Proceedings of ISAMA 2011

Tenth Interdisciplinary Conference of the International Society of the Arts, Mathematics, and Architecture

Columbia College, Chicago, Illinois

June 13-17, 2011

ISAMA 2011 is dedicated to the memory of Charles O. Perry (1929-2011)

Charles O. Perry passed away on Tuesday, February 8, 2011 at his home in Norwalk, Connecticut after a long illness. We are dedicating this conference to his memory. Charles Perry was one of the leading international sculptors whose work was inspired by mathematics. He continued in the tradition of Max Bill, Naum Gabo, and Antoine Pevsner. I first met Charlie when he was an invited speaker at the first Art and Mathematics Conference held at the University at Albany in June, 1992. As a leader in the field, he certainly energized that conference, as well as the many subsequent conferences at which he spoke. His work is an inspiration to all of us. It was also a great experience for all of us to learn from him. We will certainly miss his presence but his strong spirit will always be with us.

As a person, he was totally down to earth, and I will certainly miss our frequent phone conversations. I can close my eyes and hear him telling me entertaining stories, as well as advice on all things concerning sculpture, as well as life in general. Charlie was "una cosa vera", the real thing.

Nat Friedman,

May 11, 2011

Preface

It is a pleasure to return to ISAMA founder Nat Friedman s hometown Chicago for ISAMA 2011 and we wish to express our deep appreciation to Pangratios Papacosta for bringing the conference to Columbia College, our host institution. Columbia College is an ideal location for the conference with Millenium Park nearby. Here are the world famous attractions such as the Art Institute of Chicago and the new Renzo Piano Wing, the wonderful public sculpture Cloudgate by Anish Kapoor, and the Frank Gehry Pritzker Pavilion Concert Hall, all within easy walking distance.

We have a full five day program with talks on Monday, Tuesday, and Wednesday, excursions on Thursday, and workshops on Friday. In particular, the invited speakers are Kevin Henry, Professor of Product Design, Columbia College, Chicago; Neil Katz, Architect, Skidmore, Owings, and Merrill, LTP, Chicago; Jason Leigh, Professor of Computer Science, University of Illinois at Chicago; Mark Schendel, Architect, Studio Gang Architects, Chicago; and David Stark, Director of Adult Programs, Art Institute of Chicago.

In this volume there are a range of papers relating the arts, mathematics, and architecture. We wish to thank the authors for their participation in ISAMA 2011- you are the conference. Our purpose is to come together to share information and discuss common interests. Hopefully new ideas and partnerships will emerge which can enrich interdisciplinary education.

ISAMA 2011 Organizing Committee

CONTENTS

Ovals and Ellipses in Architecture

Javier Barrallo
The University of the Basque Country
E.T.S. Arquitectura. Plaza Oñati, 2
20018 San Sebastián. Spain

Abstract

Since ancient times, ovals and ellipses have been used to design floor plans and enclosed spaces. From the amphitheatres of Rome to the European Baroque churches, a wide variety of oval shapes have been constructed throughout the history of Architecture. The close similarity between ellipses and ovals makes it almost impossible to distinguish between them without documentation from the construction techniques. Several details have led us to think that ovals were preferred by architects and masons. Modern architecture has experienced a revival of elliptic forms, creating amazing new buildings based on torsion, juxtaposition and rotation of ovals, ellipses and superellipses.

Definition of Ovals

The word oval comes from the Latin *ovum*, egg. There is no strict mathematical definition for the term oval and many curves are commonly called ovals. All ovals are closed differentiable curves that enclose a convex region. They are smooth looking and have at least one axis of symmetry.

Amongst them, the most well known are Cassini's Ovals, named after the Italian born astronomer Giovanni Domenico Cassini (1625-1712) who studied them in 1680. They are defined as the set of points in the plane whose product of the distances to two fixed points is constant. Remember that the ellipse is defined as the set of points whose sum of the distances to two fixed points is constant, rather than the product. Cassini's ovals have the following equation, where the foci are (a, 0), (-a, 0) and b is a constant.

$$\left(x^2 + y^2\right)^2 - 2a^2\left(x^2 - y^2\right) + a^4 = b^4$$

With this definition of Cassini´s ovals, we can obtain an enormous variety of forms. These include the lemniscate of Bernoulli (when b/a=1) which is a figure with a rotated eight shape and self-intersecting, a reason why it is sometimes not considered as an oval.

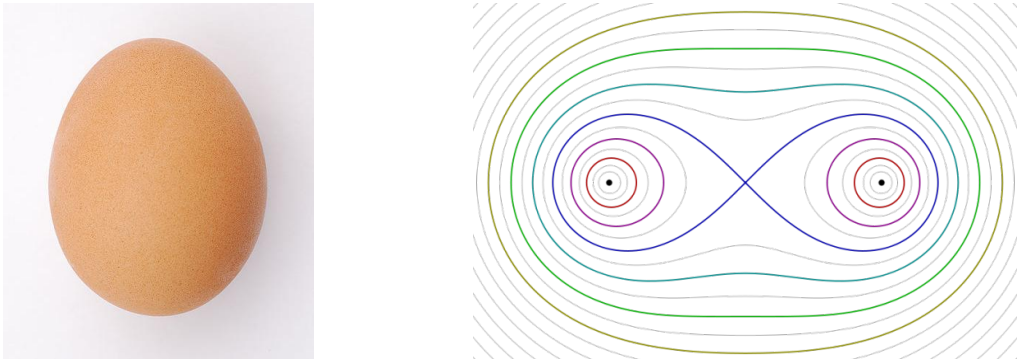

Figure 1: *A chicken egg is an oval with one axis of symmetry (left). Family of Cassini's ovals (right).*

There are many possible constructions of ovals, but we should highlight the constructions described by Sebastiano Serlio (1537-1575) in his books *Primo* and *Quinto Libri d'Arquitecttura*. Here, four simple and reliable techniques for the construction of ovals were introduced. Using the triangle, square and circle as basic geometric forms, Serlio described how to produce ovals made up from four circular arcs. This treatise has been used extensively by many architects across Europe.

Serlio's constructions have been analyzed in terms of the ovals' approximation to an ellipse. We found that Serlio's constructions do reasonably well. But other constructions by James Simpson –based on a method by James Stirling– have superior fitness. Other methods, like Vignola's construction, do especially well.

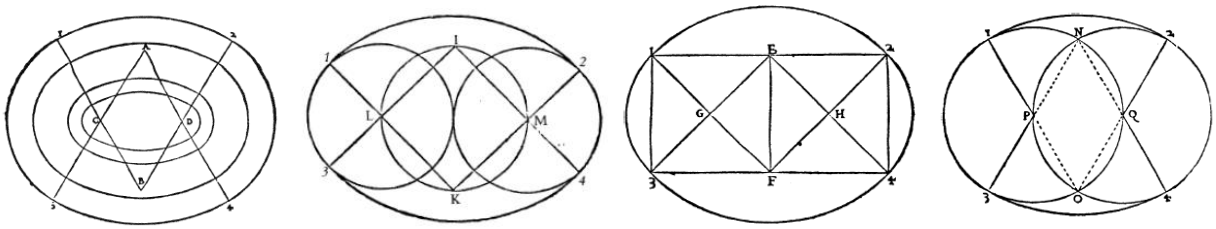

Figure 2: *Sebastiano Serlio's oval constructions (1545)*

Ellipses and Conic Sections

An ellipse is a closed plane curve consisting of all points for which the sum of the distances between a point on the curve and two fixed points (foci) is the same. It can also be defined as the conic section formed by a plane cutting a cone in a way that produces a closed curve. Circles are special cases of ellipses.

The discovery of conic sections is credited to Menaechmus in Ancient Greece around the years 360-350 B.C. These curves were later investigated by Euclid, Archimedes and Apollonius, *the Great Geometer*. Conic sections were nearly forgotten for 12 centuries until Johannes Kepler (1571-1630) discovered the elliptic nature of planetary motion as one of the major advances in the history of science.

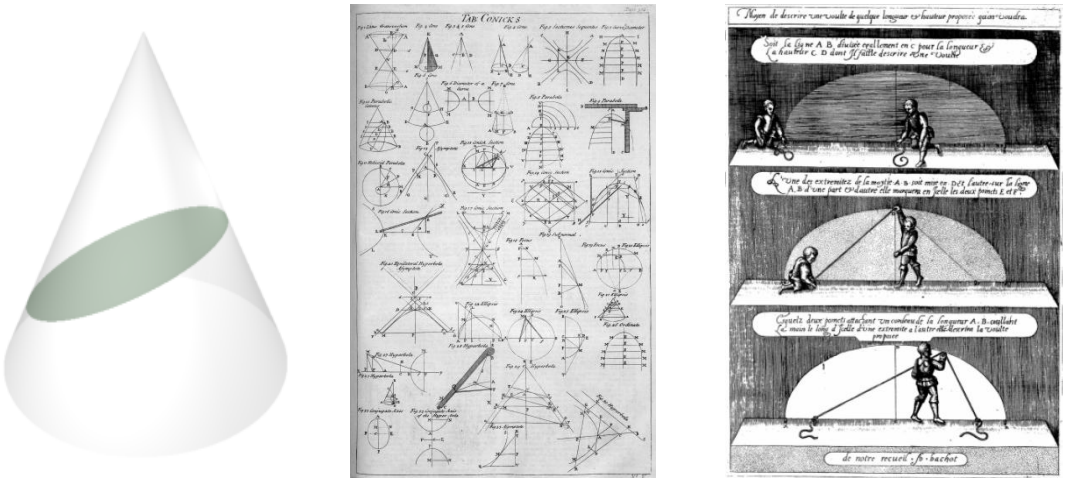

Figure 3: *Ellipse obtained as the intersection of a cone and a plane (left) Table of conics, Cyclopaedia, 1728 (center) Use of the string method to trace an ellipse, Bachot, 1598 (right).*

It must be stated that before René Descartes (1596-1650) developed analytic geometry all geometrical objects were described from basic measurements taken with rule and compass. So, the ellipse equation we usually manipulate, $(x/a)^2+(y/b)^2=1$, was unknown before the XVII century.

The only way to represent an ellipse in the ancient world was to follow pure mechanical processes like the gardener's method using two pegs as the ellipse's foci and a rope around them. Other more complex devices were the Trammel of Archimedes (also known as Ellipsograph) or the Hypotrochoid curve generator, considering the ellipse as a special case of a Hypotrocoid.

In *Astronomia Nova* (1609) and the *Codex Atlanticus* (1519) Johannes Kepler and Leonardo da Vinci respectively described how an ellipse inscribed in a circumference divides lines drawn from its major axis to the circle proportionally.

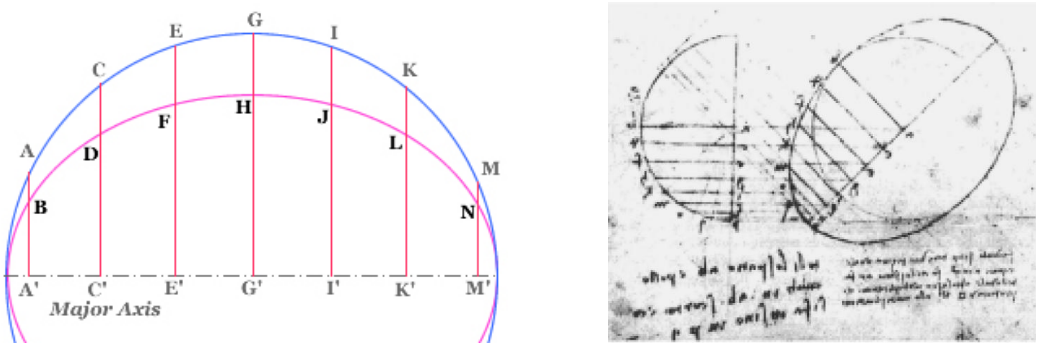

Figure 4: *According to Kepler, Point B divides line AA' in the same proportion as point D divides line CC', and so on (left). Drawing by Leonardo da Vinci from the Codex Atlanticus (right).*

The origin of Ovals in Architecture

The first buildings from antique civilizations like Egypt or Mesopotamia were rounded forms not geometrically defined which could be described as ovals. Ancient builders were looking for a simple and economical way to enclosure a space. As these techniques were improved and spaces became wider, contours became geometrically traced, probably by means of cords and pegs.

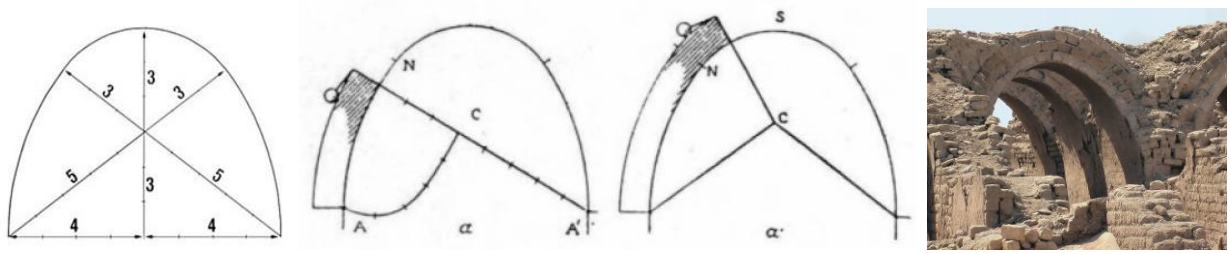

Figure 5: *Method of constructing oval arches using the Egyptian triangle 3-4-5 in the Ramesseum, Thebes (XIII Century B.C.)*

During the following centuries, the improvement of materials and edification techniques solved the constructive problems with lintels and corners and led to the introduction of rectangular shapes. Thus, during the Hellenic times ovals were not present, although the Greek discoveries in conic sections are present in their mouldings.

Roman architecture introduced the elliptic amphitheatre. This shape was introduced in response to several factors; a square or rectangular amphitheatre would result in animals and combatants stuck in corners. Circles and ellipses make better use of space and improve the view of the action. Finally, ellipses are better than circles since they have a dominant direction to structure the fights, whereas circles would lead to an impression of confusion.

As it is almost impossible to distinguish an ellipse from an oval when the major and minor axes are not too different, there has been much argument to the exact form of Roman amphitheatres. It is difficult to believe they could be elliptical for several reasons. First, because mechanical methods to generate ellipses (the gardener s method mainly) are adequate only for small ellipses. But there is an important loss of accuracy when scaling those techniques into larger ellipses produced by non constant elasticity and tension of the cord or changes in humidity and temperature. We should also consider that the gardener s method was reported for the first time by Anthemius of Tralles, one of the architects of Hagia Sophia, in the 6th century. So it is not proved it was known by Roman architects and related to conic sections.

A second reason is that since the analytic ellipse equation was unknown until the XVIIth century, it was impossible to calculate its points accurately. Ovals are made up from arches of constant curvature and any point can be easily calculated by means of trigonometry.

And a third reason is that ellipses have different curvature along its points. This generates the problem of accurately shaping constructive materials because every block has a different trace. The changing curvature also results in the problem of constructing parallel ellipses because a line made up of equidistant points from an ellipse is not another ellipse. On the other hand, concentric ovals can be easily produced, so it seems reasonable to adopt the oval form to construct the rows of benches in amphitheatres without corrupting the whole form.

Unfortunately there is no relevant literature on construction of ovals and ellipses so there is no evidence of the use of ovals in amphitheatres. Some scholars have made exhaustive analysis of the data acquired from several amphitheatres but it is not possible to get any definitive conclusions. As an example, the 662 topographic points from the Roman Colosseum showed in figure 6 do not reveal any evidence of the use of ovals or ellipses. Some minor gaps appear on both –four centred oval and ellipse– models but it must be considered that the Colosseum has suffered several collapses, including devastating earthquakes and stone-robbers.

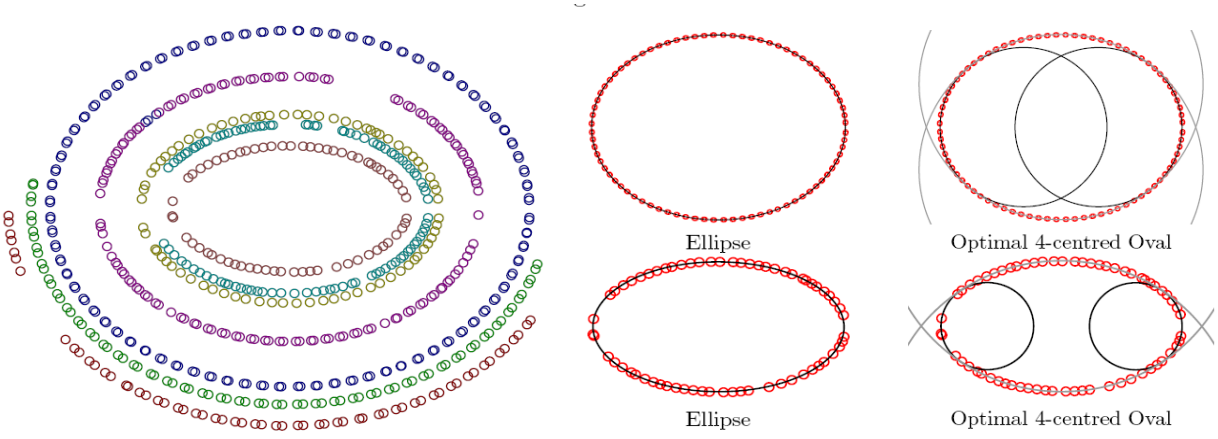

Figure 6: *Best fit curves overlaid in the Colosseum data (rings 3 and 7). The fitness of the graphical and statistical analysis does not allow obtaining a final conclusion about the use of ovals or ellipses by the roman constructors (80 AD).*

Ovals in Baroque Architecture

Baroque was the golden age of ovals, used as a new form of defining architectural space both in floor plans and domes. Baldassare Peruzi (1481-1536) was the first architect who discovered the advantages of the oval space in the church design. But it was his disciple Sebastiano Serlio who was responsible for the spread of the oval form in the late Renaissance and Baroque. In fact, many masons and architects knew that starting from Serlio's constructions, it was possible to create infinitely many ovals for any two axes.

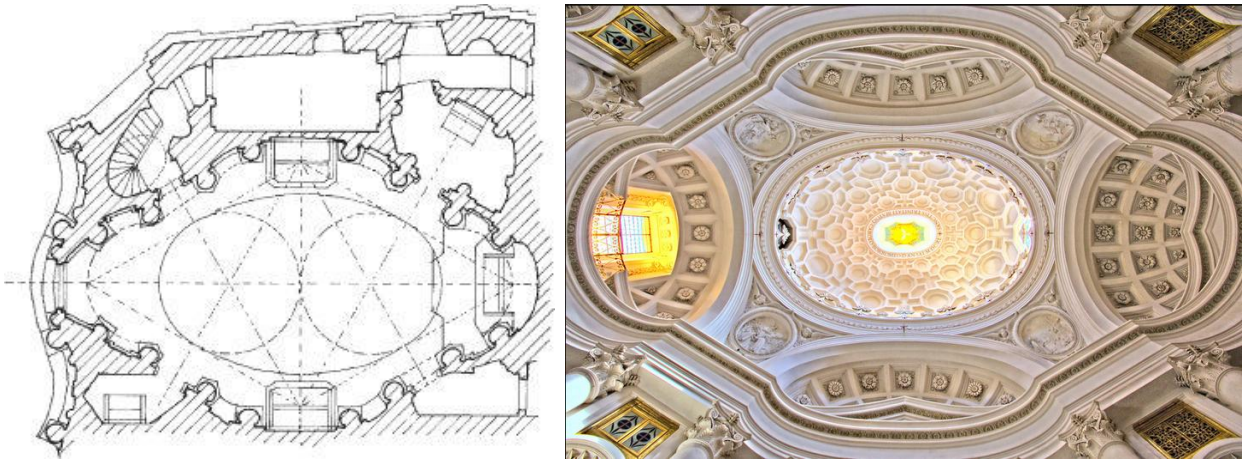

Figure 7: *Floor plane and dome of San Carlo alle Quattro Fontane designed by Francesco Borromini. It is an iconic masterpiece of Baroque architecture featuring its fantastic oval constructions.*

Giacomo Vignola (1507-1573) was the author of the first known church whose design was based on the oval shape (Sant Andrea in Via Flaminia). After Serlio and Vignola, the oval dome spread quickly not only in Italy, but in Spain, France and Central Europe. Oval shapes became a symbol of a new dynamic architecture, quite different from the classicism of the circular shapes of the Renaissance. Architect Francesco Borromini (1569-1667) designed Saint Peter's Square as the most beautiful square of Christianity. "The majestic colonnade embraces the faithful with the motherly arms of the Christian Church as they enter the piazza", in the words of Bernini. The Colonnade enclosing the oval shape becomes simultaneously a dramatic frame for the church and an impressive stage for processions and other sacred ceremonies.

Figure 8: *Saint Peter's Square in Rome, constructed by Francesco Borromini under an oval plan.*

Ellipses in Modern Architecture

The arrival of Neoclassic and Romantic Architecture in the XVIIIth century recovered the taste for classic Greco-Roman shapes. Ovals and ellipses were almost forgotten for over two centuries. It was Philip Johnson, the famous architect who first introduced the ellipse in 1986 in his Lipstick building. The unusual shape was a requirement of the developer to make the building stand out and compensate for its poor location on Third Avenue in Manhattan. According to Johnson, the elliptical shape and surrounding colonnade is reminiscent of Baroque architecture, but also succeeds in converting all exterior offices into *corners*. The three big elliptical bodies of the building are not concentric, but share a tangent line in the back of the building enhancing the elliptic shapes and lipstick appearance.

Figure 9: *The postmodern Lipstick building, New York 1986, by Philip Johnson (left) and the Tower of Winds, Yokohama 1986, by Toyo Ito (right) are two of the most iconic modern elliptical buildings.*

In Yokohama, Toyo Ito transformed a rectangular opaque concrete tower by enclosing it with an elliptical envelope. At night, the lights, neon rings and reflective surfaces react to any man made or natural forces, like ambient sounds, lights, wind forces or the time of the day. The building creates a wide variety of light patterns showing the fragile transparency of the ellipse around the inner monolithic shape.

The discussion of oval versus ellipse construction makes no sense in these times. The use of computers in geometric design allows using any pattern without differences in the final layout. It must be remarked that due to the stiffness and straightness of modern structural elements all curves are converted into polylines with straight segments and then covered by smooth constructive elements with continuous derivative.

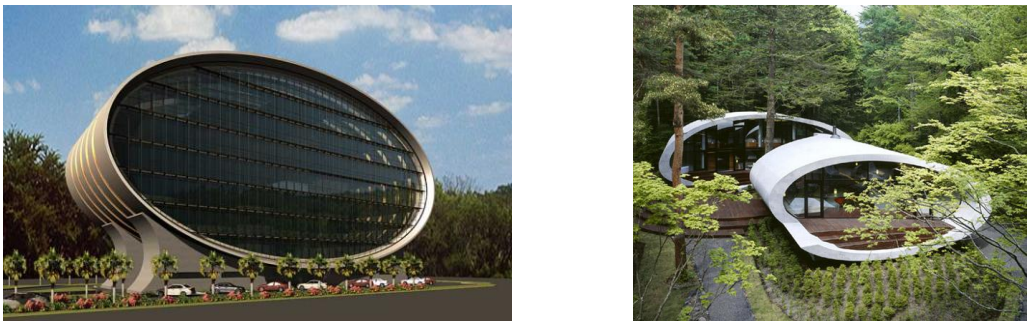

Figure 10: *The Mauritius Commercial Bank project by Jean-Francois Koenig (left) and the Shell House by Kotaro-Ide at Nagano, 2008 (right). Both building shows facades with elliptic shape.*

An ellipse is usually extended to three dimensions by means of a vertical extrusion producing a tower like structure as shown in the examples in figure 9. When the extrusion is horizontal the result resembles the examples in figure 10. When the ellipse is rotated along one of its axis the result is a quadric surface called ellipsoid, which is the analog of the ellipse in three dimensions. An example is shown in figure 11.

Figure 11: *The National Centre for the Performing Arts, usually called The Egg, is an ellipsoid dome of glass and titanium surrounded by an artificial lake. Designed by Paul Andreu, Beijing, 2007.*

Other variations are the double ellipse programs, which produce complex shapes without completely abandoning the basic geometry of the ellipse. There are several ways to juxtapose ellipses as shown in figure 12.

Figure 12: *The 73 stories Highcliff Apartments Building in Hong Kong (left) and the Bijlmer Park Theather in Amsterdam (right) are examples of juxtaposed ellipses.*

Superellipses

A Superellipse is a variant of the usual ellipse equation in which the exponent 2 is substituted by a generic value *n*. When *n*=1 the resulting figure is a diamond, when *n*=2 the figure is the ordinary ellipse and values *n*>2 produce superellipses.

Equation of the Superellipse:

$$\left|\frac{x}{a}\right|^n + \left|\frac{y}{b}\right|^n = 1$$

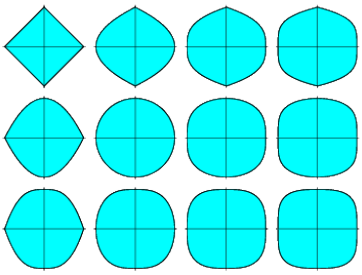

Figure 13: *Two examples of superellipses: the project of Z15 Tower, the future tallest building in Beijing (left) and the Aztec Stadium, constructed for the 1968 Olympic Games in Mexico (right). Many sport stadiums feature the superellipse in their floor plans.*

Torqued Ellipses

Torqued ellipses are weathered steel sculptures created by the American minimalist sculptor Richard Serra. The geometry of the construction consists in a set of ellipses with a continuous rotation at different heights. The surface that connects all ellipses is the torqued ellipse.

The same idea has been used in contemporary architecture, featuring the Canton Tower in Guangzhou, a 600 meter structure designed by Information Based Arquitecture with collaboration from Arup. The structure of a torqued ellipse is similar to a hyperboloid where all the circumferences contained in the planes perpendicular to the main axis are replaced by rotated ellipses of different ratios. As in the hyperboloid, the torque ellipse is a ruled surface, as can be clearly seen in figure 14.

Figure 14: *Torqued ellipse by Richard Serra at Bilbao Guggenheim Museum (left) and torqued ellipse structure in the Canton Tower in Guangzhou (right).*

A variant of the torqued ellipse is the surface constructed with rotated superellipses, which may be named as torqued superellipses. A beautiful example and maybe the only one in Architecture is the Museum Soumaya in Mexico, designed by the architect Fernando Romero. The building has a height of 46 meters and features a coating of 16,000 brilliant hexagons and looks amazing from all viewpoints.

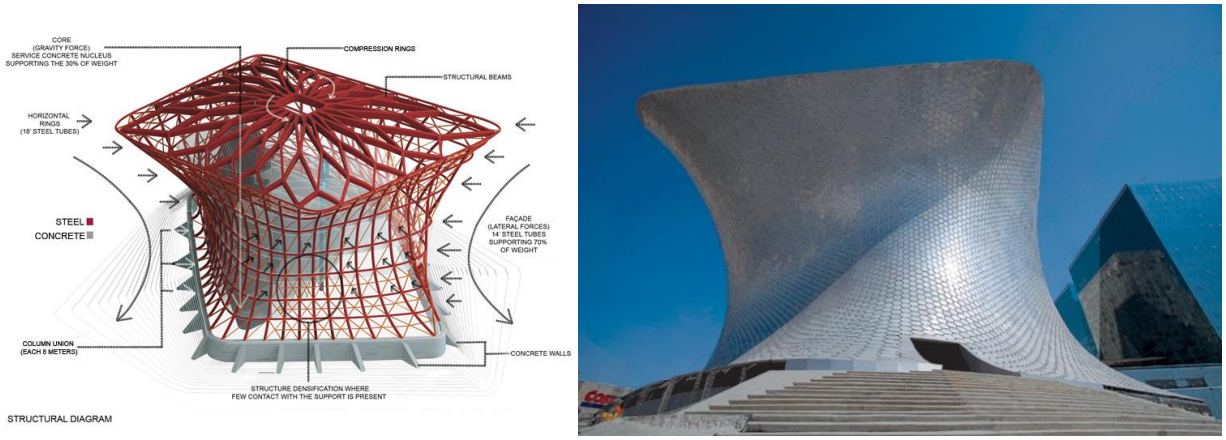

Figure 15: *Structural diagram (left) and torqued superellipse (right) from the Museo Soumaya, by architect Fernando Romero, Mexico 2011.*

Variable Oval Surface

Architect Norman Foster has made a wide use of ovals as described in Serlio s constructions 450 years ago. The Sage Gateshead is a great example of this geometry. A transversal planar four centre oval runs along a third axis changing the scale of the oval trace. The longitudinal axis modifies the shape by means of a second curve alternating convex and concave smooth curve arches.

The result is a very dynamical surface where the oval structure is almost not recognizable at first viewing and only after a detailed analysis can one deduce the hidden geometry of the building.

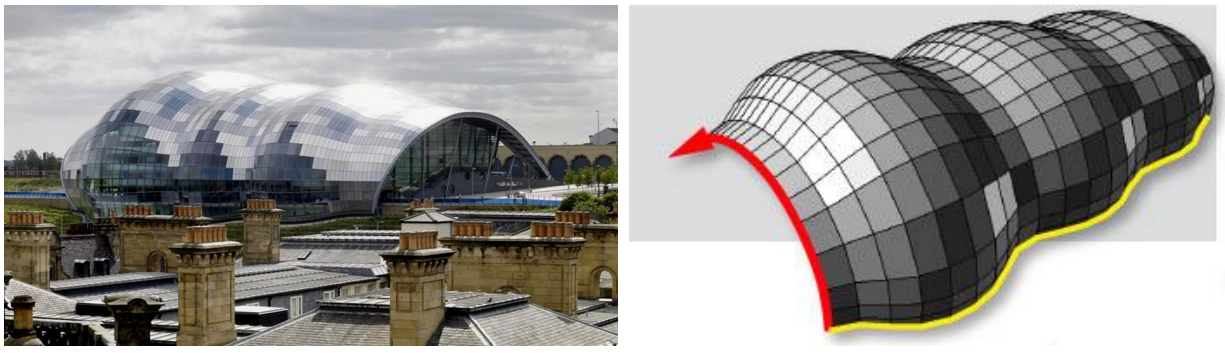

Figure 16: *The Sage Gateshead, constructed by Norman Foster in 2004. The external surface has the shape of a planar four centre oval whose scale changes as it moves along a longitudinal axis.*

References

[1] CHAPPUIS R., *Utilisation du tracé ovale dans l'architecture des églises romanes*. Bulletin Monumental 134, pp. 7-36. 1976.

[2] CHOISY Auguste, *L'art de bâtir chez les égyptiens*. Paris. E. Rouveyre. 1904.

[3] DÜRER Albrecht, *Unterweisung der Messung*. Nürnberg. 1525. (facsimile edition, Nördligen, 1983).

[4] GOYON J.C. et al., *La construction Pharaonique, du Moyen Empire à l'époque gréco-romaine*. Paris. Picard. 2004.

[5] HART V. and HICKS. P., editors. *Sebastiano Serlio on Architecture: Books I-V o Tutte L'Opere D'Architettura et Prospetiva*. Yale Univ. Press, 1996.

[6] HEATH Thomas, *A History of Greek Mathematics*. 1921. Reprint, New York. Dover Publications. 1981.

[7] HEYMAN Jacques, *The Stone Skeleton. Structural Engineering of Masonry Architecture.* Cambridge. Cambridge University Press. 1995.

[8] HUERTA Santiago, *Arcos, bóvedas y cúpulas. Geometría y equilibrio en el cálculo tradicional de estructuras de fábrica*. Madrid. Instituto Juan de Herrera. 2004.

[9] HUERTA Santiago, *Oval Domes: History, Geometry and Mechanics.* Nexus Network Journal 9, Number 2, pp. 211-248.

[10] KITAO T., *Circle and Oval in the Square of Saint Peter's. Bernini's Art of Planning*. New York. New York University Press. 1974.

[11] LAWDEN D. F., *Families of ovals and their orthogonal trajectories*. Mathematical Gazette 83, pp. 410-420. November 1999.

[12] RANKINE W. J. M., *A Manual of Applied Mechanics*. London. Charles Griffin. 1858.

[13] ROSIN P. L., *On Serlio's construction of ovals*. Mathematical Intelligencer 23, pp. 58-69. 2001.

[14] ROSIN P. L. and TRUCCO E., *The amphitheatre construction problem*. Incontro Internazionale di Studi Rileggere L'Antico. Rome. 2005.

[15] SERLIO Sebastiano. *Il Primo libro d'Architettura di Sebastiano Serlio...* Paris. 1545.

[15] SERLIO Sebastiano. *Quinto libro d'Architettura, nel quale se tratta de diverse forme de templi.* Paris. 1547.

[16] VITRUVIUS. *De Architectura*. Dover, 1960.

[17] WILLIS Robert, *On the Construction of the Vaults of the Middle Ages*. Transactions of the Royal Institute of British Architects 1, pp. 1-69. 1843.

A Fourteen-Pointed Star Polygon Design on the Mimbar of the Mosque of *al-Mu'ayyad*

B. Lynn Bodner
Mathematics Department
Cedar Avenue
Monmouth University
West Long Branch, New Jersey, 07764, USA
E-mail: bodner@monmouth.edu

Abstract

This paper will explore the conceptualization and creation of a fourteen-pointed star polygon design, found on a mimbar in the Mosque of *al-Mu'ayyad* in Cairo, Egypt, and also as Plate 169 of Bourgoin's *Arabic Geometrical Pattern and Design*. Our exploration specifically seeks to answer the question, "How did the original designer of this pattern determine, without mensuration, the proportion and placement of the star polygons comprising this design?" In addition, we propose a plausible Euclidean "point-joining" compass-and-straightedge reconstruction for it.

Introduction

The most commonly-occurring star polygons found in geometric Islamic art are those that may be created within regular n-gons (polygons with n sides) that are *constructible* in the Euclidean sense, where n = 4, 5, 6, 8, 10, 12, or 16. That is, these regular polygons may be created using only a compass to make circles or arcs and a straightedge to connect points of intersection between segments or circular arcs. For n = 7, 9, 11, 13, 14, 18…, the regular n-gons (and likewise, the corresponding regular n-star polygons) may only be constructed approximately using these tools. Of these *non-constructible* star polygons, we will explore the conceptualization and creation of a 14-pointed star polygon design found on the mimbar (or pulpit) of the Mosque of *al-Mu'ayyad* in Cairo, Egypt (shown below in **Figure 1**). This image is a cropped and rotated version of a photograph known as catalog number EGY 1217 of the *Pattern in Islamic Art: The Wade Photo Archive* [1].

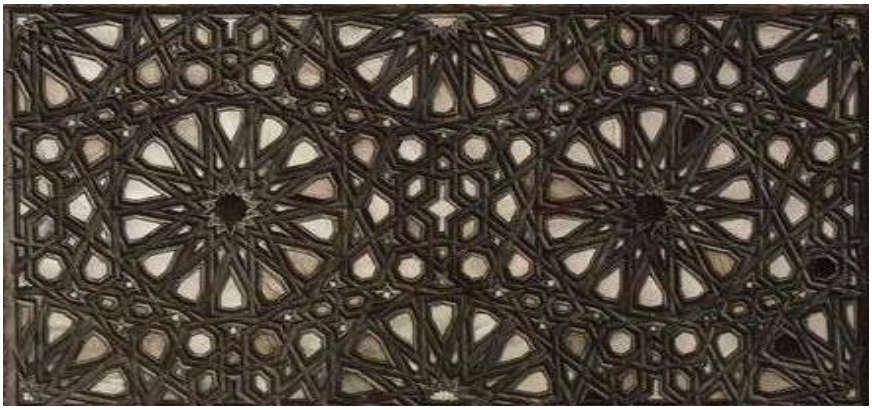

Figure 1. *Design on the mimbar (or pulpit) of the Mosque of al-Mu'ayyad in Cairo, Egypt from the Pattern in Islamic Art: The Wade Photo Archive, catalog number EGY 1217*

This same 14-star design also appears in skeletal form as Plate 169 of J. Bourgoin's *Arabic Geometrical Pattern and Design* [2], a rich published source of 190 Islamic patterns, first published in 1879 and based upon drawings of Islamic monuments in Cairo and Damascus. Our exploration specifically seeks to answer the question, "How did the original designer of this pattern determine, without mensuration, the proportion and placement of the star polygons comprising the design?" In addition, we propose a plausible Euclidean "point-joining" compass-and-straightedge reconstruction for each, using the *Geometer's Sketchpad* software program [3], the electronic equivalent of the compass and straightedge.

Construction of a "Nearly Regular" 7-gon, a 14-gon, and the 14-Pointed {14/6} Star Polygon

A straightforward technique for creating star polygons, discussed previously in [4], is to initially construct an n-gon inscribed within a circle and then draw in the corresponding regular n-pointed star by methodically joining the vertices of the n-gon with line segments (diagonals) or by methodically joining midpoints of the n-gon's edges. A figure formed in this way is mathematically designated as a $\{p/q\}$ star polygon, where p and q are positive integers that are also relatively prime, with $q < p/2$.

To create a "nearly regular" seven-pointed {7/2} star polygon, construct an approximately regular heptagon and then connect every other vertex with line segments. A very good approximate heptagon and its inscribed seven-pointed star polygon is shown in **Figure 1a.** Once a heptagon is created within a circle, a 14-gon may be generated by constructing lines through the vertices of the heptagon and the midpoints of the corresponding opposite line segments. The points where these lines intersect the circle divide the circle into 14 approximately congruent arcs and also form the vertices of the 14-gon, as shown in **Figures 1b and 1c**.

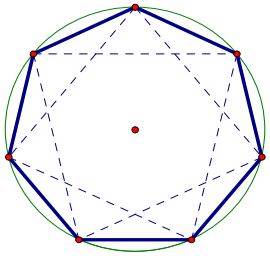

Figure 1a.

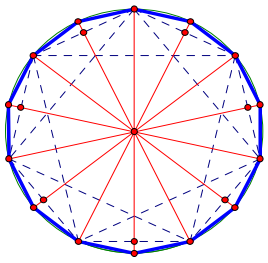

Figure 1b.

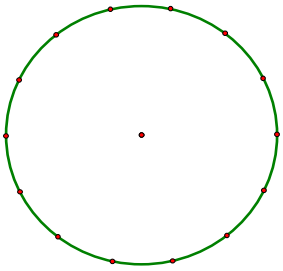

Figure 1c.

Now connect every third point with line segments until **Figure 2a** is achieved. Repeat this procedure with the points of intersection generated in the previous step and shown in **Figure 2b**. To generate the {14/6} star polygon of interest, connect every sixth point of intersection created in the previous step, as indicated in **Figure 2c**.

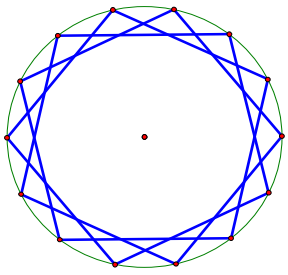

Figure 2a.

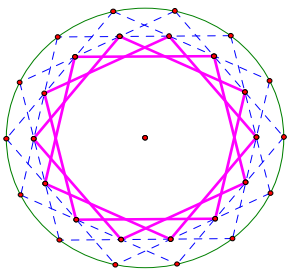

Figure 2b.

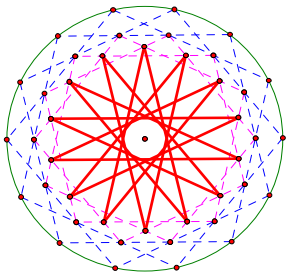

Figure 2c.

Erase the segments generated in the second step and highlight the appropriate segments to yield the image in **Figure 3a**. To create additional points of intersection from which the segments forming the hexagonal "arrow" shapes may be made, extend these segments until they intersect the segments generated in the first step; two of these chords, shown in **Figure 3b,** are used to form the arrow at the top of the fourteen-pointed star. Highlighting the segments of interest and erasing the segments generated in the first step results in **Figure 3c**. For the remainder of this paper, the 14-pointed star polygon along with the 14 arrows will together be referred to as the "*fourteen star polygon*" or the "*star polygon*" or the "*star*."

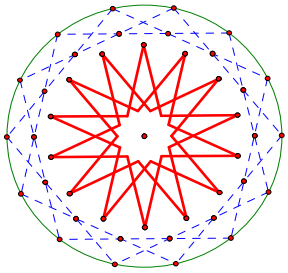

Figure 3a.

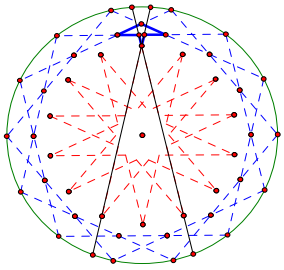

Figure 3b.

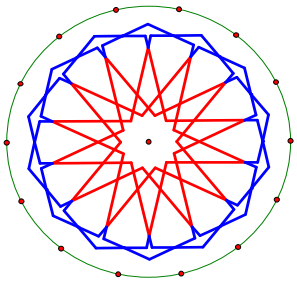

Figure 3c.

Placement of the *Stars* in Bourgoin's 14-pointed Star Designs, Plates 164 - 167

As we have already shown, generating the *stars* is a relatively straightforward process. In a previous paper [4], the author discussed this and also how to place the stars relative to one another in four other 14-star designs, Plates 164 – 167 of [2]. In Plate 165, (see **Figure 4a** on the next page), the *stars* met two at a time, with the arrow tip of one *star* just touching an arrow tip of an adjacent *star*. In Plate 166, (see **Figure 4b**), if the *stars* are surrounded by the circles used in their original construction, each circle was tangent to two others, and the two middle circles overlap, enclosing their two arrow tips that touch.

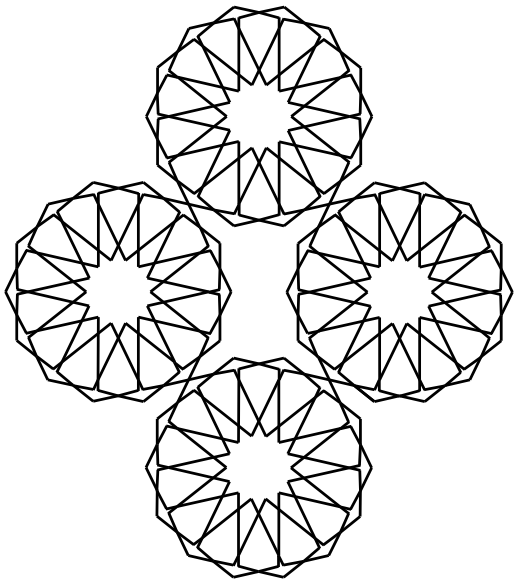

Figure 4a. *Design of Bourgoin's Plate 165*

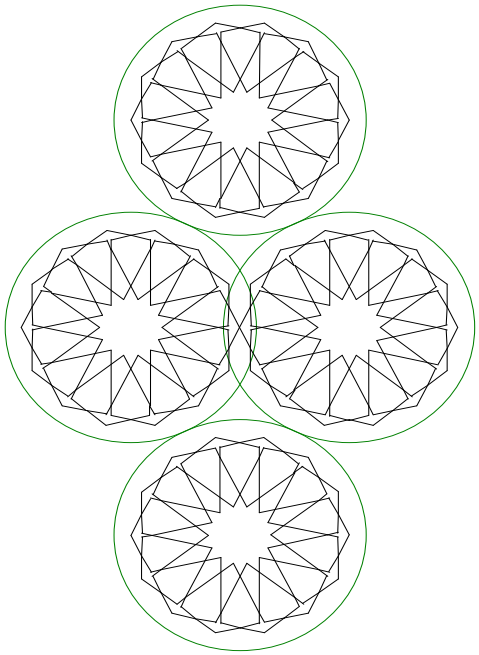

Figure 4b. *Design of Bourgoin's Plate 166*

In Plate 164, (see **Figure 4c**) the arrows of adjacent *stars* overlapped and merged to form pairs of 5-pointed stars, and the lozenge-shaped petals of adjacent *stars* just touched. In Plate 167, (see **Figure 4d**) Bourgoin has separated the four stars so that none are touching but the circumscribing circles are positioned to be tangent in pairs. Between the *stars* in all of these designs there is an area to be filled in with other polygons. (For more information on these four designs, see [4].)

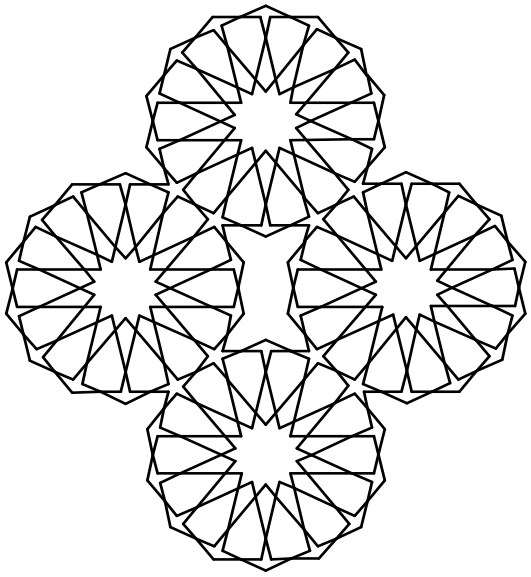

Figure 4c. *Design of Bourgoin's Plate 164*

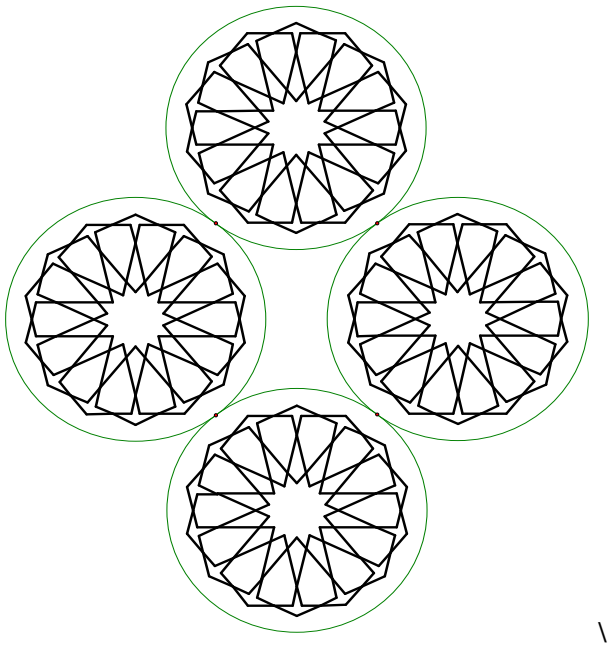

Figure 4d. *Design of Bourgoin's Plate 167*

Construction of the 14-Star Design on Bourgoin's Plate 169

One plausible method for positioning the stars in Bourgoin's Plate 169 is to use a grid of regular hexagons that are displaced by half of an edge length. The hexagonal grid, along with inscribed circles superimposed on the design, is shown in **Figure 5**. It is in the circles inscribed within these hexagons that the *stars* will be constructed, as previously discussed, and shown in **Figure 6a** on the following page.

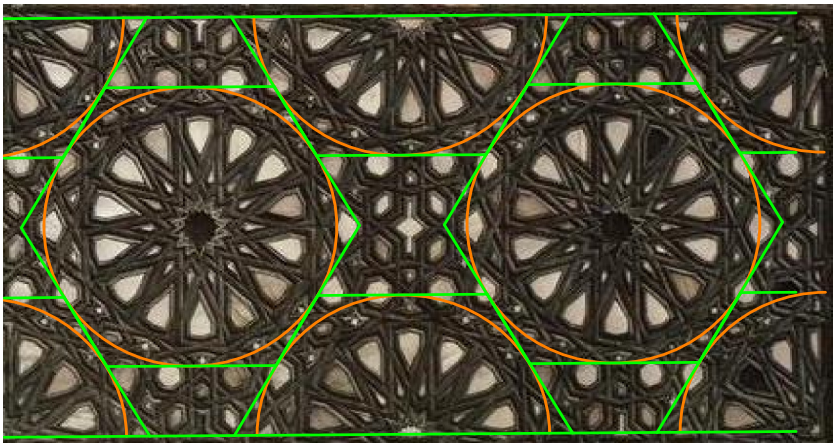

Figure 5. *Design on the mimbar (or pulpit) of the Mosque of al-Mu'ayyad in Cairo, Egypt from the Pattern in Islamic Art: The Wade Photo Archive, catalog number EGY 1217*

Erase the hexagons and extend existing line segments until they intersect other rays, thus yielding the image in **Figure 6b.**

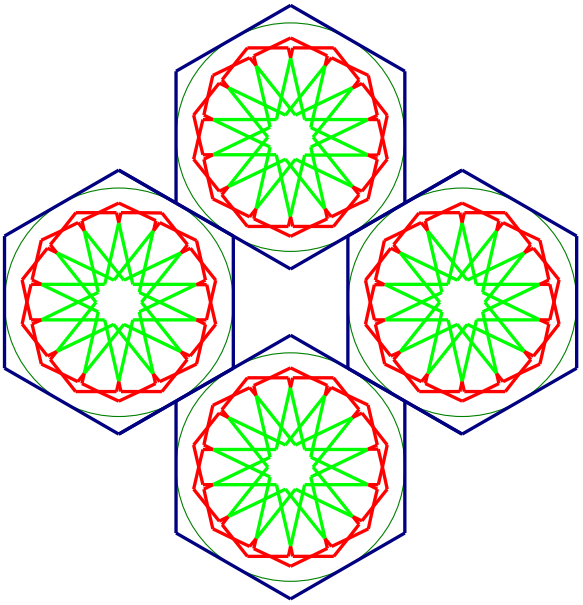

Figure 6a.

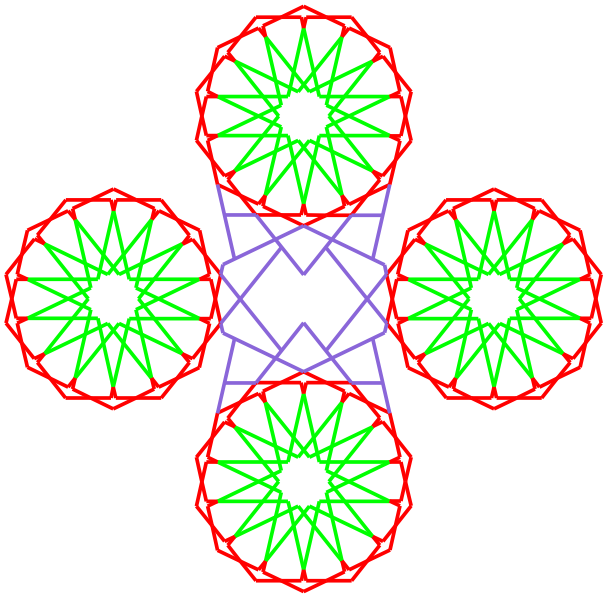

Figure 6b.

Erase the circles, construct midpoints of four segments and draw horizontal line segments between these points as shown in **Figure 6c.** Extend additional segments and erase unneeded segments to form the non-convex 12-sided polygon in the center of the figure flanked on either side by two non-convex octagons, shown in **Figure 6d.**

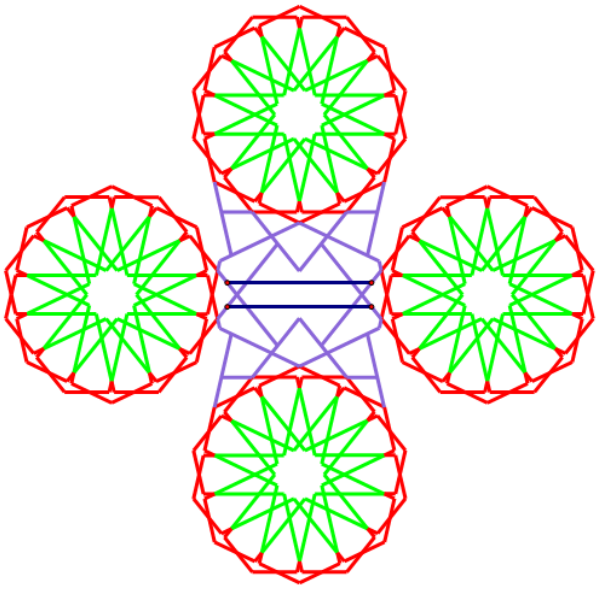

Figure 6c.

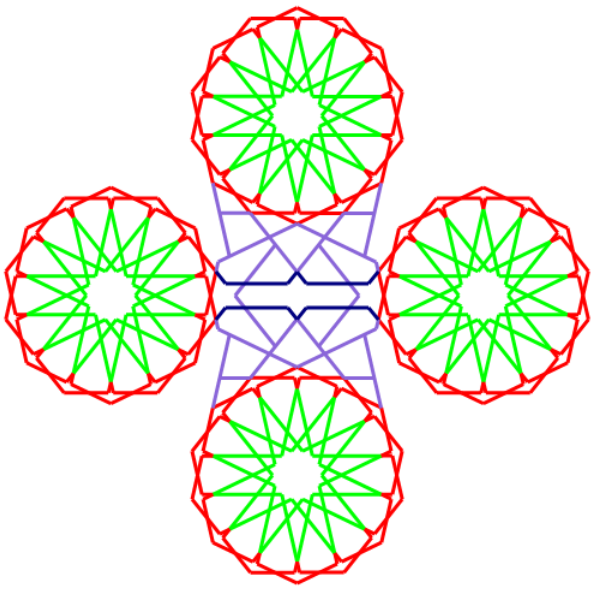

Figure 6d.

Construct two additional horizontal line segments through existing points to obtain four additional points as shown in **Figure 7a.** From these points, draw line segments to points on the *stars* to the left and right of the center space as shown and also erase unnecessary segments to produce the image in **Figure 7b.**

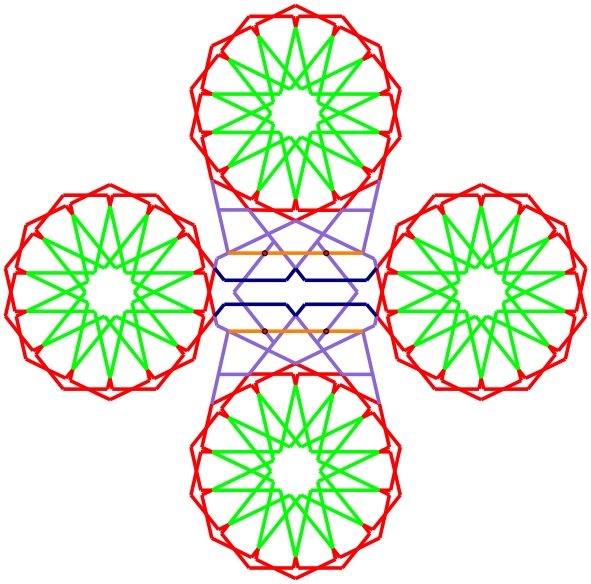

Figure 7a.

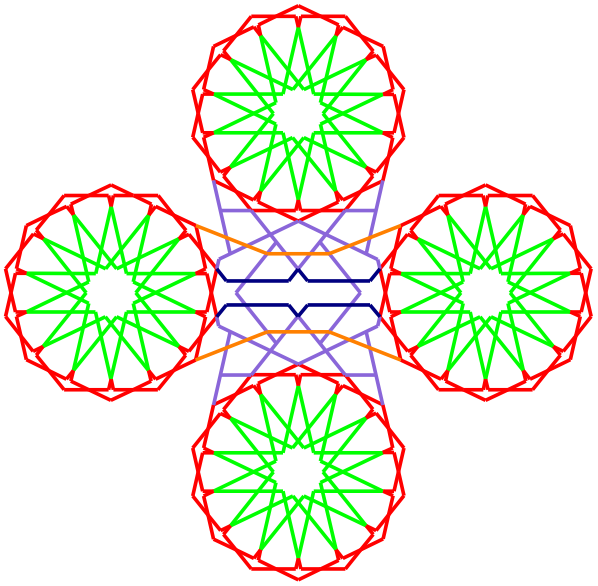

Figure 7b.

Construct midpoints of many of the segments in the center of the image so that additional segments may be constructed by joining them to themselves and to other existing points, as shown in **Figures 7c** and **7d**. The unneeded segments are then erased.

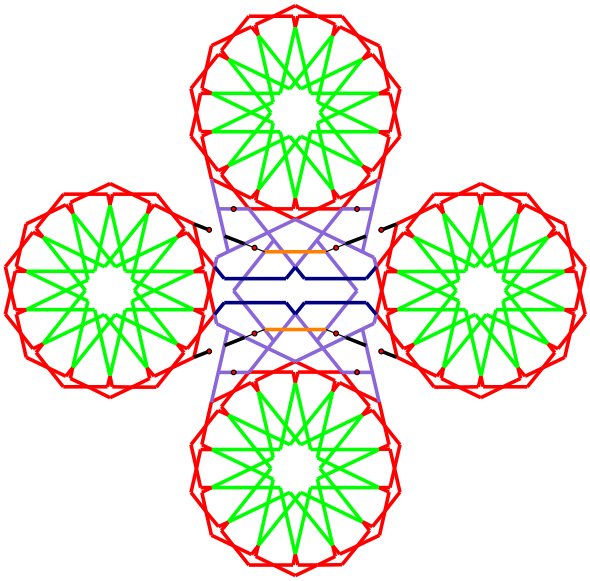

Figure 7c.

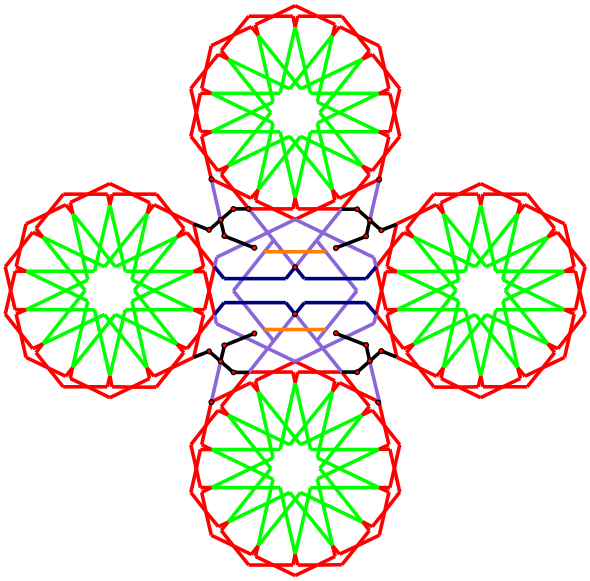

Figure 7d.

Next, construct and then bisect the horizontal line segment in the center of the design. Using the midpoint of this segment as the endpoint of two smaller segments, find their midpoints as well, as shown in **Figure 8a**. Additional line segments may now be constructed between these midpoints. By erasing unneeded line segments and highlighting the appropriate ones we obtain **Figure 8b.**

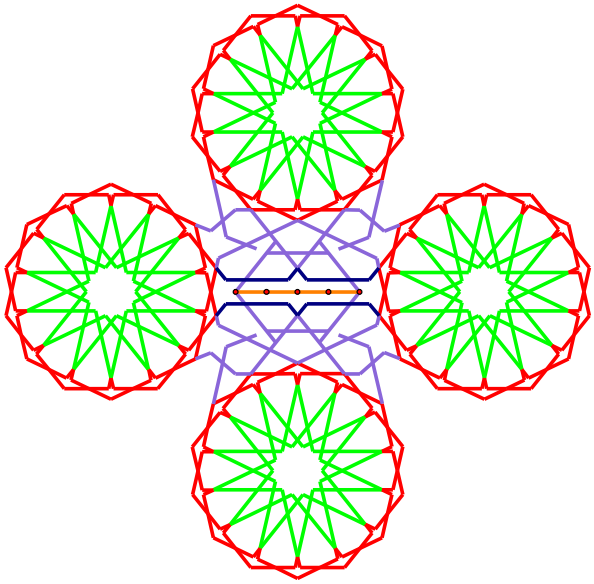

Figure 8a.

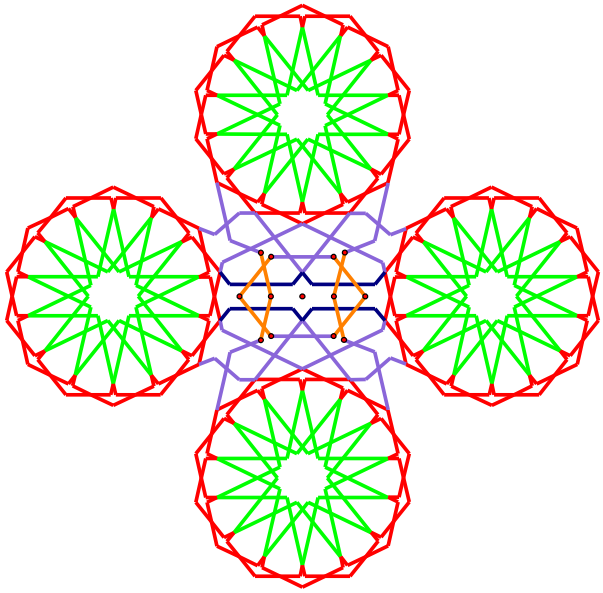

Figure 8b.

To complete the design, extend and find midpoints of some existing line segments, as shown in **Figure 8c,** and then erase the unneeded segments to produce the required image shown in **Figure 8d.** Having found a way to construct the polygons between the *stars* is sufficient to be able to continue the design indefinitely.

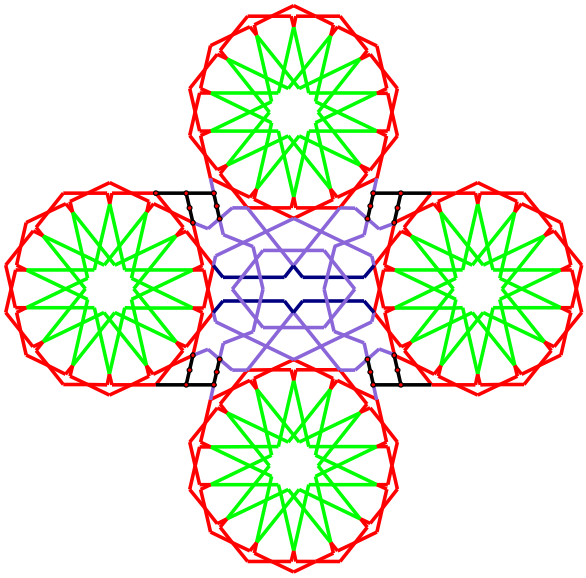

Figure 8c.

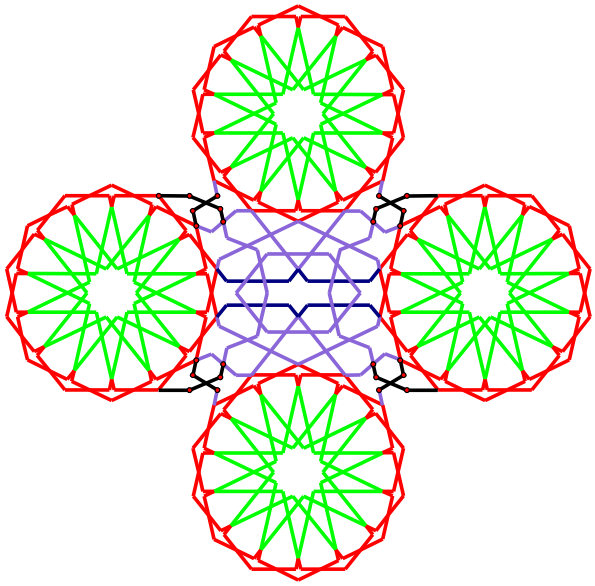

Figure 8d.

A skeletal version of four of the *stars* and the interstitial space is given in **Figure 9a,** and a colored rendition of the design, created by the author using the *Geometer's Sketchpad* and *Paint* [5] software packages, is given in **Figure 9b**.

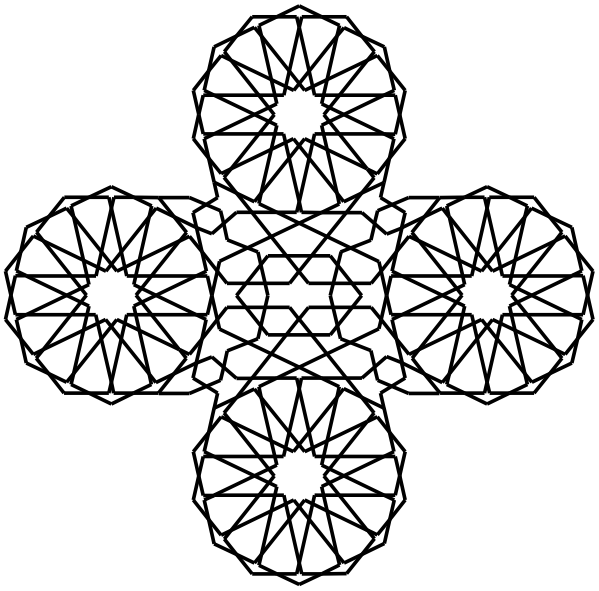

Figure 9a.

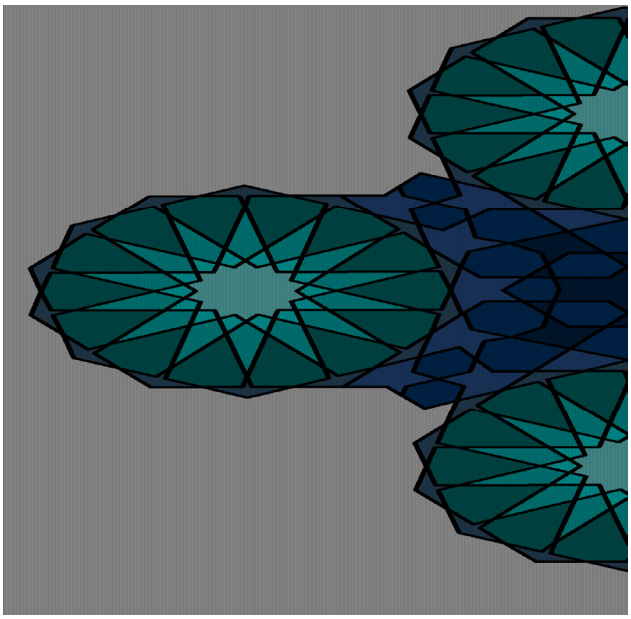

Figure 9b.

Discussion

Reconstructing the fourteen-pointed star polygon design found on the mimbar of the Mosque of *al-Mu'ayyad* (taken from a photograph known as catalog number EGY 1217, of *The Wade Photo Archive*) and also found on Plate 169 of Bourgoin's *Arabic Geometrical Pattern and Design* was relatively straightforward once the *stars* were positioned using a grid of regular hexagons that were displaced relative to each other by half of an edge length. A compass-and-straightedge "point joining" technique was used exclusively to produce the design by constructing the requisite points, circles, line segments, and midpoints. That is, no measurements of any kind (for example of angles or line segment dimension) were employed as may have been the practice of medieval artisans.

References

[1] Pattern in Islamic Art: The Wade Photo Archive, available at http://www.patternsinislamicart.com
[2] Bourgoin, J. (1973). *Arabic Geometrical Pattern and Design,* Dover Publications. Original 1879.
[3] The *Geometer's Sketchpad* software program, available at http://www.keypress.com.
[4] Bodner, B. L. (2010). "Bourgoin's 14-Pointed Star Polygon Designs," *Bridges: Mathematical Connections in Art, Music, and Science Conference Proceedings,* pp. 135 - 142.
[5] The *Paint* software program.

Enumerations of Hyperbolic Truchet Tiles

Douglas Dunham
Department of Computer Science
University of Minnesota, Duluth
Duluth, MN 55812-3036, USA
E-mail: ddunham@d.umn.edu
Web Site: http://www.d.umn.edu/~ddunham/

Abstract

Sébastien Truchet was a pioneer in applying combinatorics to the study of regular patterns. He enumerated the patterns that could be formed from square tiles that were divided by a diagonal into a black and a white triangle Following Truchet, others have created Truchet-like tilings composed of circular arcs and other motifs. These patterns are all based on Euclidean tessellations, usually the tiling by squares. In this paper we pose corresponding enumeration questions about hyperbolic Truchet tilings and show some sample patterns.

1. Introduction

About 300 years ago the French Dominican Father Sébastien Truchet enumerated Euclidean patterns that could be formed by using square tiles that are divided into two $45°$ equilateral triangles, one black and one white. The goal of this paper is to try to enumerate corresponding patterns in the hyperbolic plane. Figure 1 shows a hyperbolic Truchet pattern.

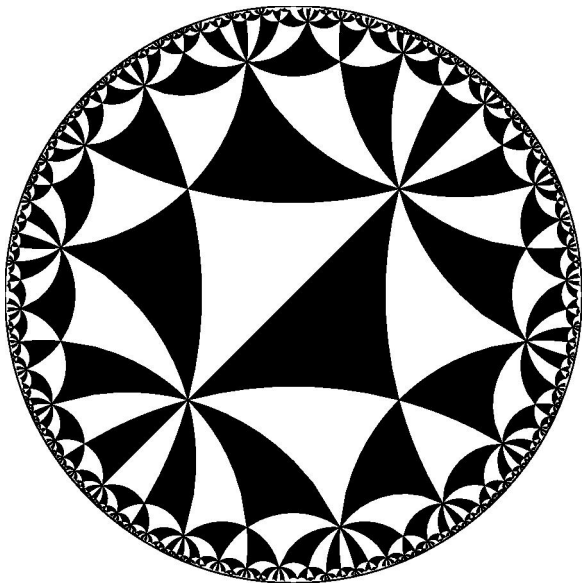

Figure 1: A hyperbolic Truchet tiling based on the $\{4,6\}$ grid.

We begin with a short history of Truchet tilings. Then we review hyperbolic geometry and regular tessellations, upon which both Euclidean and hyperbolic tilings are based. Next we examine hyperbolic patterns based on "square" grids, which are most directly related to Truchet's tilings. More generally we show how a p-sided polygon for can be subdivided by triangles for $p \neq 4$. We also investigate p-sides tiles

decorated with circular arcs. Finally, we show sample patterns and indicate possible directions of further research.

2. A Short History of Truchet Tilings

Sébastien Truchet was born in Lyon, France in 1657, and became a Dominican Father as an adult. In addition to Truchet tilings, he is well known for his work in typography and the "Roman Du Roi" typeface that is an ancestor of "Times New Roman", in particular. Truchet also designed many French canals and invented sundials, weapons, and special implements for transporting trees (from Wikipedia [11]). He published his work on tilings "Memoir sur les Combinaisons" in the *Memoires de l'Académie Royale des Sciences* in 1704 [10]. In this paper Truchet considered all possible pairs of juxtaposed squares divided by a diagonal into a black and a white triangle. This was most likely the first published systematic enumeration of simple tile motifs. In the mid 1700's, Pierre Simon Fournier created Truchet patterns based on more complex motifs [2]. In 1942 M.C. Escher enumerated 2×2 tiles of squares formed from squares containing simple motifs, thus extending Truchet's idea of 2×1 tiles (see the section *Other experiments in regular division*, pages 44–52 of [8]). In 1987 Truchet's treatise was translated into English (by Pauline Bouchet), with some history and comments on Truchet's theory (by Cyril Smith) in a *Leonardo* paper which also reproduced Truchet's figures [9]. The Smith-Bouchet paper re-ignited interest in Truchet's tilings, and also introduced the "circular arc" Truchet tile, which has been popular with other pattern creators. Since then Browne [1], Lord and Ranganathan [3], Reimann [5, 6], and Rhode [7] have extended Truchet's ideas to other 2-dimensional motifs and to 3-dimensional patterns.

3. Hyperbolic Geometry and Regular Tessellations

Truchet used the Euclidean tessellation by squares for his tiling patterns. Others have also used the other two regular Euclidean tessellations, by equilateral triangles and by regular hexagons, as a basis for their Truchet-like tilings. In this paper, we show how to extend Truchet tilings to the hyperbolic plane, which has an infinite number of regular tessellations.

It has been known for more than a century that there is no smooth embedding of the hyperbolic plane into Euclidean 3-space. Thus we must rely on models of hyperbolic geometry. Specifically, we use the *Poincaré disk* model, whose (hyperbolic) points are represented by Euclidean points within a bounding circle. Hyperbolic lines are represented by (Euclidean) circular arcs orthogonal to the bounding circle (including diameters). The hyperbolic measure of an angle is the same as its Euclidean measure in the disk model (i.e the model is *conformal*), but equal hyperbolic distances correspond to ever-smaller Euclidean distances as figures approach the edge of the disk, as can be seen in Figure 1.

There is a *regular tessellation,* $\{p, q\}$, of the hyperbolic plane by regular p-sided polygons, which we call *p-gons*, with q of them meeting at each vertex, provided $(p-2)(q-2) > 4$. If $(p-2)(q-2) = 4$, one obtains three Euclidean tessellations: the square grid $\{4, 4\}$, the hexagon grid $\{6, 3\}$, and the equilateral triangle grid $\{3, 6\}$. Figure 2 shows the regular hyperbolic tessellation $\{4, 6\}$, and Figure 3 shows that tessellation superimposed on the Figure 1 pattern.

4. Hyperbolic Truchet Patterns Based on "Squares"

The simplest Euclidean Truchet tiling is the one created by translations of the *basic square* — a square divided into a black and a white isosceles right triangle by a diagonal, as shown in Figure 4 on the left. There is another Truchet tiling obtained by rotating the basic squares about its vertices, so that the 45° vertices meet at alternate vertices of the $\{4, 4\}$ grid, as shown on the right of Figure 4. These are patterns A and D of Truchet's *Memoir* [9] and the only ones adhering to the map-coloring principle: no triangles of the same color share and edge.

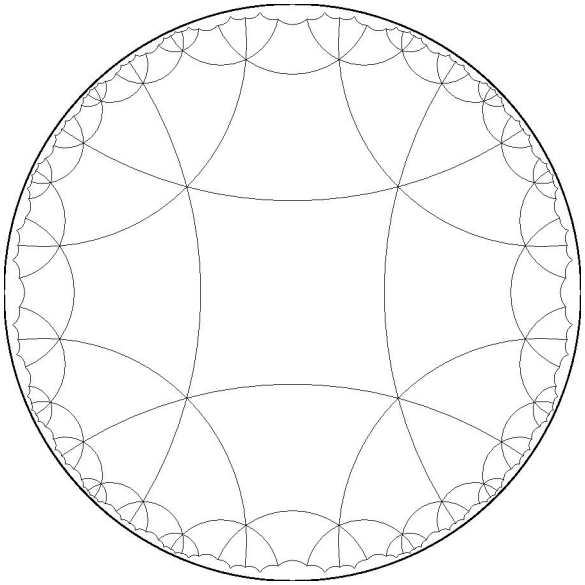

Figure 2: The $\{4,6\}$ tessellation

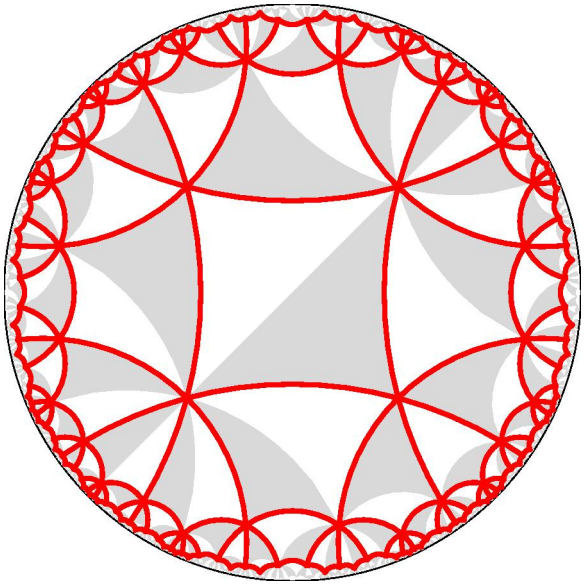

Figure 3: The $\{4,6\}$ superimposed on the Figure 1 pattern.

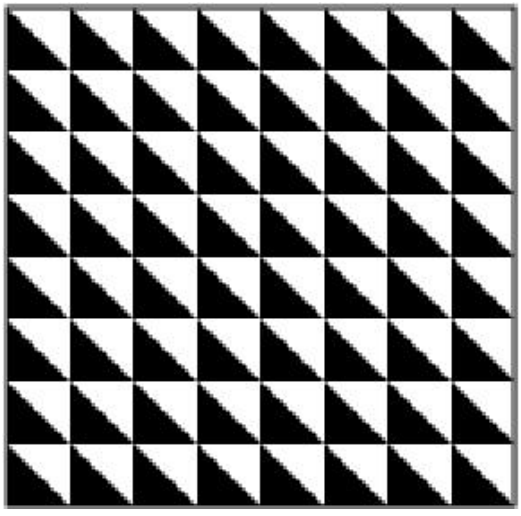

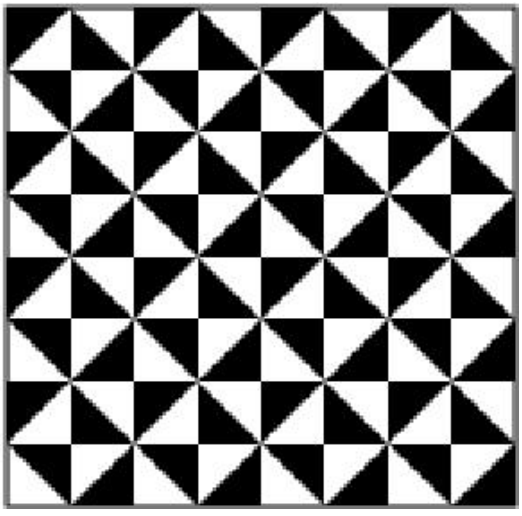

Figure 4: (a) A "translation" Truchet tiling, (b) A "rotation" Truchet tiling.

In the hyperbolic plane, if one translates a decorated 4-gon of a $\{4, q\}$ to the next 4-gon to the right, then upward, then to the left, etc., in a counter-clockwise manner about a q-vertex, the decorated 4-gon will return to its orginal position after q steps. However, the decoration will be rotated by an angle of $q\pi/2$. Therefore, to obtain a consistent tiling by a decorated 4-gon, $q\pi/2$ must be a multiple of 2π, i.e. q must be divisible by 4. Figure 5 shows the "smallest" hyperbolic example with $q = 8$.

If we apply the rotation construction in the hyperbolic case, the base angles of the black and white isosceles triangles meet at some of the vertices of $\{4, q\}$ and the vertex angles of the isosceles triangles meet at the other vertices of $\{4, q\}$. In this case q must be even to satisfy the map-coloring principle. Figure 1 shows the pattern when $q = 6$; Figure 6 shows the result when $q = 8$. In Figures 5 and 6 small circles have been placed at the vertex angles of the black and white isosceles triangles to illustrate the differences between the hyperbolic "translation" and "rotation" patterns. Truchet did not restrict himself to the map-

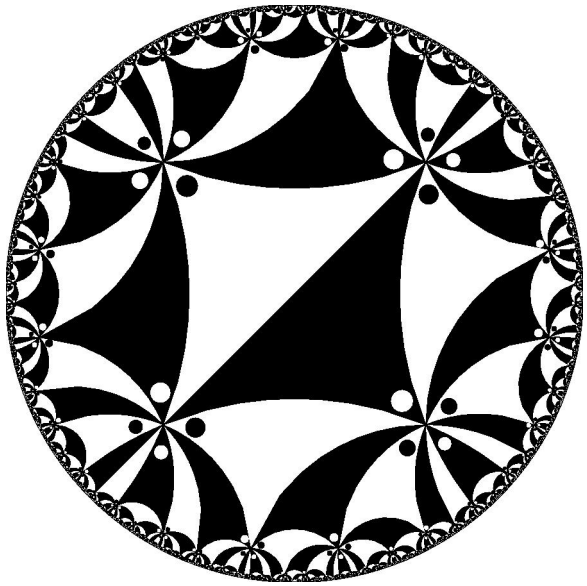

Figure 5: A "translation" Truchet pattern based on the $\{4, 8\}$ tessellation.

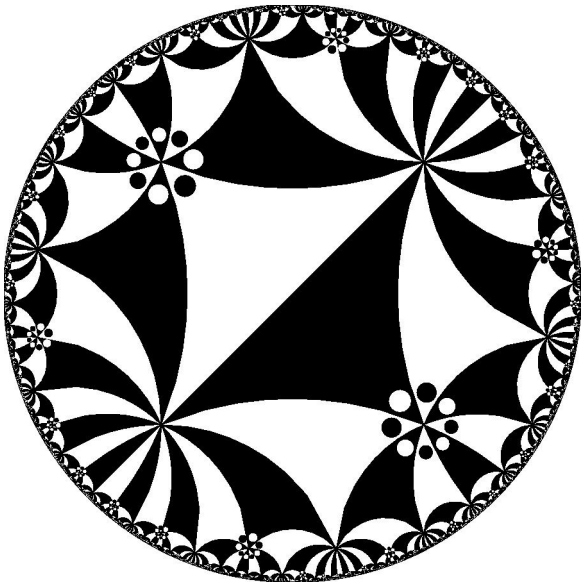

Figure 6: A "rotation" Truchet pattern based on the $\{4, 8\}$ tessellation.

coloring principle, allowing triangles of the same color to share an edge. Figure 7 shows such a pattern, F in Truchet's Plate 1 of his *Memoir* [9], which mixes "translation" and "rotation" edge matchings. Figure 8 shows a hyperbolic version of this pattern based on the $\{4, 6\}$ tessellation, which has large, alternately colored hexagons (since $q = 6$) instead of the squares of pattern F.

5. Truchet Tiles with Multiple Triangles per p-gon

In his *Memoir*, Truchet considered rectangles composed of two basic squares (each divided into a black and white triangle). Each square could be given one of four orientations, and the second square could be placed adjacent to each of the four edges of the first square, giving 64 different rectangles. However, many pairs of rectangles are equivalent by rotation, yielding 10 inequivalent rectangles — shown in Truchet's Table 1 [9]. There are only six inequivalent rectangles if reflections are allowed, but Truchet did not consider them. Truchet constructed 24 patterns from his rectangles, six on each of Plates 1, 2, 3, and 4 of his *Memoir*. He labeled those patterns with the letters A through Z and &, omitting J, K, and W (we have seen A, D, and F above).

Though it is natural to tile the Euclidean plane by rectangles, it is more difficult to tile the hyperbolic plane by "rectangles" — quadrilaterals with congruent opposite sides. Instead, we divide the p-gons of a

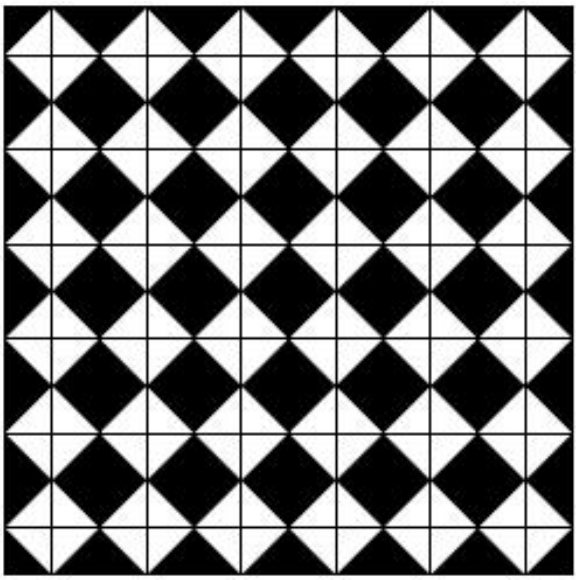

Figure 7: Truchet's pattern F, which does not adhere to the map-coloring principle.

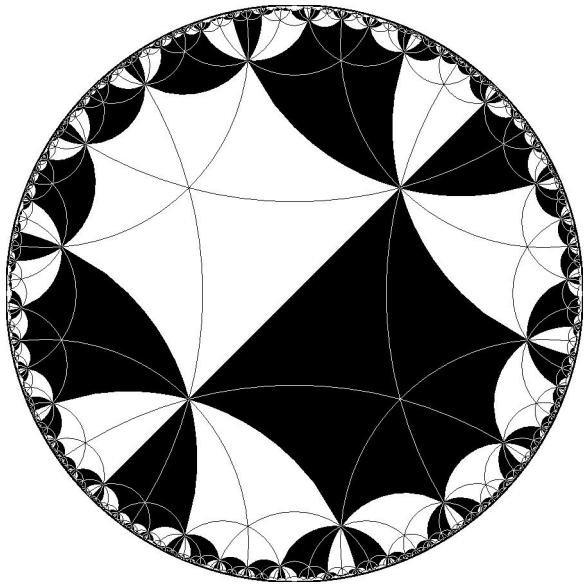

Figure 8: A hyperbolic Truchet pattern corresponding to Truchet's pattern F.

$\{p, q\}$ divided into black and white $\frac{\pi}{p}$ - $\frac{\pi}{q}$ - $\frac{\pi}{2}$ *basic triangles* by radii and apothems, since p-gons easily tile the hyperbolic plane. To satisfy the map-coloring principle, the basic triangles in the p-gon should alternate black and white, and that p-gon should be rotated about the midpoints of the edges to extend the pattern. There are two such patterns for any p and q, one obtained from the other by interchanging black and white. Figure 9 shows such a pattern based on the $\{4, 6\}$ tessellation — probably a better hyperbolic analog to Truchet's pattern A of Plate 1 than Figure 5 above.

If we do not require the pattern to be map-colored, there are many more possibilities. There are $N_2(2p)$ possible ways to fill a p-gon with black and white basic triangles, where $N_k(n)$ is the number of different n-bead necklaces that can be made using beads of k colors, and is given by [12]:

$$N_k(n) = \frac{1}{n} \sum_{d|n} \varphi(d) k^{n/k}$$

where $\varphi(d)$ is Euler's totient function (which gives the number of positive integers less than or equal to d and relatively prime to it). This can be seen as follows: we consider the perimeter of the p-gon to be the necklace, and the two basic triangles adjacent to each edge as "beads" ($2p$ beads total) of one of two colors. If we consider our "necklaces" to be equivalent by reflection across a diameter or apothem of the p-gon, there are fewer possibilities, given by $B_k(n)$ the number of n-bead "bracelets" made with k colors of beads [12]. It seems to be a difficult problem to enumerate all the ways such a p-gon pattern of triangles could be extended across each of its edges, though an upper bound would be $(2p)^p N_2(2p)$.

Figure 10 shows a $\{4, 6\}$ pattern with pairs of black and white triangles adjacent across apothems, analogous to Truchet's pattern E of Plate 1. Figure 11, also based on $\{4, 6\}$, uses the same triangles within the 4-gon as Figure 10, but extended differently across the 4-gon edges. Like Figure 8, it is analogous to Truchet's Pattern F of Plate 1.

Finally, we show patterns based on p-gons with $p \neq 4$. Figure 12 shows a tiling generated by alternating pairs of black and white basic triangles within a 6-gon. white triangles; it is analogous to Truchet's pattern N on Plate 2. Figure 13 shows a tiling generated by a symmetric arrangement of basic triangles within a 5-gon. These two patterns are not related to any patterns in Truchet's *Memoir*.

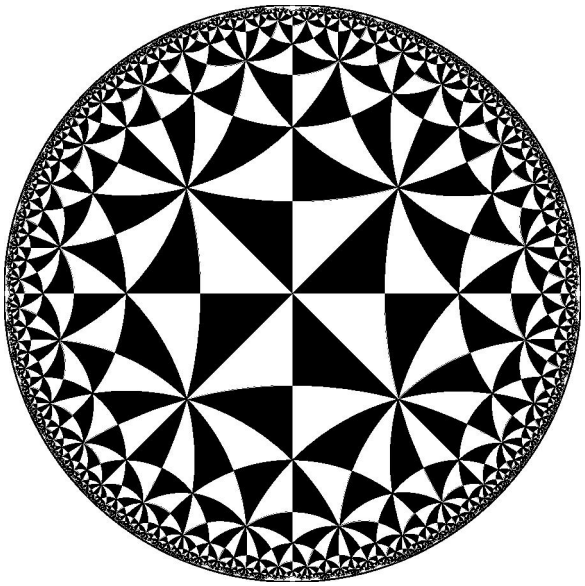

Figure 9: A pattern generated by alternate black and white triangles in a 4-gon.

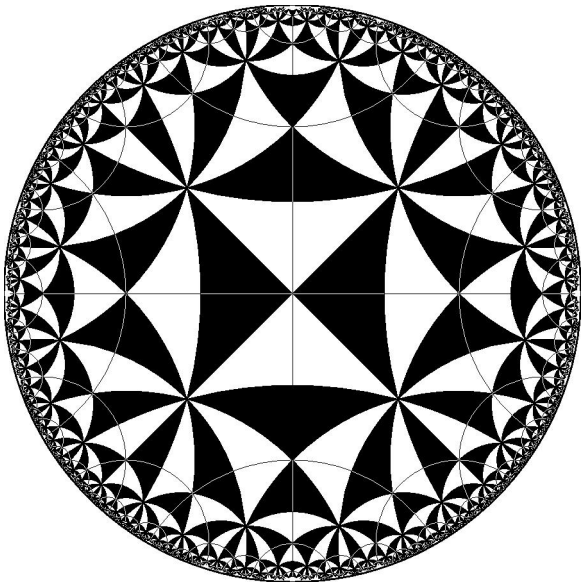

Figure 10: A pattern generated by paired black and white triangles in a 4-gon.

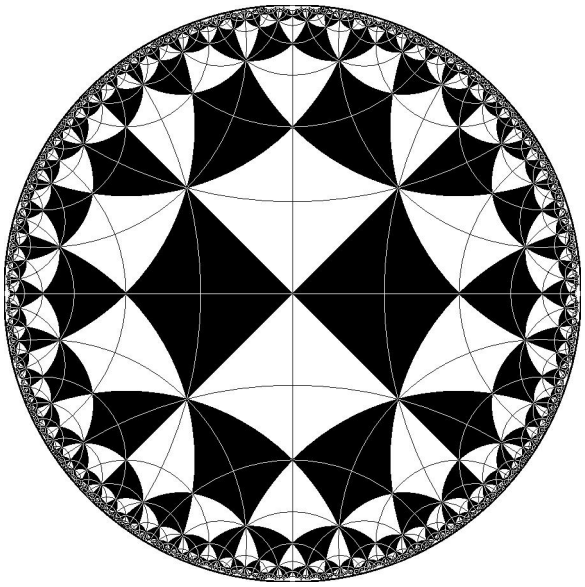

Figure 11: Another pattern generated by paired black and white triangles in a 4-gon.

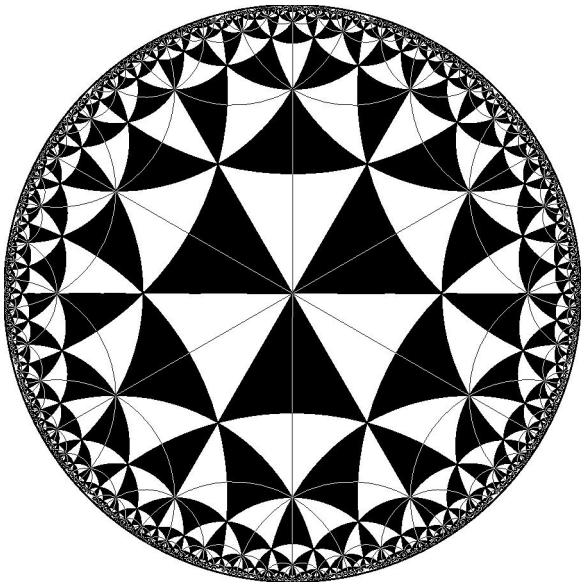

Figure 12: A simple $\{6, 4\}$ pattern.

6. Patterns with Other Motifs

Other designers have used motifs other than the triangularly divided square to make their Truchet-like patterns. One choice, first described by Smith is a motif consisting of two quarter arcs of circles with each arc connecting the midpoints of two adjacent edges of the square [9]. Such patterns can be regular, random, or even carefully arranged so as to spell words [5]. Figure 14 shows a hyperbolic pattern based on two-arcs motif (superimposed on the underlying $\{4, 6\}$ tessellation).

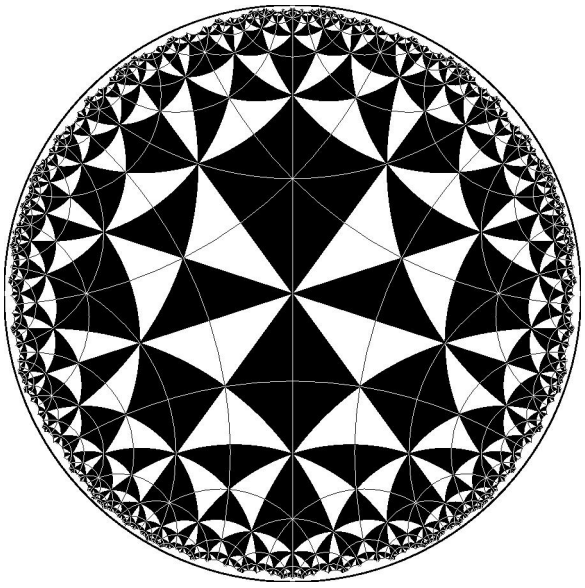

Figure 13: A new $\{5, 4\}$ Truchet-like tiling.

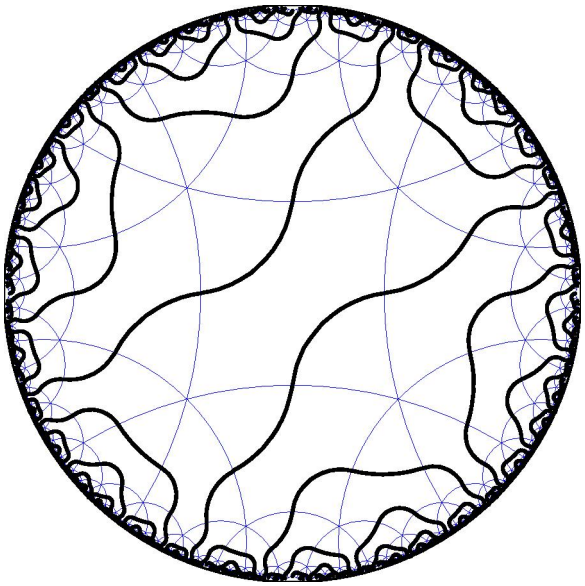

Figure 14: A hyperbolic Truchet arc pattern on a $\{4, 6\}$ grid.

One can generalize the "arcs" motif to $2n$-gons: there would be n non-intersecting arcs connecting the midpoints of the edges of the $2n$-gon. The number of possible $2n$-gon tiles is the same as the number of ways to connect $2n$ points on a circle with non-intersecting chords. It is the Catalan number $C(n) = 2n!/[n!(n + 1)!]$ as noted for Sloane's sequence A000108 [4]. As is the case with the triangle-decorated p-gons, the number of possible patterns is bounded above by $(2n)^{2n}C(n)$, though it seems difficult to get an exact enumeration.

7. Future Work

We have shown some Truchet patterns in the hyperbolic plane based on the regular $\{p, q\}$ tessellations. We have also noted some combinatorial results on the number of possible tiles for "square", triangle-decorated p-gon, and arc Truchet patterns. But there are other questions that remain to be answered about the the possible number of patterns that can be formed in a regular way from such tiles. These questions seem to be difficult.

Since some Truchet patterns have black-white color symmetry, it would also seem natural to investigate the coloring of Truchet tilings with more than two colors. Another direction of future research would be to create Truchet patterns on hyperbolic Archimedean tessellations.

Acknowledgments

I would like to thank David Reimann for his inspiration and useful discussions. I would also like to thank Lisa Fitzpatrick, director, and the staff of the Visualization and Digital Imaging Lab at the University of Minnesota Duluth.

References

[1] Cameron Browne, Duotone Truchet-like tilings, *Journal of Mathematics and the Arts*, 2: pp. 189–196, 2008.

[2] The Wikipedia page on Pierre Simon Fournier:
`http://en.wikipedia.org/wiki/Pierre_Simon_Fournier`

[3] R.A. Lord and S. Ranganathan, Truchet tilings and their generalisations, *Resonance*, Vol. 11, No. 6, pp. 42–50, 2006.

[4] The On-Line Encyclopedia of Integer Sequences, Sequence A000108 (Catalan Numbers)
`http://oeis.org/A000108`

[5] David Reimann, Text from Truchet Tiles, *Bridges 2009 Conference Proceedings,* pp. 325–326, 2009.

[6] David Reimann, Patterns from Archimedean Tilings Using Generalized Truchet Tiles Decorated with Simple Bézier Curves, *Bridges 2010 Conference Proceedings,* pp. 427–430, 2010.

[7] Sleeves Rhode patterns at: `http://xahlee.org/math/Truchet_tiles.html`

[8] D. Schattschneider, *M.C. Escher: Visions of Symmetry,* 2nd Ed., Harry N. Abrams, Inc., New York, 2004. ISBN 0-8109-4308-5

[9] Cyril Stanley Smith, The tiling patterns of Sebastien Truchet and the topology of structural hierarchy, *Leonardo*, 20(4): 373–385, 1987.

[10] Sébastien Truchet, Mémoire sur les combinaisons, *Memoires de l'Academie Royale des Sciences,* pp. 363–372, 1704.

[11] S. Truchet, Wikipedia page: `http://en.wikipedia.org/wiki/Sebastien_Truchet`

[12] Wikipedia page on counting necklaces:
`http://en.wikipedia.org/wiki/Necklace_%28combinatorics%29`

Studio Gang Architects: Lincoln Park Pavilion

Nat Friedman
nat.isama77@gmail.com

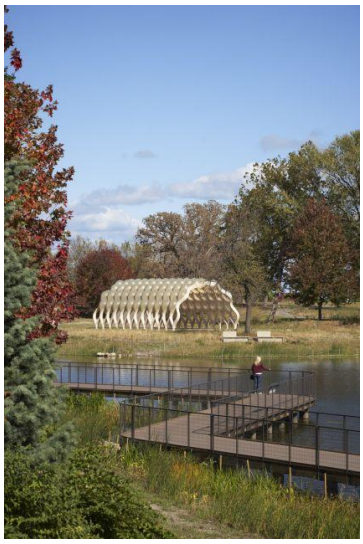

Figure 1. Studio Gang Architects, Lincoln Park Pavilion, 2010, Property of Lincoln Park Zoo, Chicago, Il. Image Steve Hall © Hedrich Blessing.
Figure 2. Interior view of Lincoln Park Pavilion. Image © Studio Gang Architects.

The Lincoln Park Pavilion, designed by the Chicago firm Studio Gang Architects, is shown in Figures 1 and 2 and is a striking example of architecture as sculpture. The Pavilion is part of a larger project that transforms an urban pond from the 19th century into a contemporary natural environment that includes a boardwalk as shown in Figure 1, with the Pavilion serving as an outdoor classroom, as shown in Figure 2.

Figure 3. Form, Space, and Light. Image Steve Hall © Hedrich Blessing.

Figure 4. Nested Fiberglass domes. Image © Studio Gang Architects.

The pavilion form is a classic arch enclosing an open-ended rectangular space. The enclosure is an elegant three dimensional tessellation consisting of curved oval windows, formed by joining prefabricated wooden wave forms. The wave forms remind one of nearby Lake Michigan. The tessellated windows are covered with fiberglass domes, except for the lowest windows which are left open. The interaction with sunlight is a beautiful example of sculptural architecture as form, space, and light, as shown in Figure 3.

Figure 5. Night view with pond. Image © Spirit of Space.

Figure 6. Night view with indoor lighting. Image Steve Hall © Hedrich Blessing.

Figure 7. Night view, detail. Image © Spirit of Space.

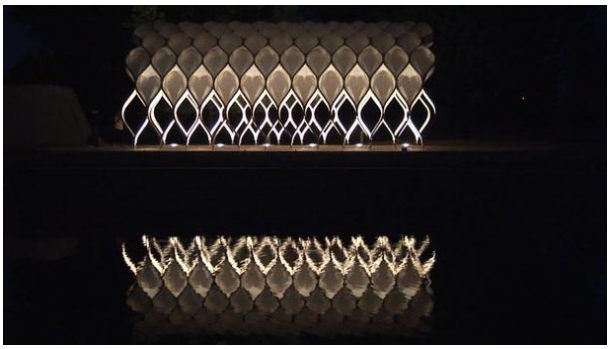

Figure 8. Night view with pond reflection. Image © Spirit of Space.

The fiberglass domes nest nicely to form a three-dimensional tessellation, as shown in Figure 4. The night views are especially striking, as shown in Figures 5-8.

The night views in Figures 7 and 8 remind one of Islamic art, as a result of the wave form joining. In conclusion, the pavilion is attractive sculptural architecture both day and night.

The photographs are courtesy of Studio Gang Architects. For additional projects, see www.studiogang.net

Linear Knot Sculptures

Nat Friedman
nat.isama77@gmail.com

Abstract

Linear knots (stick knots) consist of a finite number of connected straight line segments (rods). Linear knots are discussed that are constructed by (1) wood dowels connected with plastic tubing, (2) bent wire, and (3) welded steel rods. Sculptures of trefoil knots and figure eight knots are considered.

Trefoil Knots

Linear knots are usually discussed with reference to the minimum number of rods necessary to construct knots. For example, six rods are necessary to construct a trefoil knot. A model of a trefoil knot sculpture made with six rods of welded rebar is shown in Figure 1.

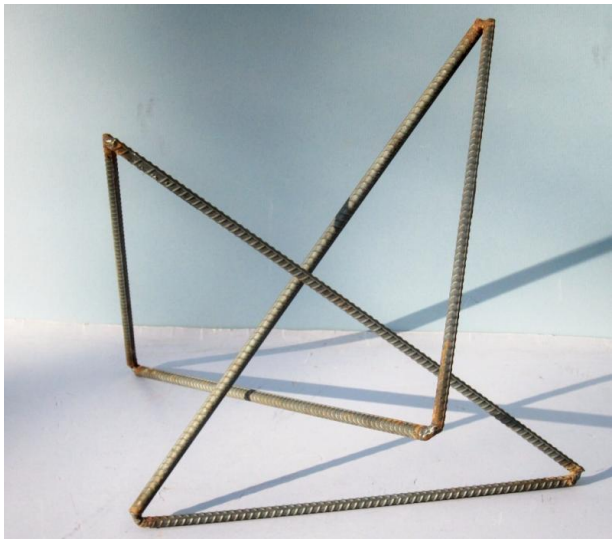

Figure 1.Trefoil Knot, 2011, Rebar steel.

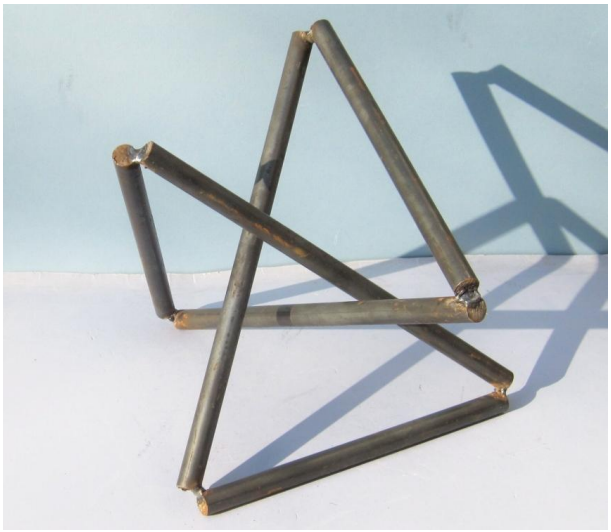

Figure 2. Trefoil knot, 2011, six 18 inch steel rods.

A trefoil knot made with six welded steel rods that are 18 inch long and 1 inch in diameter is shown in Figure 2. The welded ends will be filled in, ground down and rounded in the final version, as well as for other welded steel rod sculptures shown below.

For a trefoil knot, six rods suffice to obtain a fairly open sculpture as seen in Figures 1 and 2. Using more rods, we can obtain more interesting configurations. First we consider the trefoil knot shown in Figure 3 which is made of soapstone hand carved in Africa and can be purchased on Ebay under “knot sculptures”. It is about 7 inches high. This sculpture has an interesting double arch configuration.

Figure 3. Soapstone double arch trefoil knot.

Figure 4. Linear double arch trefoil, 2011, seven steel rods.

A linear version of the double arch trefoil is shown in Figure 4 and is made of seven welded steel rods. Three rods are 18 inches long, which form the corresponding upper arch, here with a horizontal top. The remaining four rods are 13 ½ inches long and form the lower part consisting of two parallel base rods and the two rods forming the lower arch which is an inverted V. The upper arch could be modified by replacing the horizontal rod with two rods as an inverted V.

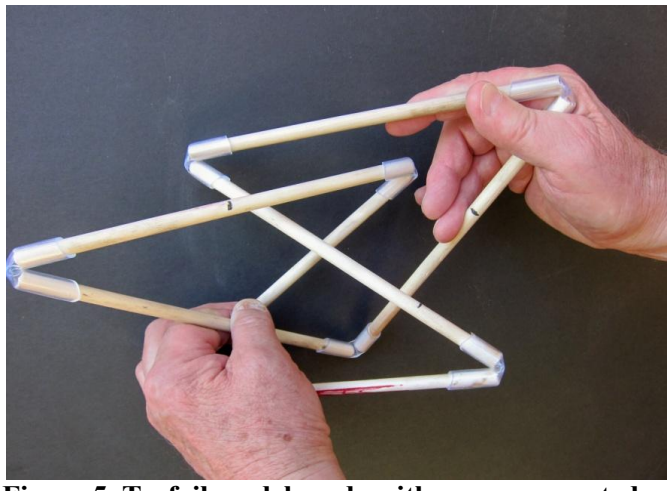

Figure 5. Trefoil model made with seven connected wood dowels.

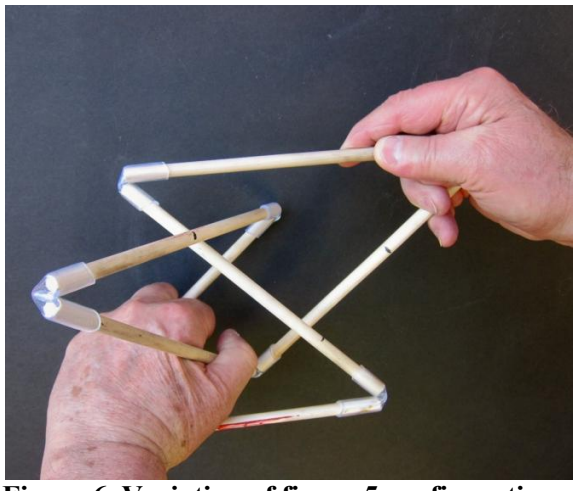

Figure 6. Variation of figure 5 configuration.

Another linear trefoil made with seven wood dowels each eight inches long and connected by plastic tubing is shown in Figure 5. This configuration was discovered by manipulating a trefoil model with seven connected dowels.

The advantage of the dowel model is that it is easy to manipulate it into different configurations. For example, the two horizontal parallel rods in Figure 5 are arranged perpendicularly in Figure 6 to obtain a different configuration.

With dowel models, there are unlimited variations and one simply plays around manipulating the model looking for appealing configurations. In order to go from a dowel configuration to an actual sculpture, it is helpful to first make a sketch or take a photograph. It is also helpful to have someone measure angles off the dowel model while you hold it. The sketch or photo and angle measurements can be used to make a bent wire model, as shown in Figure 7. For example, the dowel model has seven equal length dowels. Thus one can take a straight length of wire and mark points to divide it into seven equal lengths. The wire is bent appropriately at each marked point corresponding to the measured angles. Usually one can wing it and bend the wire by eye so as to get a corresponding wire model. This will involve some final bending adjustments so that the model "looks right" and the two ends meet. A little extra can be left at both ends to bend into a little join as shown in Figure 7.

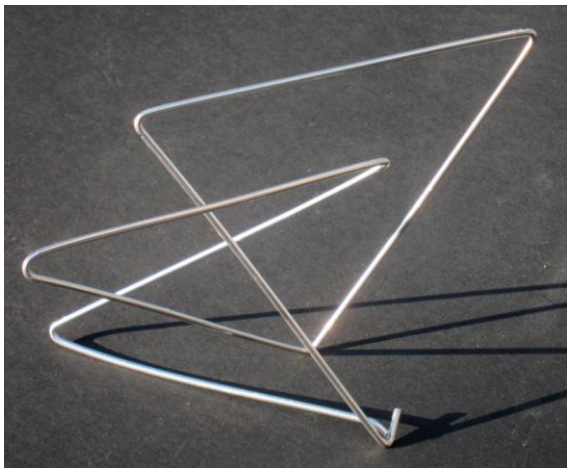

Figure 7. Bent wire trefoil model with seven segments.

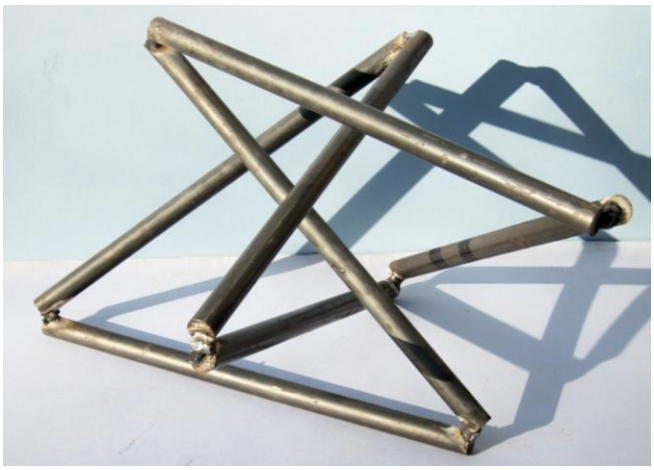

Figure 8. Trefoil knot, 2011, seven 18 inch steel rods.

The advantage of the wire model is that it is permanent and can also be used for angle measurements. Also one can manipulate it if desired and it keeps the new configuration. The wire model can now be used to construct a sculpture using welded steel rods as shown in Figure 8. Here angles are copied when welding rods. This takes some study in choosing the order of the rods to be welded so that the last two rods have a certain amount of freedom to allow them to meet. Note that the sculpture in Figure 8 corresponds to Figure 6 with the horizontal rods perpendicular.

Figure Eight Knots

The minimum number of rods in a linear model of a figure 8 knot is 7. However, configurations with 7 rods are not that sculpturally appealing. It was found that appealing figure 8 sculptures could be made with eight equal length rods. A dowel model is shown in Figure 9. Note that there are four alternating crossings.

The configuration in Figure 9 is quite flat. To obtain a three-dimensional configuration, it was found that the lower left 90 degree corner could be lowered down, and then the knot can be manipulated as shown in Figure 10. Another version of the model is shown in Figure 11. Note that the four alternating crossings can still be seen in Figure 11 but the knot is much more three-dimensional, rather than planar as in Figure 9. A corresponding wire model is shown in Figure 12. Here the ends don't meet, but this may lead to a more desirable so-called open configuration (see below), or suggest lengthening the end rods so they do meet.

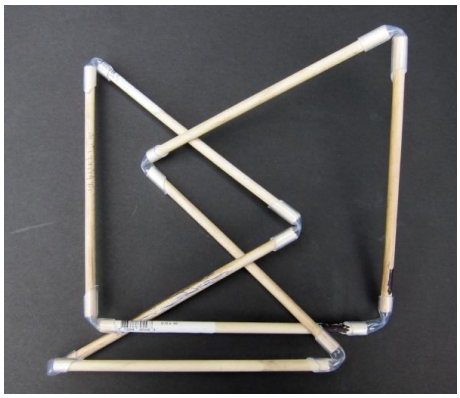

Figure 9. Figure 8 knot with eight dowels each 8 inches long.

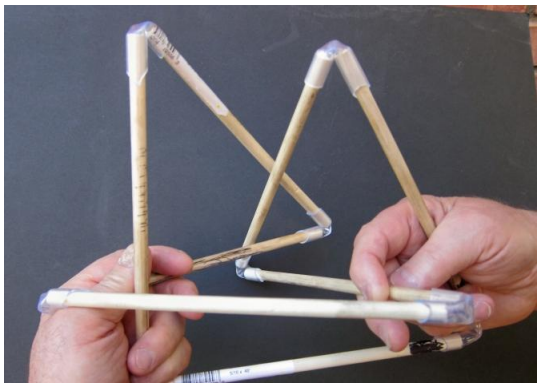

Figure 10. Figure 8 dowel model.

A sculpture corresponding to the wire model is shown in Figure 13. Another position of the same form in Figure 13 is shown in Figure 14. Recall that a *sculpture* is a form in a position and two sculptures consisting of the same form are called *congruent*. Thus the Figure 8 sculptures I and II in Figures 13 and 14 are congruent. Another congruent sculpture is shown in Figure 15.

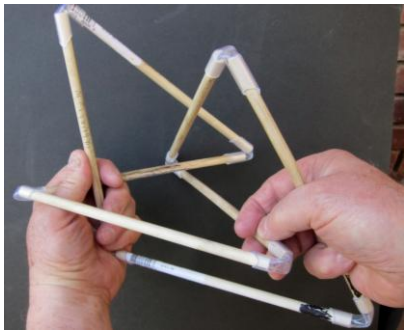

Figure 11. Alternate Figure 8 dowel model.

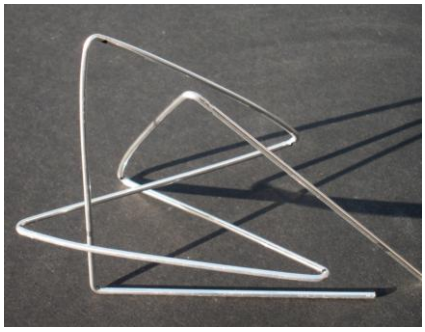

Figure 12. Figure 8 wire model.

Figure 13. Figure 8 I, 2011, eight 18 inch steel rods.

Open Knots

When one ties a knot, the ends are loose and the knot is called an *open* knot. When the ends are joined, the knot is called a *closed* knot. Open knots are not interesting from a mathematical viewpoint because they can all be deformed (manipulated, untied) into the same thing: a loose straight string. Mathematicians only consider a closed knot, which is simply called a knot. The knots we considered above are closed knots.

Figure 14. Figure 8 II, 2011, eight 18 inch steel rods.
Figure 15. Figure 8 III, 2011, eight 18 inch steel rods.

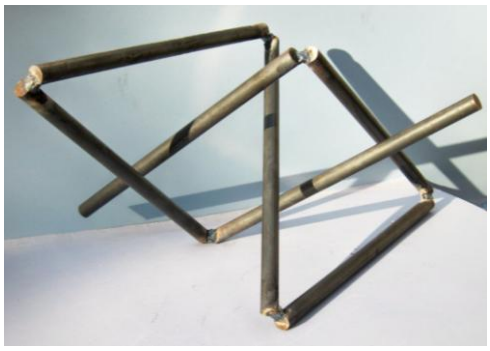

Figure 16. Open Figure 8 knot, 2011, seven 18 inch steel rods.

The main question in knot theory is when can one knot be deformed into another knot? For example, it can be shown that a trefoil knot cannot be deformed into a figure 8 knot. Intuitively, deformation allows bending, stretching, or shrinking, but not cutting and rejoining. There is a precise mathematical definition of allowable deformations. However, open knots are interesting from a sculptural viewpoint. An open figure 8 knot sculpture is shown in Figure 16.

If we consider the picture in Figure 16 as a two-dimensional diagram, the so-called *mirror image* is obtained by reversing under and over crossings. One can see that (a perfectly symmetric version of the) image in Figure 16 can be given a half-turn rotation about the center to obtain the mirror image. For example, the loose end on the left in Figure 16 crosses under and the loose end on the right crosses over. They will exchange places under a half-turn rotation. This is the idea underlying the property that the figure 8 knot can be deformed into its mirror image. Although a trefoil knot has one less crossing, it can be shown that a trefoil knot cannot be deformed into its mirror image.

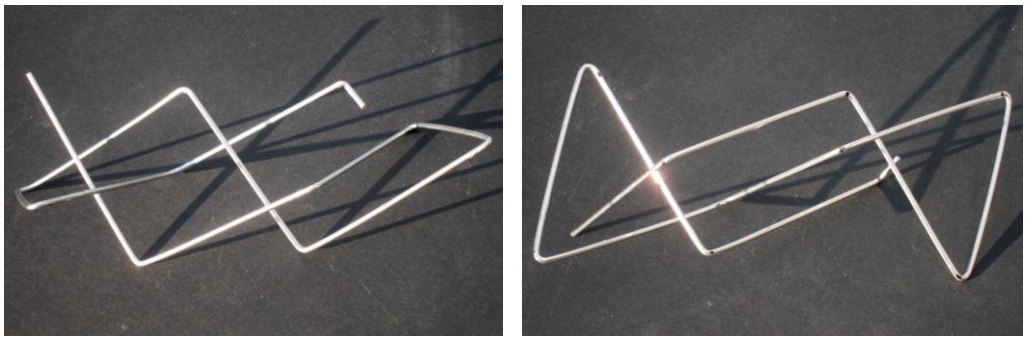

Figure 16. Two views of an open wire model of 6_3.

Another knot that can be deformed into its mirror image is knot 6_3. In a knot table, knots are listed according to the least number of crossings in a diagram of the knot and knot 6_3 is the third knot with six crossings. An open wire model of the knot is shown in two views in Figure 16. The loose right end of the wire model in Figure16 should actually be longer to correspond to the same length as the loose left end. The wire model would then rotate into its mirror image under a half-turn.

There are other knots with more than six crossings that can be deformed into their mirror images. Some of them have open versions, with the same number of crossings as the corresponding closed knot, that also rotate into their mirror images.

Mathematical Art and Surfer

Mehrdad Garousi
Freelance fractal artist
No. 153, Second floor, Block #14
Maskan Apartments, Kashani Ave
Hamadan, Iran
E-mail: mehrdad_fractal@yahoo.com
http://mehrdadart.deviantart.com

Abstract

This paper introduces Surfer, an interesting artistic-mathematical software, and presents examples of the author's contributions to the type of art generated by the software.

Introduction

Nowadays, digital software that results in a visual or audible output can be exploited as a scientific medium for creating art. Digital art incorporates different fields of art and science and, more importantly, makes it possible to exploit the very awesome interaction between pure mathematics and its visual results. Significant landmarks of such phenomena can be seen in the history of evolution of computer -generated art.

One such interesting software is Surfer [1]. Surfer is a program to visualize real algebraic geometry in real-time. The surfaces visualized are given by the zero set of a polynomial equation in 3 variables. Surfer is based on the program Surf and has been developed for the exhibition IMAGINARY [2], organized by the Mathematisches Forschungsinstitut Oberwolfach created for the Year of Mathematics 2008 in Germany [1].

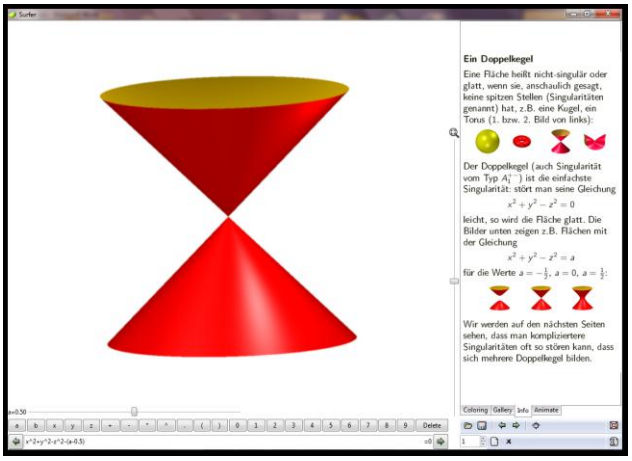

Figure 1*: Surfer interface*

The interface of the software consists of a polynomial bar, a viewer, and some coloring, lighting, and positioning adjusters, as shown in Figure 1 below. The equation bar, at the bottom of the page, contains the polynomial equation that the user would like to have generate its geometric surface, which is shown visually inside the viewer. Numbers and variables x, y and z composing the polynomial could be typed simply through the keyboard or by means of keys cited at the top of the equation bar. Viewer, covering the left half of the page, directly shows visual consequences of an equations changes instantly. Here is the very close interaction between the aesthetic part of the artist's mind or feeling and his mathematical abilities. He can change the equation to obtain more aesthetic and eye catching results. Without such a fast medium of digital computing, a useful interaction would not be possible. And such interaction is what allows the artist to try different possibilities and tame seemingly

untamable rough mathematical shapes. Without this type of interactive chase, significant mathematical aesthetics could not be discovered.

On the right hand side, buttons like coloring, gallery, info, and animate allow one to specify the colors of both sides of the surfaces, displaying galleries of preexisting equations and selecting among them to start new projects, and making an animation by means of provided gadgets.

Other buttons are open, save, back, and forward which make it possible to jump to the back or next polynomial preexisting in the gallery. The full-screen button is also very useful to have a better overall view of the shape and make minor changes.

Some other useful adjustments are cited under the Scene Properties button, which manipulate side colors, background color, illumination, material, position and resolution more professionally and numerically.

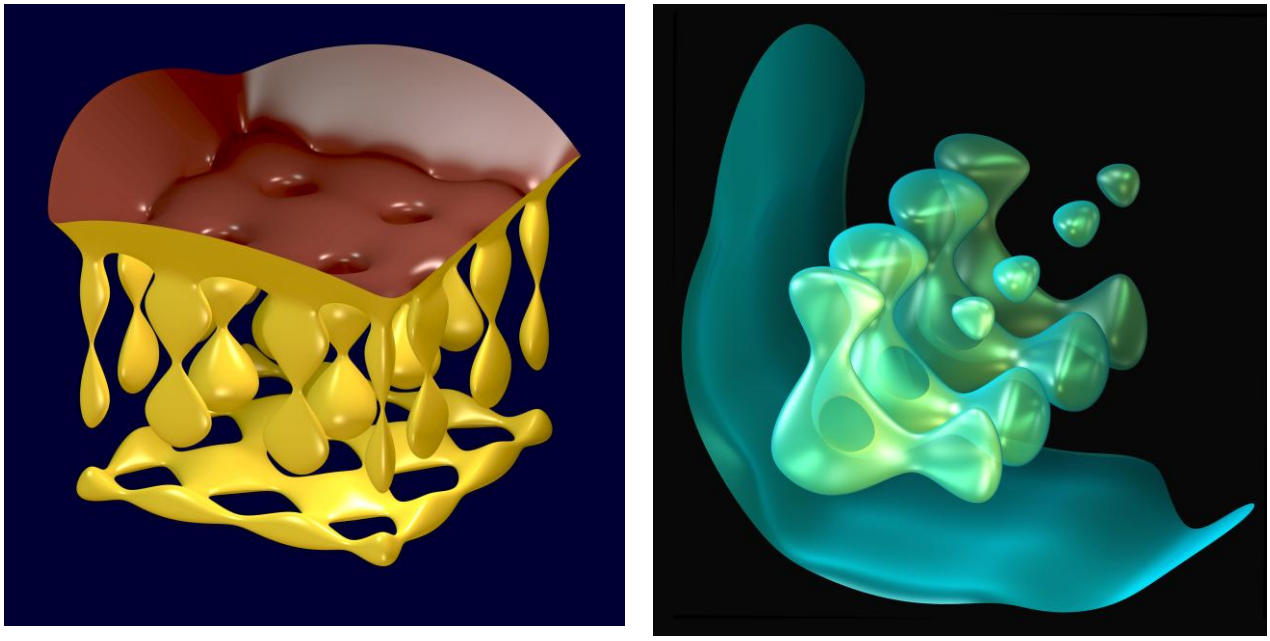

Figure 2: *Melting Chocolate (Acquired the second place at Cambridge Surfer Picture Competition, http://www.imaginary2008.de/cambridge/galerie_view.php?gal=4), (2010; © Mehrdad Garousi). Equation: (a*(-2))/125+x^8+y^8+z^9-2*x^6-2*y^6-2*z^6+1.25*x^4+1.25*y^4+1.25*z^4-0.25*x^2-0.25*y^2-0.20*z^2+0.031=0*

Figure 3*: Buddhist lads at the back seat (Acquired the third place at Zurich SURFER Image Contest, http://www.imaginary-exhibition.com/zuerich/galerie_view.php?gal=6), (2010; © Mehrdad Garousi). Equation: (a*(-5))/125+x^5+y^5+z^8-2*x^8*y^4-2*z^6+1.25*x^4+1.25*y^4+1.25*z^4-0.25*x^2-0.25*y^2-0.25*z^2+0.03125=0*

Working with SURFER is straight forward. One can just insert a polynomial in the three variables x, y and z and obtain a real time visualization of the zero set, which in general is a surface with some singularities and self-intersections. Using the cursor and a scroll bar, the surface can be rotated in every direction and the visible sector can be rescaled [3].

Surfer is very handy and recreational. Both users with profound backgrounds, such as Klaus, S. [3] and Stephan, K. [4], or lesser backgrounds can play around with equations and may attain planned or possibly random results. A significant property of surfer is the mathematical purity that is used in it to create art. It

does not have any additional tools of image processing which could lead the result further than the generative mathematics creating them. Surfer directly discloses visual results of equations with possibilities in manipulating colors and illumination of surfaces or the amount and direction of light sources. You can open the software and start examining visual changes resulting from random or logical changes in different equations that lead to significant works. This software can engage you for days and weeks resulting in mathematical prints for displaying on your walls with typed generative equations under them similar to what creators of the software, Mathematisches Forschungsinstitut Oberwolfach and the Technical University Kaiserslautern, have been doing in several competitions and exhibitions in several countries.

IMAGINARY has been shown more than 30 times in Germany, Austria, Ukraine, England, Switzerland and the US [5].

Here, I am presenting a number of my own works created entirely by Surfer. Keep in mind that opening my equations on your own might not have the same result in your viewer. Such differences are because of zoom, color and/or position issues which are not contained in the equations. They are only included inside the file which is saved via the software save button.

Surfer can be downloaded at http://www.imaginary-exhibition.com/surfer.php . More news about IMAGINARY exhibitions or competitions can be found at http://www.imaginary-exhibition.com/news.php .

Figures 2-13 show examples of the author's works.

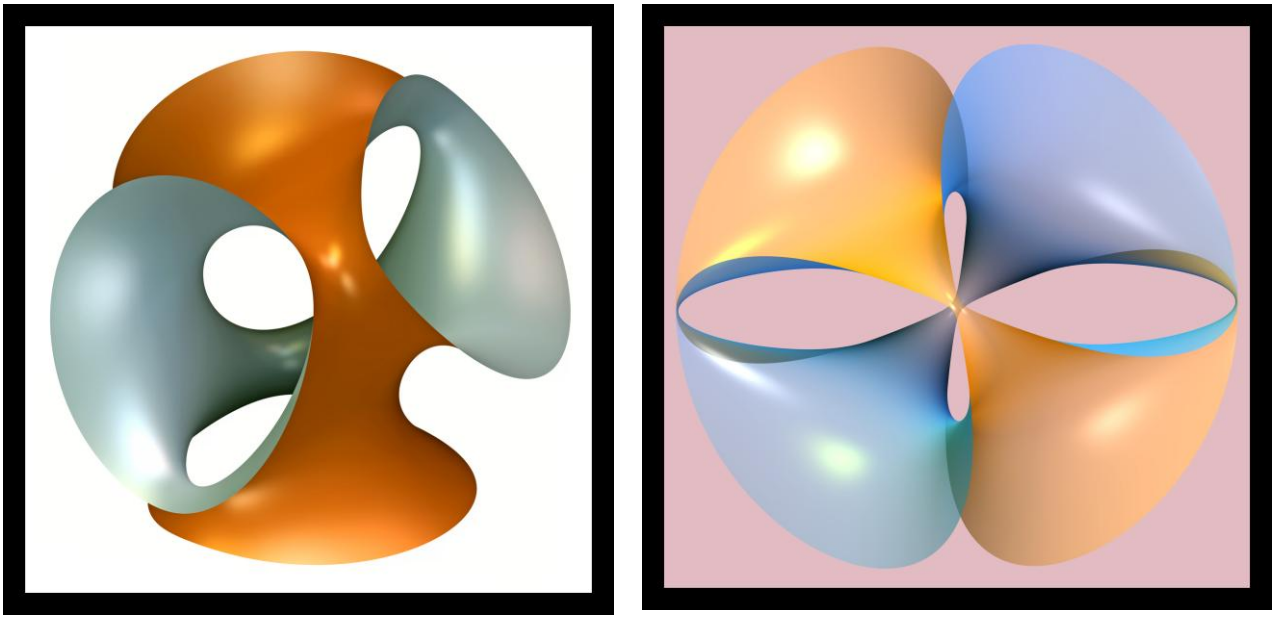

Figure 4: *Standing Mathematical Sculpture (Acquired the second place at Paris Surfer Competition, http://images.math.cnrs.fr/Resultats-de-la-competition-d.html), (2010; © Mehrdad Garousi). Equation: (x^2+y^2+z^2-(0.5+2*a)^2)^2-(3.0*((0.5+2*a)^2)-1.0)/(3.0-((0.5+2*a)^2))*(1-z-sqrt(3)*x)*(1-z+sqrt(3)*x)*(1+z+sqrt(3)*y)*(1+z-sqrt(3)*y)=0*

Figure 5*: Clover, (2010; © Mehrdad Garousi). Equation: (x^2+y^2+z^2-(0.5+2*a)^2)^2-(3.0*((0.5+2*a)^2)-1.0)/(3.0-((0.5+2*a)^2))*(1-z-sqrt(3)*x)*(1-z+sqrt(3)*x)*(1+z+sqrt(3)*y)*(1+z-sqrt(3)*y)=0*

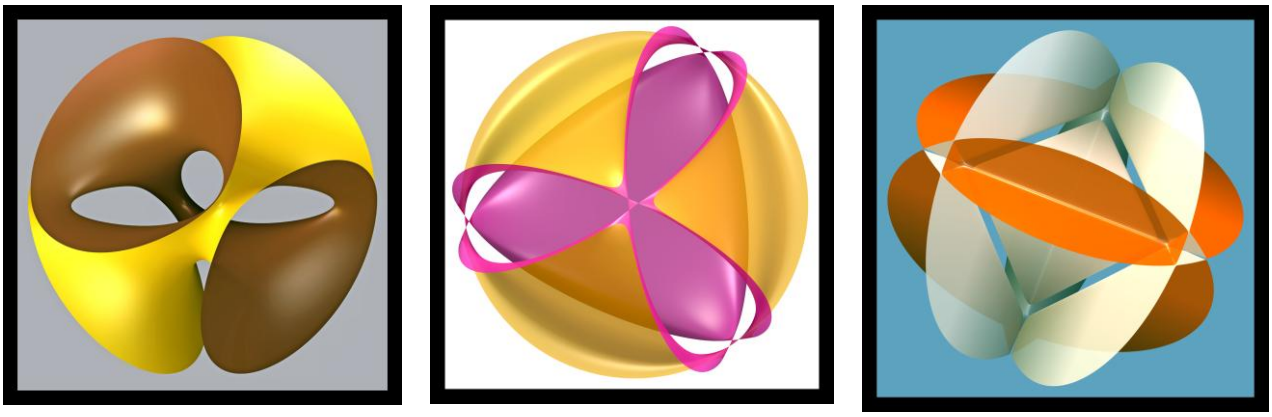

Figure 6: *3D Symmetric Sculpture, (2010; © Mehrdad Garousi). Equation: (x^2+y^2+z^2-(0.5+2*a)^2)^2-(3.0*((0.5+2*a)^2)-1.0)/(3.0-((0.5+2*a)^2))*(1-z-sqrt(3)*x)*(1-z+sqrt(3)*x)*(1+z+sqrt(3)*y)*(1+z-sqrt(3)*y)=0*

Figure 7: *Atom, (2010; © Mehrdad Garousi). Equation: (x^2+y^2+z^2-(.8+.3*a)^.8)^2-(1.5*((0.9+a+b+c)^2)-1.3)/(2.0-((0.5+2*a)^2))*(.5-z-sqrt(2)*x)*(.5-z+sqrt(2)*x)*(.5+z+sqrt(2)*y)*(.5+z-sqrt(2)*y)=0*

Figure 8: *Floating Cube, (2010; © Mehrdad Garousi). Equation: (x^2+y^2+z^2-(0.5+2*a)^2)^2-(3.0*((0.5+2)^2)-1.0)/(3.0-((0.5+2*a)^2))*(1-z-sqrt(3)*x)*(1-z+sqrt(3)*x)*(1+z+sqrt(3)*y)*(1+z-sqrt(3)*y)=0*

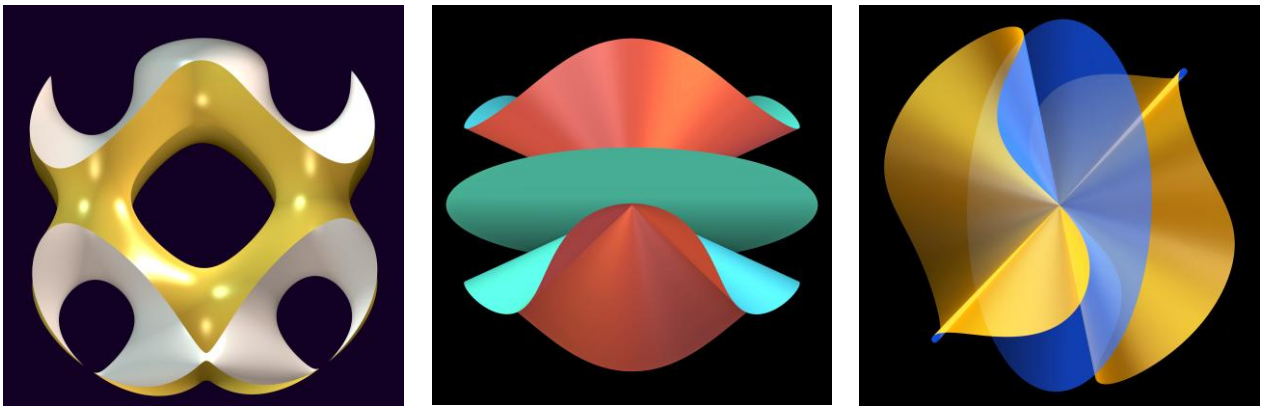

Figure 9: *The Sacred Bowl, (2010; © Mehrdad Garousi).Equation: (a*(-2))/125+x^8+y^8+z^9-2*x^6-2*y^6-2*z^6+1.25*x^4+1.25*y^4+1.25*z^4-0.25*x^2-0.25*y^2-0.25*z^2+0.031=0*

Figure 8: *Mathematical Cake, (2010; © Mehrdad Garousi).Equation: (y*x^3+x*z^3+z*y^3)*(x+y+z)=0*

Figure 11: *Blue Ellipse, (2010; © Mehrdad Garousi). Equation: (y*x^3+x*z^3+z*y^3)*(x+y+z)=0*

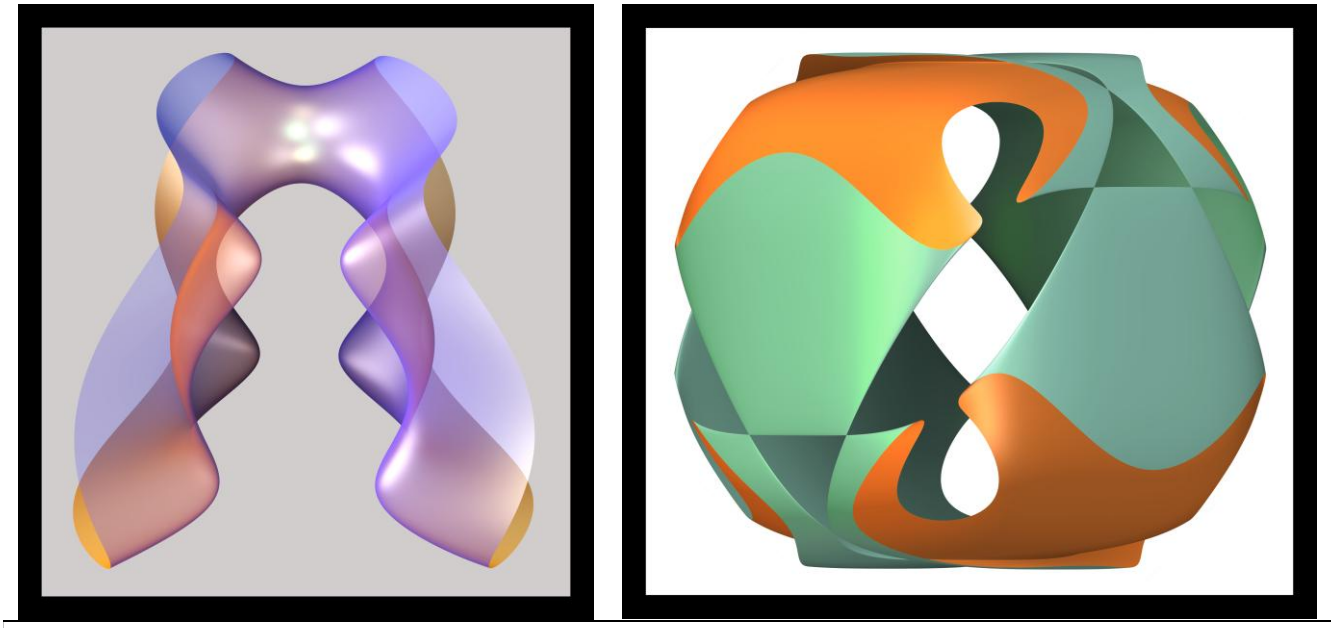

Figure 12*: Color Smoke, (2010; © Mehrdad Garousi). Equation: (a*(-5))/125+x^5+y^5+z^5-2*x^5-2*y^5-2*z^5+1.25*x^5+1.25*y^4+1.25*z^4-0.25*x^2-0.25*y^2-0.25*z^2+0.03125=0*

Figure 9: *Martian Pot, (2010; © Mehrdad Garousi). Equation: (x^4+y^4+z^4-(1.5+a)^.8)^2-(2.0*((0.6+a+b+c)^2)-1.2)/(3.0-((0.5+2*a)^2))*(1-z-sqrt(2)*x)*(1-z+sqrt(2)*x)*(1+z+sqrt(2)*y)*(1+z-sqrt(2)*y)=0*

References

[1] http://www.imaginary-exhibition.com/surfer.php .

[2] http://www.imaginary-exhibition.com/ .

[3] Klaus, S., 2009, Solid Mobius strips as algebraic surfaces, p. 8, available at http://data.imaginary-exhibition.com/IMAGINARY-Moebiusband-Stephan-Klaus.pdf .

[4] Stephan, K., 2010, The solid trefoil knot as an algebraic surface, available at http://data.imaginary-exhibition.com/IMAGINARY-Trefoil-Stephan-Klaus.pdf .

[5] http://www.imaginary-exhibition.com/wannwo.php .

Sierpinski World

Mehrdad Garousi
Freelance fractal artist
No. 153, Second floor, Block #14
Maskan Apartments, Kashani Ave
Hamadan, Iran
E-mail: mehrdad_fractal@yahoo.com
http://mehrdadart.deviantart.com

Abstract

This paper aims to show some amazing aspects of the new mathematical medium of 3D fractal imaging by a step-by-step pictorial representation of a journey in a specific 3D fractal in order to view a number of delightful scenes.

Introduction

Fractal image making has been a very popular medium of art for about four decades, creating terrific images with specific mathematical properties belonging to other fractional dimensions. Fractals result in some of the oddest man-made images in recent decades. However, their revelation was always limited to 2D representations on monitors or papers and screens until a few years ago when there were investigations in order to experience fractals in three dimensions. Now we can have some kind of three dimensional experiences of fractal dimension on our monitors [1]. Despite the flatness of 2D fractals, now we have a solid 3D shape with fractal properties in three directions. Wherever you magnify, you see awesome 3D self-similarities. In 3D fractals you can go inside a fractional dimension with everything three dimensional around you; like the real world. It can be conceived as the most realistic journey inside a world belonging to other dimensions.

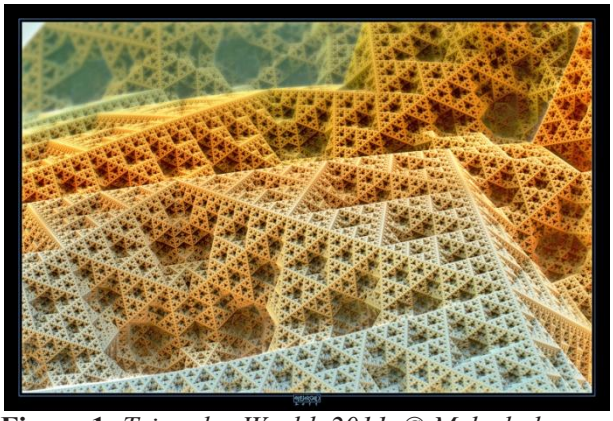

Figure 1: *Triangles World, 2011, © Mehrdad Garousi*.

Previous Work

A large class of fractal geometrical shapes, including the Sierpinski tetrahedron is self-similar. Such shapes can be constructed with an algorithm that exploit the self-similarity property of shapes [4] by repetitively take the union of transformed (e.g. scaled, rotated, translated, mirrored or skewed) copies of an initial shape. An advantage of union operation is that it is possible to ignore it since using disconnected copies will visually give the same results. With such an algorithm, the number of the copies increases exponentially in every iteration. Therefore, after a few iterations a good approximation of final shape can be obtained. Because of its simplicity, this approach is widely used to create fractal shapes. Another important property of this approach is that it is dimension independent, i.e. the same conceptual algorithm can be used both for 2D and 3D shape construction. Moreover, this algorithm is independent of the way the shape is represented, e.g., shape can

be a set of points, an implicit surface, a polygonal surface, or a NURBS surface. Regardless of the type of the initial shape, the same algorithm can be used. One of the problems with these algorithms is that the resulting fractal consists of a large number of disconnected objects. If one wants to construct a physical sculpture, s/he has to take union to obtain a connected surface that can be physically printed.

A particularly useful algorithm based on union of transformed shapes is Iterated Function Systems. Barnsley showed that a set of contractive transformation is sufficient to construct the Fractal shape by randomly applying transformations to a point [4]. Regardless of the initial position, the point will eventually attract the fractal shape and trajectory of the point will draw Fractal. IFS algorithm can also work in any dimension. A popular software xenodream is based on IFS algorithms. The problem with IFS is that the resulting 3D shapes do not describe a volume. There is still a need to convert these shapes into a surface to build a physical sculpture.

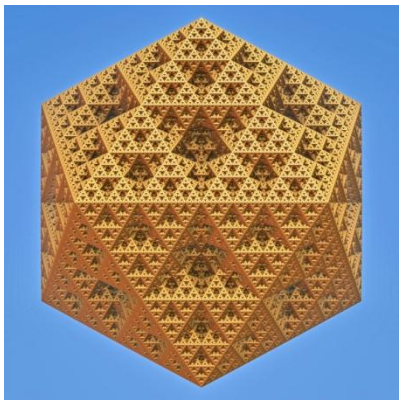

Figure 2: *Magnification of 2.3*

Figure 3: *Magnification of 10*

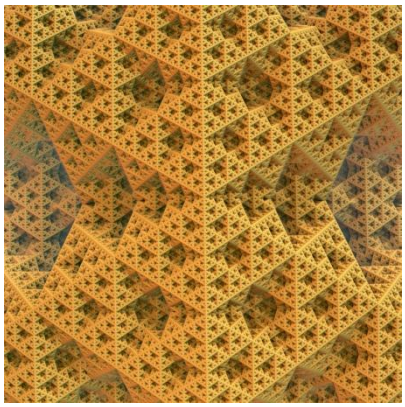

Figure 4: *Magnification of 2.3*

Another problem with these union based algorithms is that they can create only truly self-similar shapes. Regardless of the shape of the initial object, a given algorithm approaches the same target shape. These algorithms do not allow construction of different target shapes from different initial shapes. For instance, it is not possible to construct a Sierpinski octahedron since such a shape cannot be expressed union of its transformed copies.

Fortunately, union based approach is not the only way for constructing fractal shapes. A notable example is one of Mandelbrot's alternative Sierpinski triangle constructions that relies upon `` *cutting out tremas*" as defined by Mandelbrot [6]. Akleman and Srinivasan observed that an attractive property of the Mandelbort□s construction is that it can be generalized using set-difference operation [5]. The initial shape can be a convex polygon and the construction algorithm can simply be as from each convex polygon cut a convex polygon that is created by connecting the midpoints of each edge. If one interprets the ``cut" operation as an ``exclusive-or" operation instead of a set-difference, it is possible to safely apply this construction to even non-convex polygons. However, it is hard to extend this algorithm to three dimensions using set operations.

To construct a generalized Sierpinski polyhedron, we need to take a set-difference (or ex-or) of the initial polyhedron with a polyhedron that is constructed by connecting midpoints of each edge in the original polyhedron. Construction of a polyhedron by connecting the midpoints of each edge of the initial polyhedron can be hard in solid modeling. First of all, set difference is an operation that is hard to obtain

in 3-space. Second, for most cases, the faces may not be triangular and hence may not be planar, which further complicates the set-difference procedure. Akleman and Srinivasan developed a topological graph theory based procedure to obtain exclusive-or with insert-edge operations. Their method also guarantees to obtain a connected and manifold surface. Therefore, resulting shapes can be converted to physical sculptures.

All aforementioned methods are objects based and, therefore, require a large amount of data to represent a reasonably complicated 3D fractal shapes. If our goal is simply to create images of 3D Fractals, then the methods for rendering Julia sets are more suitable. It is not a well-known fact but many Fractal algorithm can be expressed as Julia-like recursive functions [10]. Moreover, Hart developed efficient algorithms to render such deterministic fractals [8 ,11] including computing the surface normal [7] and finding fast intersection with fractal surfaces [9,10]. He also created five Sierpinski Platonic shapes, which he called "the Five Non-Platonic Non-Solids"[12]. In this paper, I investigate closely Sierpinski Icosahedron, one of his creations using *Mandelbulb3D* [2].

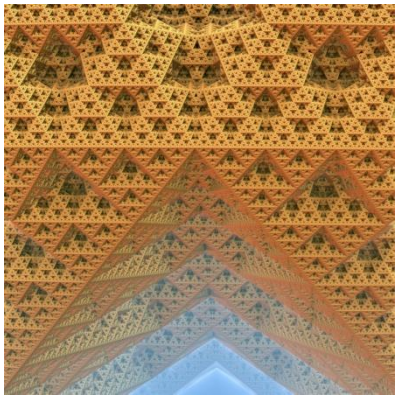

Figure 5: *Magnification of 411*

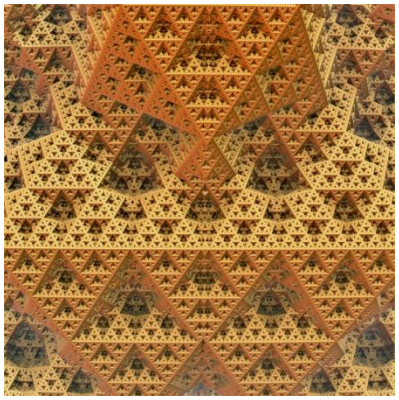

Figure 6: *Magnification of 2.8 x 10^7*

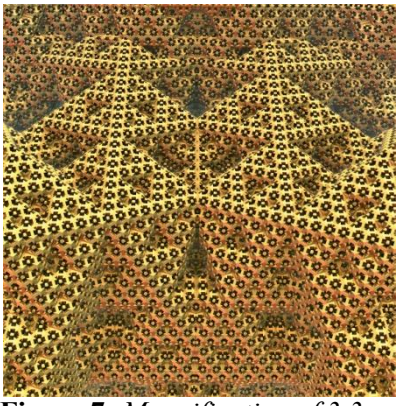

Figure 7: *Magnification of 3.3 x 10^8*

There are a few pieces of software that enable us to feature 3D fractals in our personal computers. One of the very marvelous examples that I usually use is *Mandelbulb3D* [2]. This software uses Hart's method for rendering [11]; therefore it provides excellent 3D lighting and coloring with realistic sense of space.

Examples

The most tempting property of *Mandelbulb3D* software is its awesome 3D navigator that makes it possible to wander quickly and freely without a lot of interruptions. You can walk inside completely bizarre 3D constructions and easily steer wherever you want like a first-person investigation digital game. In such a medium, the role of the artist actually changes and borders between art, esthetics, and artist outstandingly blur. Artists themselves do not know where they are going and what they will encounter at each step. They play a role as adventurers who travel through unknown environments and select certain scenes to shoot and show to others.

In *Mandelbulb3D* everything starts from a few defined fractal formulas depicted as simple 3D shapes at the center of the viewer of the software. By manipulating the defining parameters you can make minor or major changes in the viewer. Then, you can start your journey by successive magnifications and orientations. Though virtually you must be able to magnify unlimitedly, due to some current technical errors, after a large number of zooms shapes start collapsing! We all hope such limitations will be dispelled in the near future so as to be able to travel toward infinity inside 3D fractals, beyond existing confines.

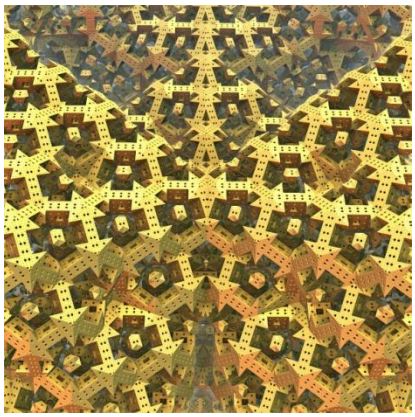

Figure 8: *Magnification of 1.5 x 10^9*

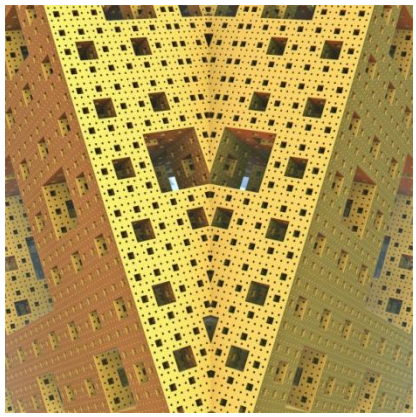

Figure 9: *Magnification of 3.18 x 10^10*

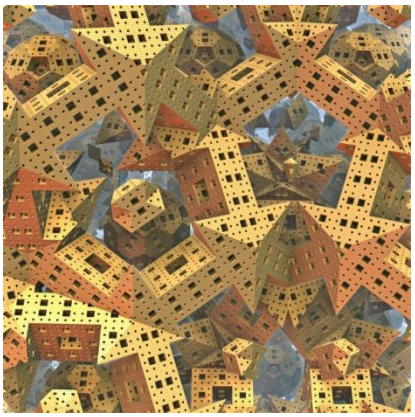

Figure 10: *Magnification of 4 x 10^9*

After specifying the desired formulas, it is possible to mix different formulas and develop hybrid formulas. This way during iterations, you can specify where formulas are carried out and where they stop. This allows one to push aesthetic limitations a little further and results in more diversity in subsequent images.

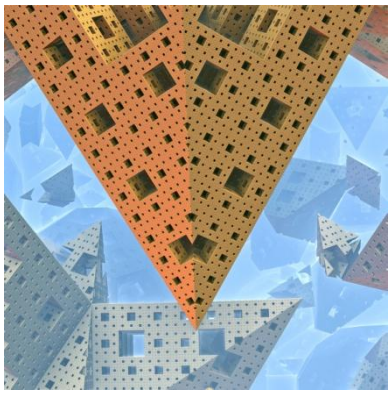

Figure 11: *Magnification of 4.1 x 10^10*

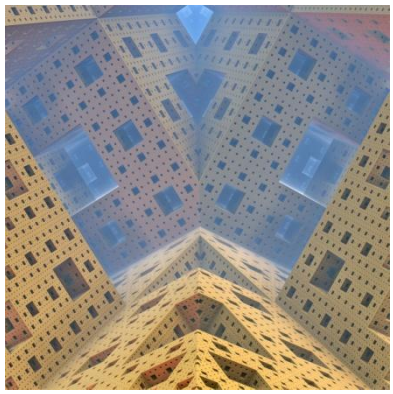

Figure 12: *Magnification of 1.39 x 10^12*

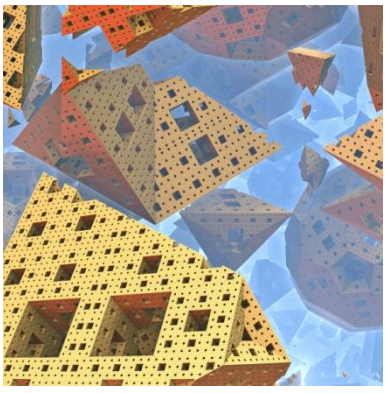

Figure 13: *Magnification of 4.8 x 10^10*

Mandelbulb3D also has another excellent property for animating fractals. It is enough to define key-frames at certain places and the software itself will calculate motions between those keys. In other words, you can have an animation of the journey you are experiencing via the navigator.

In this paper, I am going to present a pictorial report of a trip that I had in a 3D fractal from the nearest shapes to the farthest possible currently. It must be mentioned that in my first trip into this mixture of formulas I concurrently defined key-frames wherever I stopped and the result was an animation which can be watched at http://www.youtube.com/watch?v=P5EkdJRtF-4 .

In the middle of the journey, I do not know why, suddenly I decided to escape from the environment surrounding me and the last one third of the animation displays my effort to find a way out; maybe, somewhere around Figures 9, 10, and 11 that I was stuck around a magnification, going here and there.

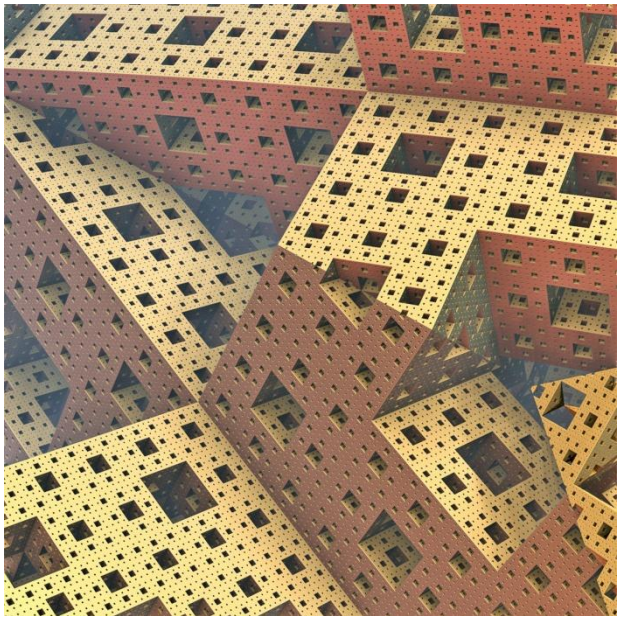

Figure 14: *Magnification of 4 x 10^11*

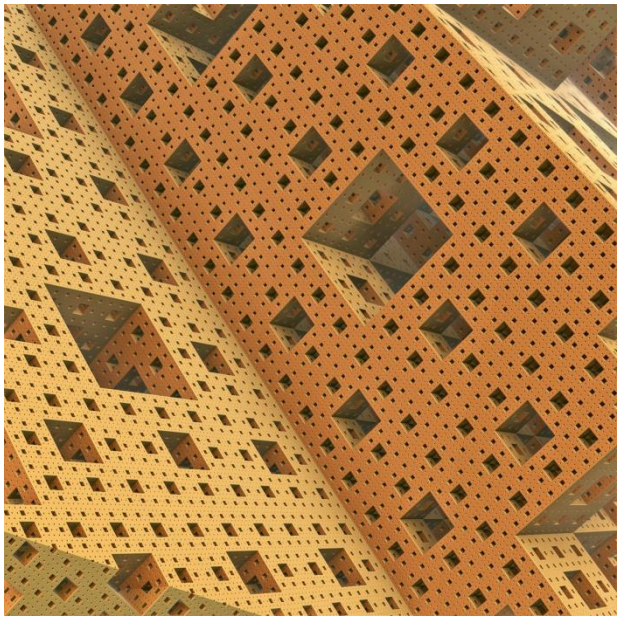

Figure 15: *Magnification of 1.7 x 10^12*

Making this animation, I did not actually know anything about what awaited me ahead and like a real traveler I started from Figure 2 and continued according to whatever was my instant aesthetic desire. It can be thought of as a subconscious trip in fractal space. During my trip I viewed a lot of interesting and eye-catching images, as shown in Figures 2 to 17. Among several scenes, I finally chose the most exciting for me to present as a still work of art, as seen in Figure 1 called *Triangles World*.

Figure 2 displays the icosahedron based on which the fractal is constructed. This fractal is wholly a blend of five different fractal formulas each of which is activated in specific iterations with specific properties. Two well-known examples of them are *IcosahedronIFS* and *Menger3* that cause the first icosahedral shape in Figure 2 and one of the most interesting parts of this journey that takes place at Figure 7. Although it is expected to have the Sierpinski pattern infinitely continuous, suddenly at a magnification of 3.3 x 10^8, a triangular pattern starts vanishing. In Figure 8 it gets clearer that a new squarish 3D pattern is showing up. Figure 9 assures us that we are going to have a Menger Sponge! Yes, a Sierpinski fractal changes to another Sierpinski fractal. This phenomenon is visible when the ending iteration number of the first fractal is executed and the iteration series of the next one starts. From Figure 10 the effects of other remaining formulas can be seen as well in form of the chaos over the arrangement and architecture of

shapes. It must be said it is also possible to have parallel formulas carried out. In the last steps, there has remained no effect of any formula except for the one causing the vivid Menger Sponge pattern in Figures 16 and 17. Finally Figure 17 displays the hatch through which I escaped from the marvelous trip I had. I obliged myself to find a real exit only because I was making an animation parallel and needed to have a good end. Artists looking for satisfying landscapes to shoot can have any kind of endless journey and finish it whenever they find something appealing or they can search, search, and search.

More of my 3D fractals can be found at http://mehrdadart.deviantart.com .

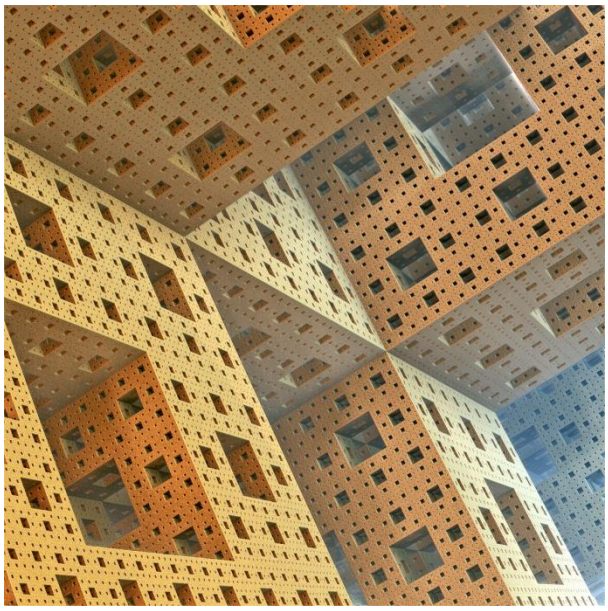

Figure 16: *Magnification of 1.15 x 10^13*

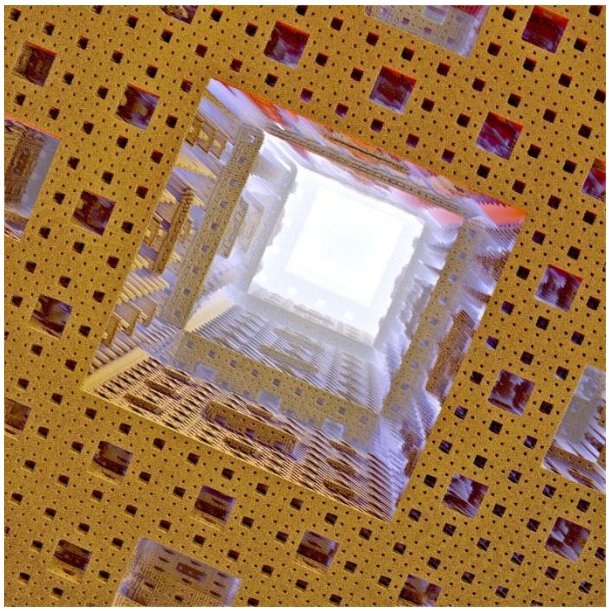

Figure 17: *Magnification of 2.62 x 10^13*

References

[1] J. Aron, The Mandelbulb: First 'True' 3D Image of Famous Fractal (November 2009). Available at http://www.newscientist.com/article/dn18171-the-mandelbulb-first-true-3d-image-of-famousfractal. html.

[2] Mandelbulb3D, http://www.fractalforums.com/index.php?action=downloads .

[3] http://www.xenodream.com/

[4] Barnsley, M. 1988. Fractals Everywhere. Academic Press, Inc. San Diego Ca.

[5] Srinivasan, V., And Akleman, E. 2004. Connected and manifold Sierpinski polyhedra. In Proceedings of Solid Modeling and Applications, 261 266.

[6] Mandelbrot, B. 1980. The Fractal Geometry of Nature. W. H. Freeman and Co., New York.

[7] Wayne O. Cochran, Robert R. Lewis, John C. Hart, The Normal of a Fractal Surface, The Visual Computer 17(4), June 2001, pp. 209-218

[8] John C. Hart, Thomas A. DeFanti, Efficient anti-aliased rendering of 3-D linear fractals, Computer Graphics 25 (3), (Proc. SIGGRAPH 91,) Aug. 1991, pp. 91-100

[9] John C. Hart, Louis H. Kauffman, Daniel J. Sandin, Interactive visualization of quaternion Julia sets, Proc. of Visualization '90, IEEE Computer Society Press, Oct. 1990, pp. 209-218

[10] John C. Hart, Daniel J. Sandin, Louis H. Kauffman, Ray tracing deterministic 3-D fractals, Computer Graphics 23(3), (Proc. SIGGRAPH 89,) July 1989, pp. 289-296

[11] John C. Hart, Computer Display of Linear Fractal Surfaces, Ph.D. Dissertation, EECS Department, University of Illinois at Chicago, 1991.

[12] John C. Hart, The Five Non-Platonic Non-Solids, in Computer Display of Linear Fractal Surfaces, Ph.D. Dissertation, EECS Department, University of Illinois at Chicago, 1991, pp 153-154.

Creative Projects in the Math Classroom

Ann Hanson
Science and Mathematics Department
Columbia College
600 S. Michigan
Chicago, IL 60605, USA
E-mail: ahanson@colum.edu

Abstract

In most math classrooms, the traditional homework assignment is to tell the students to do a certain number of problems. However, in some math classrooms, it may make more sense to give a different type of homework assignment. This assignment asks them to use their creativity to produce a "work of art". This paper will focus on the reasons why to give such an assignment, the grading process and samples of student work.

Introduction

In geometry or liberal arts math classes, having an additional way to assess student learning may be helpful to the instructor. If you assign a creative project, you will learn about the student's other talents, interests and understanding of mathematical concepts. By making this type of assignment, you will have a new way to assess students' understanding [1]. In addition, a poor math student may be able to excel in this area and thereby, give you a better understanding of his/her thinking process and knowledge of the subject matter. Also, this type of assignment forces the students to see mathematics as more than just numbers and formulas. It humanizes the subject and helps the students see that math can contribute to beautiful art. In addition, most students like to do a different type of assignment and one, which challenges their creativity in new ways. The students present their projects to the class and helps everyone to get to know one another.

Incorporating the project into the classroom

At the beginning of the semester include the creative project assignment in your syllabus. As you go over the important points on the syllabus with your class, point out that a new type of assignment will be part of their grade. If you have examples of work from previous students, this is a good time to show those successful projects. About two or three weeks before the project is due, give the students the guidelines about the type of project you want (see below) and the grading criteria (see below). Go over in detail both pieces of information.

Below is the sample criteria from the following class.

Math in Art and Nature, 56-1725
Columbia College
Science and Mathematics Department

The characteristics of the projects and grading criteria are as follows.

1) You should be creative in combining mathematics and art. You may use ideas from class; such as, line designs, tessellations, or develop your own idea related to concepts in the course or mathematical concepts. If you are not sure about your project, talk to me to make sure that your idea does relate to mathematics and to our course.

2) The project should be done with care. The amount of time and effort in creating the project is important. **NEATNESS COUNTS.** However, spending a lot of time on your project, does not guarantee that you will receive an A on your project.

3) The project should be a work of art and be ready to be hung in an art gallery. Framing or mounting your artwork will make it look more professional and look, as though, it is ready to be installed in a gallery.

The students need to have a clear understanding of what is expected of them and how it will be evaluated. In 1995 when I first started using this type of assignments in my Math in Art and Nature class, I was rather prescriptive. I told the students that they had to do a line design, a tessellation, a construction, etc. I got projects that were nice but nothing really creative or unexpected. Since then I have given the students a great deal of latitude in what they can do and I have been amazed. Once I allowed them to do a math/art project that was somehow related to our class, the projects became very interesting and diverse. Many of the students created a project using their major. Some created songs, videos, photographs and one young man made a dress out of silk which combined the Fibonacci numbers with a tessellation. There is one caveat and that is in my m class, we do some math/art creative activities during class. For example, on the day that we talk about the Fibonacci numbers, we also make a Fibonacci plaid. On the day that we discuss triangles and Pythagorean triples, we make an origami triangle box and a mathematical quilt using the Pythagorean triples. If this is not the case in your classroom, then you may want to direct the students to some math/art websites for ideas.

On the day that the projects are due, each student comes up to the front of the classroom and talks about his/her project. Then the class has an opportunity to ask the student questions about his/her work. This semester, for the first time, each student in the class graded each project. The students were given a form to complete for each project and then their results were averaged and included as part of the grade. Although my portion of the grade was the most, allowing the students to contribute to the grade negated any feeling that the teacher just gave good grades to the students that the teacher liked. It made the grading more objective and fair but more time consuming for the grading process.

The form that the students completed for each project is shown below.

Math in Art and Nature
Evaluation of student projects

Classmates name _____
In making your evaluation, keep in mind the following criteria:
Connection to the class
Aesthetic appeal (ie exhibit ready)
Number of points_____ (0 to 10)

Your name_____

The form used by the instructor to grade the projects is next.

Math in Art and Nature

Project Grading Form

Name_____ Major_____

Title of project_____

Explain how your project is related to this class._____

_____

_____

May the instructor use your project in an educational setting?_____
What materials did you use to make your project?_____

_____

_____

Why did you choose this project? How did you feel about creating it?_____

_____

_____

To be completed by the instructor after class presentation of the project

Quality Assess	Max Points	Points Awarded
Effective connection to the course	10	
Qualities of creativity & originality	5	
Overall appearance of the project (is it exhibit ready?)	15	
Quality of classroom presentation	5	
Classmates evaluation	10	
Instructor s comments		
Total	45	

Here are two examples of student projects. The first one is by Ernest Hill and is made out of odd pieces of wood. The perspective that he got is amazing since the size of the wood is not uniform. The second project is by Joseph Koch. He made is a drawing of Pythagoras and supper-imposed on it is a construction of the Lute of Pythagoras.

Having the students do a non-traditional assignment may be somewhat daunting at first. If you structure it and make some suggestions about what constitutes a math/art project, then you will be pleasantly surprised with the talent and creativity in your class.

[1]Papacosta, Pangratios and Hanson, Ann, *Artistic Expressions in Science and mathematics,* Journal of College Science Teaching, vol. XXVII, vol. 4, February 1998.

Apollonian Gaskets

Neil C. Katz
Skidmore, Owings & Merrill LLP
neil.katz@som.com

Abstract

This paper briefly discusses the concept of apollonian gaskets, and demonstrates possible variations of models generated using different initial shapes.

Introduction

An "apollonian gasket" is an iteratively-generated diagram composed of tangent circles [1,2,3,5].

The basic step in the generation process is to identify an area defined by three curves (typically the space enclosed by three mutually-tangent circles, but these curves can be straight lines, or other curves), and create within this space a circle which is tangent to the three edges which define the space[1]. Creating this circle will create three new spaces, in which the process can be repeated – it can occur recursively. We can call the space bounded by three curves, within which we can recursively create these apollonian circles, the "bounded" space.

The recursive iterations can occur for some number of generations, or until a minimum circle size has been reached. (Reaching a target minimum radius may take different numbers of generations in different areas of the diagram.)

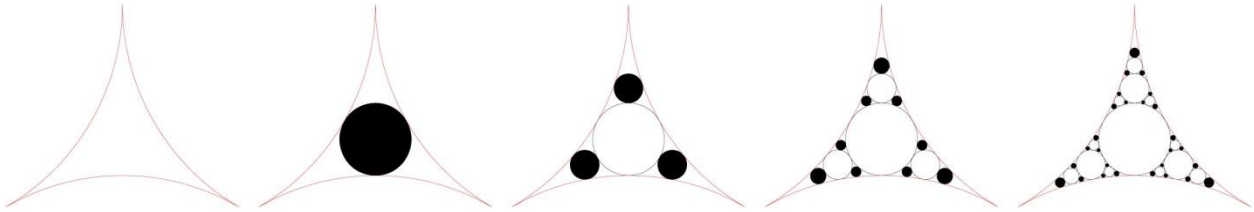

Figure 1. Starting with three mutually-tangent curves, we create a bounded space within which we can generate a set of apollonian circles. The diagram shows how we iteratively generate new circles in newly-created bounded spaces.

In the purest sense, we can begin with a single circle, and two (or more) inscribed circles as the initial figure, creating bounded spaces within which the apollonian gasket can be computed.

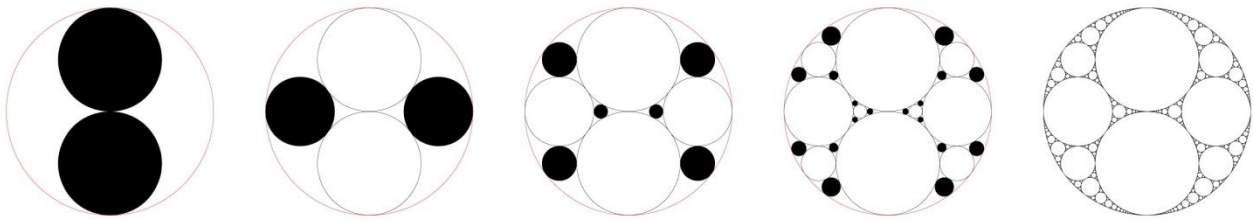

Figure 2. Creating apollonian circles within an initial figure of a circle two equal circles within it.

[1] Many of the examples presented here use straight lines and/or intersecting (not tangent) circles as their initial starting diagrams, and some use two or more-than-three curves (how this is done is explained in the text). Whether these can be considered "true" or "pure" apollonian gaskets is still unclear to the author.

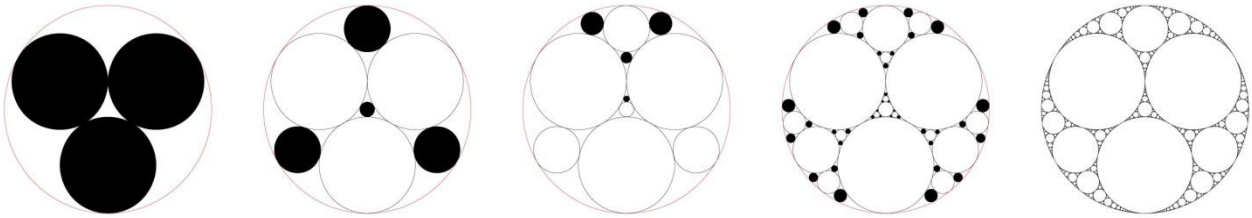

Figure 3. Creating apollonian circles within an initial figure of a circle three equal circles within it.

However, equally interesting results can be generated with different initial figures: polygons within which circles are inscribed, circles and polygons divided with lines and/or circular arcs, and other curves (such as ellipses and splines).

Related Models and Concepts

A Sierpinski triangle (or Sierpinski gasket) is a very close relative of the Apollonian gasket. It is also a recursive process, based on triangles (Sierpinski gasket : apollonian gasket :: triangle : circle). (Variations on this model/process can be explored as well.)

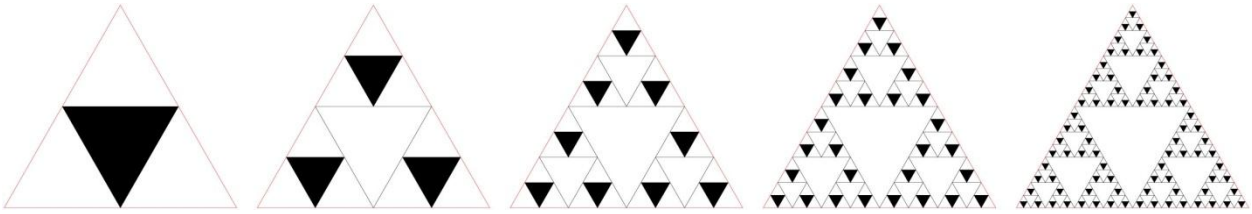

Figure 4. The generation of the the Sierpinski gasket.

The Algorithm

The algorithm used in generating the models in this paper uses (a variation of) the "smallest size" method (instead of the "number of generations" method). I found this method provided more visually-pleasing and graphically consistent results. In generating the models, I established a "critical size" value (using the circle's radius). If a computed circle was larger than this size, I added three new circles in the spaces surrounding the just-generated circle within its bounded space. As I generate the circles, I color-code them according to their size: circles larger than the critical size are green; circles smaller than the critical size are red; if a circle was exactly the critical size it was colored yellow. I could have said "only circles larger than the critical size will exist in the model", in which case there would be only green (and perhaps yellow) circles in the model, but my criteria was for the rule rather than the results, so there are in fact red circles which are sometimes much smaller than this critical value.

I was undecided about what to do about the yellow circles, which, within a roundoff tolerance, were exactly at the critical size. Should I add new circles around these (as if they were green), or should I stop there (as if they were red)? I did something in-between: instead of adding three new circles around these circles, I added just one – the largest of the three.

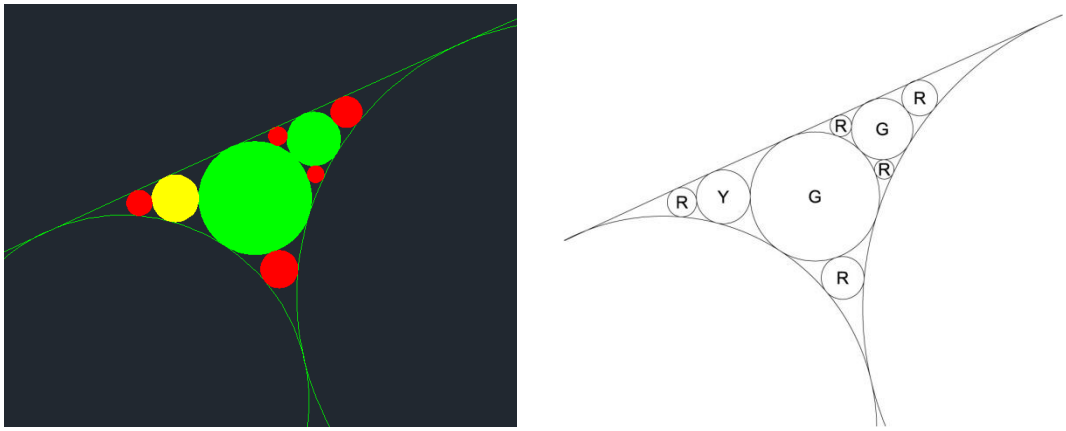

Figure 5. Using color helps determine (and demonstrate) whether to continue running the circle-generating rules in newly-created bounded spaces.

Automating this process is a bit challenging. So far I have been able to automate the generation of apollonian circles within a space bounded by three circles, if none of the circles are inside of the other circles (so they all have "positive" curvature with respect to the bounded space). In other cases, the algorithm was carried out manually, although I created some tools to ease this tedious process a bit, and the color-coding was essential in deciding, after adding a new circle, whether or not to continue creating circles in that same bounded space.

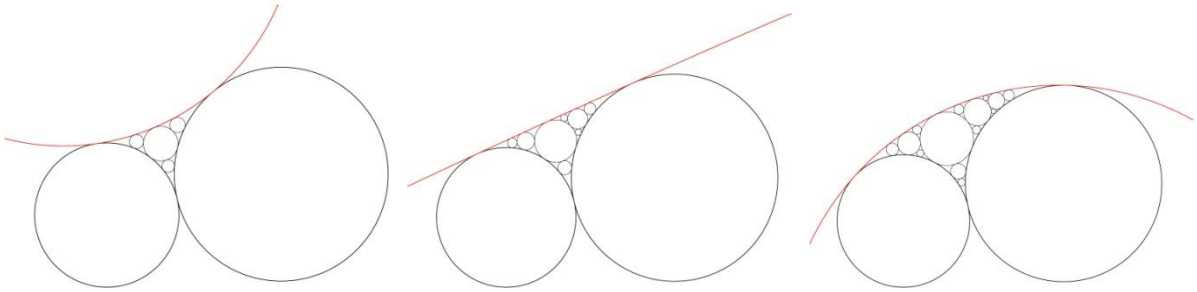

Figure 6. The red curve generates different types of bounded spaces. In the figure on the left, the red curve has "positive" curvature with respect to the bounded area, and is similar to the other curves which bound that same space. In the middle figure, the curve is a straight line, and has "zero" curvature. In the figure on the right, the red curve has negative curvature with respect to the bounded area.

A Couple of Surprises

It is not the intention of this document to be mathematically rigorous. There have been papers written which go into depth on the geometry of the circles[2].

In generating these models, and experimenting with various initial figures and visually and/or geometrically interesting patterns, I came across two very interesting discoveries.

In generating apollonian circles, each new circle typically requires three curves as its generator. Sometimes two or four (or more) curves can be used. If we start with a regular polygon – a square, a

[2] Many of these papers, interestingly, describe the "curvature" of the circles by applying numeric values to the circles, which is the inverse of the radius of the circle (smaller circles have greater curvature and higher numbers; larger circles have smaller curvature; straight lines have a curvature of 0; and if a circle is concave instead of convex (for example, is tangent to two others in such a way that it encompasses both of them) then it has a negative curvature -- there are incredibly interesting (and beautiful) relationships among these numeric values. Since a circle's radius is more comfortable for me to work with as I'm generating and studying these forms, these are the values that I'm using in generating new circles, and comparing them.

pentagon, … (a triangle already has three edges, and will generate apollonian circles in the typical way), we can generate a circle which is tangent to all of the edges, and then normal apollonian circles can be added in the spaces near the vertices of the polygon. If the polygon has greater than three sides and is not regular, it may not work. So if more than three curves are used, there must be symmetry, such that the resulting circle touches each of the generating lines and yields resulting spaces which are bounded by three curves (or are also symmetrical in a similar way).

If two circles intersect, the area shared by the two circles can accommodate another circle within it, which is tangent to the original two. The two circles can be equal (in size) or not, and one of them can in fact be a straight line.

One of the "surprises" was not really a surprise at all. I started with two initial figures to generate two sets of apollonian gaskets: two golden rhombuses, with acute angles of 36 and 72 degrees (the same rhombuses used in Penrose tilings). Since these rhombuses are full of golden relationships, I wondered if the resulting apollonian circles would also have golden relationships. They do (at least the initial generation). I think it would not be surprising if later generations also had similar properties, but I have not found these. Looking at curvature values instead of radius values might make some of these relationships easier to see.

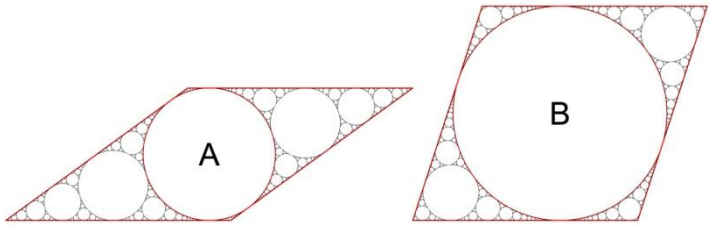

Figure 7. Within initial figures of golden rhombi (rhombus A has an acute angle of 36° and rhombus B has an acute angle of 72°) we generate a set of apollonian circles. The first circle in each of the rhombi creates four new bounded spaces within which the process can continue in the typical way described. The radii of the first circles have a golden relationship (B/A = 1.618…).

The second discovery was shocking. I started with a circle and a chord going through it. We can say that two sets of apollonian gaskets then are generated for each circle - one set on each side of the chord. If the chord is the diameter of the circle, the sets are symmetric and identical. But as the chord moves away from the diameter, each set will be different.
The initial circle which is added between the line and the circle (a case where only two curves (instead of three) are used to generate this "first-generation" circle) has its tangent point at the middle of the part of the line which is contained inside the circle. This is true in both parts of the circle which is divided by the line. Unless the line is the diameter of the circle, these first generation circles will be unequal in size (this seems obvious and intuitive). What was startling to me was that the second-generation circles (which uses the original encompassing circle, the line, and each first-generation circle as its generators) will be identical in size!, regardless of where the line is placed.

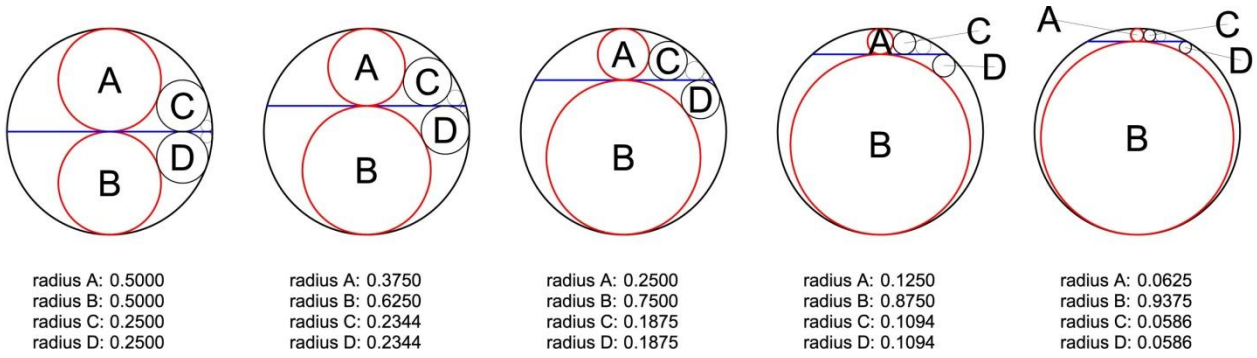

Figure 8. Diagram showing the interesting and surprising relationship of second-generation apollonian circles generated within the two bounded areas of an encompassing circle and a chord. As the chord location varies, the initial circles (A and B) will be different (obviously), but the next generation circles will be equal (not at all obvious).

Extending the Concept to 3D and Higher Dimensions

It has been shown that the concept of apollonian gaskets can be extended from two dimensions (using tangent circles) to three dimensions (using tangent spheres) and surfaces [2,4,6]. We can create three-dimensional analogies to some of the two-dimensional diagrams presented here, using planes where straight lines have been used, and polyhedra where polygons have been used[3]. It seems likely that this can be extended to higher dimensions as well.

References

[1] B. Mandelbrot, 1980. *The Fractal Geometry of Nature*. W. H. Freeman and Co., New York.

[2] J. Kocik, *Clifford Algebras and Euclid's Parametrization of Pythagorean Triples*, in Advances In Applied Clifford Algebras, Volume 17, Number 1, Pages 71-93, 2007.

[3] P. B. Thomas and D. Dhar, *The Hausdorf dimension of the Apollonian packing of circles*, Journal of Physics A: Mathematical and General Volume 27 Number 7, Pages 22-57, 1994.

[4] R. D. Mauldin, M. Urbanski, *Dimension and Measures for a Curvilinear Sierpinski Gasket or Apollonian Packing*, Advances in Mathematics, Volume 136, Issue 1, 1, Pages 26-38, June 1998.

[5] Paul Bourke, *An introduction to the Apollonian fractal*, Computers & Graphics, Volume 30, Issue 1, Pages 134-136, February 2006.

[6] E. Akleman and P. Edmundson. *A Vertex Truncation Subdivision Scheme to Create Intriguing Polyhedra*. In Proceedings of Bridges: Mathematical Connections in Art, Music, and Science, Win?eld, Kansas, August 2004.

[3] This is similar, for example, to extending the Sierpinski triangle to become the Sierpinski tetrahedron or Sierpinski pyramid [1].

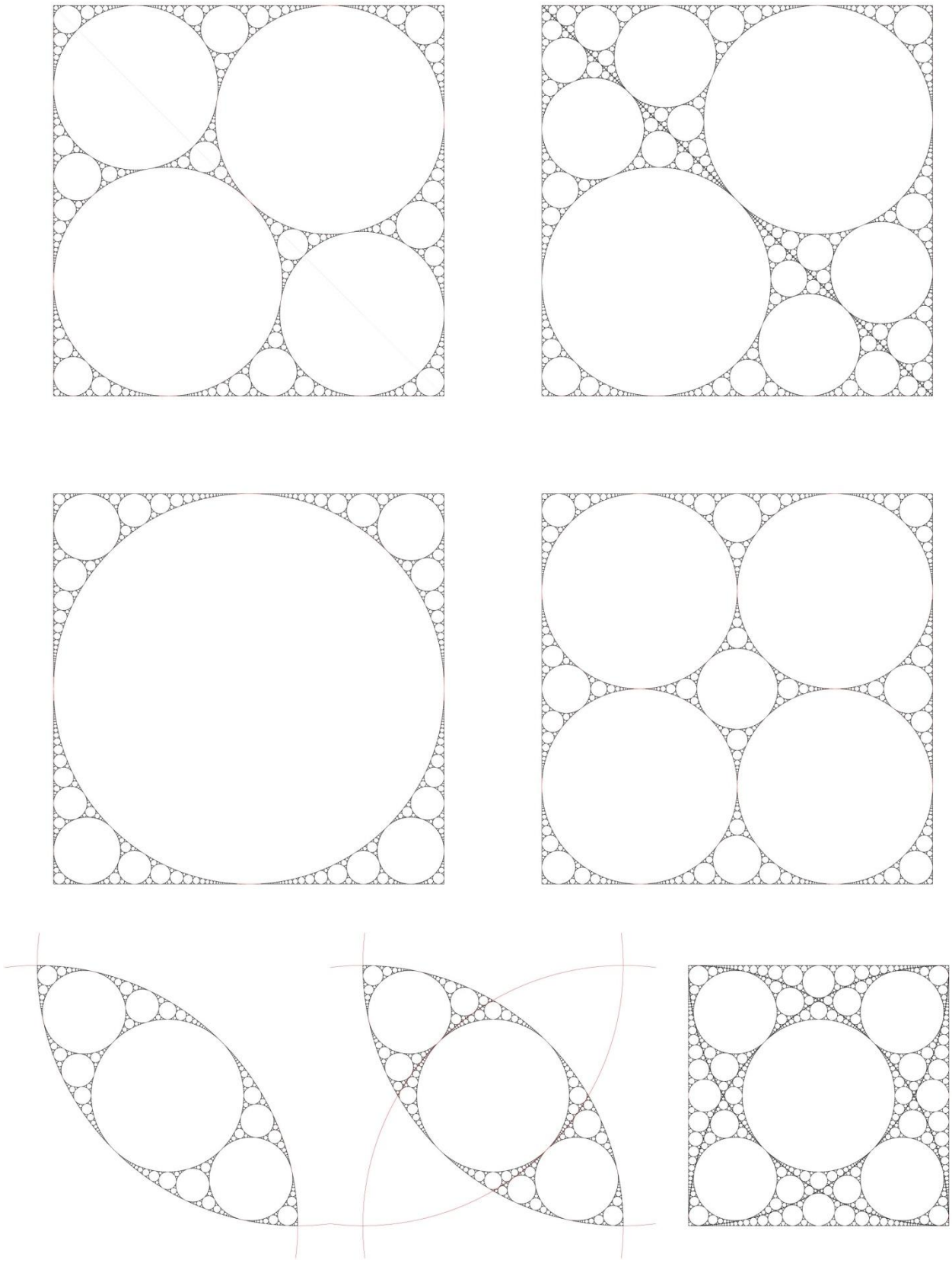

Figure 9. Sets of apollonian gaskets modeled within a square.

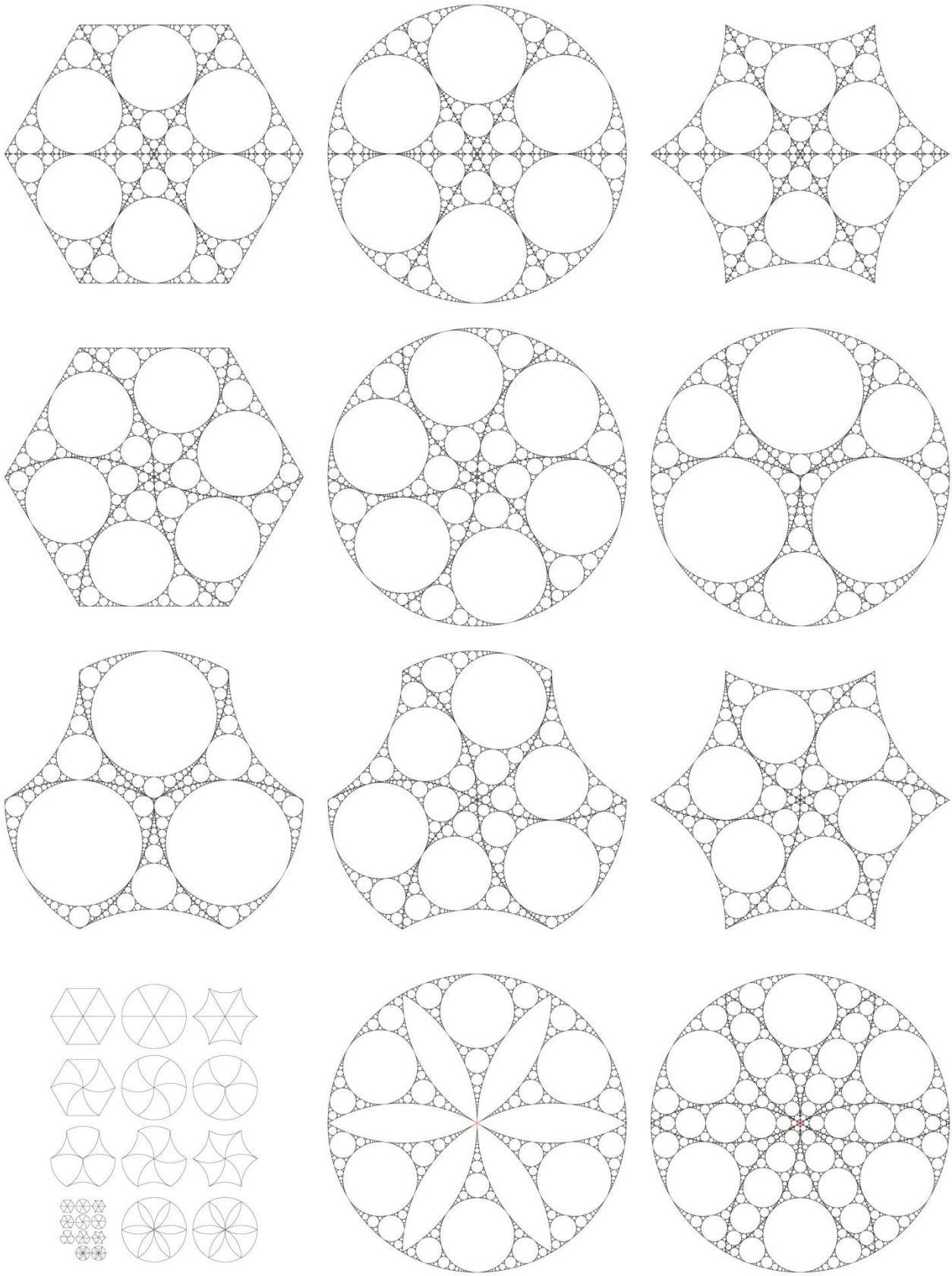

Figure 10. Sets of apollonian gaskets in a hexagonal configuration. A set of 'triangular' modules was created, which are repeated to created these models. Combinations of these modules can also fill a plane.

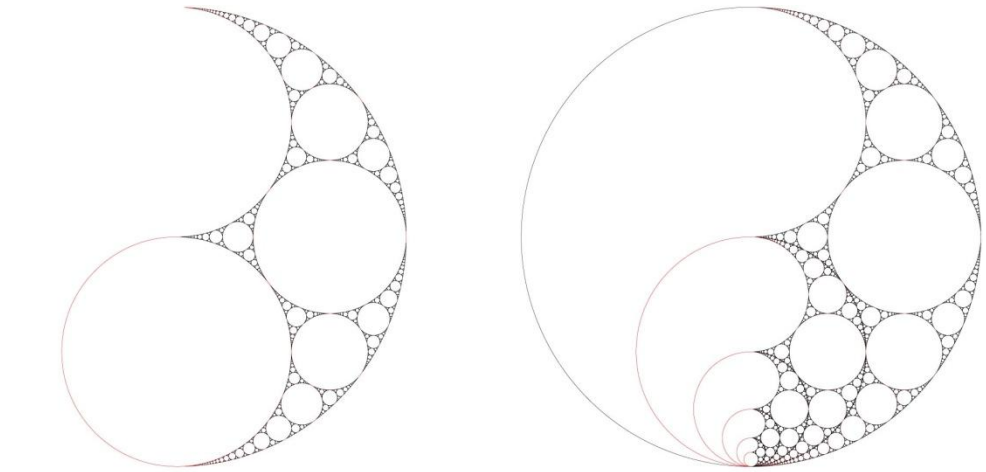

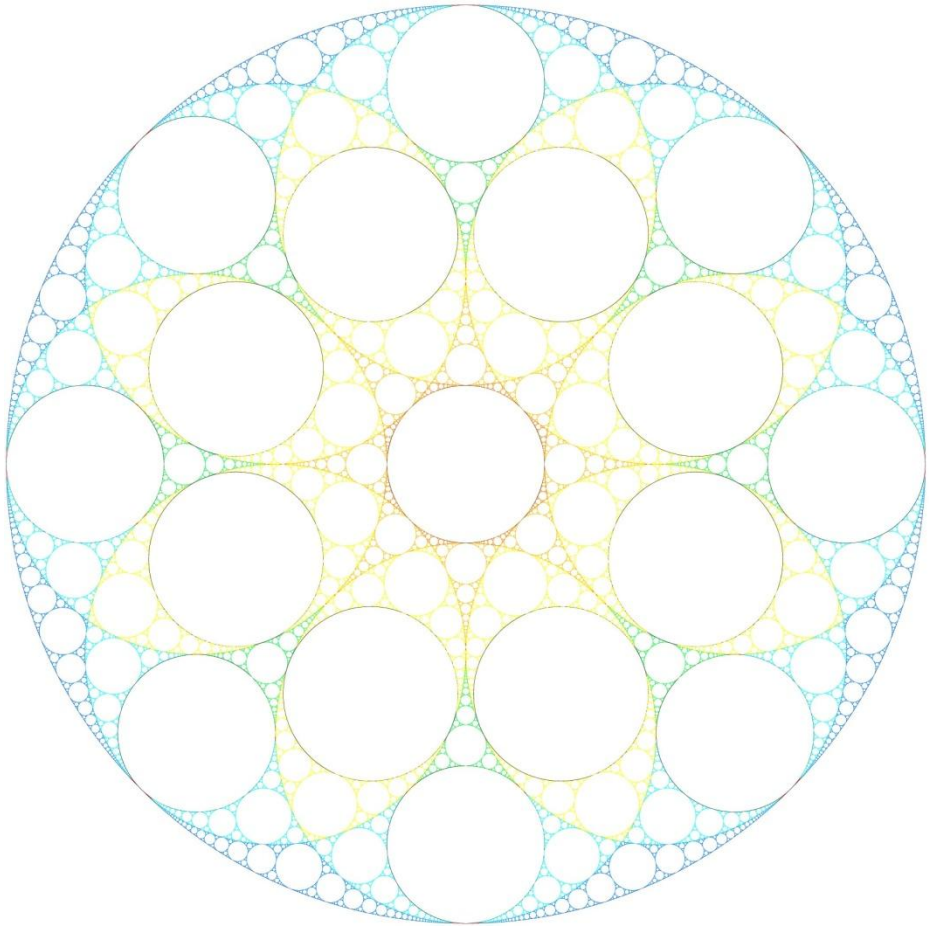

Figure 11 (top). Apollonian gaskets modeled in a circle can recursively be applied to circles within the model.

Figure 12 (bottom). Color can be used in various ways: circles can be color-coded by size, or by generation. In this example, circles were color-coded based on their location in the overall geometry of the model.

Truchet Tilings Revisited

Robert J. Krawczyk
College of Architecture
Illinois Institute of Technology
3360 South State Street,
Chicago, IL, 60616, USA
E-mail: krawczyk@iit.edu

Abstract

Repeating patterns in architecture are utilized in elements at a variety of scales; scale of a facade, perforated ceilings, and wall reliefs to carpeting and tile stonework. The Truchet tiling concept can now be reconsidered as one means to develop a modular non-repeating pattern. This paper explores some of the basic concepts of Truchet tilings and variations developed; and some current examples of using these methods with digital generation and fabrication methods.

Background

A number of formal repeating pattern concepts and system exist for designers and architects to utilize. They may as simple as uniform tilings and patterns, frieze and wallpaper groups, or complex as systems that can use randomness for placing individual patterns. Grunnbaum and Shephard offer a comprehensive and systematic treatment of the subject [1]. With the greater introduction of digitally based generative systems, algorithmically generated patterns, and greater means of digitally controlled fabrication, the concept of many-of-one is becoming one-of-many. As real-time steaming fabrication evolves, the need for non-repeating patterns will be easier to satisfy.

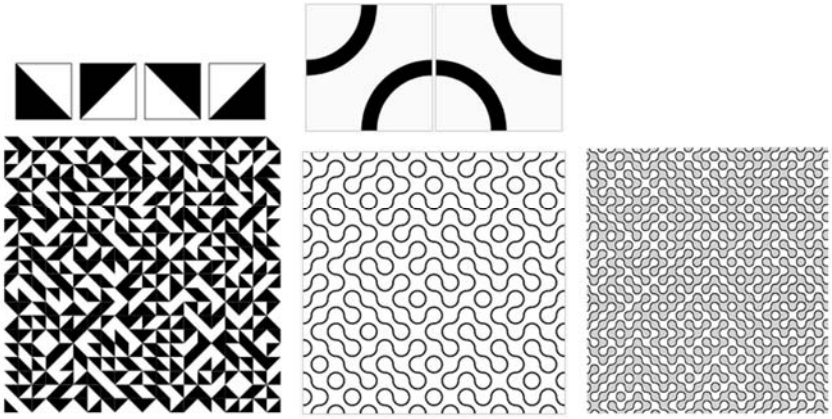

a. *b.* *c.*

Figure 1: *Truchet pattern, Smith variation, Smith shading.*

One such patterning concept which can be revisited is the modular shape combinations first observed and developed by Father Sebastien Truchet. Father Truchet (1657-1729) was of the French clergyman living in Lyon. He is known for being active in areas of mathematics, hydraulics, graphics, and typography. An

excellent repository of links to Truchet's writings and plates can be found on Jacques.Andre's website [2]. Figure 1a displays one of the many periodic patterns he developed. In 1704 he published "Memoir sur les combinaisons" in which a number of plates were developed to show periodic patterns. In 1722, P. Dominique Douat further elaborates on Truchet tilings [4]. Lord & S Ranganathan cover both Truchet and Douat's patterns [5]. The Andre website also includes the writings of Douat [2].

One of the basic concepts that one can see of Truchet tilings is that adjacent tiles can create much larger contiguous edge connecting patterns. In 1987 Cyril Smith analyzed the structure of Truchet's tilings and first abstracted them into simple diagonal lines and then into two arcs starting and ending at edge midpoints, Figure 1b [6]. Smith wrote about the closures that were being formed, circles; and also showed an example that was color filled to further highlight these positive and negative, concave and convex patterns, Figure 1c.

In 1977, Martin Gardner wrote about non-periodic tilings on dart and kites that included arcs connecting midpoint edges [7]. Later, 1989 and 1990 Clifford Pickover also wrote about arc tiles used the generation of random tiling patterns [7][8]. C. Browne further investigated the shading of the Truchet tilings by including examples using triangular and hexagonal tiles [10][11].

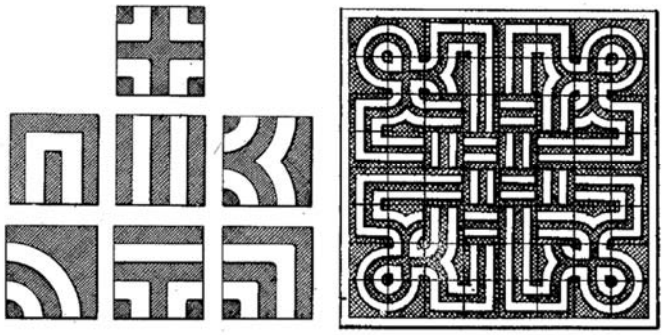

Figure 2: *Toy Designing Blocks by Graham, 1934.*

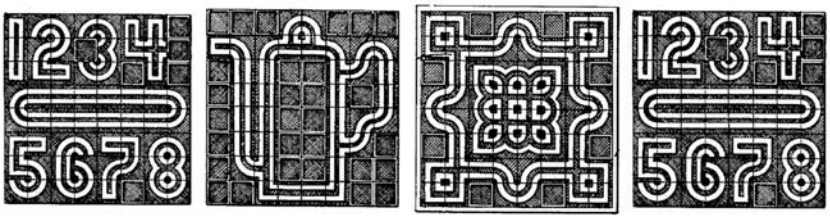

Figure 3: *Examples of Graham's Toy Designing Blocks.*

Following non-academic research and writing, we find that in 1934, a patent for a Toy Designing Block was granted to Tom C. Graham, 1,973,564, Figure 2 and 3 [12] This patent expired and 1991 patent 5,011,411 was granted to a Method of Making a Non-Repetitive Modular Design to Andreas F. Loewy, Figure 4 [13]. It expired in 2003 for nonpayment of maintenance fees. Researching previous art of these patents also uncovered US Patent 1,4,53,728 Means for Devising Ornamental Designs granted in 1923 to F. J. Rhodes, Figure 5 [14]. It has at least of the modular patterns that appear later, the two arcs at the midpoints.

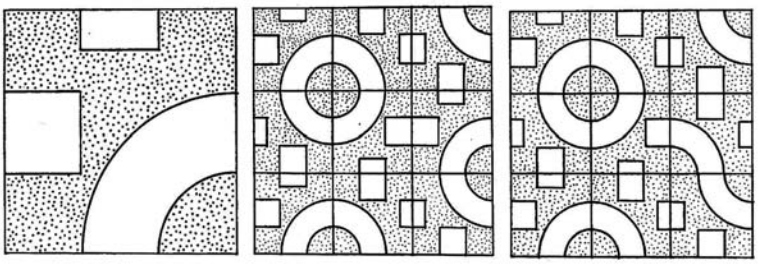

Figure 4: *Examples of Loewy modular design.*

As demonstrated by Loewy, the concept of how the adjoining edges could extend to a larger design was well understood, as seen here in his description:

"Each module is made in the following manner. Assume that the regular polygon has n sides. First, one chooses a set of points on one of the sides of the polygon, the points being distributed symmetrically around the midpoint of the side. Then, one duplicates this arrangement of points on each of the remaining sides. Next, one connects pairs of points with lines, such that every point is connected to one line. The lines can be straight or curved, but they must be continuous. The lines are drawn such that the resulting pattern is not symmetrical around any imaginary straight line joining any pair of vertices of the polygon. Finally, one can optionally fill in some or all of the spaces defined by pairs of lines, or by one or more lines and one or more sides of the polygon, with color or with some other design element." [13]

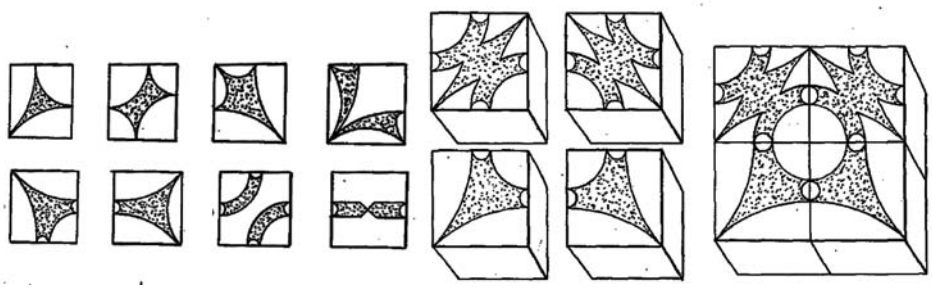

Figure 5: Examples of Rhodes ornamental design, 1923.

More recently, US Patent 3,464,145 Set of Blocks for Generating Designs was granted to P. C. Martin in 1969, Figure 6 [15] and US Patent application 10/792,627, System of Combinable Patterns that Generates Artful Designs submitted in 2004 by Pablo Fernando Cha included many of the same concepts as others before him, Figure 7 [16]. This application was abandoned in 2008.

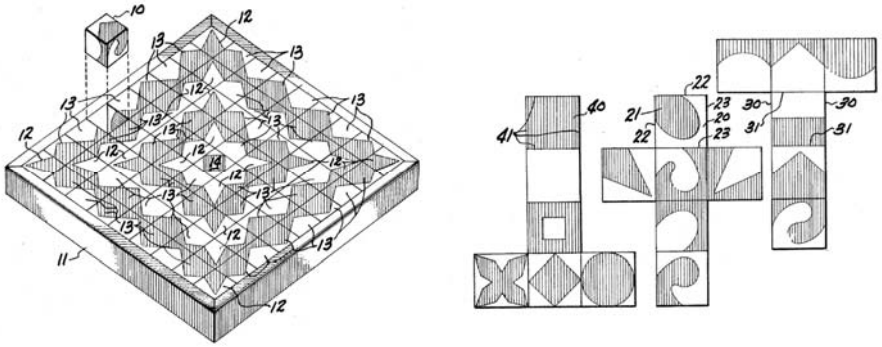

Figure 6: *Examples of Martin blocks, 1969.*

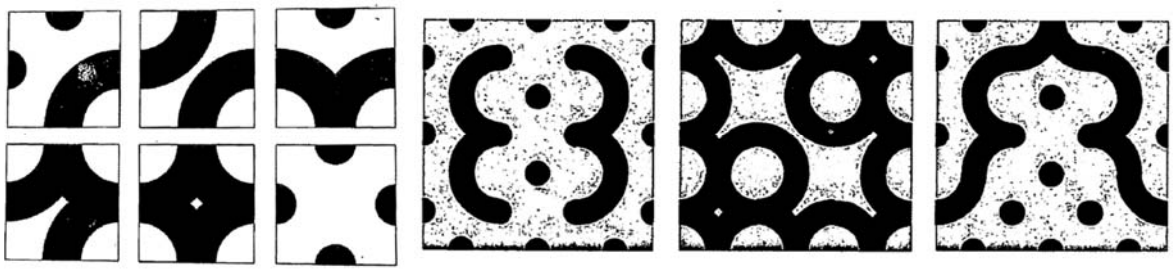

Figure 7: Examples of Cha ornamental design, 2004.

It should be noted that none of the patent descriptions ever mentioned the work of Truchet, Smith, or any others noted here; and also none of the writings of Smith and others ever mention the work being applied and granted for patents.

The Truchet tilings have also appeared in three-dimensions, Figure 6 as in Browne [10]. Bowne also includes a diagram that has the tiling on the face of a cube; it is a diagram for the resulting surface model. Browne also extends these three-dimensional models with the use of spheres.

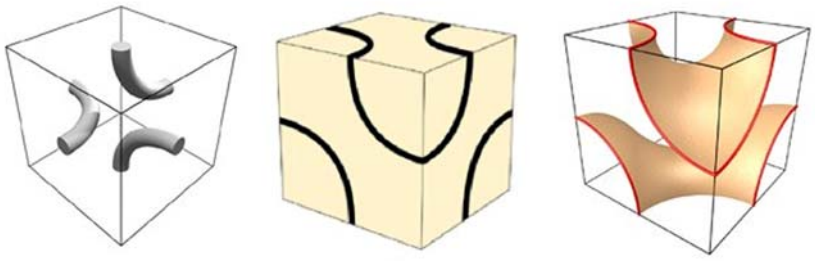

Figure 8: *Examples of three dimensional Truchet-like modules.*

Developing Truchet-like Tilings

The initial interpretation of the underlying concept of Truchet tilings was the connection of the midpoints of adjacent edges. We have seen in the patent search that others have also developed tiles using two and three equal subdivisions of edges. We have also seen the edge points connected with arcs and with straight line segments or ribbons. To further explore this tiling concept, a number of versions were developed in 2005, with two and three edges points were developed. From that series a total of three tiles emerged. Figure 9 displays the first set of tiles developed. It these tiles symmetry is across the diagonal. The ribbon connector was used to develop a coloring density between the foreground and background. The initial tiles were fabricated with a laser cutter using two tones of wood, in this case, inexpensive 1/8" MDF, Medium Density Fiberboard. Referring to Figure 10, the backing, the bottom layer, was simply a 11 inch square of light toned MDF and the top layer consisted of a series of 1.25 inch ribbons of a darker toned MDF. The plan for these wooden tiles was to attach them to a wall surface in a manner that they could be reoriented individually on a regular basis. The full fabrication of this version was never realized.

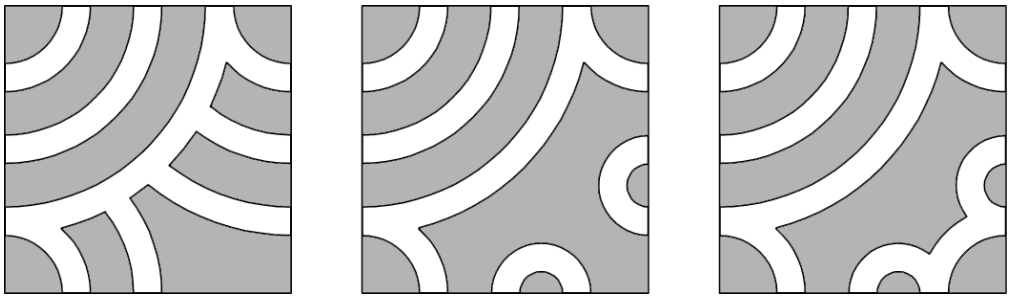

Figure 9: *Initial tile patterns developed.*

Figure 10: *Laser cut tiles, using two tones of wood.*

Theses initial tiles were also replicated in a 20 inch square array, randomly rotating each tile as it was placed. Figure 11 displays a black and white version of these images, a color series of these were also developed and titled Paths [17]. The Path series explores using a single tile or randomly selecting one from two or more different tiles. Using multiple tiles in a single tiling offered a greater opportunity for variation.

Figure 11: *Image printed version of the random tilings.*

The Path series also mimics the concept Sol LeWitt developed in his Wall Drawings, in particularly #358, 1981, which consists of arcs drawn from opposite corners of a square grid pattern [18]. The Wall drawings consisted of drawn arcs or lines connecting opposite corners of a grid where his crew was instructed to determine the orientation of the arc or line as they executed each individual module. In this case, the software replaces the crew and an algorithm using a random function computes the rotation of the module, replacing the decision of the individual crew person. Each time a tiling pattern is pattern executed a unique piece is generated.

For an installation at the 2010 Art Loop Open, an interactive modular tiling piece was proposed and selected. A version of the tiles was developed as a four inch magnet. A set of steel sheets were placed in a six by three foot frame. A total of 128 magnets were placed on the surface and viewers were encouraged to pick up any one of them, rotate it, and place it back. Figure 12 displays a single magnet and some initial arrangements, and Figure 13 shows the complete installed piece onsite.

Figure 12: *Printed magnet tiles, red ribbons on black background.*

Figure 13: *Installation at 2010 Art Loop Open in Chicago.*

Research has also found similar tile designs, both as a square tile and a triangular tile configuration by Japanese architect and designer Asao Tokolo, shown in Figure 14 [19]. His website does not cover the design development of these tiles nor how they originated. His designs consist of five edge points and are more free-form in the ribbon shapes included.

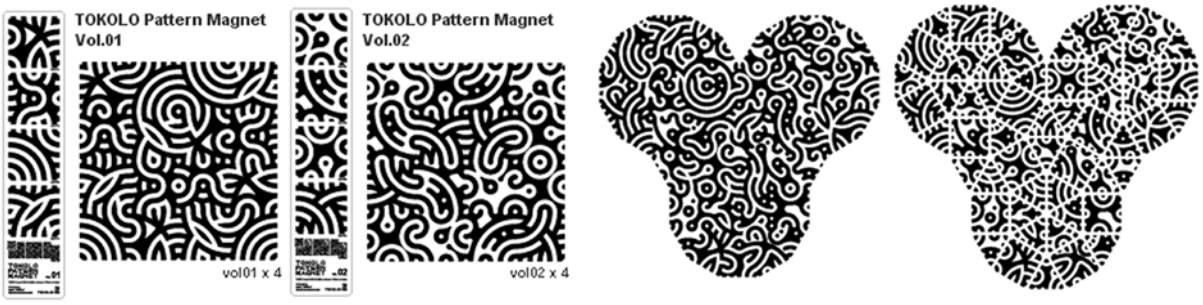

Figure 14: *Magnet* designs *by Asao Tokol*

The wall piece let to an interest to developing a larger, more variable piece that could also be interactive but possibly more three-dimensional. This let to developing a series of tile designs that could be placed on

the surfaces of a cube. The solid ribbons that were in the print and magnet tiles were recreated as three much thinner ribbons. The intersection of the multiple banded ribbons forms a very interesting blending and when laser cut and assembled into a cube, give the cube a very light and lacy appearance.

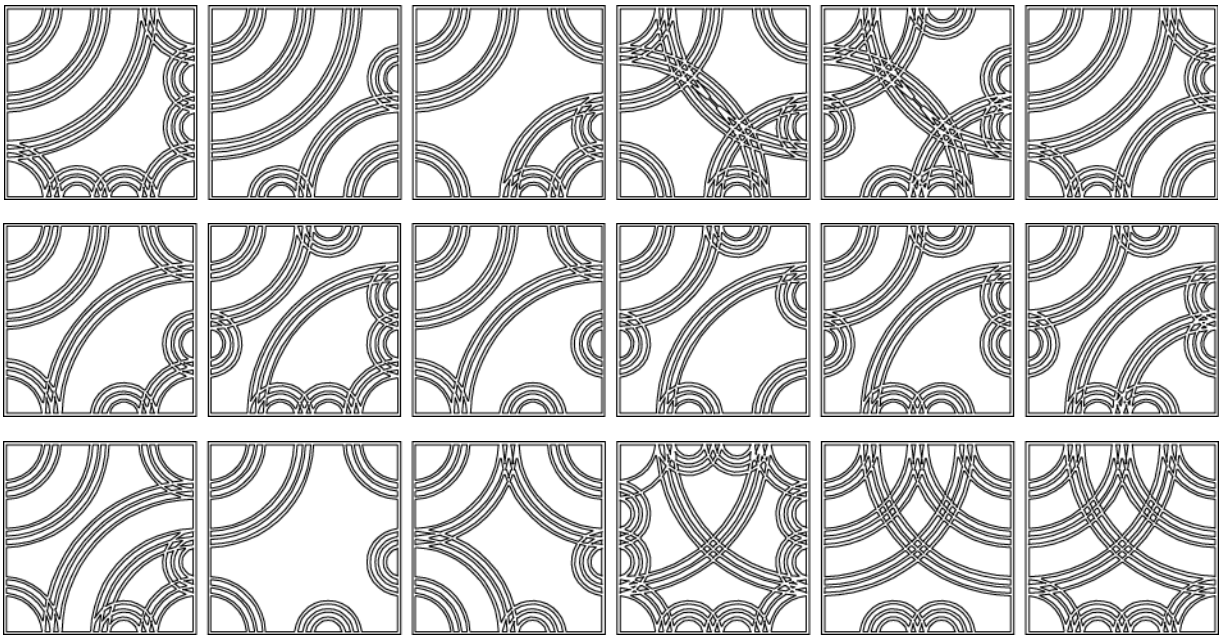

Figure 15: *Tile designs for cube surfaces, diagonal symmetry.*

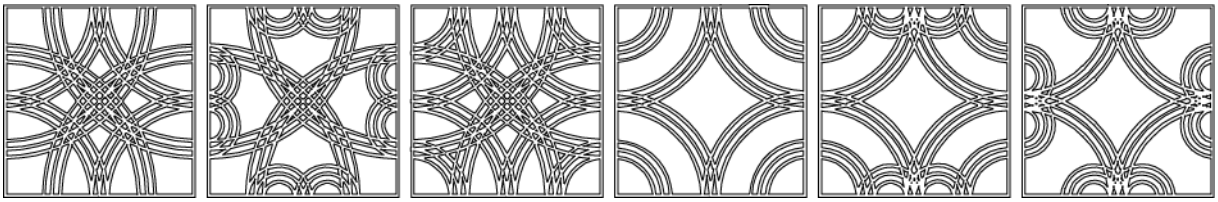

Figure 16: *Tile designs for cube surfaces, horizontal and vertical symmetry.*

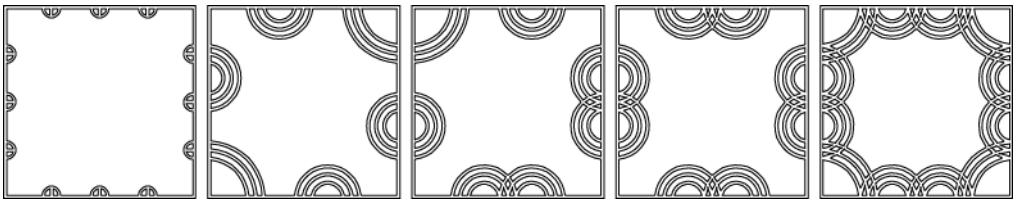

Figure 17: *Tile designs for cube surfaces, terminators.*

Figures 15, 16, and 17 display some of the designs that were developed. All display some symmetry and all consist of simple arcs connecting any the three edge points. The last set includes a series of terminators for the ribbons. These will in a future study be filled in with color and generated as prints using a random selection individual modules and random orientation.

Figure 18: *Laser cut cubes.*

Figure 18 displays the final assembled laser cut six inch cubes. An overlapping edge was developed so the cubes could be easily assembled. The most similar item currently on the market is a block game titled Motif Cubes Wooden Block Game, designed by newartifacts, a group of artists and designers from Uruguay, South America. These consist of nine 1 3/8 inch painted cubes, Figure 19. Browne also has developed a series of games that are based on Truchet-like tilings of all different shapes, three-dimensional and two-dimensional [20].

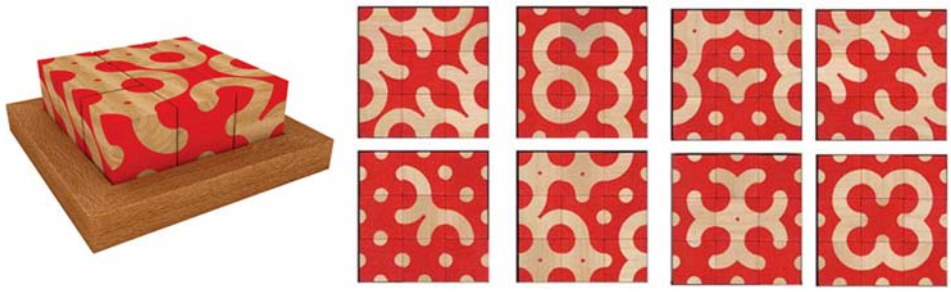

Figure 19: *Motif Cubes.*

These studies begin to demonstrate some of the possibilities of using a modular design element with random selection and random orientation to generate repeating patterns that would most likely not actually repeat. With the utilization of a digitally driven fabrication system, each piece manufactured could be a unique combination of basic elements. In some emerging technologies, such as, large scale carpet printers, if the design were to be streamed horizontal row by row, a very large area could be manufactured without any repetition. Otherwise, less technical demanding tiling systems such as carpet, wall, and ceiling tiles and panels could be economically manufactured while still offering a very great variety of unique installations.

References

[1] B Grünbaum and G C Shephard, Tilings and Patterns, W H Freeman, 1987.

[2] J. Andre, Website for S. Truchet, http://jacques-andre.fr/faqtypo/truchet/

[3] S. Truchet, Memoir sur les combinaisons, Memoires de l.Academie Royale des Sciences, pp.363-72, 1704.

[4] P. Dominique Douat , Methode pourfaire une infinite de desseins differents avec des carreaux mipartis de deux couleurs par une ligne diagonale: ou observations du Pere Dominique Douat Religieux Carme de la Province de Toulouse sur un memoire insere dans l'Histoire de I'Academie Royale des Sciences de Paris l'annee 1704, presente par le Reverend Pere Sebastastien Trunchet religieux du meme ordre, Academicien honoraire, Paris, 1722.

[5] E A Lord & S Ranganathan. Truchet tilings and their generalisations. Resonance 11 (2006) 42-50.

[6] C S Smith, The tiling patterns of Sebastien Truchet and the topology of structural hierarchy, Leonardo, Vol.20, pp.373-385, 1987.

[7] M. Gardner, "Extraordinary Non-Periodic Tilings That Enrich the Understanding of Tiles", Scientific American 236, No. 1, 110-121 (1977).

[8] C. A. Pickover, "Picturing Randomness with Truchet Tiles." J. Recr. Math. 21, 256-259, 1989.

[9] Pickover C. Picturing randomness with Truchet tiles. Computers, pattern, chaos, and beauty: graphics from an unseen world. New York: St Martin's Press; 1990. p. 329–32.

[10] C. Browne, "Truchet curves and surfaces," Computers & Graphics, 32:2, 2007, 268-281.

[11] C. Browne, "Duotone Truchet-like Tilings," Mathematics and the Arts, 2:4, December 2008, 189-196.

[12] T. C. Graham, Toy Designing Block, US Patent 1,973,564, 1934.

[13] A. F. Loewy , Method of Making a Non-Repetitive Modular Design, US Patent 5,011,411, 1991.

[14] F. J. Rhodes. Means for Devising Ornamental Designs, US Patent 1,4,53,728, 1923.

[15] P. C. Martin, Set of Blocks for Generating Designs, US Patent 3,464,145, 1969.

[16] P. F. Cha, System of Combinable Patterns that Generates Artful Designs in US Patent application 10/792,627, 2004.

[17] R. J. Krawczyk, Path Print Series, bitartworks.com

[18] G. Garrels, Editor, Sol LeWitt: A Retrospective, Yale University Press, 195, 2000.

[19] A. Tokolo, tokolo.com

[20] C. Browne, www.cameronius.com/games/

Creating the Mandala

Margaret Lanterman
Department of Art, Media and Design
DePaul University
1150 West Fullerton, Chicago IL. 60613
Email: mlanterm@depaul.edu

Abstract

The author will discuss the artistic/mathematical structure of the mandala, it's brief history, and the procedure for producing a mathematically derived example.

Introduction

The beautiful melding of art and mathematical form that we know as the mandala seems to stem from pre-history as a desire to find a realm where humans and the sacred could interface.

The question of where to begin the discussion of the Mandala is an interesting one, as the form itself suggests a wonderful continuity and the possibility of eternity. The origin of this structure resides in a simple, dimensionless dot in its very center, with mathematical radiations formed by triangulation, reflection and rotations - a unit that reflected eternity and all of nature.

This art form is commonly associated with the Buddhist religion and is known as a template for deep meditation and spiritual sustenance, a means to connect the divine with the simple world of humanity. The mandala presents as a circular design, arranged in layers and radiating out from the center. The source of the name seems to be derived from the Sanskrit word for essence, *manda*, and the word for container, *la*. Thus, we have the container of essence, the great circle that through geometric patterning embodies the essence of god and all of nature. Through mathematics and art, comes the perfect prayer.

Looking at the earliest levels of Indian and Indo-European religion (the Rig Veda and its associated literature) there is also another math-art connection. Tapping into the cognitive connections of math and music, another source lies in the Vedic ceremonies in which hymns or mantras were chanted, perhaps in rounds. These hymns and chants were thought to have the power to create patterns for creatures and natural elements, thus serving as a generative world model. Visual art imagery was added to re-enforce and enhance the effect, embodying mathematical patterning in the process.

By 1500 BC a form of mandala was highly developed by Hindus. The earliest 3-D stupas were built in 300-400 BCE by Emperor Ashoka, who undertook the task of building monuments on important Buddhist sites; by 800 AD Javanese temple complexes were treasured as architectural models of the mandala, and this embodiment of sacred space has carried forward through all of time and many traditions.

Today Buddhist monks create sacred mandalas to give home to the presence of the Buddha, and as a "blueprint" to connect the peace and continuity of their deity to the supplicant, to connect

the universe with man and all of nature. They study for three years to learn the concepts and techniques of math and art necessary to achieve their ultimate creative goal.

Many cultures have incorporated the beauty of the mandala in their practices. Islamic mosques appear as mandalas with a dome, and they use the same art/math to allow thoughts and emotions to soar towards Allah. Navajo Indians create sand paintings, medicine wheels and dream catchers with much the same mathematical structure. Mandala concepts can be seen in Celtic knots, often contained in a circular structure and using some of the same mathematical and artistic processes in the endless or unbroken line that crosses over itself many times but always returns to the original path.

Christian rose windows and the marble floor in such architecture as the Chartes Cathedral put art/math to good use in the same mandala patterns. Even in the political geographical realm the circle was and still is a way to divide or claim area and extend holdings.

With all of this rich and wonderful history to support the effort, the remainder of this paper will look at the procedure and possibilities of creating individual mandalas.

Design

Through this project the participant will be able to explore permutations of a basic design, the effect of various color interactions, and possibly create a meditative tool for future use in resolving problematic issues of mind or spirit. Using the components of geometry and the devices of repetition, reflection, rotation and proportion, the participant will create an aesthetically pleasing design radiating from a center point in the format know as the mandala.

Materials

- ✓ Watercolor paper
- ✓ Tracing paper
- ✓ Paint and drawing tools

Procedure

1. Plan your design. Consider curves, arcs, coils, circles, spirals, isosceles triangles, interconnected lines, and other geometric forms.

   Participants will receive a template of a circular form divided into four quarters around a center point. Consider the center of the circle as the point of radiation or rotation. This center should be considered as an energy source from which the design flows. Lines will materialize from the center and will intersect to create geometric or organic patterns.

   Start by designing one single quarter of the mandala using the elements of line, repetition of form, radial symmetry, reflection, and color interaction. This will then serve as the pattern to complete the entire Mandala.

Design interpretations can include any combination of form, line and color. Consider repetitions employing reflection, translation and rotation symmetries. Apply gradations in scale to introduce proportion. Consider also interconnecting forms. The forms that you use may be symbolic to you, or simply aesthetic choices. Each quadrant of the design will reflect the other three, creating a visual continuity.

If you wish to simulate a traditional Buddhist prayer mandala form, you will include a center, which is free of dimension, as the source of energy. From this center draw a circle approximately one third of the way out from the center to represent dynamic consciousness. The circle should be inscribed in a square, which represents the physical world.

2. Tape a piece of tracing paper over your completed design and trace it onto the tracing paper. Rotate the tracing paper and repeat this procedure until you have filled all four quadrant of the tracing paper.

3. Flip the tracing paper graphite side down and tape it on to your water color paper, being careful to line the center point precisely in the middle. Using your pencil, draw over your image again. This will transfer the graphite onto your watercolor paper.

   Remove the tracing paper and check that the image is completely transferred.

4. You are now ready to consider your color choices. You may of course choose any color system or perhaps work intuitively. If you would like some symbolic references, consider the following:

   In western thinking, energy is often symbolized by the warm colors of reds, yellows and oranges. Greens and blues are psychologically cool colors and can be said to represent nature, growth and calm. White may represent peace, purity or wisdom, while black signifies such things as sophistication, death, mourning, or an unknown depth.

   In Buddhist thinking, there are specific connotations for each color. White can represent the move from ignorance to the wisdom of reality. Yellow represents the change of pride to the wisdom of sameness. Red signals attachment becoming discernment, while green suggests jealousy turning to accomplishment. Blue symbolizes the turn from anger to wisdom.

Conclusion

The mandala is one of the most ancient of art forms, and has had cultural and spiritual significance from pre-historic times to the present. Some form of it appears in most of the world cultures. This circular form, radiating from a center, has proven to be highly satisfying and significant enough to promote extended application and research. The creation of personal mandalas have been found to promote relaxation, awakening, mental stimulation and both aesthetic and mathematical extensions. The author has laid out a simple procedure for participants to work within the framework created in ancient times.

In practical terms this project has been designed to include concepts of radiation, reflection, line quality, shape and color interaction. There is considerable opportunity for playful interaction within the format. The artist may choose the application of traditional symbolism or select personal interpretation of color and form. In accepting the discipline of the structure, the artist can then guide his or her creative inventiveness.

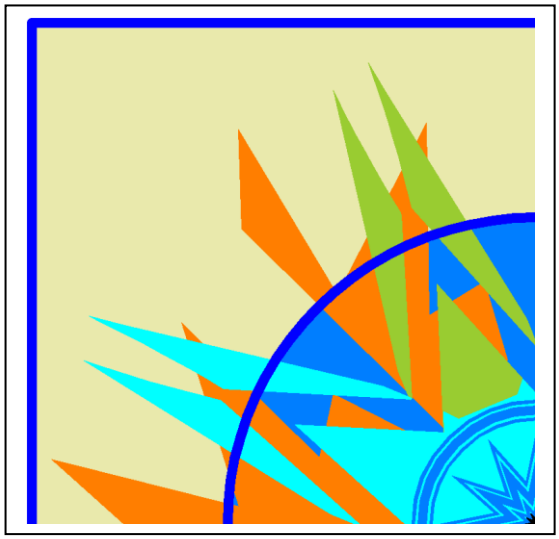

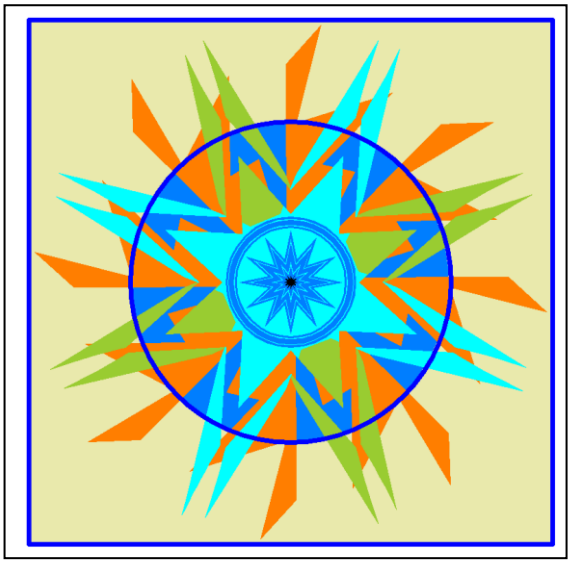

Perceptions of Three

Donna L. Lish
129 Center St.
Clinton, N.J. 08809
E-mail: dlish5@embarqmail.com
Web: libeado-designs.com

Abstract

The creative process is an interweaving of the artist's experiences, intuition, and intellect, which altogether impact the art that is generated. The journey is equally as vital as the destination.

Introduction

As an appreciator of the mathematical realm, I was first cognizant of an attraction to the number 3 as it pertained to my art making. Besides realizing that many of my sculptural forms consisted of groupings of three units, I noted a connection in the actual construction: three beads in patterns, three-stitch increments in knitting, and increases of three in crocheting.

The magnetism of three permeated daily practices while preparing to work in my studio. I refined as much as possible prior to stitching, immersed in images within the stream of consciousness. This part of the ritual was accompanied with stacking rocks in threes, purported to maintain focus for the day. Taller monoliths followed, odd-numbered, towered in decreasing sizes. The divine balance was achieved to enhance my productivity and calm.

The relevance of my connection with three went on: I have three children, three academic degrees; three decades of teaching experience; three seats in my living room, three brooches on each jacket lapel (or odd number), and while researching energy and crystal healing, I placed three crystals in each arrangement of them. Certain aspects of three have been relevant to the refinement I attain in my art.

In Pythagorean theory, numerical three represents perfect harmony: "the union of unity (one) and diversity (two).The symbolism of 3 is linked with the triangle" (O'Connell, p. 208). On the history channel ("Ancient Aliens", April 13, 2011) scientists referred to the Pythagorean right angle triangle resulting from imaginary lines which link massive rock formations at Carnac, France, the Armenian Stone Henge, and the high plateau city of Sicyon (Greece). Theoretically, the formations are believed to have mathematical significance which dates to the Stone Age: advanced math clues, a riddle or a sign.

Another reference is the certain frequency in which humans vibrate in three dimensions. At the thirty third latitudinal parallel (a double 3) is the ultimate attainment of consciousness ("Ancient Aliens", 2011). In Islamic art, "the 3 symbolizes human consciousness and the principle of harmony" (O'Connell, P. 116). "Three is associated with adjectives divine, power, success, prosperity, safety, and positivity (O'Connell, p. 500).

Pertinent to magic, three has the empowerment of change. In a mojo bag containing three objects or an odd number of them, called gree grees, these charms are selected because "the universe operates on odd

numbers in order to keep things moving….Three wants to tumble into four, whereas four is solid and fixed rather than flowing" (Heaven, p. 38).

The third phase of the universe is cited in "Quantum Shift of the Global Brain", in which "society's evolutionary path is rapidly decided" (Laszlo, p. 30). The areas of environmental and social shifts manifest in bifurcations, "the place where systems have two branches or peaks" (Guralnik, p. 139). The power of selection at this fork is mirrored in visualization and problem solving as the artist selects which alternative will yield superior refinement of form or subject.

Figure 1- Splash Ring, 30in.x30in.x5in., beaded, netting stitch

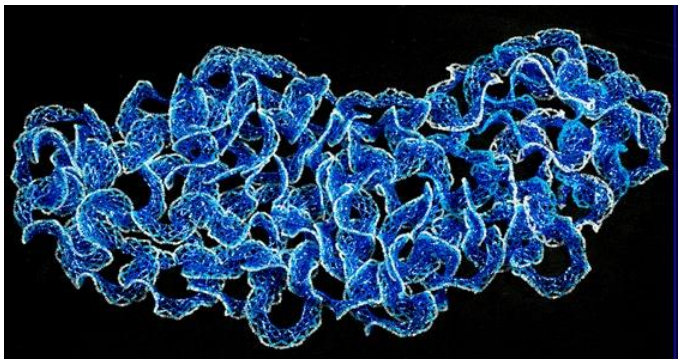

Figure 2- Agitation, 33in.x27in.x 4in., beaded,netting stitch

The beauty of three in three-dimensional art is evident in Figure 3 in the reference, "Golightly", a triple twist Mobius (Friedman, Hyperseeing, 8/2007), and Figure 5 in the reference, "Bronze Triple", Mobius (Friedman, Hyperseeing, 8/2007). An extreme application including properties of three is the four-dimensional hendecatope where "colored beams represent the edges of triangles…." (Lanier, p.28). (In the fourth dimension each side is 3-D, the principles of which are challenging to identify, especially in diagram form on a two-dimensional page). As complex as this construction may seem, it is still imbued with aesthetic options for interpretation in the eyes of this sculptor.

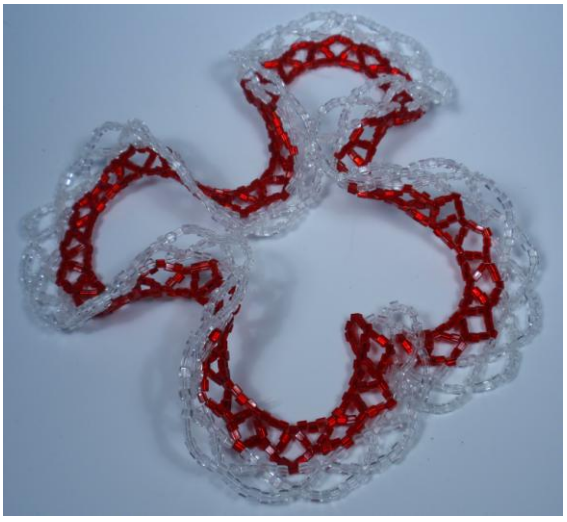

Figure 3, Beaded Curvature, 11in.x10in.x3in., beaded, netting stitch

Figure 4, triangle dye ribbon strip, crocheted mylar

The concept, as well as the reference to the tetrahedron (three-sided pyramid) has possibilities in consolidating with triangle needlework to achieve variations in surface pattern and positive and negative

curvature of hyperbolic planes. This application requires experimenting to envision models of fundamental architecture, a dynamic concoction of stitches and materials in impressive scale. This is my obsession.

Figure 5- Steel Curves, 12in.x12in.x3in., knitted steel wire

Figure 6- Perpetual Meander, 8in.x10in.x10in., rubber, crocheted

I was attracted to artists' applications of curvature. In Irene Rousseau's "Art as Metaphor for the Fourth Dimension", she features two "hyperbolic mosaic sculptures which symbolically represent the concept of infinity" (Rousseau, Hyperseeing, Spring, 2009). My notes on her presentation are: concepts of infinity in negative curvature; interpretation of infinite structures within boundaries recognize the circle as the outer edge of those limits. My studies on this configuration are seen in Figures 1-3.

Figure 7- Black-White+, 10in.x10in.x8in., rubber, crocheted

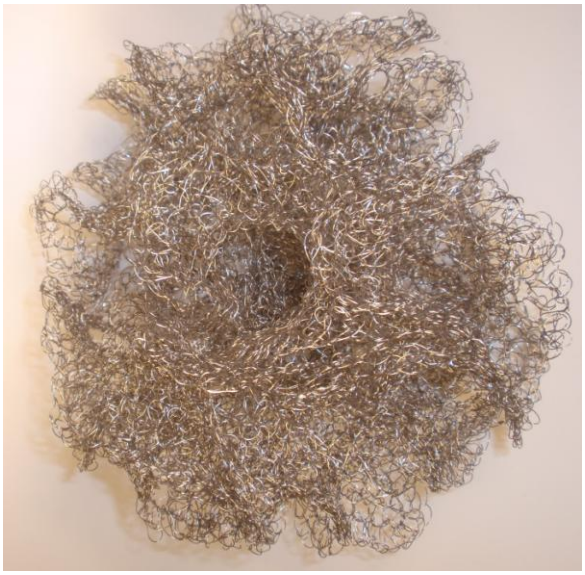

Figure 8- Curvature,12in.x12in.x8in., stainless steel, crocheted

In “Triangle-Strip Knitting”, James Mallos writes the strategies of using algorithms to enhance accuracy of knitting or crocheting units for 3-dimensional shapes. My focus is the crocheted continuity of strips of triangles, loosely following the information in his paper. Figure 4 is an ongoing strip. Triangles can be stitched together to achieve curvature in 3 dimensions. Pursuant to instruction, I crocheted the first triangle, then slip-crocheted back down the last side to proceed to each additional triangle in the strip. The orderly repetition enabled me to complete multiples and to maintain size uniformity and color variations using dye sublimation ribbon, a recycled light, yet rigid material. Presently, these works are limited to use indoors though massive in scale.

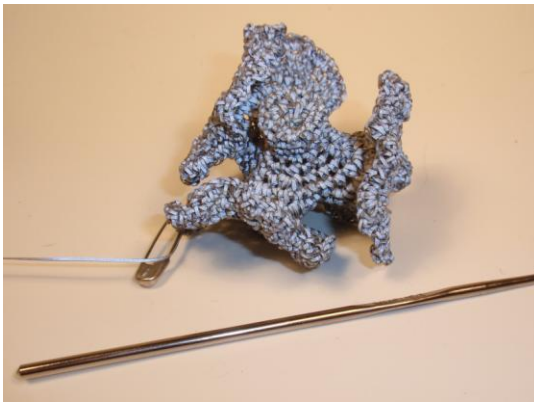

Figure 9, Hyperbolic Plane, 3in.x3in.x3in., retroglo reflective fiber

Figure 10- Third Eye, synthetics, metallics,glass, crocheted

Figure 11- Third Eye (detail), 12in.x12in.x4in., synthetics, metallics, glass, crocheted

Daina Taimina’s crocheted models of hyperbolic planes were the necessary elements of research to integrate within my schema. Surface ruffles were reminiscent of the mnemonic capacities embedded in brain folds. My objective is a universal visual language- to view and unravel the mysteries, through consultation of one’s own memory, human’s limited physiology. These images of infinite expanses led to using novel materials like rubber and steel in my own departures, seen in Figures 5-12. Each study is based on increments of 3 stitches- increases and single crochets. Expansive diversions await rendering as this preliminary undertaking unfolds.

Coalescence of all resources has enriched and refined the direction of the journey. The work portrayed in the figures represents cosmic ideation of preliminary impressions. Until the work is assembled, it is merely a thought, an essence limited to the language that can clarify the initial spark. Until that idea is acted upon, memory of it is invisible and must be transformed in order to be physically represented. It is the sole power of the artist to perform this extraordinary translation.

References

[1] Devadoss, Satran, “The Shape of Nature”, The Great Courses Publications, c. 2010

[2] Friedman, Nat, “Larry Frazier:Topological Surfaces”, Hyperseeing, August, 2007

[3] Guralnik, David, Webster’s New World Dictionary, Simon and Schuster, c. 1970

[4] Heaven, Ross, Charing, Howard, “Plant Spirit Shamanism”, Destiny Books, c. 2006

[5] Lanier, Jaron, “Jaron’s World”, Discover Magazine, April, 2007

[6] Laszlo, Ervin, “Quantum Shift of the Global Brain”, Inner Traditions, 2008

[7] Mallos, James, “Triangle-Strip Knitting”, Hyperseeing, Summer, 2010

[8] O’Connell, Mark, Airey, Raje, Craze, Richard, “Symbols, Signs, and Dream Interpretation, Metro Books, c. 2007

[9] Taimina, Daina, “Crocheting Adventures with Hyperbolic Planes”, A.K. Peters, Ltd., c. 2009

[10] Tapson, Frank, “Barron’s Mathematics”, Oxford U. Press, c. 1996

[11] Stahl, Saul, “Geometry from Euclid to Knots”, Dover Publications, c. 2003

Figure 12- Three curves, 6in.x6in.x4in. (largest), wool, hemp, crocheted

Perceptions of Three Workshop

Donna L. Lish
129 Center St.
Clinton, NJ 08809
Web: libeado-designs.com
Email: dlish5@embarqmail.com

Description

Estimated Length: 1-1 ½ hours (modified to available time)
Materials provided by the instructor

In this workshop I will introduce two models of construction of forms: paper doll triangle strips, and varied triangle multiples to implement and affix in experimental 3-D configurations. From these maquettes, participants will select an appealing sample to expand into a balanced, sturdy sculpture, of approximately shoe box size. Diverse papers (printed and solid), nontoxic adhesives, joining elements, scissors and other tools will be provided. Problem solving skills will be implemented.

Octoids: Sculpting Between Octahedron and Sphere

Stephen Luecking

School of Computer Science and Digital Media
DePaul University
sluecking@cs.depaul.edu

The edges of an octahedron inscribed in a sphere will project as arcs dividing the sphere into quadrants. Flattening one or more of these arcs onto the corresponding edges of the octahedron causes the affected quadrants to lose their double curvature and reduces their surfaces to conical, cylindrical and planar surfaces. The sculptor dubs the figures thus created as octoids and cites approximately 143 possible variations that his sculptures might take. He also offers methods for the efficient manufacture of these sculptures.

Introduction

The octahedron inscribes in a sphere, and its edges project onto the sphere as orthogonal great circles that divide the sphere into quadrants. The sphere may then be seen as an octagon all of whose edges comprise 90° arcs and whose faces have swelled tangent to one another and doubly curved. Have only select edges of the octahedron round into these quarter arcs, and portions of the expanded octagon (or octoid by the sculptor s parlance) and its surface will take on the conical, cylindrical and planar features determined by the combinations of straight and curved edges. The solid figures this generates offer considerable interest as sculptures. Further the sculptures are then amenable to combinatorial fabrication in which each octoid forms from eight modules in various combinations of spherical, conical, cylindrical or planar surfaces.

Inflating an Octahedron

To create an octoid from an octagon (Figure 1a) selectively inflate an edge or edges into 90° arcs and treat these as bounding curves of new surfaces to supplant the original faces.

Figure 1b depicts an octagon with one edge inflated. The two adjacent faces sharing that edge now meet on the arc so that each curves into a conical surface. Similarly Figure 1c has had two meeting edges inflated. Subsequently the face bounded by the two arcs and the straight base of the triangular face rounds into a cylinder, while the two faces adjacent at the arcs grow into conical surfaces. In Figure 1d all three edges of a single face have arced outward forming that face into a spherical segment and the three adjacent faces into quarter cones.

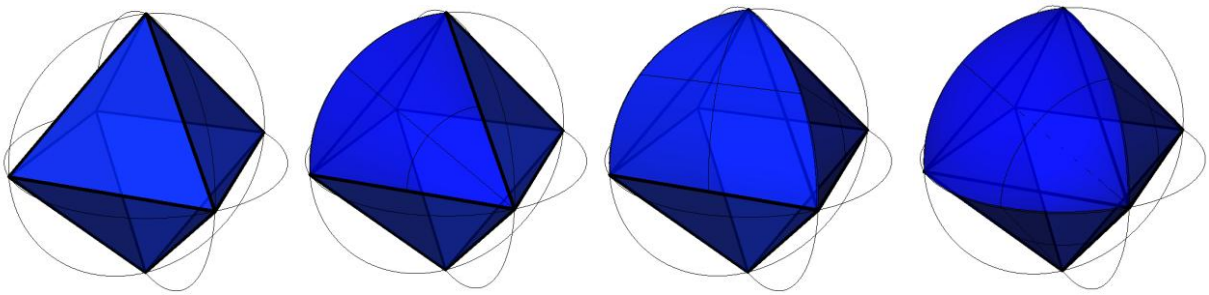

Figure 1. a) inscribed octagon b) one edge inflated c) two meeting edges inflated d) all edges of one face inlated.

Deflating a Sphere

To create an octoid from a sphere (Figure 2a) selectively deflate a quadrant arc or arcs into 90° chords corresponding to the edges of an inscribed octagon.

Figure 2b features a single arc deflated into the edge of the inscribed octahedron to create adjacent cylindrical surfaces. Figure 2c deflates two meeting arcs into the corresponding edges of the inscribed octahedron to yield a cone segment flanked by two cylinder segments. With all of the arcs of a single quadrant deflated the sphere quadrant deflates into a triangular face with the adjacent quadrants transform into cylinder segments.

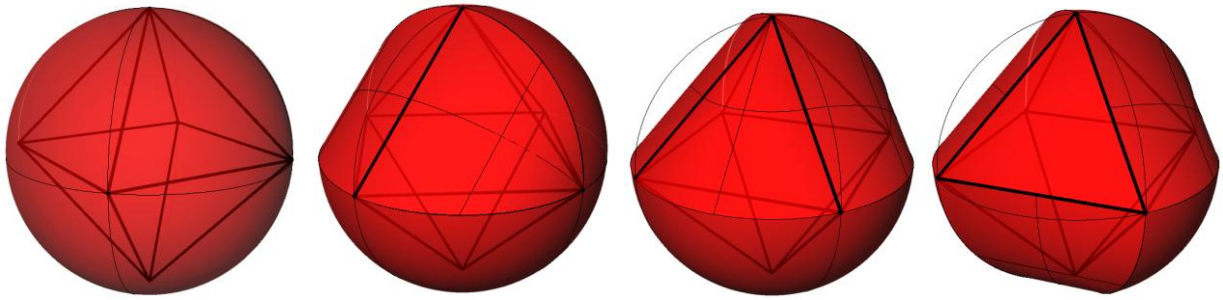

Figure 2. a) circumscribed sphere b) one surface arc deflated c) two surface arcs deflated d) three surface arcs deflated.

Fabricating an Octoid Sculpture

Three orthogonal intersecting disks may serve as the armature for a sphere (Figure 3). Modifying those disks by cropping them at their quadrant chords can result in five additional sections (Figure 4) for creating the orthogonal armatures of any potential octoid. The sculptor cut these from thin plywood, then slotted them to intersect in order to then tightly glue them together into an armature (Figure 5).

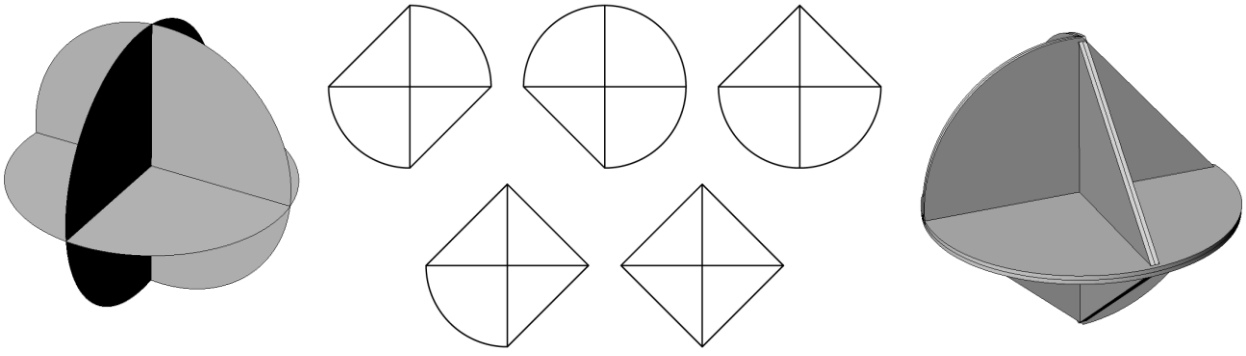

Figure 3. Armature for a sphere. Figure 4. Armature sections for creating octoids. Figure 5. Assembled octoid armature.

The sculptor drew schematics for the potential configurations of octoids (Figure 6) and followed these for fitting pre-cut plywood sections into armatures. To date 72 of the possible armatures have been assembled and filled using an alkyd-based spackling compound applied in thin layers. After smoothly sanding the spackle, then priming and re-sanding to a porcelain-like finish, the sculptures were ready for the final finish of a metallic lacquer. To date 24 have reached the finished stage (see gallery below).

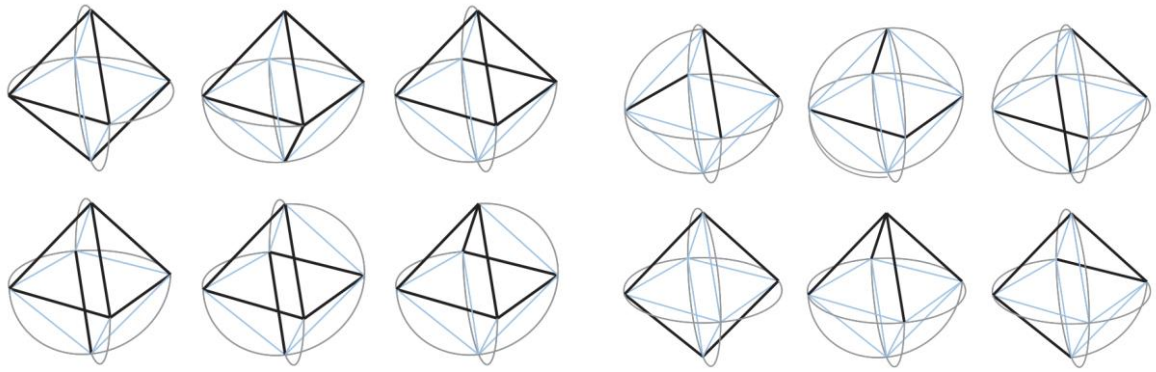

Figure 6. Sample schematics for octoid layout. Dark lines represent the configuration of collapsed edges of the octoid.

Octoid Gallery

Digital Painting by the Numbers

Stephen Luecking
School of Computer Science and Digital Media
DePaul University
243 S. Wabash Ave, Chicago IL. 60604
Email: sluecking @cdm.depaul.edu

Abstract

Colors in computer graphics may be selected and printed with precision by applying the RGB and HSL color models that are standard in PC operating systems. We access these models through MS Word and apply the numerical coding used by programmers to identify and mix colors in common visual relationships.

Introduction

Most graphic programs have color-selecting tool that are typically used intuitively by artists, often employing a slider controlled with the mouse. To refine their color choice the artists may resort to numerically adjusting the color. Graphics programs usually have an interface of numbers specifying percentages between 1 and 100 that is easily understood by the average user. Both of these tools, the slider and the percentage adjuster are programmed using the RGB color model included in the operating system. This same model is readily accessible in its basic form through most common office programs that have some minor graphic capabilities, such as Microsoft Word or PowerPoint. This workshop accesses that model and introduces methods within such programs for selecting and mixing colors with a precision at the limits of human vision.

Color Models

A color model is any system for numerically specifying color, especially within a computer environment. There are several of these depending on the use demanded of the model. However, all are built over the RGB model, which is present in all operating systems.

The RGB primaries are red, green and blue, so that the model specifies color based on the amount of each primary present in a color. The model designates these amounts from a low of 0 to a high of 255. This is a total of 256 or 2^8, otherwise known as 8 bits, for each of the three primaries. There are then a total of 8 bits each of red or green or blue in a color. This means that the total number of possible colors that may be designated is 256 x 256 x 256 or 2^8 x 2^8 x 2^8, or 2^{24} , 24 bits of color. This number, is double that perceivable to the average human and only perceivable to a few trained colorists. Thus 24 bit color is considered full color.

These 17,000,000+ colors can array according to three axes of red, green and blue that are set orthogonal like the X, Y and Z axes of a standard orthogonal grid. Consequently the color space of the RGB model fits into a cube (Figures 1 and 2). The model denotes the position of each color in that space by a scale of 0 to 255 along each axis. Thus this model and all color models requires three values, or coordinates, to specify a color. In RGB the three coordinates are values between 0 and 255, including the achromatic colors between black and white. RGB color is additive, meaning that a full complement of all three primaries (255,255,255) produces white. A lack of all of these, or 0,0,0, indicates black. Any triplet of values that are all the same number will lie on the grayscale since no one primary dominates.

A model very closely related to RGB is CMY, which uses the primaries cyan, magenta and yellow. This model is subtractive, meaning that a full complement of the primaries yields black. It is meant to replicate the mixing of colors with filters. Figures 3 and 4 illustrate the CMY color space. The triple 0,0,0 enumerates white and the triple 255,255,255 enumerates black, exactly the opposite of RGB. Sophisticated graphics programs also supply the CMYK model, where K indicates black. This model imitates mixing with inks, where black ensures the accurate printing of very dark colors. Although inks and paints mix color subtractively, there are no pigments pure enough to produce a black when mixed. Without K the darkest color is a deep, slightly muddy gray.

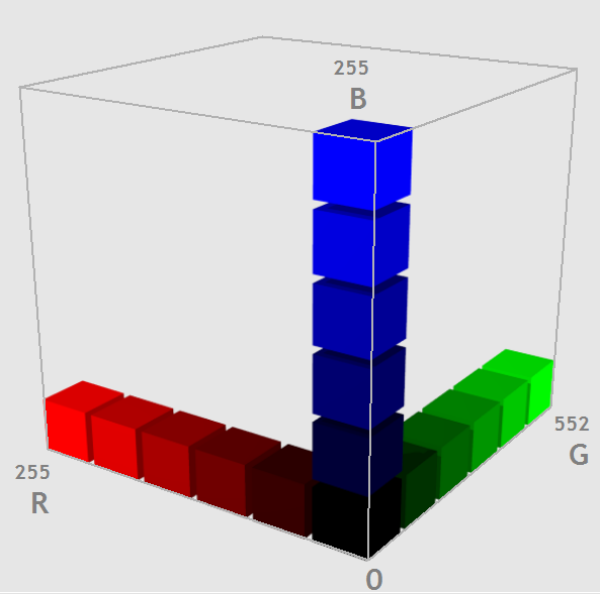

Figure 1. RGB color axes.

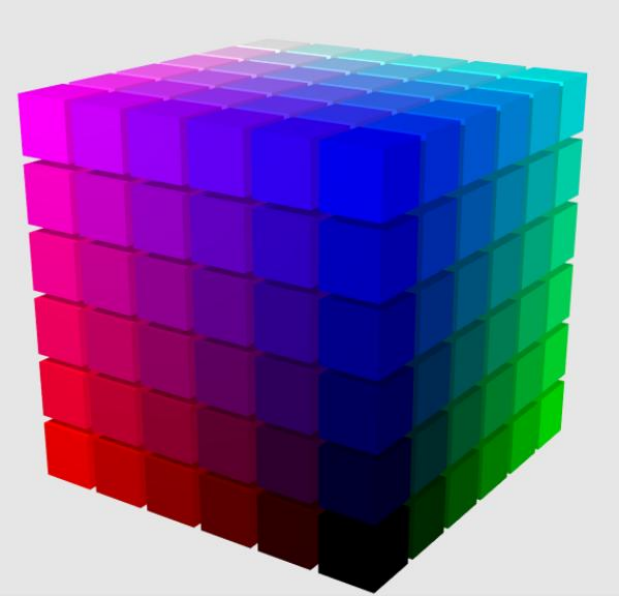

Figure 2. RGB color space.

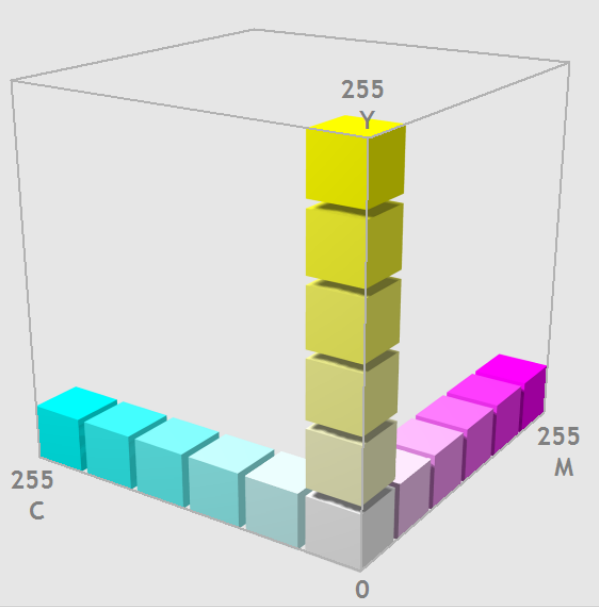

Figure 3. CMY color axes.

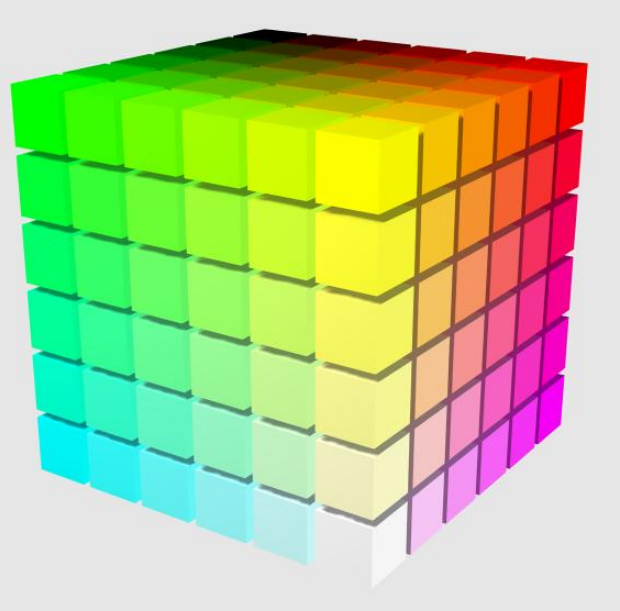

Figure 4. CMY color space.

Mixing Color in RGB

To mix colors in the RGB model from older Word programs click on the paint can at the bottom of the screen after selecting the desired shape. To find the paint bucket in newer versions of Word click on the Drawing Tools tab that appears at the top of the screen upon selecting the shape. Click on More Fill Colors and then on Custom tab in Colors window. This opens access to RGB.

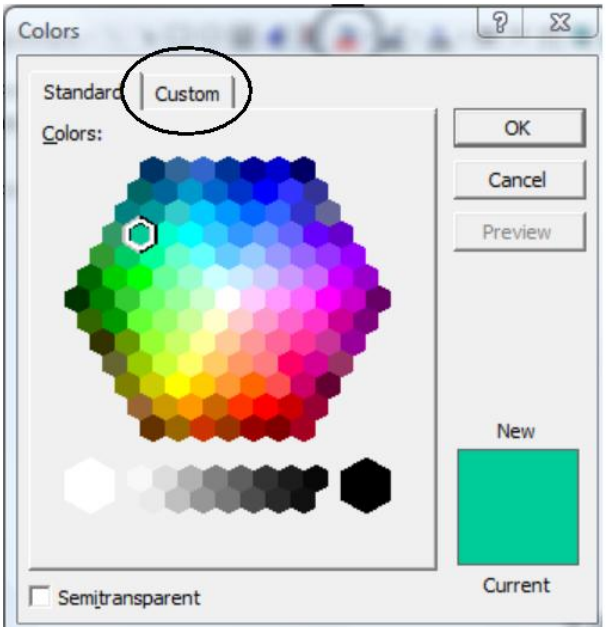

Figure 5. Standard Colors window.

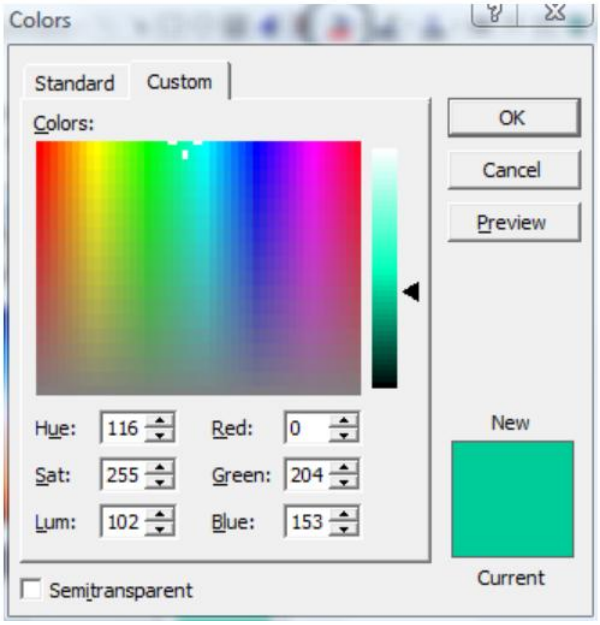

Figure 6. Custom Colors window.

To create a pure red enter 255 at Red and 0 at Green and 0 at Blue for a value triplet of 255,0,0. This ensures that red will not be changed by the inclusion of another primary. The same holds true for the other two primaries: the triplet for green is 0,255,0 and that for blue is 0,0,255 (Figure 5). Since 255 is the highest value, then lowering that value toward 0 while maintaining the other three values at 0 will darken, or *shade*, the primary color toward black.

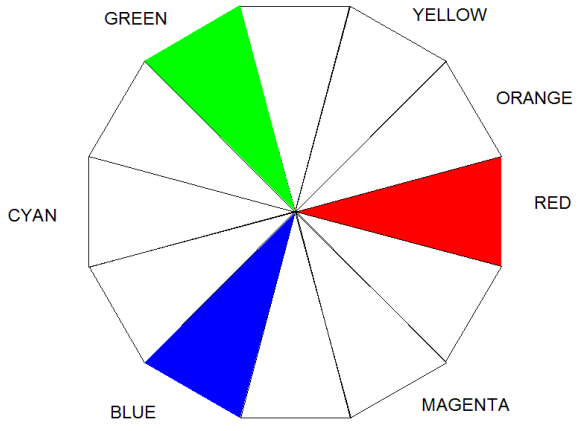

Figure 7. Red, green and blue placed on the color wheel.

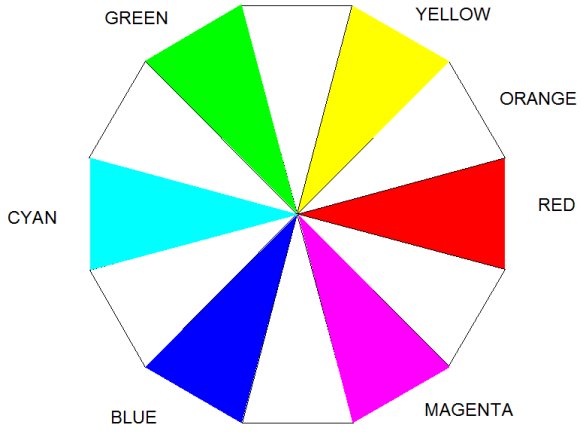

Figure 8. Cyan, magenta and yellow added to the color wheel.

The secondary colors in RGB are cyan, magenta and yellow. On the color wheel above each lies midway between the primaries used to mix them. Thus cyan falls between green and blue; magenta falls between blue and red; and yellow falls between red and green. Note that this differs significantly from paint mixing. A pure secondary demands two pure primaries so that the triplet for a secondary color has two values at 255 and one at 0. Thus yellow has R and G values of 255, but a B value of 0. Raising the value for B while keeping the R and G values at 255 will cause the color to lighten, or tint, toward white as the triplet approaches 255,255,255. Blue, then, is the *complement* of yellow, since its addition to yellow creates white. Similarly red is the complement of cyan (0,255,255), and green is the complement of magenta (255,0,255).

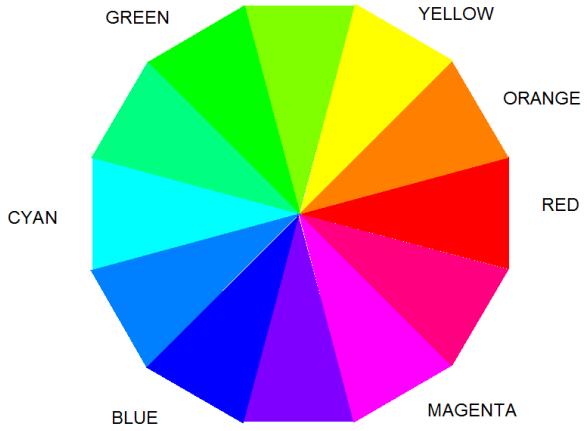

Figure 9. The RGB and CMY, or physical color wheel.

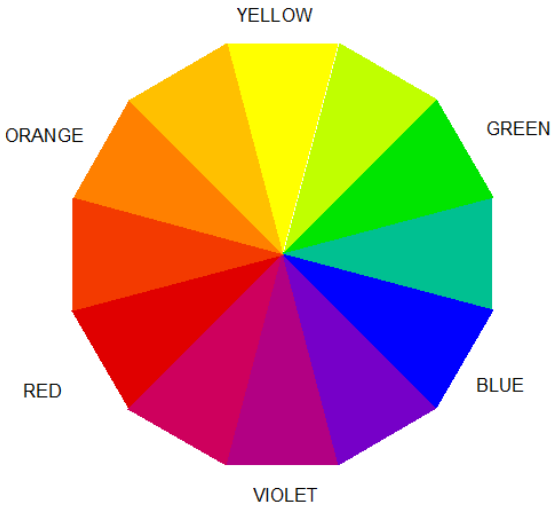

Figure 10. The RYB, or artist's color wheel.

Finding the complement of a given hue requires the simple procedure of subtracting the triplet for the given hue from the triplet for white. Thus the complement for the hue 255,17, 0 is 0, 238,255.

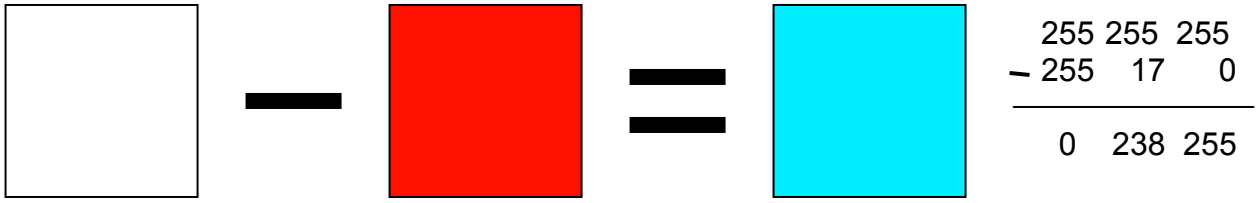

Figure 11. Calculating an RGB complementary pair.

Mixing the six tertiary colors will fill out the color wheel. The tertiary colors are a mix between a secondary color and a primary color. Between red and green are the tertiary colors orange (255, 128,0) and yellow green (128,255,0). Since orange is more red than green the red remains at its full strength of 255, but green is reduced by half to 128. Similarly, cyan green is 0, 255, 128 since green dominates over blue. Note that red becomes 0. Filling out the color wheel: cyan blue = 0,128, 255, magenta blue = 128,0, 255 and magenta red = 255,0,128.

The color wheel may not look like that normally used by painters, where the primaries are RYB, red, yellow and blue. The RGB and CMY color wheels (which appear the same as one another) are physical models of hue relationships. The RYB color wheel is a good guide for mixing with artists' paints. Since it contains a broader range yellow, it also corresponds to the range of colors most distinguishable by the human eye.

Mixing Color in HSL

In the Custom tab of Word's Colors window is a second model based on hue, saturation and luminosity: the HSL model. Note that, like RGB, HSL has three dimensions, which are based on other aspects of color rather than the three primaries.The HSL model has 256 different hues beginning at 0 for red and then circling the color wheel and returning almost to red again at 255. Saturation is a measure of the hue in a color, lowering as it fades toward the *achromatic* scale of white, grays and black. Since a pure hue has maximum saturation its S value is 255, while the S value of all 256 colors on the achromatic scale is 0. Luminosity measures the lightness or darkness of a color. For this reason the L value of each pure hue is automatically set at 128. As a color lightens its luminosity rises toward 255; as it darkens it descends toward 0.

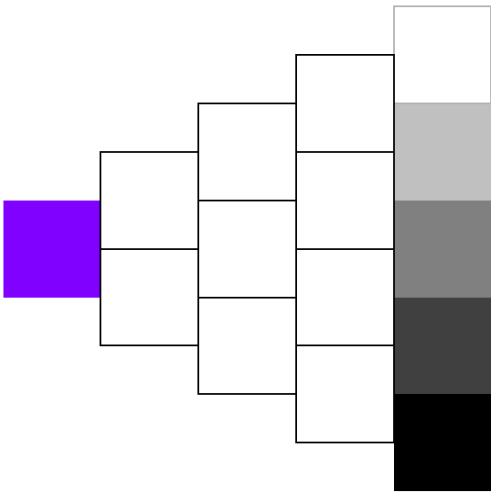

Figure 12. Pure hue and achromatic scale on the hue triangle.

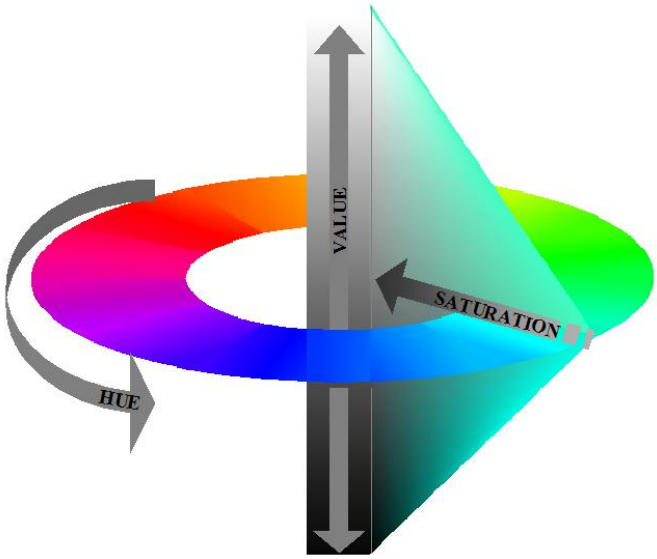

Figure 13. HSL color space/

The clearest demonstration of the HSL model is the mixing of a hue triangle. This triangle has rotated sideways so that its base is vertical and its apex points to the side. It features a pure hue at its apex and an achromatic scale along its upturned base. The colors on this scale move from maximum saturation as they move from the pure hue to the achromatic scale. At the same time, they spread toward white and black.

Choose a pure hue, specifying its H value and setting the S value to 255 and the L value to 128. The triplet for blue magenta in the apex of the triangle in Figure 12 is 192, 255, 128 in HSL.

Mixing a gray scale: to create a middle gray lower S to 0 and keep L at 128 for a triplet of 192,0,128. Since there is no hue in the gray scale any H value will work. In this case the H value is just a placeholder, so it is included in the triplet for gray. In order to create white and black keep S at 0 and move L to 255 and 0, respectively. White will equal 192,0,255 and black will equal 192,0,0; light gray will equal 192,0,192, or mid way between the L values for white and gray, similarly dark gray will equal 192,0,64.

The upper side of the triangle is *tinted* toward white. Mix the tints of a hue in the scale by raising the L value incrementally from 128 to 255. There are four steps so each increment is ¼ of 128, or 32. The descending side of the triangle is *shaded* toward black. Mix the shades of a hue in the scale by lowering the L value incrementally from 128 to 0. There are four steps so each increment is 32. There are three tones in this scale. These are: the mid tone (192,128,128) a high tone (192,64,160) and a low tone (192,64, 96). The mid-tone lies halfway between the pure hue and the middle gray. To mix simply halve

the S value to 128. The high and low tones on this scale are in a row of 25% saturation with S values of 64, or ¼ of 256. In this row the top color has an L of 224 and the bottom color has an L of 32 for a difference of 192 to yield increments of 64 between the four colors.

Often a hue triangle is paired with its complement so that the two hue triangles are mirrored into a horizontal diamond. The difference between two complementary hues in HSL is 128, or ½ of 256. In this case the H value is 192 □128, or 64. Mix this hue on the right apex of the scale in Figure 14. Finish out the right triangle by using the same SL values as the left triangle and a consistent H value throughout. Note that in this scale, all colors on the same horizontal row have the same luminosity value. Those in the same vertical column have the same saturation value (Figure 14).

A set of all 256 hue triangles sharing the same gray scale will yield the HSL color space, which is a double cone depicted in Figure 13.

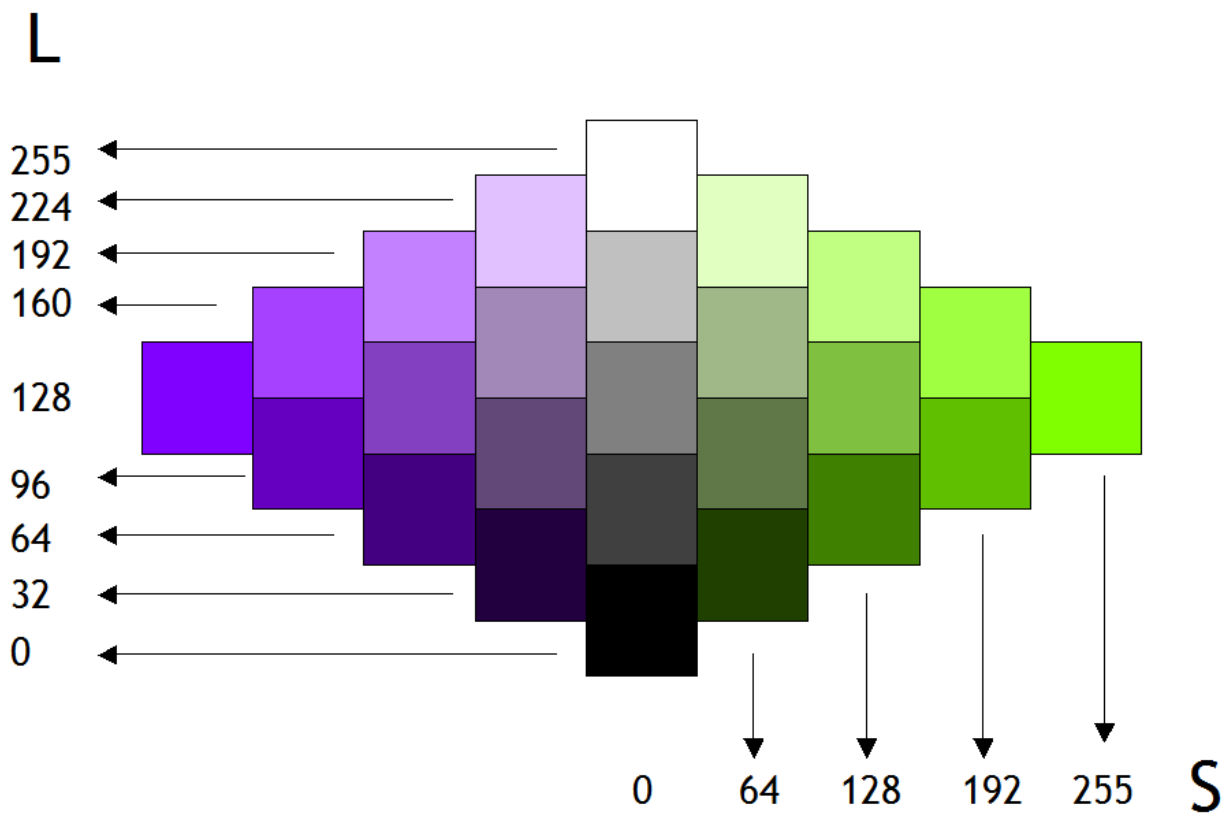

Figure 14. Scale of complements.

Middle Mixtures and Transparency

Often color harmonies are based on a scale mixed between two key colors of the composition. The scale for the example in Figure 15 has as its endpoints two key colors plus the gradation between them. The three colors inside this scale are called middle mixtures. The two colors were selected for their contrast. A check on the HSL triplet for the green reveals it to be 57, 255, 179. Its RGB triplet is 204,255,102. The orange has an HSL value of 21,255,102. It has an RGB value of 205,102,0.

At the center of Figure 15 below is the table of calculations for the differences between the numerical codes of the two colors as determined under both the HSL and RGB models. The differences are then

divided by 4 to determine the increments in each value. In this case H differs by increments of 9 (36 divided by 4), S will not differ, and L differs in increments of 19 (77 divided by 4). In the case of the RGB values the increments of change will be 0 for R, 38 for G and 25 for B.

Flanking this table are the scales of gradients containing the middle mixtures produced by both models. The RGB coding is perceptually accurate while that produced by HSL coding is not. HSL is ineffective for the straight-line mixing between two arbitrary colors, while RGB is excellent. The HSL model is good for selecting color or for mixing within a single hue. RGB is good for mixing between two given colors.

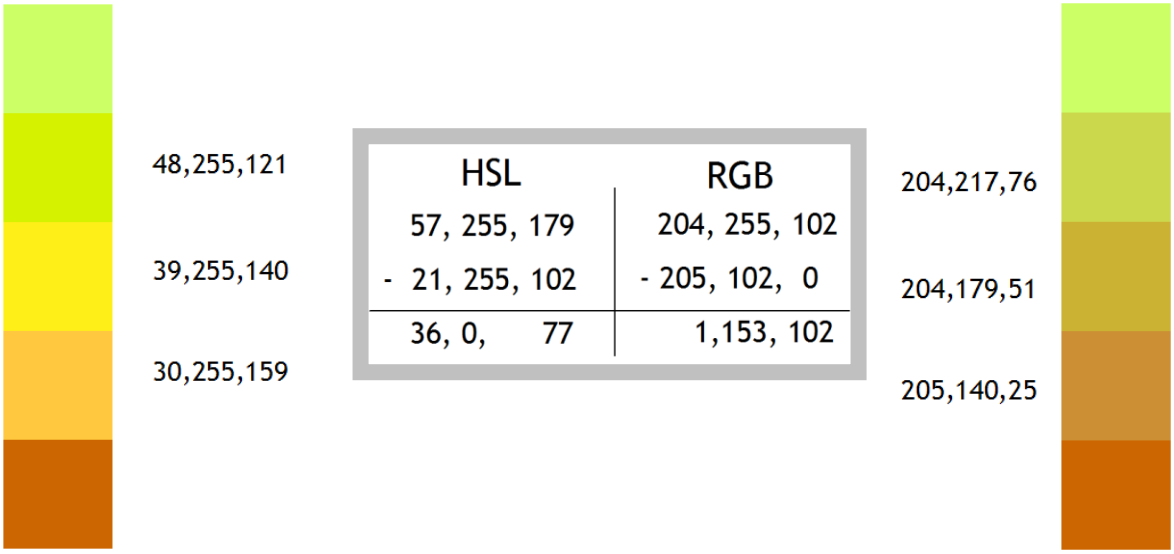

Figure 15. Middle mixing in HSL and RGB

Artists employ middle mixtures in order to create transparency effects. The samples in Figure 16 use each of the three middle mixtures to color the area of intersection of two shapes of the original colors. Each produces a transparency: one where the green is forward, one where the two shapes lie on the same plane and one where the orange is forward.

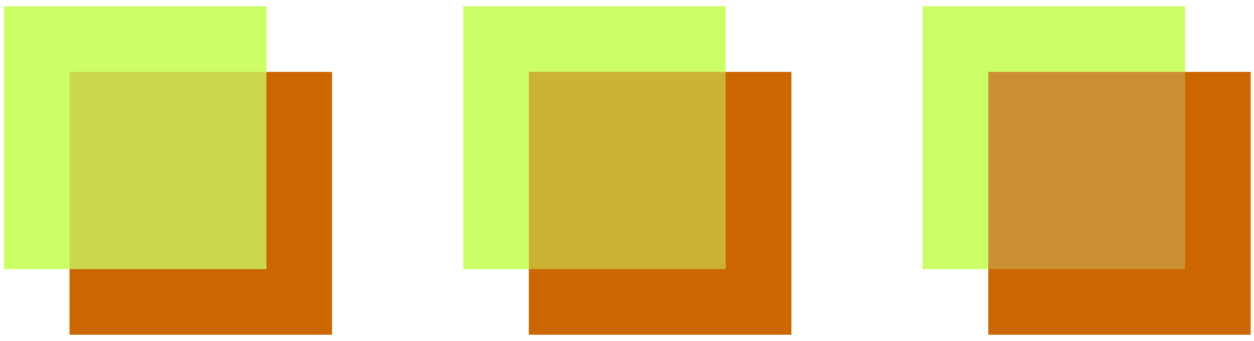

Figure 16. Transparencies created with the three middle mixtures on the RGB scale in Figure 16.

Figure 17 has added middle mixing between the original green and orange colors and the white of the paper. The triplet for the green when averaged with white (255,255,255) becomes 230,255,179; the orange becomes 230,179,128. The area of intercept, however, remains the same as in Figure 16. Note how in Figure 17 the middle transparency creates an additive effect and strongly conveys the feel of two translucent tissues overlaid on a white surface.

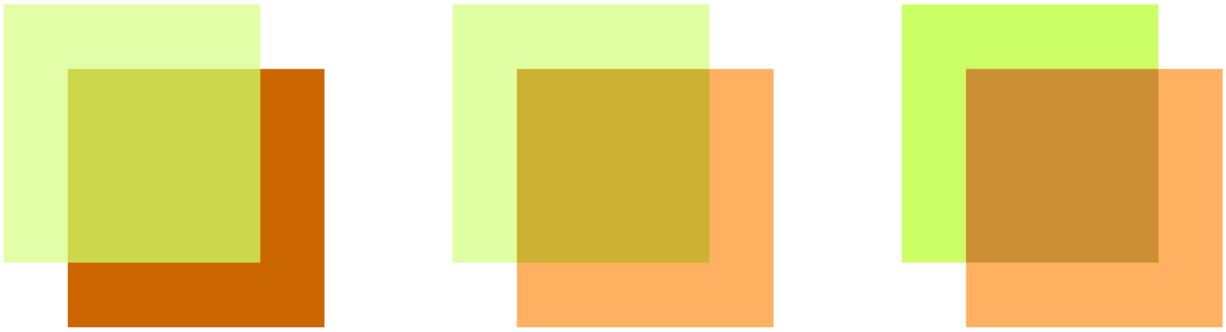

Figure 17. Transparencies featuring middle mixtures with the background color.

Conclusion

Operating systems incorporate two complementary color models. The HSL model is excellent for color selection or mixing a single color. Artists familiar with hue, saturation and luminosity can modify color by raising or lowering the numerical values for each dimension until the color visually matches the color sought by the artist. However, once colors are chosen mixing between the colors becomes the task of the RGB model.

Building a Scherk Surface from Paper Tiles

Stephen Luecking
School of Computer Science,
Telecommunications and Information Systems
DePaul University
sluecking@cs.depaul.edu

Abstract

Double curved surfaces such as a sphere or, in the case of this paper, a hyperbolic paraboloid are problematic to create from paper, a material more amenable to developable surfaces. However, one can break a double curved surface into polygonal facets that do an acceptable job of visually approximating that surface. By this means one can unfold the polygonal surface structure into a flat pattern that may be printed, cut and scored, and then folded into the desired surface. In this case the surface to build is the Scherk periodic minimal surface.

Introduction

A hyperbolic paraboloid (hypar) module in the proper configuration offers some intriguing possibilities for deploying saddles in space in order to tile periodic minimal surfaces. One especially elegant tiling scheme derives from the structural geometry presented by Peter Pearce in his book Structure in Nature Is a Strategy for Design. Pearce presents the case where the 90º regular saddle hexagon and the 60º regular saddle rhombus can tile space to form a continuous system of tubular surfaces. As it turns out either of these three-dimensional polygons will tile to form the Scherk periodic minimal surface (Figure 1). Pearce notes that both of these saddle polygons subdivide into identical hypar surface patches in the form of a kite. Consequently this patch serves as the single, common module for building Scherk's surface. In order to craft this module from paper the builder must first triangulate the kite's surface and then unfold the triangular faces into a 2D pattern.

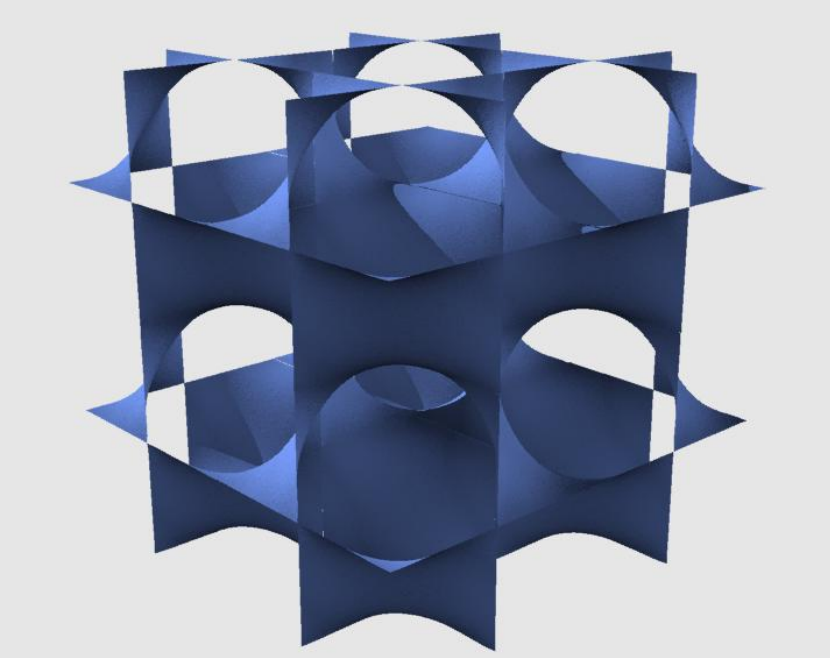

Figure 1. Scherk periodic minimal surface.

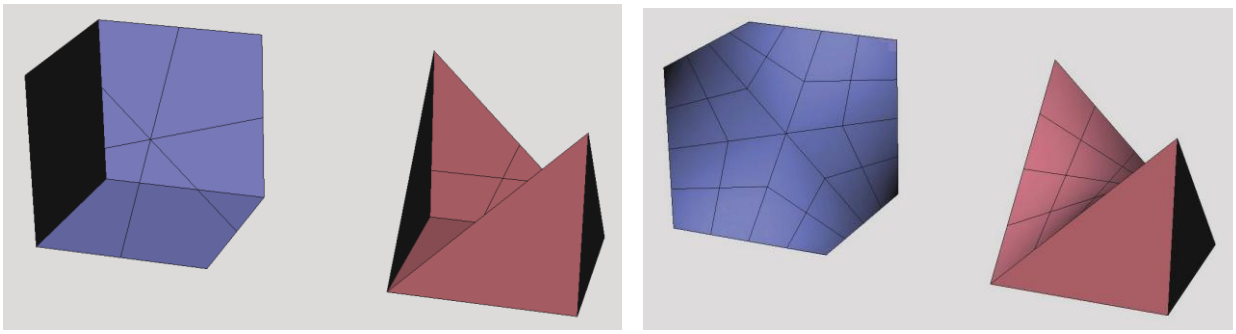

Figures 2 and 3. Creating the 90º saddle hexagon and the 60º saddle quadrilateral from the cube.

Saddle Polygons

Pearce derives a host of saddle polygons by extracting their edges from a dense grid of all possible cubic symmetries that he terms the Universal Node System, a grid matrix of cubes whose interiors and faces are traversed by their diagonals. A more direct method for constructing these two saddles exploits the relationship each bears to the cube. Edging the saddle hexagon is a transit of six edges on the cube, splitting the cube in half; edging the saddle rhombus is a transit of four diagonals of the cube also splitting the cube in half (Figure 2). In each case half of the faces of the cube are removed to reveal edges of the respective polygons. With the addition of the armature of mid-edge diagonals as shown in Figure 2 the stage is set for building the saddles from a circuit of hypar surface patches in the form of a kite (Figure 3). It turns out that the kites for both saddle polygons are congruent, allowing the 60º regular saddle rhombus and the 90º regular saddle hexagon to intersect by their identical kites (Figure 4).

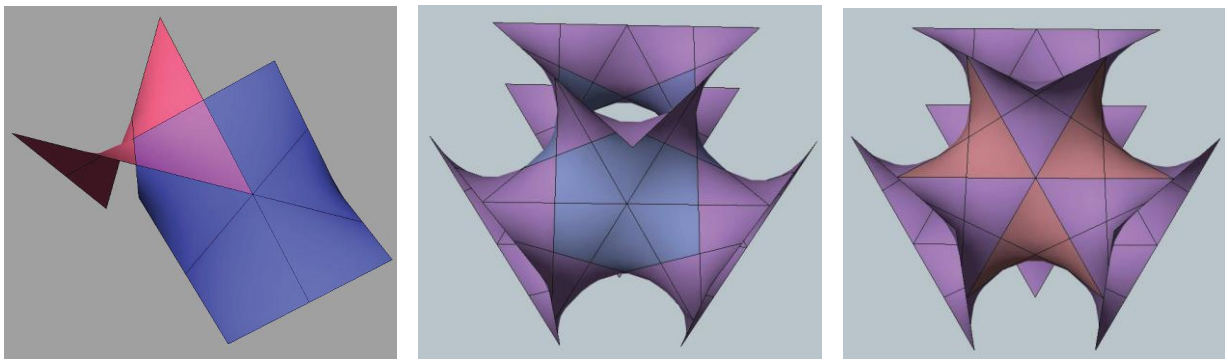

Figure 4. In both saddle polygons the mid-edge diagonals divide the surfaces into the same hypar kite. Figure 5. Scherk surface tiled with the 90º saddle hexagon. Figure 6. Scherk surface tiled with the 60º saddle quadrilateral.

With a little experimentation the possibilities for three-dimensional tiling of these saddle polygons become apparent. Either polygonal surface repeats to generate a continuously curving surface, which develops into tubular foam that displays some elegant symmetries (Figures 5 and 6).

Module Design

For the purposes of tiling only a single module, the shared hypar kite alone, suffices. By triangulating the hypar kite it is possible to build physical representations of these surfaces from folded paper modules (Figure 7). The simplest such triangulation uses four triangles such that each triangle has as its base one

side of the kite and as its apex the saddle point of the hypar located at the intersection of the hypar's mid-edge diagonals (Figure 8).

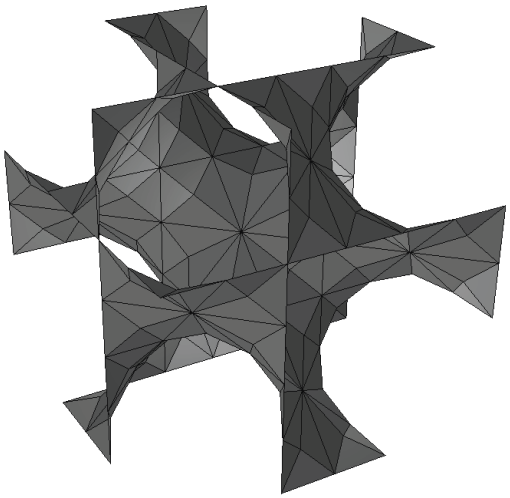

Figure 7. Triangulated periodic surface.

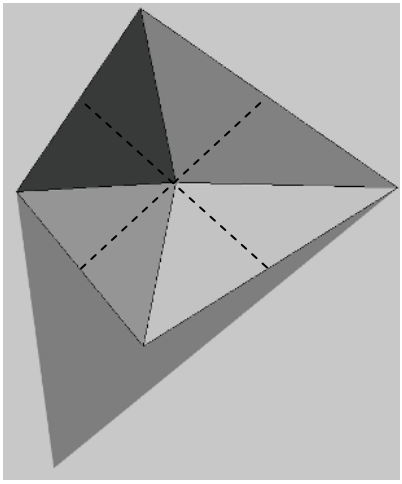

Figure 8. Triangulated kite.

Six kites orienting their curvature in alternating up-and-down directions and glued in a radial pattern by their long edges yields the 90º regular saddle hexagon, while four kites joined about a center by their short edges produces the 60º regular saddle rhombus (Figure 9). Thus the two polygons intersect by the same kite (Figure 10).

Based on figure 10 it is apparent that four 90º hexagons will tile around a common point, and that six 60º rhombuses will tile around a common point, to produce the same surface.

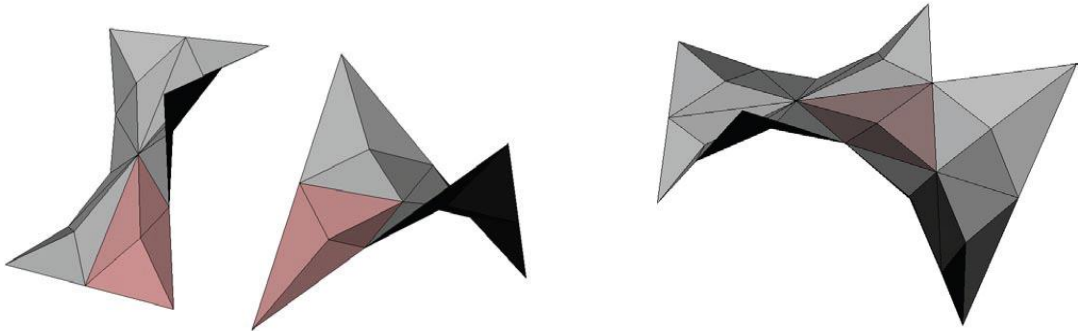

Figure 9. 90º regular saddle hexagon and 60º regular saddle rhombus triangulated from kites. Figure 10. Overlap of these polygons as a kite.

Figure 11a is a portion of the Scherk periodic surface constructed from these kites. Figure 11b reveals the same surface with one of its 90º hexagons outlined. The hexagon works as a kind of architrave at the juncture of a Scherk surface□s tubes. The 60□rhombus, on the other hand, wraps around the tubes (Figure 11c). These figures also reveal that at each juncture four tubes meet with four hexagonal architraves bridging between them in tetrahedral symmetry (Figure 12). The angles of intersection correspond to the intersecting edges of packed rhombic dodecahedrons.

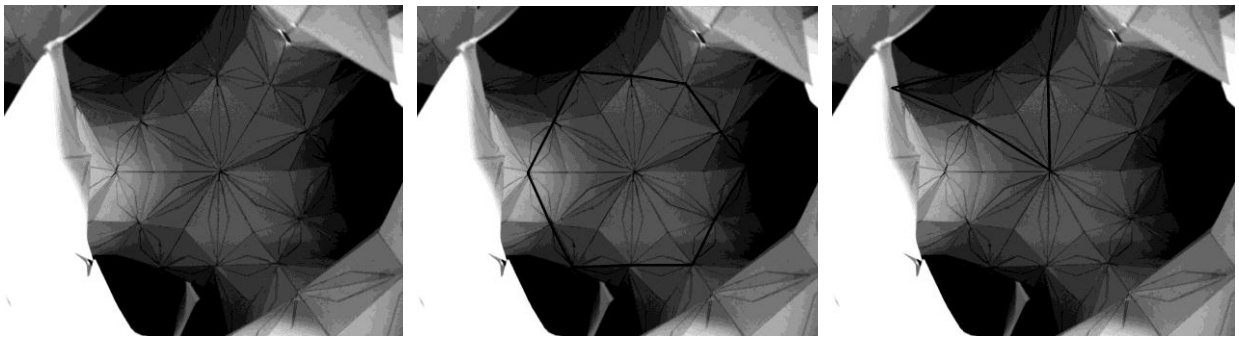

Figure 11a. A view of the paper Scherk surface through one of its hollows. Figure 11b. The 90º regular saddle hexagon on the Scherk surface. Figure 11c. The 60º regular saddle rhombus on the Scherk surface.

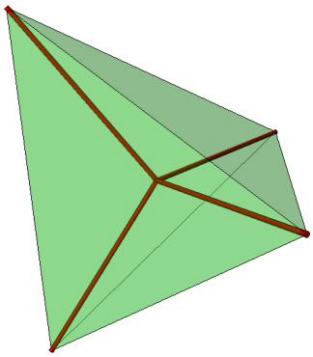

Figure 12. Center of a tetrahedron connectedto its vertices.

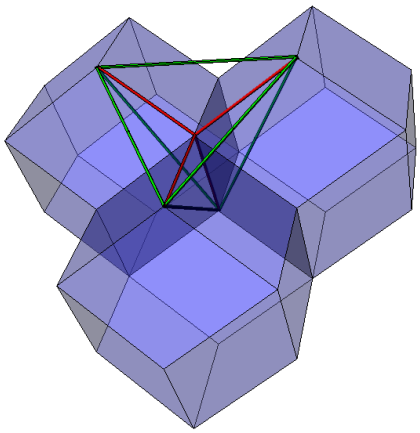

Figure 13. Tetrahedral junction of rhombic dodecdahedrons.

Figure 14 diagrams the pattern for folding and assembling the kites. There are two patterns, one the mirror of the other. Trial and error proved that, since any two adjacent kites are flipped relative to one another, mirroring the patterns aided assembly.

The kites hinge together with folded rhombuses keyed to the length of their edges. The rhombuses in turn generate a highly symmetric decorative pattern across the surface and transform what might have been a distractive joining into an enhancement of the surface.

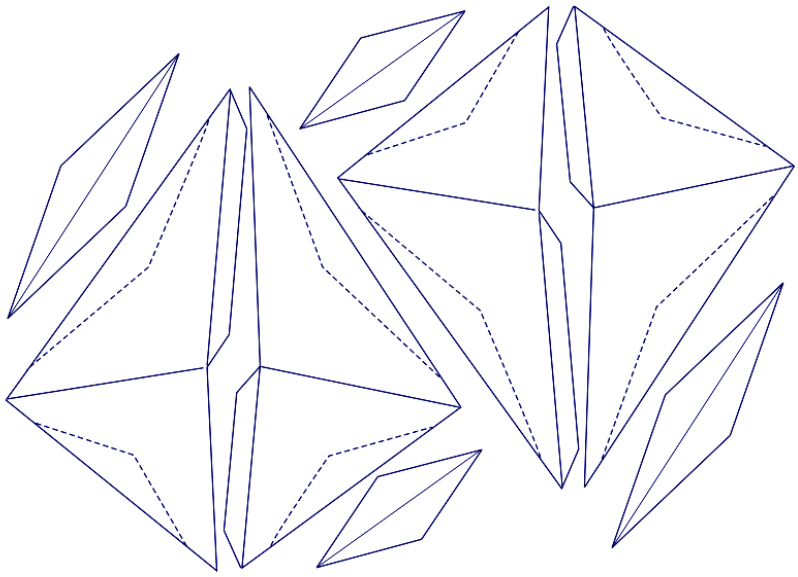

Figure 14. Patterns for the triangulated hypar kite and the rhombic connecting tabs.

Sculpture From a Space Filling Saddle Pentahedron

Stephen Luecking
School of Computer Science,
Telecommunications and Information Systems
DePaul University
Email: sluecking@cs.depaul.edu

Abstract

A variety of polyhedrons whose edges are non-planar may be bounded by minimal saddle surfaces. By virtue of their saddle formation these surfaces can mate and, in cases where the polyhedron's edges derive from a cubic lattice, they may pack space. One such space packing polyhedron possesses five saddles and is thus dubbed a pentahedron. The subject of this paper is a pentahedron, which will pack space along the course of a Scherk periodic minimal surface. The pentahedron may then be utilized as a module for constructing sculptures comprising minimal surfaces of simple and complex saddles. This paper demonstrates sculptural studies built from paper constructions of this pentahedron.

Introduction

Peter Pearce in his book Structure in Nature Is a Strategy for Design offers a host of space filling polyhedrons, whose edges are straight, but whose "faces" are saddle surfaces. Pearce derives these by extracting their edges from a dense grid of all possible cubic symmetries that he terms the Universal Node System, a grid matrix of cubes whose interiors and faces are traversed by their diagonals. Part and parcel of their space-filling property comes the option of assembling these as modules to create more complex sculptural forms. The saddle polyhedron under consideration here is a pentahedron all of whose surfaces are hyperbolic paraboloids, or *hypars*.

Of key interest is the one face that is a 60º regular saddle rhombus. This surface bears the capability of tiling the periodic version of the Scherk minimal surface (Figure 1). This surface divides the 3D space it occupies into two complex halves, one of which may be filled while the other remains empty. This creates sculptural interest by virtue of the dichotomy between strongly formed volumes and their complementary masses. If the pentahedrons pack such that the 60º regular saddle rhombuses all remain open, then the packed space will comprise equal regions of mass and volume, bordered by the Scherk surface.

This paper surveys the creation of the saddle polyhedron required to effect such a space and the sculptural possibilities it offers.

The Pentahedral Module

Figure 2 displays three views of a digital model of the pentahedron. The third view reveals its essentially cubic symmetry. Four of the surfaces of this figure, all hypars, flank the sides of the 60º regular saddle rhombus that constitutes the fifth face of this polyhedron.

Figure 3 demonstrates the joining of two pentahedrons by matching the flanking surfaces and leaving their saddle rhombuses exposed. Note that this joining creates a continuous surface tiled from the rhombuses.

Figure 4 portrays an alternate joining by matching the pentahedrons by the 60º regular saddle rhombuses. The figure that results is the regular saddle tetrahedron. This figure will pack space as in Figure 5. The pentahedron will pack space by virtue of its ability to join to form the saddle tetrahedron. This is the basis for the pentahedron s ability to serve as a module for creating sculpture.

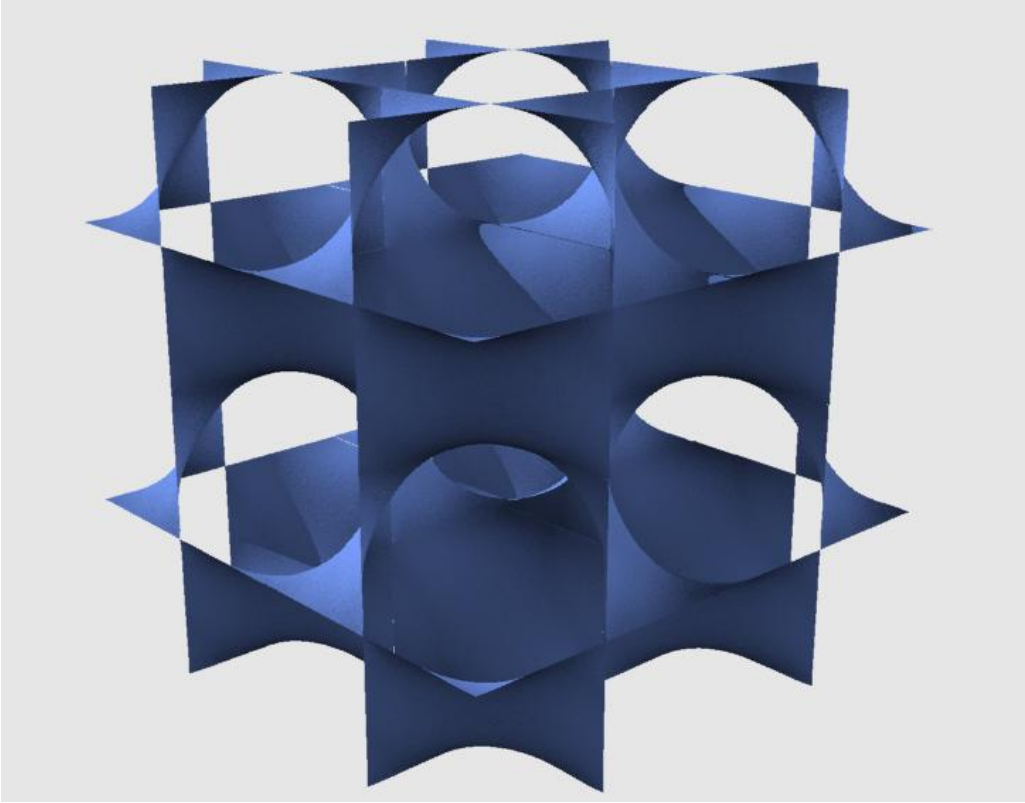

Figure 1. Scherk periodic minimal surface.

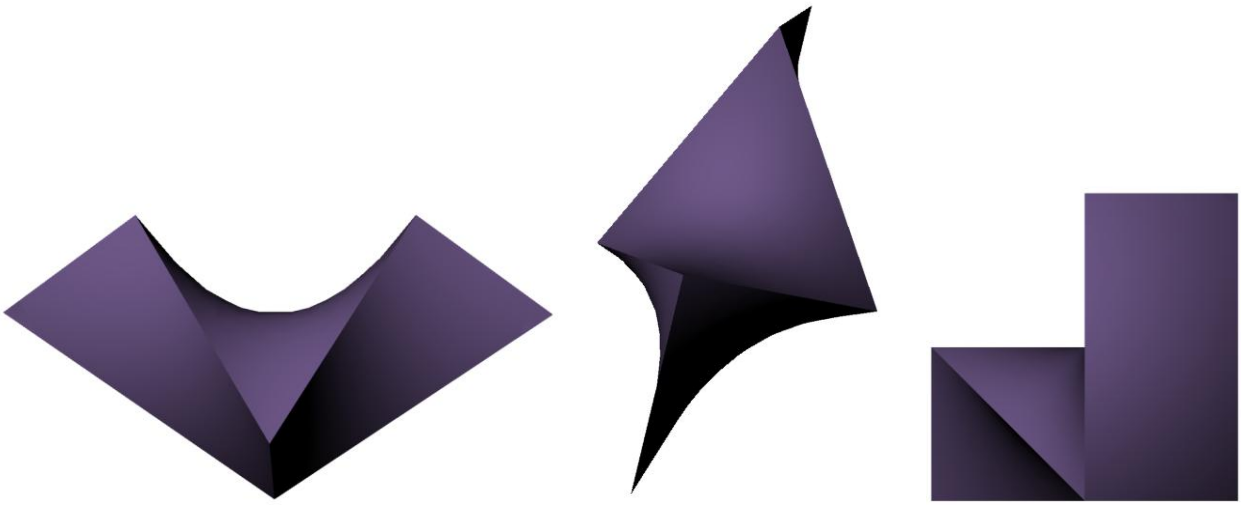

Figure 2. Three views of the saddle pentahedron.

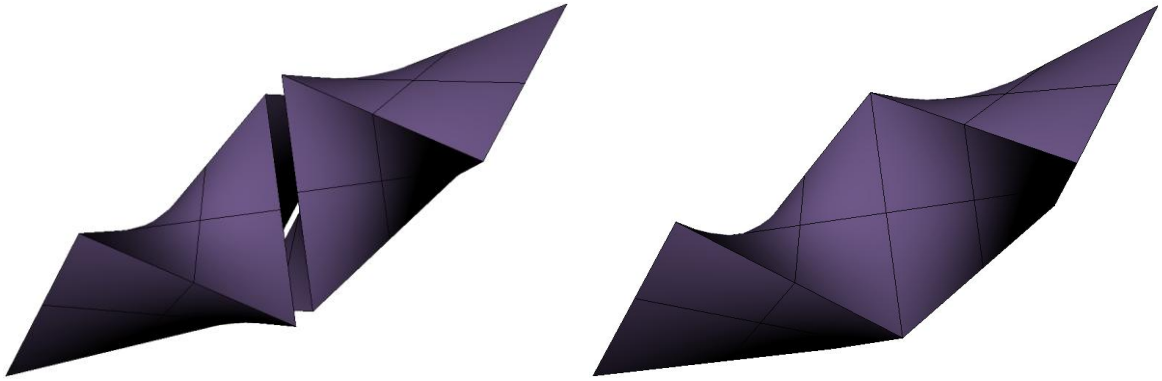

Figure 3. Two pentahedrons joining at their flanks.

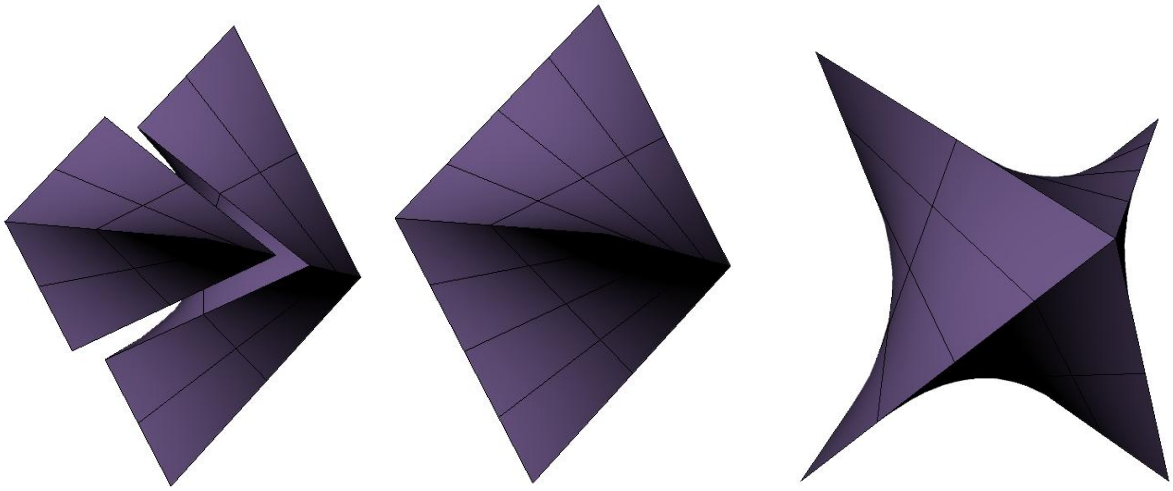

Figure 4. Two pentahedrons joining into a saddle tetrahedron.

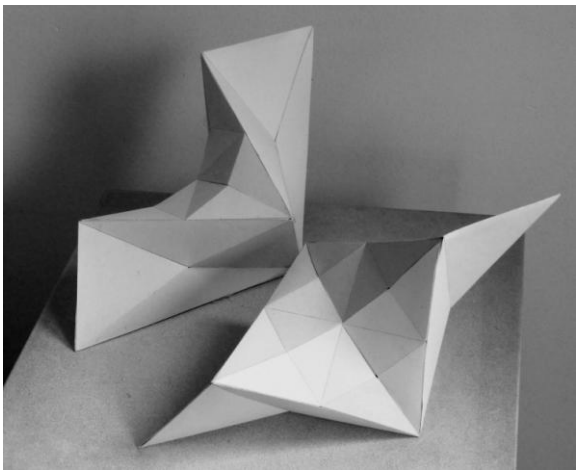

Figure 5. Packing the regular saddle tetrahedron. Figure 6. Triangulated paperboard models of the pentahedron.

Sculptures from Pentahedrons

A triangulated model of the pentahedron (Figure 6) displays the same joining properties as does its fully curved counterpart (Figure 7 and 8). All of the sculptures comprise six of the pentahedron modules in symmetrical arrays. Each portrays a different segment of the Scherk surface. Figure 9 depicts two positions of the sculpture Claw. This construction forms the segment of the Scherk surface at the juncture of three of its "tubes". (The periodic version of the Scherk surface may be imagined as a network of tubes, such that the four tubes meet at each juncture in tetrahedral symmetry.)

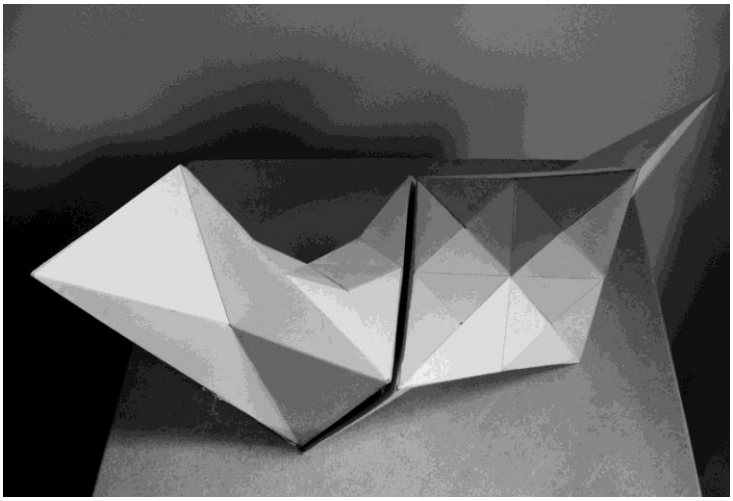

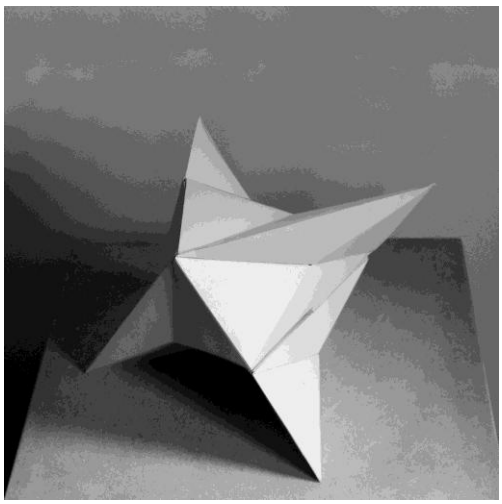

Figure 7. Two pentahedrons joined at the flank. Figure 8. Two pentahedrons joined at the 60º regular saddle rhombuses.

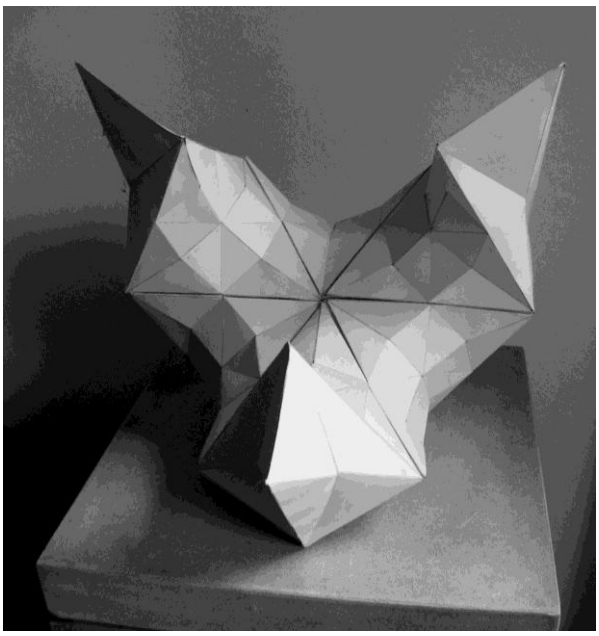

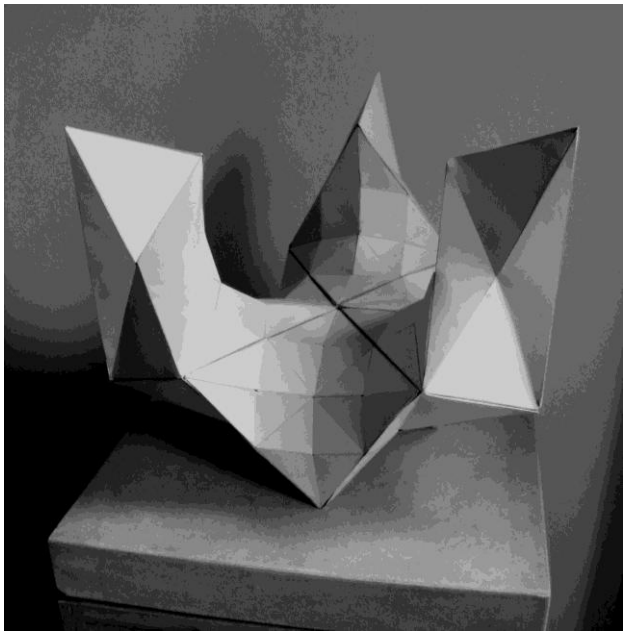

Figure 9. Claw, positions 1 and 2, paperboard, 2010.

Claw presents the meeting of three half tubes and the architrave that provides continuity between the tubes. Repeating Claw four times and joining all four copies will form the juncture of all four tubes.

As seen in Claw, six pentahedrons proved sufficient to create a formally intriguing sulpture. Figure 10 displays a study for the sculpture Star Torus, also comprising six pentahedrons in a similarly intriguing sculpture. Star□s inner surface is the band surrounding the girth of one of the tubes. This surface matches the torus segment on the outer surface of the study for Rotator in Figure 11. Both sculptures present identical segments of the Scherk surface. They differ in that the space each packs is on opposite sides of that surface.

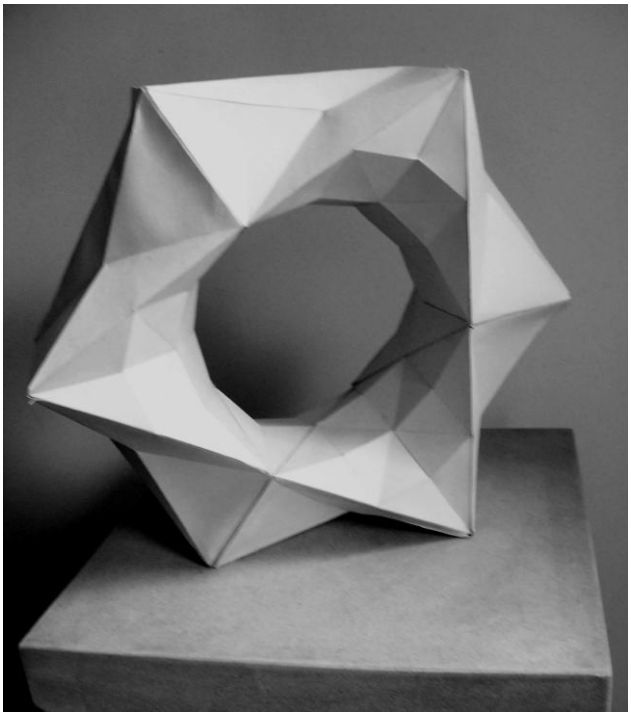

Figure 11. Star Torus, paperboard, 2010.

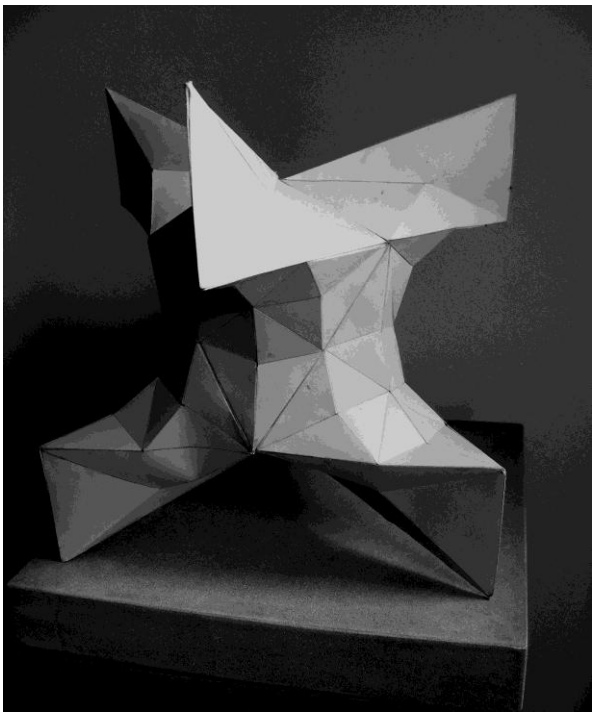

Figure 12. Rotator, paperboard, 2011

Extra Ways to See: An Artist's Guide to Map Operations

James Mallos
Sculptor

Silver Spring, MD, USA
E-mail: jbmallos@gmail.com

Abstract

A map operation converts one mathematical model of a surface into another, and can thereby suggest to the artist or artisan different ways of building or decorating a given surface. A truchet tile technique is presented that allows many common map operations to be represented by truchet tiles of triangular shape. These map operations can also be defined pictorially by their action on a monogon embedded in the sphere. Truchet tiles for twenty-one map operations are illustrated along with examples of their use in the design of weaving and tensegrity structures.

Introduction

Familiarity with map operations can spark the visual imagination. For example, it might be surprising that a map with all triangular faces (think of the edges of an icosahedron projected onto the sphere) can be trivially converted into a map with all quadrilateral faces, or into one with all pentagonal faces, or into a design for a weaving, or into a design for a tensegrity structure. Seemingly alchemical changes like these are effected by map operations. The operations themselves are quite simple, so simple that many can be represented visually by truchet tiles; that is, by specially patterned tiles designed to fit together, side-by-side, to help visualize a larger pattern. This article illustrates truchet tiles for many map operations and gives some examples of their practical use.

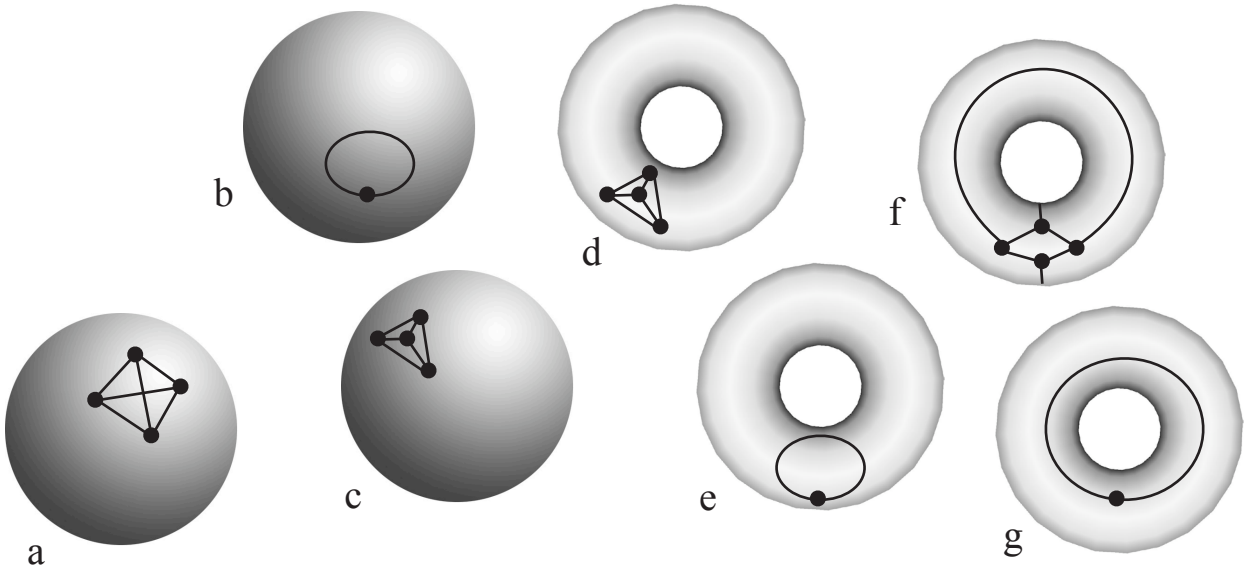

Figure 1: *Which of these are maps? Only b, c, and f.*

Definition of a Map. Abstracting the definition of a *map* given in [1]:

A map is a graph drawn on a closed surface in such a way that:

a) the vertices are represented as distinct points on the surface,
b) the edges are represented as curves on the surface intersecting only at the vertices,
c) if we cut the surface along the graph, what remains is a disjoint union of connected components, called faces, each topologically equivalent to an open disk.

Examples: a monogon (i.e., a single vertex with a self-loop) is a map when drawn on the sphere; on the torus it can be drawn several different ways, but none succeeds in being a map because one of the faces will fail to be a topological disk. The skeleton graph of a tetrahedron is a map when drawn on the sphere without crossings—and also a map if drawn on the torus in a particular way (see Figure 1.) In computer science terms: if a graph encodes the topology of the surface it is drawn on, then it's a map.

A practical use of maps is to mathematically describe a surface we are interested in making or decorating.

Map Operations. Map operations are procedures that convert one map into another [2-3]. Map operations are known under various guises in different fields, most notably in Conway's polyhedron notation [4], in computer graphics, where they appear as various *subdivision schemes* [5-8], and in geodesic dome design, where they appear as various *geodesic breakdown schemes* [9].

Many map operations can operate indiscriminately on map faces that are monogons, digons, or n-gons. Many map operations (namely, the achiral ones) work just as well on surfaces that are orientable and nonorientable, and surfaces of any topological genus. This wide scope of application is why we should indeed prefer to speak of *maps,* not limiting ourselves to polyhedra or computer graphics surface models.

Some map operations are fundamental: *identity, dual,* and *reflect* are of first importance (reflect [4], unfortunately, is one that cannot be accomplished with truchet tiles.)

Some map operations are composite, meaning that they can be accomplished by performing a sequence of other map operations in a specified order (note that map operations are not generally commutative.) But, since truchet tiles cannot compose map operations—nor can the visual imagination do this very easily—some composite map operations are presented here.

Names and Notation. I have strayed from Conway's operation names only in the case of *medial* and *radial,* terms well established in the graph theory literature. Conway's concise notation system can be a little cryptic for the novice, and, in any case, with twenty-one (and counting) map operations, a suitably mnemonic mapping to the 26 letters of the alphabet is beyond reach. Instead, I adopt here the two-letter function notation common in the map operations literature. For the names of map operations not in Conway, I have adopted Hart's *propellor* and *reflect* [4], and elsewhere followed precedents in the map operations literature, but I have rejected subscripts and numerals, and insisted that "action" names be in verb form. Two operations well-known in the computer graphics literature, have been dubbed with the first two letters of the names of the authors most associated with each [5-6]. A composite operation which is particularly useful in ring weaving has been dubbed *ring.*

Having abbreviations of operation names allows one to write out composite operations and identities in function notation. For example, the fact that a map and its dual yield the same medial is expressed:

$Me(M) = Me(Du(M))$.

Order, Type, and Chirality. Map operations can be ranked in orders according to the number of edges they place in the resultant map when the base map is a monogon drawn on the sphere. For example, *identity, dual,* and *reflect* make up the first order, each placing a single edge in the resulting spherical map. *Subdivide, parallel, radial,* and *medial* make up the second order, each placing two edges in the resulting spherical map... and so on.

Map operations can also be typed according to whether, like *identity,* they *include* the original vertex of the monogon base-map, or, like *dual*, they *delete* it. The former will be called *i-type,* and the latter *d-type.*

Map operations that are *chiral* come in left-handed and right-handed varieties (thus they cannot be used on a surface that cannot be oriented, such as a mobius strip.) All four of the *chiral* map operations in the present collection are fifth order.

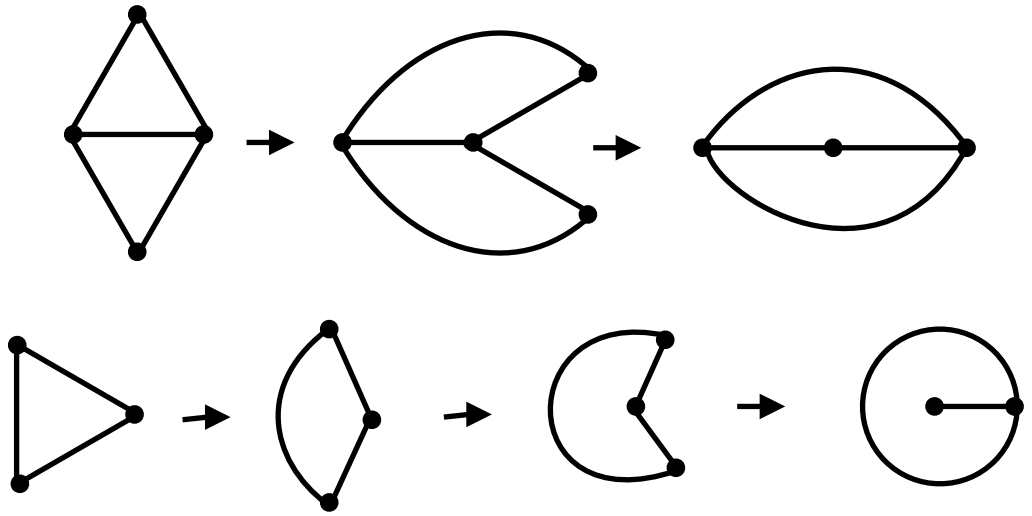

Figure 2: *Stretchy triangular tiles can stretch to tile digons (above) and monogons (below.)*

Representing Map Operations with Truchet Tiles

Stretchy Tiles. The truchet tiles contemplated in this paper are stretchy. That is, we will imagine that a patterned triangular tile can be stretched to conform to any size or shape of triangle. A vertex angle can be stretched open to 180 degrees—enabling two such tiles to tile a digon (see Figure 2.) Even further, a vertex angle can be stretched open to a full 360 degrees, enabling it to tile a monogon by itself. Note that the stretched triangles still have three sides in these tilings—they are topologically still triangles.

Though paper or ceramic tiles cannot stretch in this way, it is possible to mathematically define a mapping (texture-mapping) carrying a pattern or texture from an equilateral triangle onto a half-circle or full circle. If the truchet pattern represents fiber elements (weaving) or building elements (tensegrity) the pattern joins across tile boundaries are equally valid when the the tile has been stretched in this way.

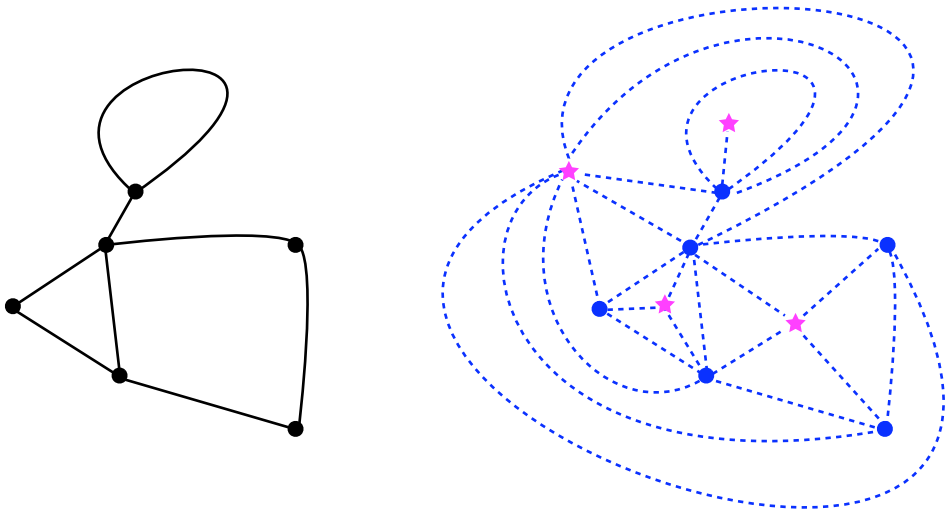

Figure 3: *Kis on an arbitrary map. Every face in the resultant map is a triangle.*

Kis First. To effect map operations with truchet tiles that are all of the same shape, we need to give priority to a particular map operation. Conway's name for it is *kis*. A truchet tile that pictorially defines kis will be introduced later, but in every case we will need to perform kis algorithmically as a preliminary to laying down tiles. The preliminary use of kis erases the base map (i.e., the map we are performing the operation on,) and replaces it with a set of "chalk" guidelines whose ultimate fate is to lie hidden behind truchet tiles (see Figure 3.)

Algorithm for the Preliminary Kis:

```
with pink chalk, mark a new vertex in the
center of each face in the base map,

with blue chalk, draw edges connecting the
new vertex to each of the old vertices
surrounding that face,

erase-and-redraw, using blue chalk, all of
the old vertices and edges of the base map.
```

The kis operation subdivides every face of the base map into triangles, including monogon faces, digon faces, and faces that were triangles to start off with. It thereby eliminates the need for truchet tiles in any other shape: all we need are tiles in the shape of kis triangles. We will refer to these as *kis-truchet tiles*. Note that kis-truchet tiles are not rotationally symmetric. That is why the new vertices are colored pink: to mark how the kis-truchet tiles should be oriented.

Illustrating Kis-Truchet Tiles. There are two ways to illustrate a kis-truchet tile. Drawn as a one-third portion of an equilateral triangle (see Figure 4,) a kis-truchet tile looks familiarly like other truchet tiles. Alternatively, since they are stretchy, a kis-truchet tile can be illustrated tiling a monogon on the sphere. A way to visualize the stretching involved is to cut a kis-truchet triangle out of paper and roll it into a cone with the pink vertex at the apex. Viewing the cone end-on reveals the tile wrapped inside a teardrop-shaped monogon (see Figure 5.)

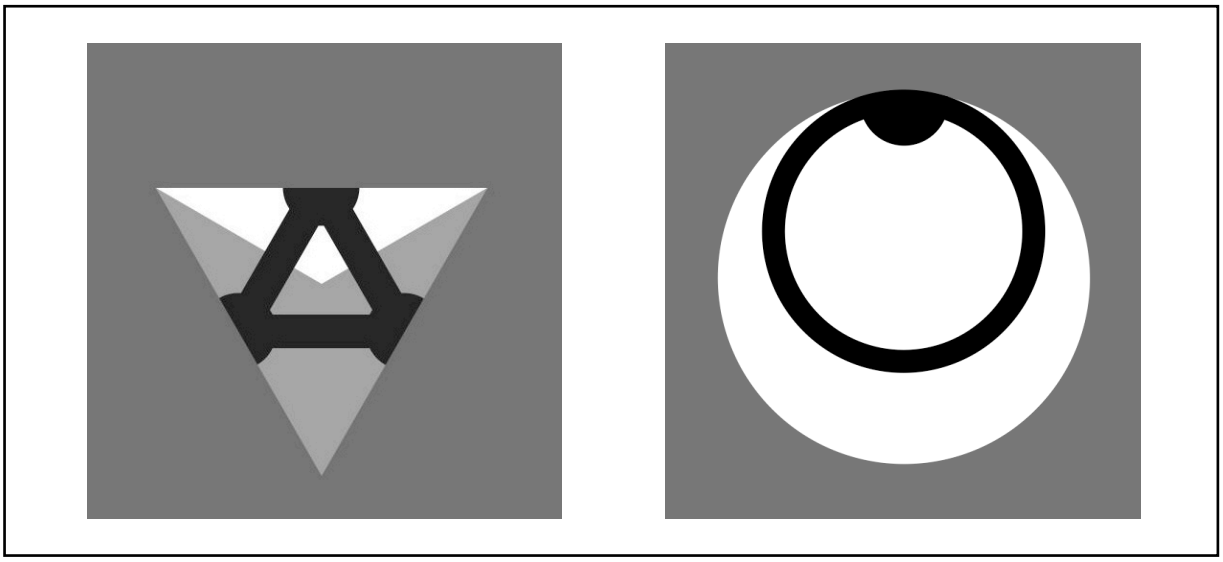

Figure 4: *A kis-truchet tile for medial shown as 1/3 of a triangle, left, and tiling a monogon, right.*

The Chart of Map Operations.

In the following Chart, kis-truchet tiles for twenty-one map operations are illustrated, both as one-third portions of equilateral triangles and as tilings of a monogon on the sphere.

In interpreting the illustration of the monogon tiling, one should imagine that the sphere is wearing the self-loop and vertex of the monogon base-map like a belt and buckle around its equator. Imagine yourself to be standing "buckle-to-buckle" with the sphere looking down on its northern hemisphere. (A glance in the Chart at the monogon representation for *identity* shows how this looks.) In the chart, all the kis-truchet triangles are shown with the pink vertex pointing down in order to make it easier to mentally roll them into the cones that would correspond to the monogon representation.

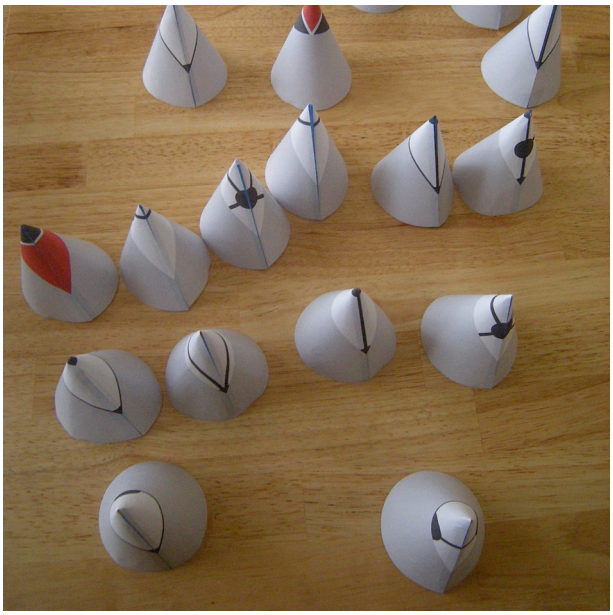

Figure 5: *Kis-truchets rolled into cones with the pink vertex at the apex.*

The sphere also has a southern hemisphere which is tiled by any map operation. If we were to turn the sphere over (still keeping it buckle-to-buckle to us) the tiling of the southern hemisphere would reveal itself to be exactly like that of the northern hemisphere. Alternatively, if we prefer to keep things stationary and view the southern hemisphere through the northern hemisphere with "x-ray vision," the southern hemisphere looks like a mirror image of the northern hemisphere. In consequence, each point on the *equator* is directly (left or right) across from a point on the opposite limb of the sphere that is its other half. This *perimetral bilateral symmetry,* along with the practical needs to produce a connected map and, in general, avoid 1-valent and 2-valent vertices, are the main constraints on useful map operations.

Chart of Map Operations

Map Operation Order-Type	Monogon Representation	Kis-Truchet Triangle	Identities Properties	Aliases
Identity Id() 1i	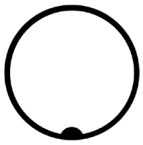	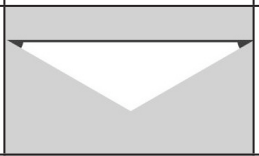	Id(M) = M	
Dual Du() 1d	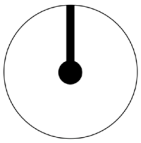	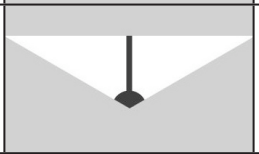	Du(Du(M)) = M	Poincare Dual
Subdivide Su() 2i	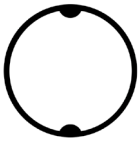	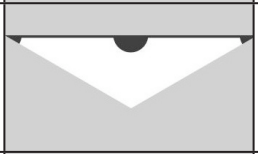	Su(M) = Du(Pa(Du(M))) Inserts 2-valent vertices in edges.	Su1, 1-Dimensional Subdivision
Parallel Pa() 2i		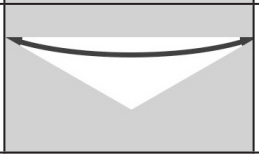	Pa(M) = Du(Su(Du(M))) Doubles all edges.	Parallelization
Radial Ra() 2i		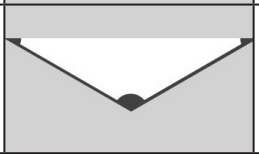	Ra(M) = Du(Me(M)) Ra(M) = Ra(Du(M)) Result is bipartite & quadrangle-faced.	Join
Medial Me() 2d	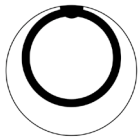	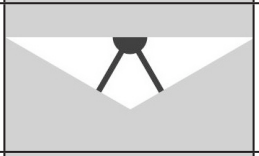	Me(M) = Du(Ra(M)) Me(M) = Me(Du(M)) Result is 4-regular & chess-colorable.	Ambo, Midpoint Subdivision, Mid-Edge Subdivision
Kis Ki() 3i		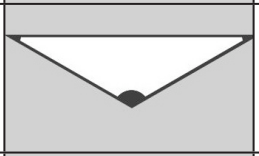	Ki(M) = Du(Tr(Du(M))) Result is triangle-faced.	P_3, Su2, 2-Dimensional Subdivision, Stellation, Omnicapping
Truncate Tr() 3d		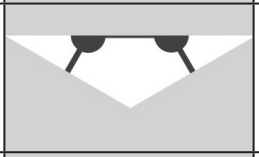	Tr(M) = Du(Ki(Du(M))) Result is 3-regular.	Truncation
Leapfrog Le() 3d	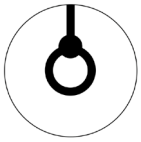	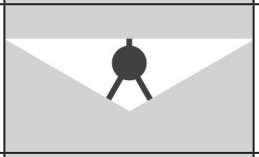	Le(M) = Du(Ki(M)) Le(M) = Tr(Du(M)) Result is 3-regular	Tripling, Dual √3 Trisection
Chamfer Ch() 4i		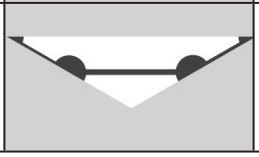		Q, Quadrupling

Ortho **Or()** 4i	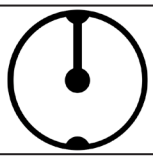	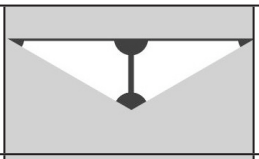	Or(M) = Ra(Ra(M)) Or(M) = Du(Ex(M)) Result is bipartite & quadrilateral-faced.	P_4, Tetrangulation, Edge Bisection, Catmull-Clark Subdivision, Primal Quadrilateral Quadrisection
Lo **Lo()** 4i		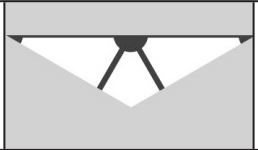	Lo(M) = Ko(Du(M)) Superposes Me(M) and Id(M).	2v Geodesic Breakdown, Loop Subdivision, Primal Triangle Quadrisection
Ko **Ko()** 4i	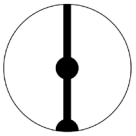	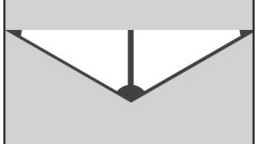	Ko(M) = Lo(Du(M)) Superposes Ra(M) and Du(M).	Primal √3 Trisection
Expand **Ex()** 4d		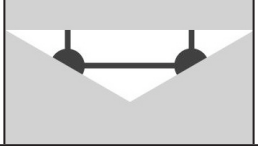	Ex(M) = Me(Me(M)) Ex(M) = Du(Or(M)) Result is 4-regular & chess-colorable.	Cantellation, Mrs. Stott's Expansion Operation, Doo-Sabin Subdivision, Dual Quadrilateral Quadrisection
Ring **Ri()** 4d	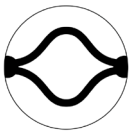		Ri(M) = Me(Su(M))	
Propellor **Pr()** 5i *chiral*				
Capra **Ca()** 5i *chiral*		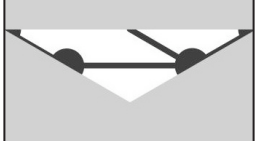	Ch(M) + chiral edge.	Septupling
Gyro **Gy()** 5i *chiral*		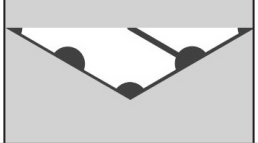	Gy(M) = Du(Sn(M)) Result is pentagon-faced.	P_5, Pentangulation
Snub **Sn()** 5d *chiral*			Sn(M) = Du(Gy(M)) Sn(Du(M) = Sn(M) Result is 5-regular. Ex(M) + chiral edge	
Meta **Mt()** 6i	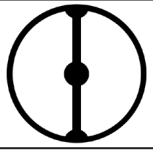	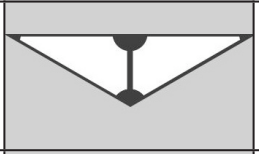	Mt(M) = Ki(Ra(M)) Mt(M) = Du(Be(M)) Result is triangle-faced.	Full Bisection, Barycentric Subdivision, 2-D Subdivision, Dual Triangle Quadrisection
Bevel **Be()** 6d	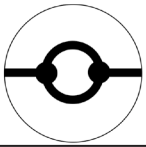	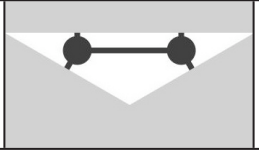	Be(M) = Du(Mt(M)) Be(M) = Tr(Me(M)) Result is 3-regular.	Omnitruncation

Practical Applications

Plain Weaving. A common problem in weaving is imagining the reverse face of the work. For example, a crossing of a vertical thread with a horizontal thread will—as we might expect—look different on the reverse face, but a crossing of two oblique threads looks the same! Confusion multiplies when one tries to weave a non-orientable surface such as a mobius strip. The surest resort is a technique known in knot theory as Tait's coloring of link diagrams [10], but first suggested in relation to weaving by Snelson [11] and fully developed by Roelofs [12].

In *plain-weaving* [13], which is weaving where every element passes over and under in strict alternation, and no three elements cross at the same point, each opening in the fabric is surrounded by a helical arrangement of weaving elements. Any such helix can be assigned a left- or right-handedness using the same rules as for an ordinary screw. This handedness is intrinsic, it does not change with the way we look at the opening. What is more, in plain-weaving each fabric opening shares edges exclusively with openings of the opposite handedness. Such a spatial arrangement is mathematically termed a *proper face 2-coloring*, or *chess coloring* [14]. Also, since elements of a plain-weaving cross strictly two-at-a-time, the map of a plain-weaving is 4-regular. Thus, more useful than a pictorial representation of a plain weaving, is a chess-colored, 4-regular map for it. If such a map is imagined to be inked "right through the paper," it becomes a reliable guide to both faces of the weaving.

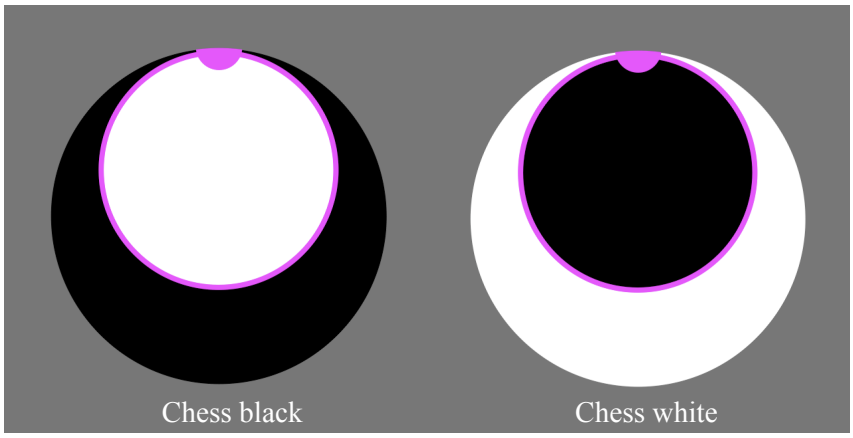

Figure 5: *Monogon representations of chess-colored medial tiles for plain-weaving.*

The map operation *medial* always yields a four-regular, chess-colorable map. In fact, a map M is a medial map of some map N if and only if M is four-regular and its faces can be chess-colored [15]. Medial is the refore the whole story for plain-weaving. All plain-woven baskets correspond to medial maps, and any given map can be converted into a design for plain-woven basket via the medial operation and a chess coloring. Medial can be understood as the projection onto the surface of the topological twisting operation in [13].

Ring Weaving. *Ring weaving*, a.k.a. *chain mail*, is often a variety of plain-weaving. A design for the commonest plain-weave chain mail is generated from any map by chess coloring the map resulting from the map operation *ring,*

Ri(M) = Me(Su(M)).

Coloring Operations. A suitable chess-coloring can be pre-marked on the truchet tile for a map operation since such a coloring is essentially unique. If a map is chess-colorable, then its dual map is *bipartite,* meaning that its vertices can be colored black and white in such a way that no two vertices of the same color are linked by an edge. Bipartite maps are important in the study of Riemann surfaces, where the map operation *subdivide* is used to generate bipartite maps which are colored according to the convention that the "old" vertices are colored black. It seems useful to generalize this coloring convention. Define a (meta) map operation, *bipartite black,* Bb(Xx(M)), as the operation that generates the bipartite-colored map (if such exists) of the map Xx(M), using the convention that all the "old" vertices in Xx(M) are to be black. *Bipartite white,* Bw(Xy(M)), generates the inverse coloring. Dually, define *chess black,* Cb(Yy(M)), as the operation that generates the chess-colored map (if such exists) of Yy(M), using the convention that all the "old" faces of Yy(M), are colored black. Chess white, Cw(Yy(M)), generates the inverse coloring. Figure 5 shows the action of *chess black* and *chess white* on medial.

Tensegrity. Pugh [16] describes three categories of tensegrity structures, *diamond, zig-zag,* and *circuit.* All three can be associated with map operations. The diamond tensegrity pattern is isomorphic to *snub.* The compression elements, or struts, of the tensegrity structure, correspond to the chiral edge of snub; the remaining non-chiral edges (which, by themselves, could equally well have been generated by the map operation *expand,*) correspond to the tension elements, or tendons, of the tensegrity structure. A monogon tiling for *snub* with the strut indicated by a thicker line is shown in Figure 7a. When the base map is a triangle on the sphere, this map operation produces the famous 3-strut, 9-tendon, T-prism. When the base map is a tetrahedron, the result is the equally well-known 6-strut, 24-tendon, expanded octahedron.

The situation is a bit messier for the *zig-zag* and *circuit* tensegrity patterns. These patterns have elements that crossover each other without actually touching—thus breaking one of the rules for maps. A stratagem is to portray these patterns with the (narrow) tendons overlying the (wide) struts—not indicating that they pass in front, but rather that they may pass either in front or behind—as the curvature of the surface dictates. Such "floating" tendons and struts are non-physical, but the problem of deciding whether tendons or struts pass in front is fully determined, in practice, by the spatial coordinates of their endpoints. (If the surface the tensegrity structure conforms to is sufficiently curved, strut-tendon and strut-strut collisions are avoided.) In *circuit,* the tendons and struts both align with the edges of *medial,* but struts join in the common vertex only on alternate passes (see Figure 7b.) In *zig-zag,* tendons align with the edges of *truncate,* while struts align with an additional chiral edge which crosses over a tendon at the equator (see Figure 7c.)

Figure 7: *Monogon representations of tensegrity patterns.*

Texture Mapping Examples of practical uses of map operations are shown in Figure 8. These images were realized by texture-mapping a triplet of kis-truchet tiles (in effect, a truchet tile composing a full equilateral triangle) onto 3-D models having all-triangle meshes using Processing [17].

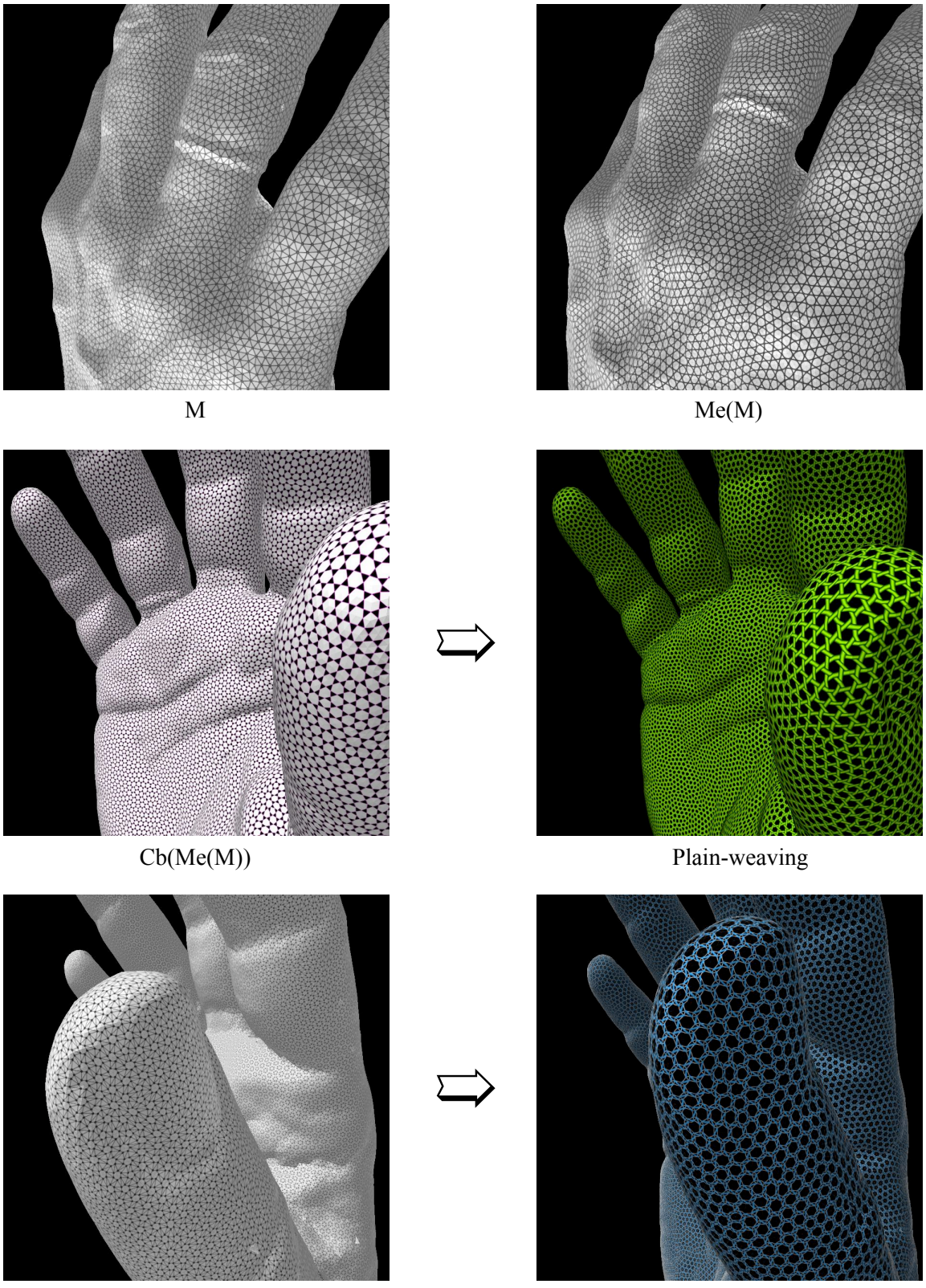

Figure 8: *Practical applications of map operations. Model courtesy of INRIA via the Aim@Shape Shape Repository.*

References

[1] S. K. Lando, A. K. Zvonkin, and D. B. Zagier, *Graphs on Surfaces and Their Applications,* Encyclopedia of Mathematical Sciences, Low Dimensional Topology, p. 28, Springer-Verlag, 2004.

[2] T. Pisanski and M. Randic, *Bridges between geometry and graph theory*, Geometry at Work, C. A. Gorini, ed., pp. 174-194, Mathematical Association of America, 2000.

[3] M. V. Diudea, M. Stefu, P. E. John, A. Graovac, *Generalized operations on maps,* Croatica Chemica Acta, CCACAA 79 (3) 355-362, 2006.

[4] G. W. Hart, *Conway notation for polyhedra,* www.georgehart.com/virtual-polyhedra/conway_notation.html

[5] C. Loop, *Smooth Subdivision Surfaces Based on Triangles.* Master's thesis, University of Utah, 1987.

[6] L. Kobbelt, *√3-Subdivision,* Proc. ACM Siggraph 2000.

[7] J. Peters and U. Reif, *The simplest subdivision scheme for smoothing polyhedra,* Purdue University, 1996

[8] P. Oswald and P. Schroder, *Composite primal/dual √3-subdivision schemes,* Computer Aided Geometric Design, vol. 20 n. 3, pp. 135-164, 2003.

[9] H. Kenner, *Geodesic Math and How to Use It*, chap. 5, Univ. of California Press, 1976.

[10] D. J. A. Welsh, *Complexity: Knots, Colourings and Counting,* p. 23, Cambridge Univ. Press, 1993.

[11] K. Snelson, *Space frame structure made by 3-D weaving of rod members,* U.S. Pat. 6739937, 2004.

[12] R. Roelofs, *About weaving and helical holes,* Bridges 2010.

[13] E. Akleman, J. Chen, Q. Xing, and J. Gross *"Cyclic plain-weaving on polygonal mesh surfaces with extended graph rotation systems,"* Proc. ACM Siggraph '2009.

[14] Deza, M., and Dutour, M., Zigzags and central circuits for 3- or 4-valent plane graphs, www.liga.ens.fr/~deza/Sem-ZigCc/ZigCcConf.pdf

[15] D. Archdeacon, *Representativity,* The Handbook of Graph Theory, J. L. Gross and J. Yellen eds., chap 7.7, F4, p. 724, CRC Press, 2003.

[16] A. Pugh, *An Introduction to Tensegrity,* Univ. of California Press*,* 1976.

[17] www.processing.org

Sundials and Astrolabes

Susan McBurney
Western Springs, IL 60558, USA
E-mail: smcburne@iit.edu

Abstract

The discipline of mathematics has evolved over the millennia in response to practical needs of the times as well as to the pursuit of ways to describe and analyze the world around us. Many fields have contributed to, and benefited from, efforts of mathematicians to discover new and elegant methods of problem-solving. Among these fields is the science of astronomy—explaining the workings of the universe. This paper is designed to provide a very basic introduction to the mathematics of astronomy by examining two popular astronomical instruments, the sundial and the astrolabe. It also hopes to illustrate the combination of mathematics, utility, and artistry exhibited by medieval astronomers and craftsmen as shown by their beautifully constructed tools and instruments.

The Adler Planetarium and Astronomy Museum

It is an honor for Chicago to host the ISAMA conference for the second consecutive year. In the theme of combining mathematics and the arts with the city's cultural offerings, the author would like to call attention to the Adler Planetarium and Astronomy Museum, beautifully situated on the lakefront, and its outstanding collection of mathematically inspired astronomical instruments. In particular, they house the largest astrolabe collection in North America. Astrolabes were portable instruments used to observe objects in the sky and derive from the readings a variety of information such as time of day, longitude, time of sunrise and sunset, and even prayer times and direction to Mecca. Sundials, armillaries, and many other instruments are also on display. The exhibit "The Universe in your Hands" in particular examines the world of medieval European and Islamic astronomers from the period 1200 to 1800 AD.

This paper will provide a brief fundamental course in the mathematics of astronomy by examining two basic instruments, the sundial and the astrolabe, and their underlying mathematical structure.

Sundials

Figure 1: *Equatorial Sundial*

The sundial, of course, is familiar to us all. In its simplest form one can push a stick vertically into the ground and get a sense of the current time by watching the relative length of the shadow cast by the sun's rays. It is the longest at sunrise and sunset and the shortest at noon when the sun is at its daily highest point in the sky The actual length of the shadows will vary from day to day as the sun advances through the seasons. The longest shadows will be cast on Dec. 21, (Dec. 22 in 2011) the day of the winter solstice when the sun is lowest in the sky. The shortest shadows will occur on June 21, the summer solstice, when the sun is highest in the sky.

The angle θ of the sun's rays at noon can be illustrated by the diagram of Figure 2, where H is the height of the stick (gnomon) and L is the length of the shadow. The tan (θ) = H/L, or $\theta = \tan^{-1}$ (H/L).

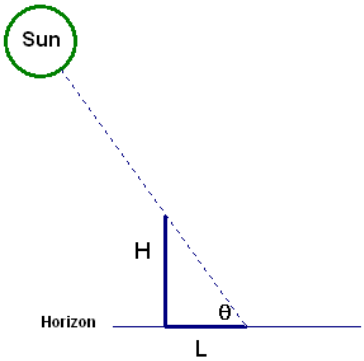

Figure 2: *Simple sundial*

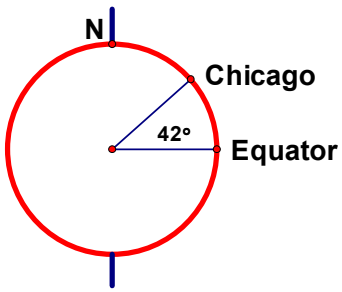

Figure 3: *Chicago latitude*

However, an additional factor influences θ, namely the latitude of the observation. If latitude is known, then θ can be determined for any day of the year. Stationary sundials must be designed for a particular latitude and portable ones must be adjustable or used only at the designated latitude.

Chicago has a latitude very close to 42°. See Figure 3. To design a horizontal sundial for Chicago, one should use a gnomon erected such that the angle it makes with the base is 42°, 12 o'clock noon is pointing due north, and the base is exactly horizontal. The hour markings do not divide 180° equally, but instead can be calculated in the following manner. The goal is to find the angle X of the hour marking in relation to the noon marking. See Figure 4. The hour (T) is expressed relative to noon, (11 am is -1, 1 pm is +1, etc.) and multiplied by 15 (width of a time zone, 360 degrees/24 hours). The tangent of 15T is then multiplied by the sin of the latitude (for Chicago, sin (42°) = .669) and the angle X is the angle whose tangent is this final result. That is, $X = \tan^{-1}$ [tan (15T) sin(42)]. A table of values for Chicago is provided for common daylight hours in Figure 4 to save calculation stress. For morning hours, subtract from 12 and measure in counterclockwise direction.

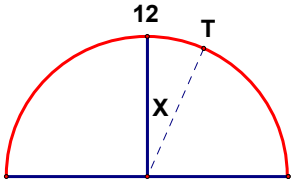

HR (T)	X degrees	HR (T)	X degrees
noon	0.0		
1	10.2	4	49.2
2	21.1	5	68.2
3	33.8	6	90.0

Figure 4: *Hour placement on sundial for Chicago, Latitude 42°*

The time read from a sundial is *sun time* at that particular point. Three adjustments must be made to find *local clock time*. First, adjust for the east-west longitude variance of the sundial from the center of the time zone. The time zones are positioned equally around the circumference of the earth (with many local variations). Beginning at Greenwich, England where the prime meridian is located, the 24 hours of the day are each allotted 15 degrees of width (360/24). Each zone spans its central line of longitude, its central meridian. The time meridians occur every 15°. Chicago's longitude is 87.897° which puts it about two degrees east of the time zone meridian at a longitude of 90°. Every degree is equivalent to four minutes (60 min. in an hour / 15 degrees per hour). That means that the sundial reading must have about eight minutes *subtracted* from it to agree with local clock time.

The second correction is very straightforward. If Daylight Savings Time is in effect, add one hour.

The third correction is somewhat more involved. Adjustment must be made for the Equation of Time. Briefly, because the orbit of the earth around the sun is elliptical and because the earth is tilted to the plane of its revolution, the sun seems to move faster in the summer. That is, it seems to cross a greater portion of the horizon in one hour than in the winter. See Figures 5 and 6.

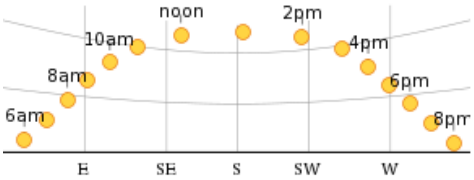

Figure 5: *Path of sun on 6-21-11 Summer solstice Daylight Savings Time, in Chicago*

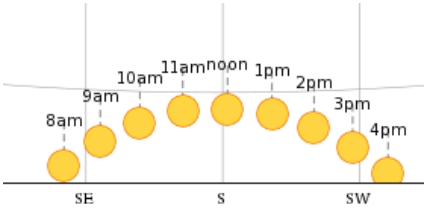

Figure 6: *Path of sun on 12-22-11Winter Solstice In Chicago*

This variance is not linear, so the easiest way to account for it is to reference a chart of average variance according to the time of year. See Figure 7.

	Minutes		Minutes
January	9	July	5
February	14	August	5
March	9	September	-5
April	0	October	-14
May	-3	November	-15
June	0	December	-5

Figure 7 : *Monthly adjustment to sundial reading for Equation of Time [1]*

This variation shown on a graph is much more varied. The yearly cycle shown as a figure is a lovely figure-eight curve known as an *analemma*. It is interesting to note that even in Vitruvius' time (1st c. B.C.) it was known and studied. He gives a full treatment in his books of how to treat the construction of sundials with this in mind [4].

Astrolabes

Figure 8: *Astrolabe*

Some of the most beautiful instruments in the Adler's collections are the Eastern astrolabes, constructed by Islamic artisans in the 12-18th century. These instruments had a myriad of uses, but to understand the operation it is best to give a simple example, finding the time of day. Also, some basic concepts must be explored.

The *altitude* of an object in the sky is the angle a line of sight to the object makes with the horizon.

The earth makes one revolution around the sun in one year. During the course of this journey, different stars appear at night, changing as the earth moves to a new position in its orbit. The band of stars seen is known as the *zodiac* and it changes slightly each night. At the spring equinox (March 20) the constellation Aries

traditionally appeared on the eastern horizon at sunrise. This occurrence is used as the beginning reference point for a measurement of the *longitude* of a star. Longitude is expressed as degrees along the ecliptic from the point of the vernal (spring) equinox.

Now, if one can measure the altitude of an object in the sky and one knows what it's longitude should be for a particular date at a particular latitude, then it is possible to obtain the time of day. That is one basic operation of an astrolabe. Here are the specifics of making such a measurement.

The backs of astrolabes are inscribed with date and zodiac scales as well as angle measurements.

With the astrolabe suspended vertically, on the back rotate the pointer (called an alidade) so that the object is viewed through the sights. Read the angle of the object with the horizon from a scale. This is the *altitude* of the object.

Rotate the alidade to the date of the observation and read the object's (sun or star) *longitude* on the zodiac from the engraved scale.

Transfer these two readings to the front of the astrolabe. The front base of the astrolabe is engraved with hour markings, a horizon line separating day from night, and altitude scales. Laid on top of the base is a perforated plate called a *rete*. The rete can be rotated also and shows pointers to specific stars *at a specific latitude* and a circle representing the *ecliptic* path of the sun. This is the path that the sun seems to take in the course of a year. Of course it is caused by the movement of the earth around the sun. See Figure 9.

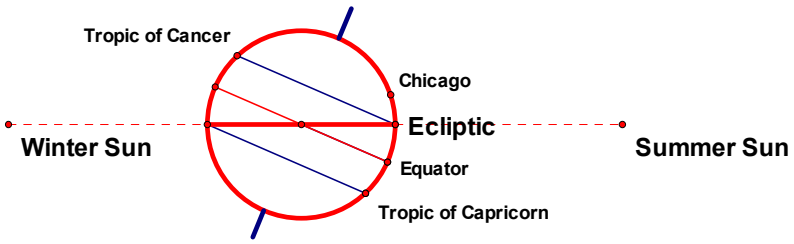

Figure 9: *The ecliptic, the apparent annual path of the sun*

Rotate the front pointer (called the rule) to the longitude on the ecliptic (zodiac) obtained in the previous step. Rotate the rete and rule together until the rule points to the altitude measured in the first step. Now the time can be read from the time scale.

Although the description seems cumbersome, this was a valuable tool for finding time in the days before mechanical clocks and watches. Many other calculations could be made as well depending on the information encoded on the astrolabe. For instance, time of sunrise and sunset, location of particular stars, even the occurrence of eclipses. Islamic devices often included tables or scales for direction to Mecca, or could be used to determine daily prayer times. The craftsmanship of the devices was raised to exceedingly fine levels and many instruments are of themselves, works of art in addition to being beautiful mathematical models of the universe.

References

.
[1] C. J. Budd and C. J. Sangwin, *Mathematics Galore*, Oxford University Press, 2001
[2] Amy Shell-Gellasch, Ed., *Hands On History*, Mathematical Association of America Press, 2007
[3] Wolfram Alpha, *Sun Path*, http://www.wolframalpha.com/
[4] Vitruvius, *Chapter VII*, www.gutenberg.org
[5] Stephenson, Bolt and Friedman, *The Universe Unveiled*, Adler Planetarium & Astronomy Museum and Cambridge University Press, 2000
[6] http://astrolabes.org/

Tessellation Patterns from a Simply Decorated Triangle

David A. Reimann
Department of Mathematics and Computer Science
Albion College
Albion, Michigan, 49224, USA
E-mail: dreimann@albion.edu

Abstract

Geometric tilings have been a key element of architectural design throughout history. This paper describes the construction of patterns using a decorated triangle and gives several surprising examples demonstrating the use of this motif. Even with this very simple design element, a wealth of interesting patterns is possible. Such patterns can be useful in very large field architectural tilings.

1 Introduction

Geometric tilings have been a key element of architectural design throughout history. One of the most simple tessellations of the plane is the common triangular lattice, where six equilateral triangles meet at every vertex. In such a tessellation, the underlying polygons can be thought of as tiles. These tiles can also be decorated with a simple motif to produce more intricate patterns. M.C. Escher was a master at decorating tiles with people and animals, breathing life into otherwise cold geometric structures.

Even simple motifs can enhance a tiling's visual interest. For example, Truchet [1] explored the patterns obtainable from a single square tile that was bisected along a diagonal between opposite vertices. Smith [2] published an article containing a translation of Truchet's original paper with some commentary and new ideas including the use of a random tiling rather than a structured pattern. Smith also included a variant of the Truchet tile that replaced the triangular segmentation with two quarter-circle arcs, resulting in a tiling that is comprised of an aesthetically pleasing, meandering set of mostly closed curves. Pickover [3] proposed using randomly placed Truchet tiles as a way to visually detect patterns in binary data, noting "the eye perceives no particular trends in the design." However, he does note small features such as circles and dumbbells. Browne [4] noted a variety of interesting shapes are possible. The author [5] described how these simple shapes can be combined to define a font that can be used to embed textual information in the patterns.

A challenge in decorating polygonal tiles with arcs arises when the underlying polygon contains an odd number of sides. Browne [6] investigated filled patterns on regular polygons regions defined by arcs connecting midpoints of polygon sides. Browne uses a motif containing a bifurcation to decorate a triangle. The author's previous work [7] investigated motifs on regular polygons where each side was subdivided into an equal number of segments and connected using Bézier curves. The author's design uses two components to decorate an equilateral triangle having side length L. The first is a circular arc of radius $a = L/2$ that connects the midpoints of two sides and the second is a short line segment from the midpoint of the remaining side in the direction of the triangle's center. This tile decoration is shown in Figure 1. This paper describes the construction of patterns using a decorated triangle as motif and gives several surprising examples demonstrating the use of this pattern.

2 Methods and Results

There are six possible orientations in which a tile as decorated in Figure 1 can be placed. The arc is centered at one of the three vertices, giving three possible orientations of the triangle. Because the triangle has two

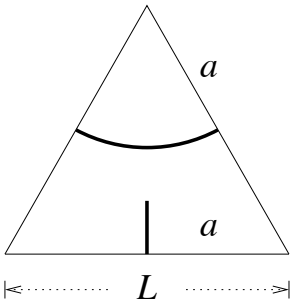

Figure 1: *The basic decorated equilateral triangle having side length L. The motif is comprised of two components. The first component of the motif is an arc of radius $a = L/2$ having endpoints that are at the midpoints of two sides. The second is a short line segment that starts at the midpoint of the third side and extends towards the center of the triangle.*

orientations in the underlying tessellation, this results in six possible orientations. An example showing a random placement of tiles is given in Figure 2. A variety of shapes is present, including circles, short line segments, and longer linear features. Because the decorations of the tile are close to the line segments that would connect the midpoints of the triangle's sides to the center, the pattern is similar to the dual of the triangular tessellation (the hexagonal tessellation).

Some striking regular patterns are also possible using this simply decorated tile. Figure 3 shows four repetitive patterns that exhibit translational symmetry and four patterns that are constructed on a hexagonal lattice. Figure 4 shows an example of a frieze pattern. Figure 5 illustrates how this motif can be used to embed text in the pattern.

3 Discussion

Even with this very simple design element, a wealth of interesting tessellated patterns is possible. One reason for the visual appeal of the patterns is the arcs of adjacent tiles are not only continuous, but also have a continuous first derivative resulting in a visually smooth transition regardless of tile orientation. In addition, the meandering paths created are roughly equally spaced, providing a relatively uniform filling of the plane. The tension present between the both local similarity and positional regularity and the irregularity of randomly generated curves provides excitement and movement not present in the underlying triangular or hexagonal tessellations. Symmetric patterns are easy to create and can be mixed with random tile orientations to create patterns with consonance and dissonance. These patterns can be useful in very large field architectural tilings.

4 Acknowledgments

This work was supported by a grant from the Hewlett-Mellon Fund for Faculty Development at Albion College, Albion, MI.

References

[1] Sebastien Truchet. Memoire sur les combinaisons. *Memoires de l'Academie Royale des Sciences*, pages 363–372, 1704.

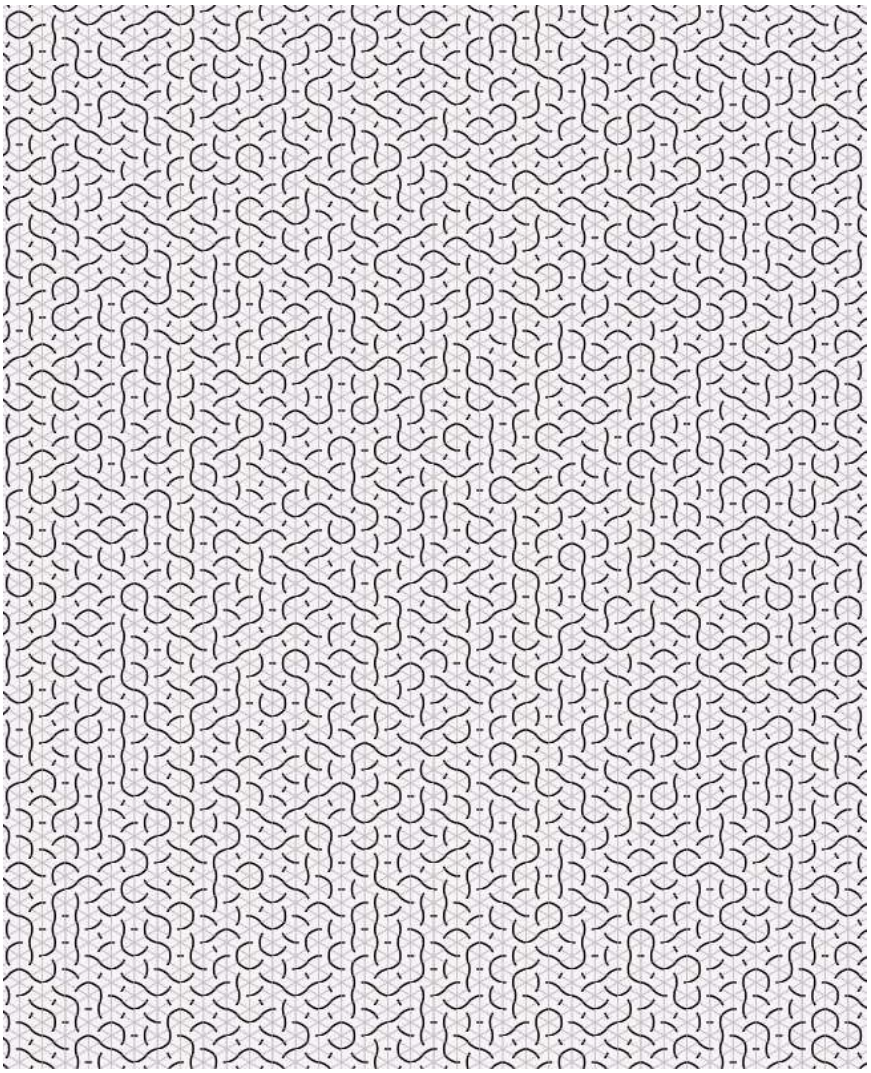

Figure 2: *A field of randomly placed tiles. The triangular lattice is shown in light gray. Note the variety and complexity of shapes created by the simple motif.*

[2] Cyril Stanley Smith. The tiling patterns of Sebastien Truchet and the topology of structural hierarchy. *Leonardo*, 20(4):373–385, 1987.

[3] Clifford A. Pickover. Picturing randomness with Truchet tiles. *J. Rec. Math.*, 21(4):256–259, 1989.

[4] Cameron Browne. Truchet curves and surfaces. *Computers & Graphics*, 32:268–281, 2008.

[5] David A. Reimann. Text from Truchet tiles. In Craig S. Kaplan and Reza Sarhangi, editors, *Bridges Banff: Mathematics, Art, Architecture, Culture*, pages 325–326, Banff, Alberta, Canada, 26–29 July 2009.

[6] Cameron Browne. Duotone Truchet-like tilings. *Journal of Mathematics and the Arts*, 2:189–196, 2008.

[7] David A. Reimann. Patterns from Archimedean tilings using generalized Truchet tiles decorated with simple Bézier curves. In George W. Hart and Reza Sarhangi, editors, *Bridges Pécs: Mathematics, Music, Art, Culture*, pages 427–430, Pécs, Hungary, 24–28 July 2010.

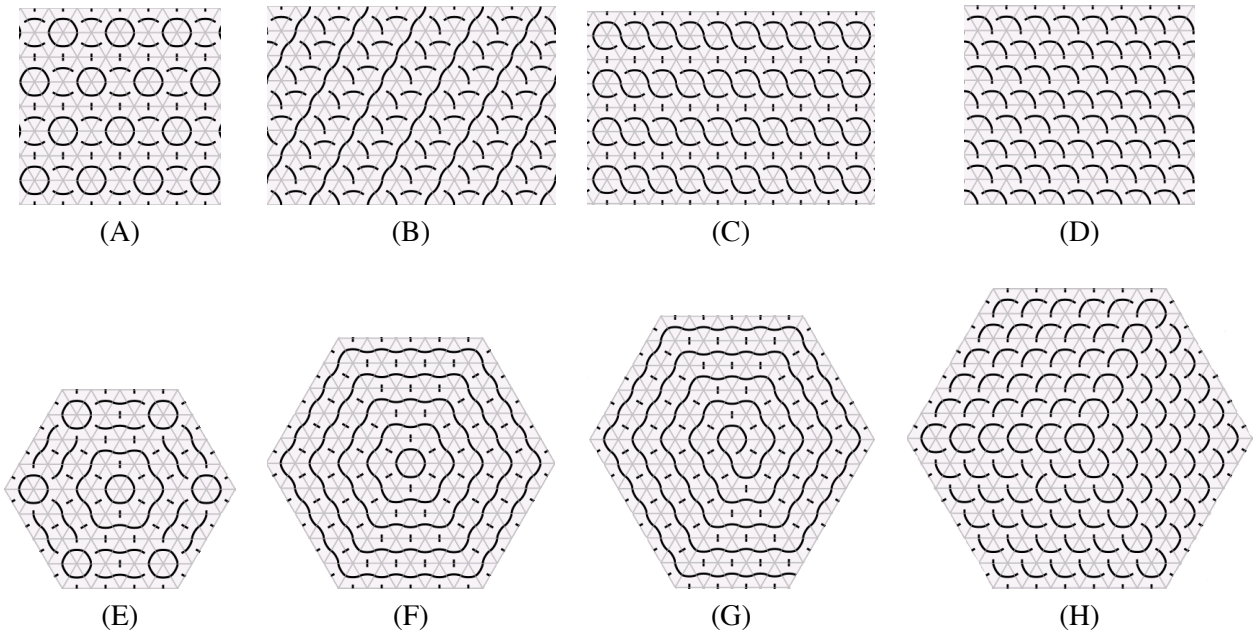

Figure 3: *Eight patterns possible using the simple motif show in Figure 1. Patterns that can be extended infinitely far in all directions are possible, as shown in A through D. Patterns created on a hexagonal lattice with six fold (E and F) and three fold rotational symmetry (H) are also possible. Space-filling curves, such as spirals (G), can be easily created.*

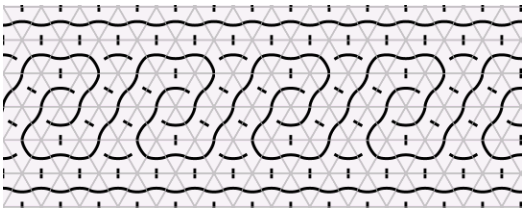

Figure 4: *An example of a frieze pattern obtainable from the motif in Figure 1.*

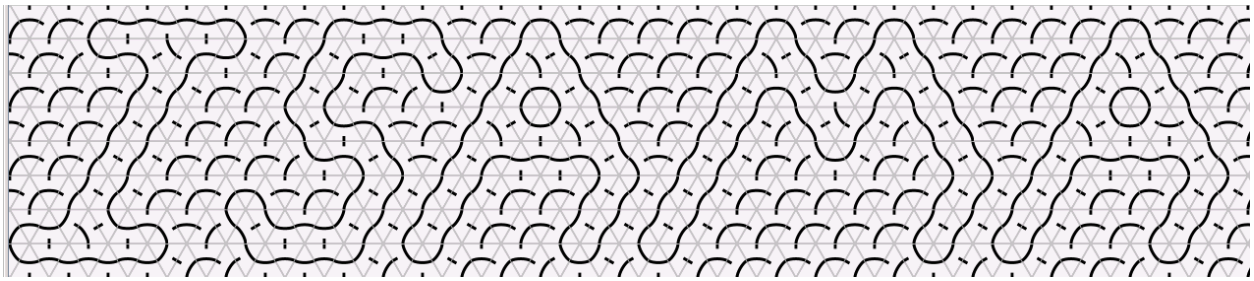

Figure 5: *An example showing how letters can be placed in a pattern comprised of modular triangular units decorated with the motif in Figure 1. The example text reads ISAMA.*

Filling Space with Random Fractal Non-Overlapping Simple Shapes

John Shier
6935 133rd Court
Apple Valley, MN, 55124, USA
E-mail: johnart@frontiernet.net

Abstract

We present an algorithm that randomly places simple shapes (circles, squares, triangles, and others) without overlap in two dimensions. We describe the mathematics of the process in detail with some conjectures about its properties. The distribution of the areas of the shapes is a power law with varying exponents (typically around -1.3 for visual art). When the algorithm continues "to infinity" it fills all space, while the shapes have an infinite total perimeter. We show several uses of this algorithm to produce visual art.

An Illustration

A picture is worth ten thousand words
-- Confucius (?)

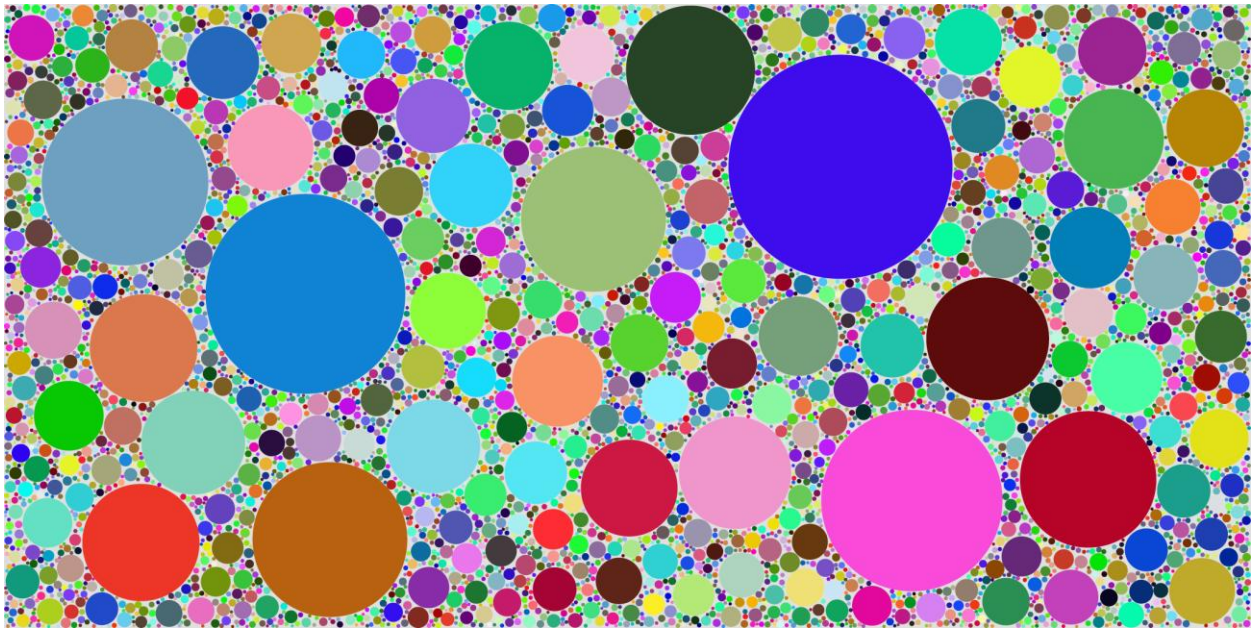

Figure 1: *5000 nonoverlapping fractal circles. The random colors provide the high contrast needed to see the full detail of the image. The successive circle areas decrease by a power law, while their placement is by random search. Such processes have been found to apply to a wide variety of geometric shapes, and in the limit will completely fill all space if properly set up. The image shows the property of "statistical self-similarity", reproducing the same distribution of circle sizes at all length scales.*

Statistical Geometry

Geometry studies the spatial arrangements of shapes (lines, polygons, circles, ...).

"Statistical" and "geometry" are words not usually seen together, so some explanation of this little-explored subject is called for.

Geometry is a huge and ancient subject. Certain branches of geometry have been much used in art and decoration. Tilings of the plane go back a long way, are pleasing to the eye, and have been especially prominent in Islamic art and decoration. Plane tilings pose the question "How do you fill the plane without gaps using a limited number of geometric shapes?" — typically polygons bounded by straight lines. The result is a pattern which covers a bounded region with a finite number of shapes.

A related area of geometry is that of "packings" -- incomplete or maximally-dense filling of a region by circles and other simple shapes. Circle packings alone have a large mathematical literature. The usual rule in circle packings is that one finds a set of circles which all touch (are tangent to) each other. Such tangent packings are called "Appolonian" after the ancient Greek mathematician Appolonius of Perga who first described such a pattern. Such packings don't fill the whole region. These packings have seen relatively little use in art. The packings of interest here are non-Appolonian and violate the rules of formal mathematical circle packing.

Traditional decorative geometric patterns are models of order and regularity, with every shape having an exact location and no elements of randomness.

One might ask: "Can you cover a bounded region with an *infinite* number of regular shapes?" Several examples of this are known, such as the Sierpinski carpet [1], but they have found little use in art, perhaps because their appearance is not particularly attractive to the average eye. Such constructions are largely recursive.

The geometric construction described here poses a different question: "How do you cover a bounded region *non-recursively* with an infinite number of ever-smaller randomly-placed simple shapes (triangles, squares, circles) such that in the limit they completely fill it?" Despite much searching, I have not found any prior account of such an algorithm.

Geometry is a subject of great exactitude. There are precise rules for edges, angles, and vertices. There is no place for randomness or uncertainty. But if you look at the pictures hanging on the wall of an art museum what you see combines elements of both randomness and order. A street scene, for example, has the regular structures of streets and buildings, and the turbulent swirl of vehicles and pedestrians. There is an attractiveness to an image which combines elements of both order and randomness. Nature itself combines randomness and order. All oak trees have a regular branching structure which the eye easily recognizes. But the details differ from one tree to another in a random way.

The geometry described here would startle Euclid.

Conventional tilings have exact symmetry -- it is one of their charms. The shapes making up the pattern have rotation, translation, mirror, and other symmetries. The statistical geometry patterns of interest here have individual shapes with symmetry (square, circle, etc.) but there is no symmetry at all in their placement. What they do have is what might be called fractal symmetry (or "statistical self-similarity") —

a regular progression in the sizes of the shapes. The eye recognizes this kind of symmetry. Apparently even untrained observers see this, although they don't know what to call it.

Rules of Construction

Suppose that we have a bounded region of area A. We intend to fill it with similar geometric shapes having a sequence of areas A_1, A_2, ... (to infinity). The areas A_i are to be computed using a mathematical rule with no randomness.

The algorithm begins by placing shape A_1 somewhere within the region. It then proceeds to generate random positions x,y within the region for the following shapes in the sequence, and for each one tests whether the given shape A_n overlaps any previous A_m. If it does not overlap, this is a "successful placement" and x,y and the size and shape of A_n are placed in a file and the process repeated for the next shape A_{n+1}, or else a new trial position is generated.

If the shapes are to completely fill the area A in the limit, it is evident that one must have

$$A = \sum_{n=1}^{\infty} A_n \qquad (1)$$

The area A_n of the n-th shape is to be chosen according to a mathematical rule. It is evident that the rule must be such that the sum above is convergent. The sequence of areas A_n should follow some ever-smaller rule: $A_n = g(n)$ for the n-th shape.

Many functions obey the obvious requirements: $exp(-an)$, $exp(-an^2)$, and power laws $1/n^c$. Here a and c are parameters which need to be chosen such that Eq. (1) is satisfied. (The sum in Eq. (1) does not converge for all values of c when a power law is used. See [2] for details.)

If the sum in Eq. (1) is less than A, the region will never be completely filled. If the sum is greater than A, the process of seeking random unoccupied positions for ever-smaller shapes will come to a halt at some point for lack of space.

Power-law functions $A_n = A_1 n^{-c}$ (exponent c) are the only ones which have been found to work in computer trials. Useful c values for art lie between 1 and 2. The "tailing off" of $g(n)$ must be slow enough that there is always room in the lacy "gasket" of unoccupied space for another placement. The gasket must get narrower at just such a rate that allows this.

For a power law Eq. (1) becomes

$$A = A_1 \sum_{n=1}^{\infty} \frac{1}{n^c} = A_1 \zeta(c) \qquad (2)$$

The sum can be recognized as the series which defines the Riemann zeta function [2] so that

$$c = \zeta^{-1}(A / A_1) \qquad (3)$$

where $\zeta^{-1}( )$ is the inverse zeta function. Thus this process does not have a unique power law exponent, but rather an exponent which varies depending on the choice made for the ratio of A_1 to total area A. It may be that this is the first-ever practical application of the Riemann zeta function.

In the above calculation it is assumed that all shapes will be placed completely inside the bounded area A. This is easy to do computationally. Other choices such as periodic or cyclical arrangements are possible but so far unexplored.

It has been found that the process also works if the sequence in Eq. (2) does not begin with $n = 1$, but starts with some higher value of n. Here the Hurwitz zeta function [2] replaces the Riemann zeta function. Or one can have various laws for A_i versus i for the first N terms and then go over to a power law for $n > N$, as long as Eq. (1) is satisfied.

The process has been used with circles, squares, nonsquare rectangles, and equilateral triangles. The process has been found to run smoothly when set up as described.

By construction the shapes are non-touching (non-Appolonian). With finite-accuracy computing they sometimes touch and may even seem to be slightly overlapping in images. This results from finite precision and roundoff error.

Observed Properties

The remarks here apply to the case where one starts with $n = 1$ as in Eq. (2).

This process operates within a very narrow window. For a given choice of A and A_1 there is only one value of c which works.

It isn't obvious to me why a power law is the unique choice here. Perhaps a rigorous proof of this is possible for this simple "model" system.

While the total area of the shapes has been set up to go to a particular limit, the perimeter grows without limit as n increases. This is characteristic of fractal sets (e.g., Sierpinski [1]).

It has been found in computational experiments that the process does seem to run on "forever" if a power law is used as described above. Sequences of up to 500000 shapes have been computed in this way with no sign that the process will quit (but it does slow down a lot). If the process described here is viewed as a way of measuring area, it reveals a rather surprising property of space.

The process uses random iterations of x,y to find a successful placement. The total (cumulative) number of iterations n_{it} needed follows an increasing power law in n, $n_{it} = n_0 n^f$, with an exponent f. Study of computed data shows that $f \cong c$, i.e., the (negative) value of c is the same (within statistical error) as the (positive) value of f. (It is not at all obvious to me why this should be so.) Thus there is a smooth and regular increase in the average amount of computation for each new shape. This says that the useful (big enough) space for placement is going down by a power law since the probability of placement is a measure of the available area. This supports the idea that the process will always find a place for a new shape "to infinity" in a finite number of iterations.

The following data was found using estimates from computation runs with the stated c values. The mean-square estimates of f and n_0 are thus subject to some uncertainty since we deal with a random process.

$c = 1.15 \quad f = 1.1513 \quad n_0 = 2.70$
$c = 1.24 \quad f = 1.2429 \quad n_0 = 8.09$
$c = 1.31 \quad f = 1.3038 \quad n_0 = 34.3$

The power law for n_{it} does not apply to the first few placements since they are exceptional. Usually enough "slack" is left after the initial placement that the algorithm has an artificially easy time for the first few placements. As n increases the process goes over more and more to a "steady state".

For a given n, the number of iterations needed can be 1, 2, 3, ... Study of histograms of these numbers shows that for large n the distribution is accurately represented by a decaying exponential function. This agrees with the fact that the Poisson distribution goes over to an exponential form when the probability of an individual event (here a successful placement) is << 1.

With its lengthy searches over the "back list" of shapes and their positions, this is a very slow and inefficient algorithm, although simple and easy to code (less than 50 lines of C code for the central loop). Of simple shapes, the square runs fastest. Improved searches should be possible.

One can define a crude measure of the "effective width" of the lacy "gasket" by taking the ratio A_{gask} (the original area A with holes cut out for every shape) divided by the perimeter P_{gask} of all shapes (both functions of n, where n is the number of shapes placed).

$$eff\_width(n) = A_{gask} / P_{gask} \qquad (4)$$

How does this compare with the size of the i-th shape? In the circle case we can define a dimensionless ratio b by

$$b(n) = A_{gask} / diam \cdot P_{gask} \qquad (5)$$

where *diam* is the diameter of the n-th circle. This has been computed using data from a run of the algorithm, and also from formulas. Data from a computer run with c = 1.24 is as follows:

$n = 1000$ $b = .4197$
$n = 2000$ $b = .4140$
$n = 3000$ $b = .4114$
$n = 4000$ $b = .4096$
$n = 5000$ $b = .4086$

One can see that while b is not quite a constant versus n, it has a very slow variation. A check of this versus computation using formulas gave agreement to nearly 4 decimal places (satisfactory in view of numerical and statistical accuracy). What this means is that as n increases the "effective width" of the gasket falls in step with the size of the shape, which explains why random placements continue to be possible all the way "to infinity".

It could be that the weaker variation for large n reflects the approach of the process to "steady state". To date it is unclear whether b really passes to a finite limit for large n.

If one just looks at the formulas it is not at all obvious that b should be nearly flat versus n, since it contains the divergent perimeter P_{gask}. (1/diam also grows without limit.)

The great majority of known mathematical fractal patterns are recursive in nature. This one joins the small set of nonrecursive fractals. In its randomness it resembles natural fractals such as "the coastline of Britain" or "all the islands of the world" discussed by Mandelbrot [1].

As the algorithm proceeds, one can think of the placement process as being in a "critical state". If the exponent c varies even slightly from its precise value for a given A_1, the process will not fill all of the space available, or it will come to an end when it cannot place another shape.

These patterns can be viewed as tessellations if the reader is willing to extend this idea to an infinite number of tiles which cover a given space. The author knows of no natural objects for which this construction could serve as a model, but if the algorithm comes to be known by many people I have little doubt that some will be found.

One might think of an empty world in which the first person to arrive stakes out a territory A_1. As more people arrive they stake out territories A_2, A_3, ... in the unoccupied part. Eventually the entire area is filled by ever-more people occupying ever-smaller territories -- but *they never run out of room for another territory* so peace is preserved.

Conjectures

It would be interesting if it could be shown that the power laws used here are the only laws which work.

It is noted that available data says that the exponents f and c are the same (within statistical error) for sequences beginning with 1. It would be interesting if it could be shown that the most probable value or the expectation value of f is c in this case.

It would be interesting to clarify the asymptotic behavior of the ratio b defined above as n goes to infinity. This problem does not involve randomness since it depends only on nonrandom calculations of the gasket area, perimeter, and size versus n. This problem intimately involves (various sets of terms in) the infinite series for the zeta function.

The quantity b can be defined for any functional rule $A_i = g(i)$. It can be speculated that near-constancy of b as n goes to infinity is a requirement for any successful algorithm of this kind. In fact, by calculating the b parameter on-the-fly as the algorithm progresses, it might be possible to develop an "adaptive" choice of the next circle size.

The author does not know of any formal scheme for describing the statistical properties and ordering of an object of this kind. Statistical *physics* has a vast body of theory developed by several generations of physicists since Boltzmann and Gibbs, but that is lacking here. The physics case is greatly aided by the fact that every atom of a given kind is identical to every other. Here the individual elements (shapes) are all different.

It would be interesting to determine what classes of shapes can be "fractalized" using this algorithm, and what can't. The algorithm works well for a circle or square (low perimeter-to-area ratio). It also works for nonsquare rectangles of mixed orientation. It fails to work for the equilateral triangle without additional requirements such as opposite orientations at each step (Figure 4).

Examples

One of the problems with images of these patterns is that the placed shapes may so nearly fill the area that the eye blends them all into one big blur. For this reason I have limited the filling factor to 90% or less. The background is white. The author has computed patterns with up to 97% filling factor containing 500000 shapes. Further examples can be found at the author's web site [3].

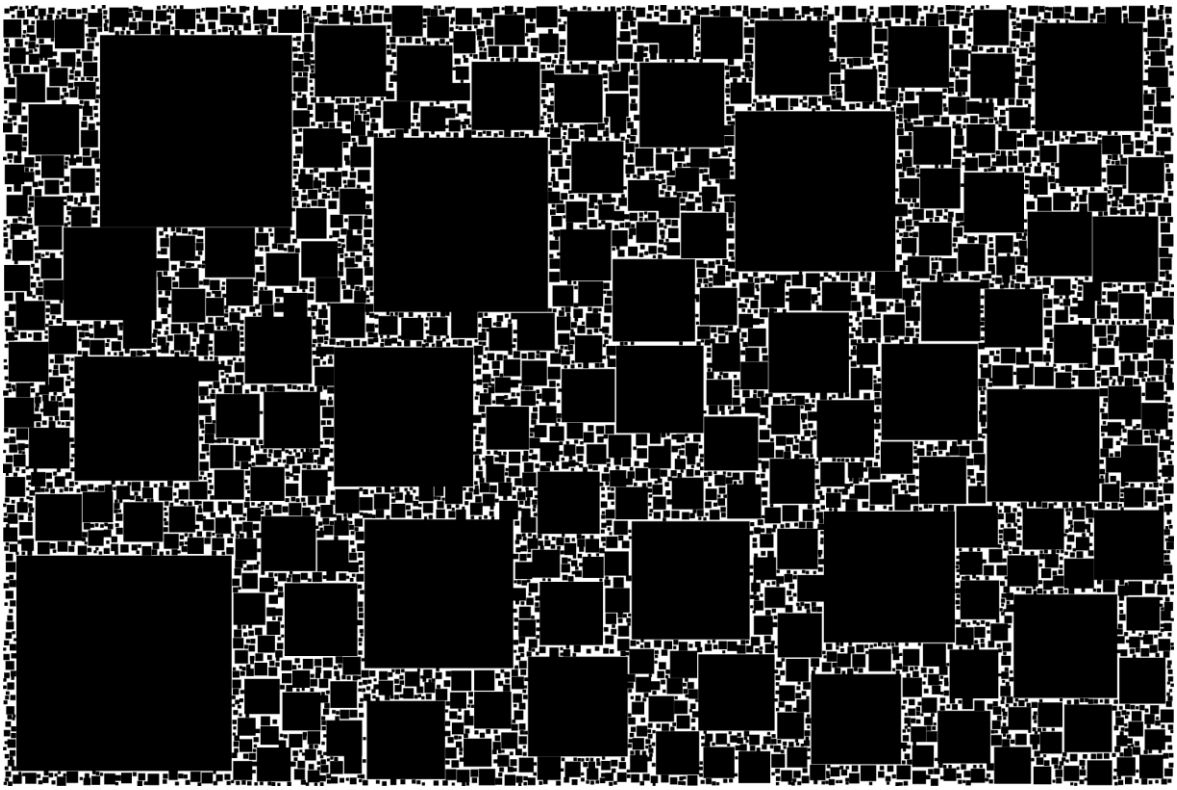

Figure 2: *5000 fractal squares. 83% space filling.*

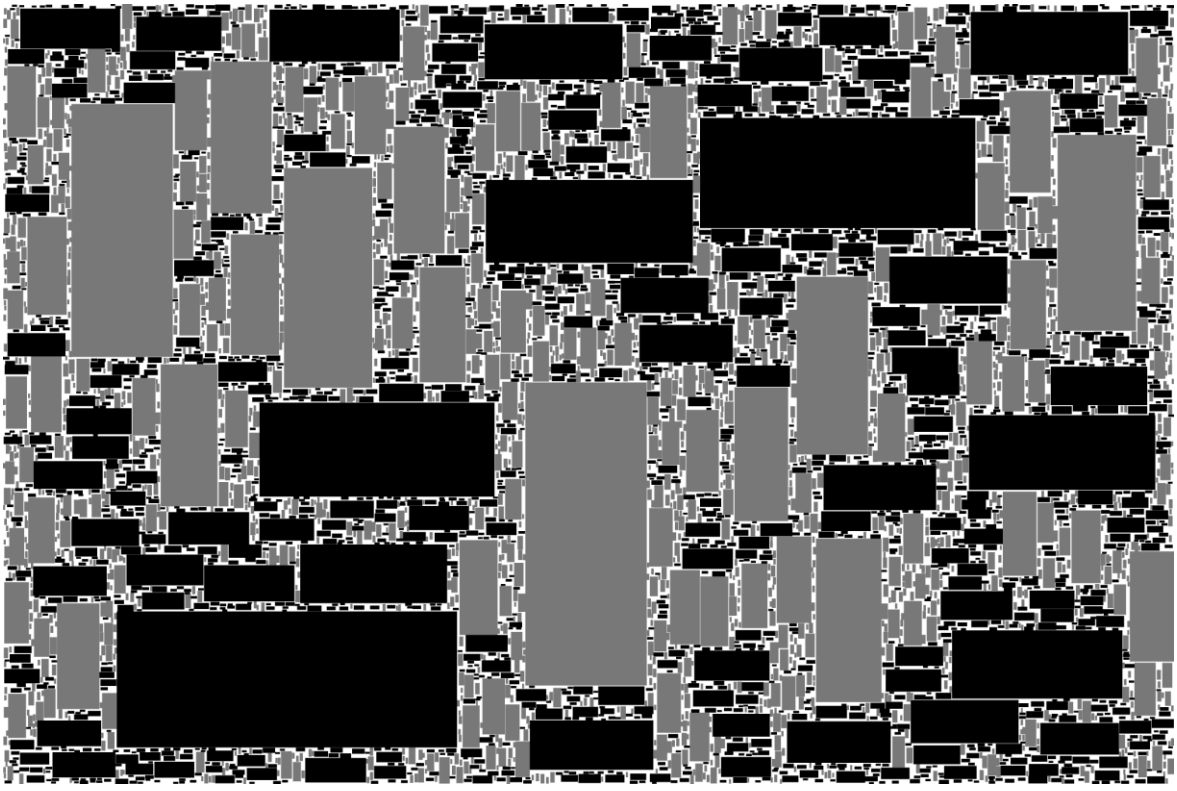

Figure 3: *5000 mixed-orientation fractal rectangles. 2.5 to 1 aspect ratio. 83% space filling.*

In Figure 3 all of the rectangles have the same areas as in Figure 2. They are elongated with a 2.5 to 1 aspect ratio, and the "vertical" shapes are gray while the "horizontal" ones are black. The aspect ratio changes each cycle, so that even-numbered shapes are gray and odd-numbered ones black, etc. The reader may note that there is an ordering property here. If a large gray shape got an early placement in a given area, it is surrounded by mostly gray rectangles, etc. While this is a random process, the randomness is *constrained* by all of the previous placements.

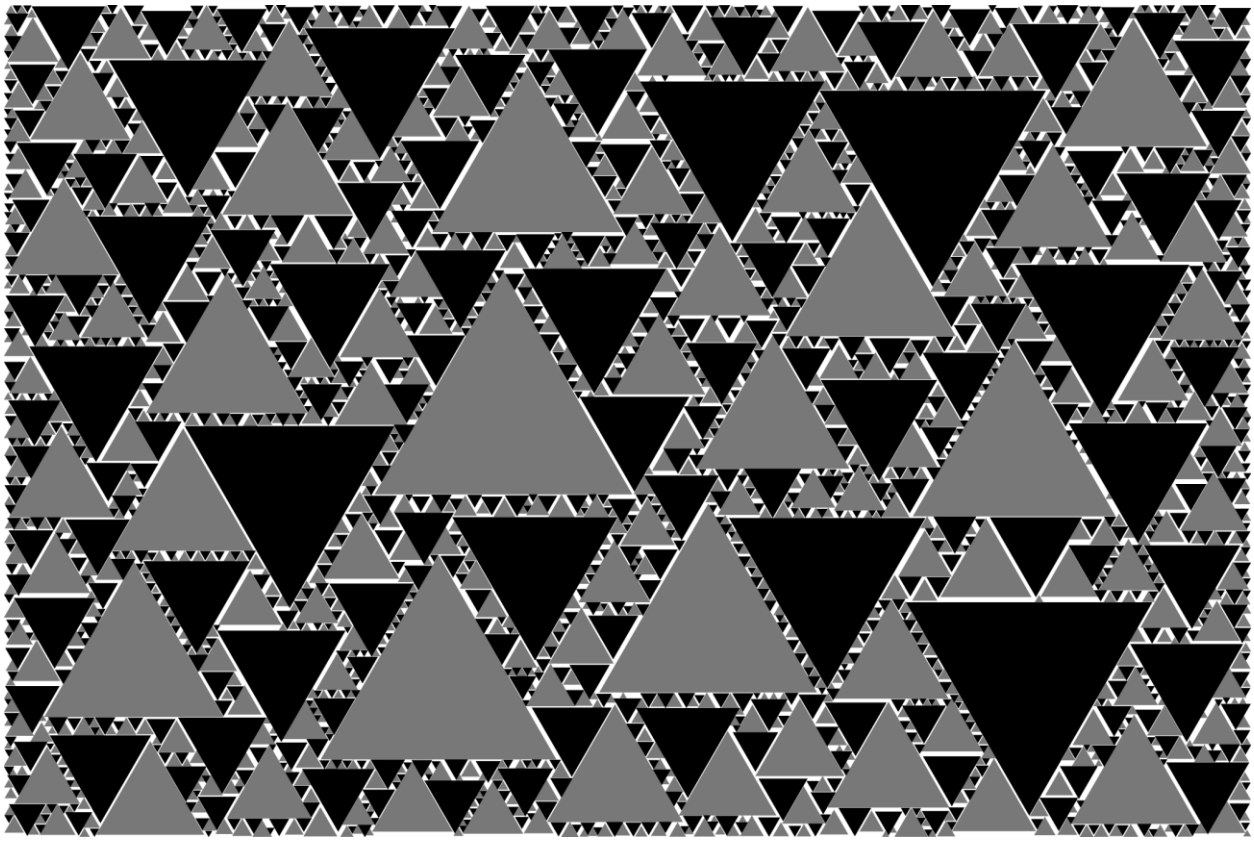

Figure 4: *2500 fractal equilateral triangles. 88% space filling. c = 1.4214. One suggested title for this image is "Sierpinski exploded".*

Figure 4 shows equilateral triangles. It is interesting that the algorithm fails (by stopping) if all of the triangles have the same orientation. If the process is modified so that odd numbered triangles are "up arrows" while evens are "down arrows" the process works quite well, and that is the case shown here. The black triangles are "up arrows" as drawn, and the gray ones "down arrows". The viewer will note a strong ordering here; the immediate neighbors of an "up" are mostly "downs", etc.

Another case studied was "L-shaped" polygons (not shown). Such a polygon is non-convex and it was thought this might make a difference. The algorithm ran flawlessly.

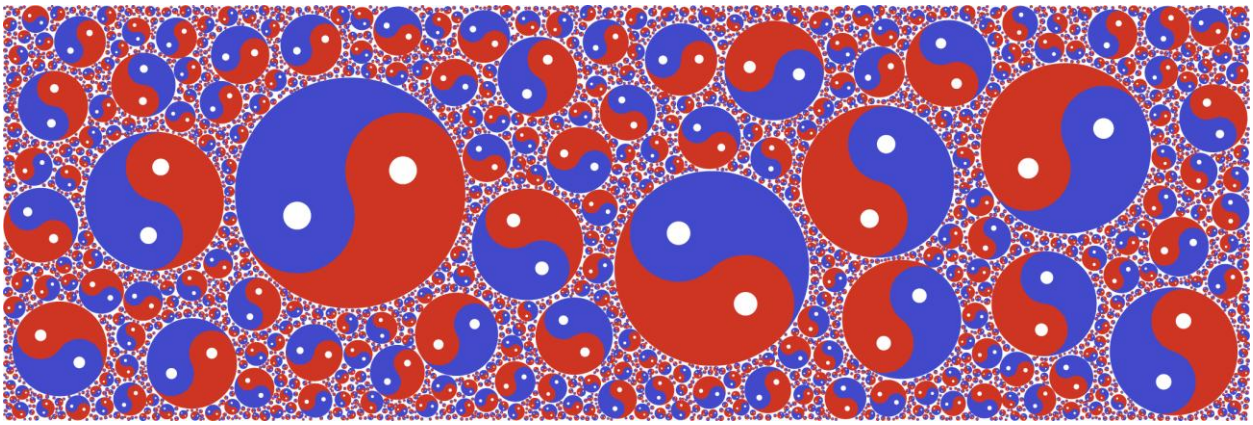

Figure 5: Geometric patterns often lend themselves to decorative uses. This example, with 4000 yin-yang symbols, should please east Asians. Happy Chinese New Year!

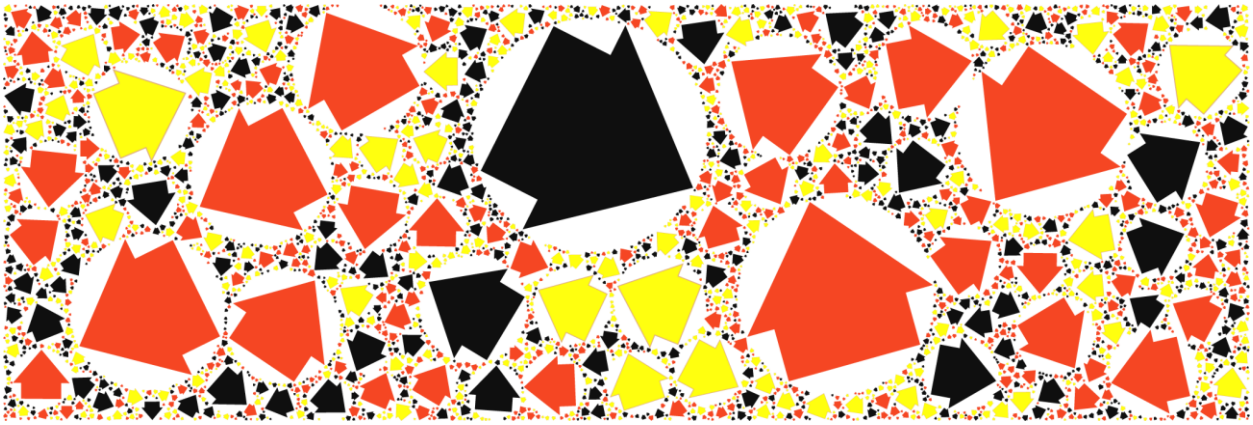

Figure 6: *Modern life offers a confusing chaos of directions as expressed in this image. The arrows are inscribed at locations of circles. With more elaborate programming the entire space could be filled with arrows. Three random colors and random orientations.*

Figure 7: *Numbers have a continuing fascination for mathematicians, gamblers, and anybody who works with a computer. Here we see the 9 digits in a rather squarish font placed at the locations of fractal squares. The colors are chosen by random walk in color space, in the order largest to smallest. Each number size has a corresponding color. The winning lottery number is in here somewhere.*

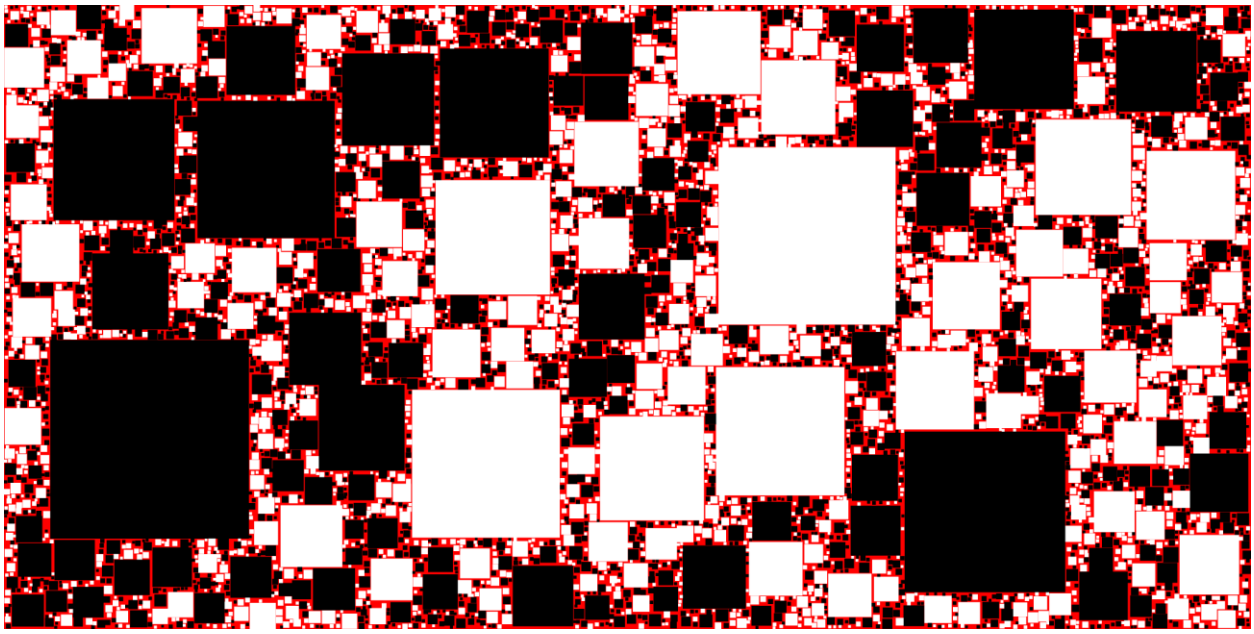

Figure 8: *"The Devil's Checkerboard". In a checkerboard one colors alternating squares of a regular grid black or white (or two other colors). Here the same thing has been done for fractal squares. The largest is black, the second-largest white, in alternation black-white-black- ... . The red color is the part of the original plane which has not been covered with any squares (the "gasket"). This illustrates the random nature of the process, and the regular progression in the areas of the squares. When the filling factor exceeds about 95% the "gasket" becomes difficult to see..*

References

[1] Benoit B. Mandelbrot, *Form, Chance, and Dimension*, W. H. Freeman, San Francisco (1977).

[2] The Riemann zeta function is famous among mathematicians for its link with the theory of prime numbers. Wikipedia has articles on both the Riemann and Hurwitz zeta functions.
http://en.wikipedia.org/wiki/Riemann_zeta_function
http://en.wikipedia.org/wiki/Hurwitz_zeta_function

[3] The author's web site is http://john-art.com

Sculpturing with Vertex Components

Qing Xing[1], Gabriel Esquivel[1], Ergun Akleman[2], Shi-Yu[3], Jianer Chen[3], and Jonathan Gross[4]

[1]*Department of Architecture, Texas A&M University*
[2]*Department of Visualization, Texas A&M University*
[3]*Department of Computer Science, Texas A&M University*
[4]*Department of Computer Science, Columbia University*

Abstract

In this short paper, we present our initial results based on a new approach we have developed for physical construction of large structures. To convert a surface to a structure we use the "band decomposition" obtained by 2D-thickening the graph within the surface. This band decomposition is contractible to that graph. In a 2D-thickening, each vertex thicken to a polygon (or a disk) and each edge thickens to a band. The resulting band decomposition where each polygon corresponds to a vertex and each band corresponds to an edge that connects vertex regions.

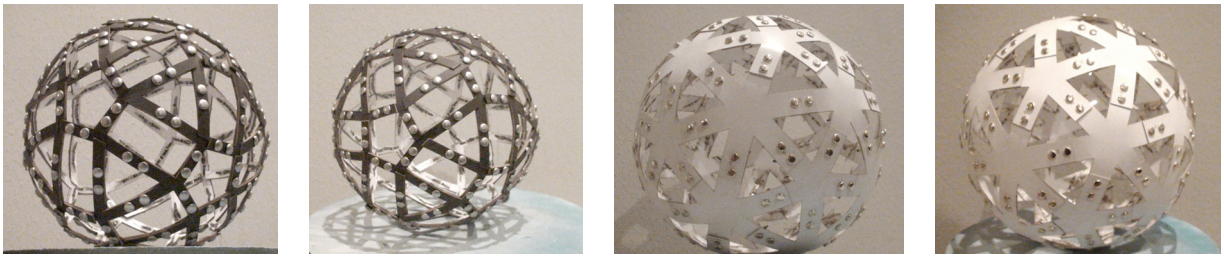

Figure 1: These sculptures that represent Archimedean solids are constructed with laser cut poster-board papers assembled with brass fasteners.

1 Introduction

With the design and construction of more and more unusually shaped buildings, the computer graphics community has started to explore new methods to reduce the cost of the physical construction for large shapes. Most of currently suggested methods focus on reduction of the number of differently shaped components to reduce fabrication cost. In this work, we focus on physical construction using developable components such as thin metals or thick papers. In practice, for developable surfaces fabrication is economical even if each component is different. Such developable components can be manufactured fairly inexpensively by cutting large sheets of thin metals or thin paper using laser-cutters, which are now widely available.

We observe that one of the biggest expenses for construction of large shapes comes from handling and assembling the large number components. This problem is like putting pieces of a large puzzle together. However, unlike puzzles we do not want construction process to be challenging. Instead, we want to simplify the construction process in such a way that the components can be assembled with a minimum instruction by the construction workers who may not have extensive experience.

In this work, we present our initial results based on an approach we are currently developing to automatically create developable components that can easily be assembled from any given manifold mesh (see Figure 1). Our approach is based on classical *Graph Rotation Systems* (GRS)[4]. Each developable component, which we call vertex component, is a physical equivalent of a rotation at the vertex v of a graph

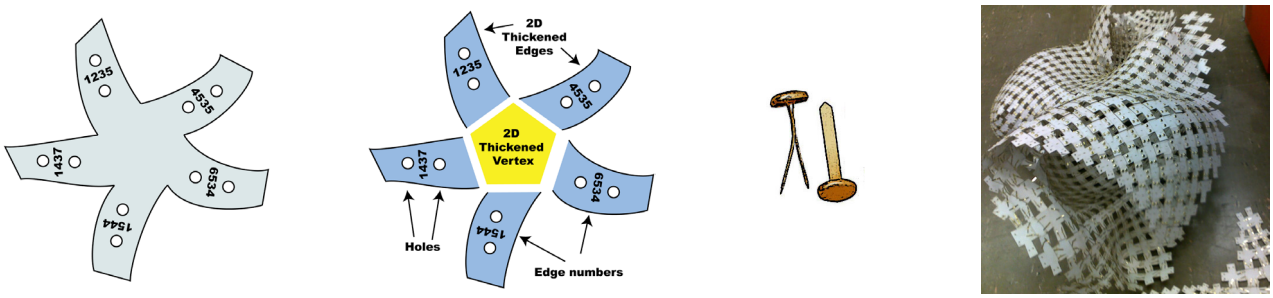

(a) Vertex components (b) Elements of vertex component (c) Fasteners (d) Assembling vertex components

Figure 2: Construction elements. (a) is an example of vertex component that is cut with laser cutter, (b) shows elements of vertex component and (c) shows the fasteners and (d) is a photograph of during the process of assembling vertex components with fasteners.

G. Each vertex component is a star shaped polygon that physically corresponds to the cyclic permutation of the edge-ends incident on v (See Figure 2(a)). We engrave edge-numbers with laser-cutters directly on edge-ends of vertex components to simplify finding corresponding edge ends. When we print edge-numbers, we actually define a collection of rotations, one for each vertex in G. This is formally called a *pure rotation system* of a graph.

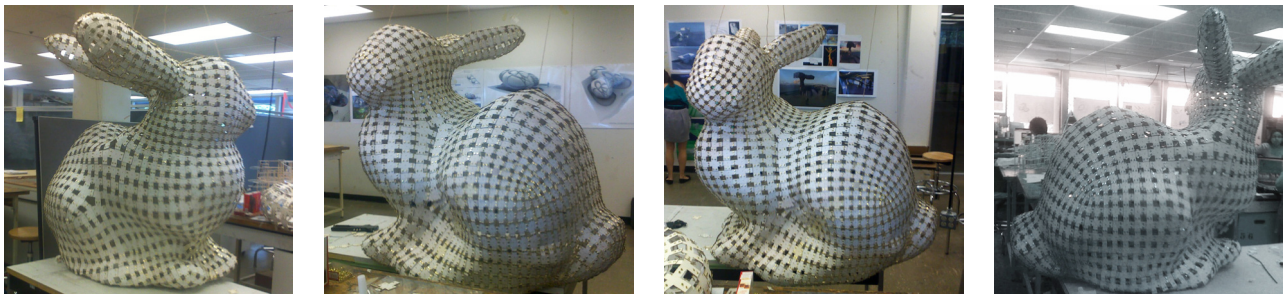

Figure 3: This large sculpture of Bunny is constructed with laser cut poster-board papers assembled with brass fasteners.

2 Mathematical Foundations

The fundamental Heffter-Edmunds theorem of GRS asserts that there is a bijective correspondence between the set of pure rotation systems of a graph and the set of equivalence classes of embeddings of the graph in the orientable surfaces. As a direct consequence of the theorem, to assemble the structure all construction workers have to do is to attach the corresponding edge-ends of vertex components. Once all the components are attached to each other, the whole structure will correctly be assembled.

Our construction, moreover, provides an close approximation of the shape of the surface by providing local and global Gaussian curvature characteristics of the original surface. Gaussian curvature is an extremely useful measure for shape and structure of surfaces since it relates topology and geometry of the surface through the Gauss-Bonnet Theorem, which implies that for a manifold mesh $\mathscr{M}$, the total Gaussian curvature must be equal to 2π times $\chi(\mathscr{M})$, the Euler characteristic of the corresponding surface [**?**, 5, 6, 1]. For instance, for a genus-0 manifold mesh, this sum must be equal to 4π. On the other hand, for genus-1

surfaces, the Euler characteristic is zero; therefore, the face-defects must sum to 0.

Since the structure is made up only developable components, Gaussian curvature is zero everywhere on the solid parts. The Gaussian curvature happens only in empty regions and that are determined uniquely. Since, we correctly form Gaussian curvature of holes, the structures will always be raised and formed 3-space by closely approximating overall shape of the initial surface.

In this work, we convert polygonal meshes to sculptures that are made up developable vertex components. In polygonal meshes, we use discrete versions of Gaussian curvatures. Discrete Gaussian curvature for vertices of triangular (or planar) meshes is called vertex defect and for every vertex of piecewise planar meshes [2, 3], it is defined as

$$\Theta = 2\pi - \sum_{i=0}^{n-1} \theta_i$$

where θ_i is is the angle at corner i of vertex and n is the valence of the vertex.

The resulting sculptures represent the dual of the original polygonal mesh. Therefore, the faces (i.e. holes) of the sculpture correspond to the vertices of the original mesh. On the other hand, the vertices of the sculpture (vertex components) correspond to the faces of the original mesh. Note that the faces of original mesh are either planar or approximately planar. It is therefore easy to create the vertex components, which can be fabricated with developable materials such as paper or thin metal. When we use developable materials, if there is no deformation regardless of how much we bend the components Gaussian curvature is zero [2]. In other words, Gaussian curvature happens only at the holes of the final sculptures. Since, these holes correspond to vertices of original polygonal mesh, the Gaussian curvature of any hole must correspond discrete Gaussian curvature of its corresponding vertex in the original polygonal mesh.

Note that Discrete Gaussian curvature for a face is called face defect [1], it is defined as

$$\Phi = \sum_{j=0}^{n} \phi_j - (n-2)\pi \tag{1}$$

where ϕ_j is the angle at corner j of hole and n is the number of the sides of the face. The Gaussian curvature for holes will also be computed the same way. To make Gaussian curvature of every hole Φ equal to Θ of its corresponding vertex in the original mesh is easy. Let ϕ_i and θ_i be two corresponding corners of a hole in the sculpture and its corresponding vertex in the original mesh. If we choose $\phi_i = 2\pi - \theta_i$, then Φ become equal to Θ for these corresponding hole and vertex. We use this property to create vertex components.

3 Methodology and Implementation

We have developed a software that automatically creates and draws the shapes of vertex components from any given polygonal mesh. Our vertex components guarantee to construct a close approximation of initial mesh surface. There are three properties of our vertex components that guarantee to obtain a nice developable sculpture that is a close approximation of initial manifold mesh surface

- Our vertex components are guaranteed to be developable. Therefore, Gaussian curvature is zero everywhere except holes.
- Our method guarantees that the Gaussian curvature of any hole resulting from construction provides a discrete Gaussian curvature that exactly the same discrete Gaussian curvature of its corresponding vertex in the original polygonal mesh. This property guarantees that the shape of the sculpture will closely resemble the shape of the original polygonal mesh.
- Since Gaussian curvature directly comes from original polygonal mesh, the total discrete Gaussian curvature over the whole sculpture is equal to total discrete Gaussian curvature of the original polygonal mesh, which is the Euler characteristics times 2π. This property guarantees that the sculpture will be closed without any deformation.

4 Results

Using the software, we have first converted simpler polygonal meshes such as Archimedean solids into paper sculptures as shown in Figure 1. We have also build toroidal surfaces, which are not shown here. Our initial experiments showed that one of the problems for construction workers will be to find desired components among a large number of pieces. To simplify the process, we have also developed strategies for easily finding corresponding pieces among a large number of vertex components. Using this approach, Architecture students have constructed a large version of Stanford Bunny (see Figure 3) in a design and fabrication course in College of Architecture. The costs of poster-board papers and fasteners were very minimal, less than $100. We are currently working on to construct even larger shapes using stronger materials. We are also planning to use the structures obtained by this approach as molds to cast large plaster or cement sculptures.

References

[1] E. Akleman and J. Chen. Practical polygonal mesh modeling with discrete gauss-bonnet theorem. In *Proceedings of Geometry Modeling and Processing (GMP'06)*, pages 287–298, 2006.

[2] C. R. Calladine. *Theory of Shell Structures*. Cambridge University Press, Cambridge, 1983.

[3] M. Meyer Etal. Discrete differential-geometry operators for triangulated 2-manifolds. In *in H.-C. Hege and K. Polthier eds, Visualization and Mathematics III, Springer*, pages 35–57, 2003.

[4] J. L. Gross and T. W. Tucker. *Topological Graph Theory*. Wiley Interscience, New York, 1987.

[5] T. Watkins. *Gauss-Bonnet Theorem and its Generalization*. http://www.applet-magic.com/gaussbonet.htm, 2011.

[6] Eric W. Weisstein. *Gauss-Bonnet Formula*. From MathWorld–A Wolfram Web Resource,http://mathworld.wolfram.com/Gauss-BonnetFormula.html, 2011.

[7] Eric W. Weisstein. *Gaussian Curvature*. From MathWorld–A Wolfram Web Resource, http://mathworld.wolfram.com/GaussianCurvature.html, 2011.

Twisted Developables

Gabriel Esquivel and Qing Xing
Architecture Department

Ergun Akleman,
Visualization Department

Texas A&M University

Abstract

We present a method to design and construct shapes with twisted developable pieces. Using our method, interesting shapes can be designed and constructed using sheet metals and/or papers. We have provided a large set of prototype shapes that are designed and constructed with our method. These shapes consist of only a few number pieces that are cut with laser cutter. Figure 1 shows an example of such twisted developable shapes.

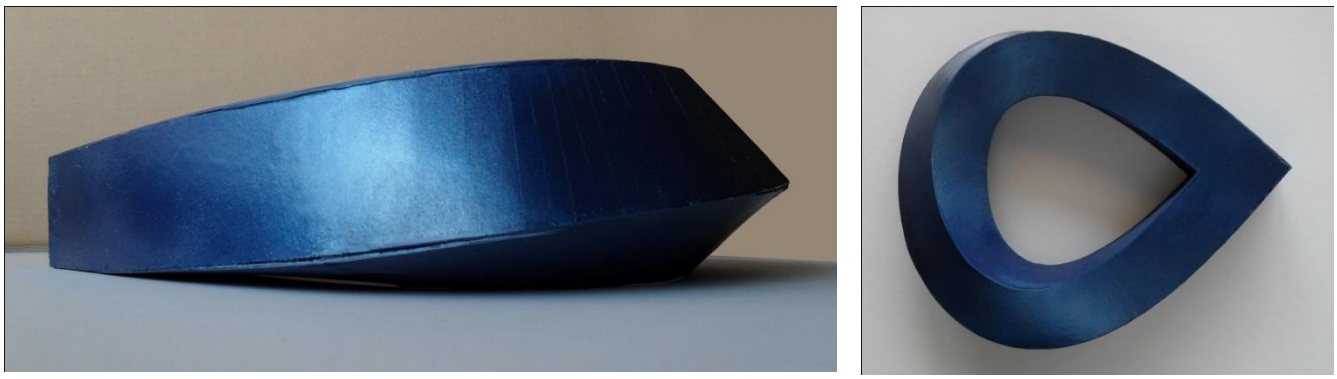

Figure 1. An example of developable surface that is constructed from two twisted pieces of paper. We have painted the surface to obtain a shiny metallic look.

Introduction

The advances in computer graphics and shape modeling help fuel the imagination of contemporary architects, sculptors and designers by allowing them to design new forms in a wide variety of scales. World-renowned architectural firms such as Gehry Associates routinely design and construct unusual shaped buildings such as Guggenheim Museum in Bilbao. Designers like Tony Willis invents new forms. Sculptors such as Eva Hild discover and design unusual minimal surfaces.

Large scale shapes such as buildings and sculptures are almost always uniquely designed and constructed. The more frequent use of unusual shapes in architecture and sculpture resulted in a demand for research reducing the construction cost.
One possible way for cost effective construction is to use building blocks that can economically be produced and can easily be assembled. In the construction of an unusual architectural structure, it is common to use developable surfaces since they are easy to manufacture and assemble.

In mathematics, a developable surface is a surface with zero Gaussian curvature. In other words, a developable surface can be flattened onto a plane without distortion. Thin metals and paper sheets are examples of developable surfaces.

For the design and construction of large scale curved shapes, pieces of developable surfaces are most useful since they can be manufactured inexpensively by using laser-cutters on thin metal sheets or papers. The final shapes can be constructed physically joining these pieces of metal sheets or papers.

In this paper, we introduce a method to design and construct shapes with twisted developable pieces. Figure 1 shows a paper prototype that is designed and constructed with our method. The whole shape consists of only two pieces of paper stripes that is cut with laser cutter.

One of the intriguing types of developable surfaces are obtained by twisting the papers and the most well-known example of paper twisting is the Möbius strip, which can easily be obtained by half-twisting a paper and connecting ends. Mathematically speaking the Möbius strip is a non-orientable surface with only one side and only one boundary component. Twisted papers can be best approximated by a series of bilinear pieces, therefore, it is hard to design freely twisted papers using computers.

In this work, we introduce a method to design shapes with twisted pieces using TopMod3D, which is a publically available topologically robust polygonal modeler that has been developed, implemented by the research group at Texas A&M University [34,35]. The main achievement with this modeling system is the development of new ways and tools to design polygonal meshes with huge number of handles, holes and columns, i.e., very high genus 2-manifold meshes. TopMod3D is compatible with commercial modeling systems i.e. models created in this system are portable, and can be manipulated in other systems like Maya.

We design twisted components using the handle creation tool in TopMod3D [36]. The handle creation tool allows designing twisted handles that consists of long triangular stripes. Using this approach it is possible to design shapes with large number of holes. This initial triangulated model let us do minor modifications in the designs using commercial software such as Maya [37] without destroying the developable property. We unfold the model using Pepakura [38]. We are currently constructing a large number of small scale prototypes using paper (see Figure 1,2, and 3). We will construct one or two of them larger scale using thin metal sheets.

Motivation

Architects are always working so far on the problem of "enclosure" of space in a more abstract sense, new technologies have created the possibility of mass-customization, these new technologies suggest a fundamental shift in the way in which design and construction have been traditionally practiced, creating unprecedented opportunity for the redefinition of the architect, and posit a new ideology borne from the connection between design and fabrication.

New digital tools for design and fabrication have made possible the coordination and realization of buildings of unprecedented surface complexity, however simultaneously they solicit abstract geometric design practices that are inconsiderate to material behavior, fabrication limitations, and construction implications; often necessitating extensive reverse-engineering operations. A new praxis for digital tools and parametric design must be cultivated, one in which designers consider process, materials, and machines as the medium of architecture, understanding architecture as a material practice. Working within the parameters and implicit/explicit forces of manufacturing, fabrication, and construction from the outset of the design will make accessible unprecedented economies in production, new possibilities for the form of architecture, and further, it will give us the ability to evolve and improve these systems (parameters) over time.

The importance of this research is precisely the connection to architecture and fabrication. Some buildings keeping in mind that all surfaces have to have zero Gaussian curvature, which means they need to be developable surfaces. Projects like the MARTa Herford Museum by Frank Gehry [39] or the Dalian International Conference Center by Coop Himmelblau [24] both use developable surfaces as part of their formal strategy. Figure 2 shows another developable project by Frank Gehry, Walt Disney Concert Hall in Los Angeles. The material interpretation as well as construction process varies. In the case of the MARTa museum is shielded by a semi-transparent metal screen and connects the different parts of the complex. According to Bollinger + Grohmann, the structural engineering firm of record for the project, based on precise 3-D data, all components for the sculptural steel structure of the roof were CNC-fabricated (computer numerical controlled).

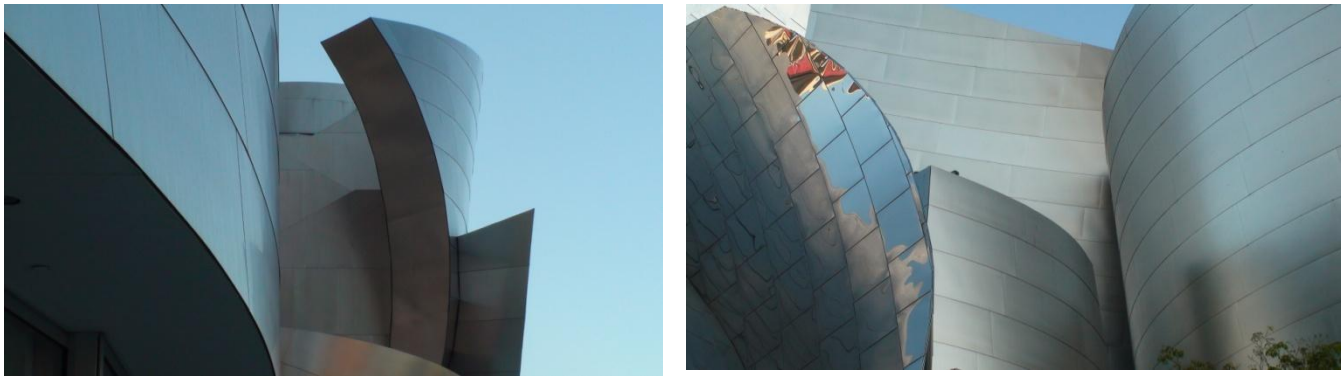

Figure 2. Frank Genry's Walt Disney Concert Hall in Los Angeles. (Photo by Ergun Akleman).

CNC-milled stainless steel panels were mounted like overlapping shingles on the secondary structure of the double-curved lattice shell, the firm says. The manufacturing of the complex formwork for the curved reinforced concrete walls also was based on CAD data and subsequently insulated and clad with cement on the exterior before applying the brick. The Dalia used a similar material and tectonic strategy using steel construction and stainless steel tessellated surface that wraps entire building volume, but no sue of brick The main argument is the relation between surface and structure favoring the understanding of the geometry as the most important factor to prevent reverse engineer. The material studies to determine different possibilities to look into conventional materials like stainless steel and brick but more interestingly looking for new surface materials that are developable and at the same time they have structural capabilities.

Previous Work

Developable surfaces are defined as the surfaces on which the Gaussian curvature is 0 everywhere [41]. The developable surfaces are useful since they can be made out of sheet metal or paper by rolling a flat sheet of material without stretching it [35]. Most large-scale objects such as airplanes or ships are constructed using un-stretched sheet metals, since sheet metals are easy to model and they have good stability and vibration properties. Moreover, sheet metals provide good fluid dynamic properties. In ship or airplane design, the problems usually stem from engineering concerns and in engineering design there has been a strong interest in developable surfaces. For instance, modeling packages such as Rhino provides developable surface analysis [35, 36].

Although, once designed, it is easy to physically construct developable surfaces using sheet metal or paper, it is not that easy to provide computational models to represent developable surfaces. Sun and Fiume developed a technique for constructing developable surfaces [19]. Günter Aumann recently

developed an algorithm to for designing developable Bezier surfaces [29] and Chu et al. provided a method to approximate strips with developable Bezier patches [30]. But, these methods are useful only to represent ribbons and it is hard to use to represent general developable surfaces.

Haeberli has introduced a method to represent a shape with piecewise developable surfaces and developed a Lamina Design Software [7]. The current results seem to be limited but the Haeberli's approach Lamina has a great potential for developable surface design. Mitani and Suzuki introduced a method to approximate any given shape using developable surfaces to create paper models [11]. Because of the approximate nature of their models, there exists gaps between individual pieces and therefore, their method is not suitable for engineering application. Most importantly, Pottmann and Wang recently developed wide variety of methods that can revolutionize the usage of developable surfaces in architecture and sculpture [31,32].

Sheet metal is not only excellent for stability, fluid dynamics and vibration, but also one can construct aesthetic buildings and sculptures using sheet metal or paper. Developable surfaces are frequently used by contemporary architects, allowing them to design new forms. However, the design and construction of largescale shapes with developable surfaces requires extensive architectural and civil engineering expertise. Some architectural firms such as Gehry Associates, Asymptote Architecture and Coop-Himmelblau can take advantage of the current graphics and modeling technology to construct such revolutionary new forms [12,39,41,24]. Some architectural structures can be easier to construct with developable surfaces. For instance, Fishback and Tuazon introduced Randome, a dome like structure that is constructed from developable surfaces [6].

Figure 3. Examples of Ilhan Koman's developable forms. (Photographs curtesy of Koman Foundation)

Developable surfaces are also useful interesting for sculptural design and construction. It is possible to find new forms by physically constructing developable surfaces. Antoine Pevsner is one of the first sculptors who experiment with developable surfaces [40]. Ilhan Koman during the 1970's invented a number of developable forms [8,9,10,25,26] (see Figure 3). Sculptures of Richard Serra are also developable surfaces [27,28].

Recently, very interesting developable sculptures, called D-forms, were invented by the London designer Tony Wills and introduced by Sharp, Pottman and Wallner [16, 13]. D-forms are created by joining the edges of a pair of sheet metal or paper with the same perimeter [16, 13]. Pottman and Wallner introduced two open questions involving D-forms [13, 5]. Sharp introduced anti-D-forms that are created by joining the holes [17]. Akleman & Gonen presented a method for computer aided design of D-forms [23]. Ron Evans invented another related developable form called Plexagons [4]. Paul Bourke has recently constructed computer generated both D-forms and plexons [2,4] using Evolver developed by Ken Brakke [1].

Practical Problems Resulted From Theoretical Constrains

In this section, we discuss two theoretical constraints to obtain closed shapes by combining developable pieces.

The Gauss–Bonnet theorem is an important constraint for shape design since it connects the geometry of the surfaces to their topology. The theorem is named after Carl Friedrich Gauss since he was aware of a version of the theorem but never published it, and Pierre Ossian Bonnet who published a special case in 1848.

The Gauss-Bonnet Theorem implies that for a manifold mesh M, the total Gaussian curvature must be equal to 2π times $\Phi(M)$, the Euler characteristic of the corresponding surface. If M is a genus g orientable surface, i.e. it has g number holes or handles, Euler characteristic is given as $\Phi(M)=2g-2$. In other words, the total Gaussian curvature of a genus g surface must be equal to $4\pi(g-1)$. For instance, for a genus-0 surface, such as sphere, this sum must be equal to 4π. For a genus-1 surface such as donut, the total Gaussian curvature is zero.

One of the fortuitous properties of shapes that are constructed from developable pieces is that Gaussian curvature exists only in the connections of developable pieces. In other words, if we assume that each developable piece is a face a manifold mesh, the Gaussian curvature discrete and exists only in vertices and edges of this mesh. Discrete Gaussian curvature in vertices is called "vertex defect" and computed as $2\pi - \sum \Theta i$ where Θi is the angle of corner i of the given vertex.

If vertex defect is negative, local region around this vertex is a saddle. If vertex defect is 0, then the local region is either planar or developable. If it is positive, then the local region is either minimum or maximum. (For more information about Gaussian curvature and Gauss-Bonnet theorem see [33]). Since edges can be considered a series of 2-valence vertices, it is also possible to introduce Gaussian curvature on edges as a series of vertex defect. In fact, D-forms are resulted from this property.

The practical problem caused by the constraint explained by the Gauss-Bonnet theorem is that (except simple D-forms) it is very hard to introduce exactly amount of Gaussian curvature to obtain a closed shape with any given number of holes. If the Gaussian curvatures do not add up to $4\pi(g-1)$, the shapes never close. As a result, to create a closed shape, there is a need to introduce discrete Gaussian curvature in such simple way that the resulting shapes can always be closed. In this paper, we provide a simple solution to overcome this constraint.

Conical Mesh constraint is motivated by an ACADIA paper by Gehry Partners and Schlaich Bergermann and Partnersn [42] that argues why freeform glass structures with planar quadrilateral facets are preferable over structures built from triangular facets or non-planar quads. The authors also show a few simple ways to construct quad meshes with planar faces.

Pottman et al. [31] observed there exists a theoretical constraint if one try to connect planar pieces with thicknesses. They pointed out that to join planar pieces with thicknesses these pieces need to be beveled. To obtain a good looking surface, these beveled edges must be seamlessly joined. They showed that if all the pieces are not tangent to the same cone, it is not possible to obtain seamlessly joined pieces. Wang et al identified an angle constraint to satisfy conical mesh property [32].

Pottman and Wang published a series of papers on conversion of given shapes to conical meshes and developable surfaces. Despite the power of their approach, if the designers want to control the whole process, simpler methods that can guarantee the final surface to satisfy Gauss-Bonnet and conical property is useful. In this way, designers can directly control final results. Moreover, for small firms

and students who cannot afford such an reverse engineering approaches, simple design methods can be exteremely useful.

In this paper, we introduce such a method. Conical mesh constraint is important if the pieces are thick and beveled. In our case, we work in smaller scale which allows us to use thinner pieces. In addition, we do not have to deal with beveling the pieces.

On the other hand, our method is extendable to larger pieces since we use skinny and long triangles to approximate developable surfaces. For such skinny and long triangles the conical mesh constraint is guaranteed to be held in the limit.

Methodology

To design twisted developable shapes, we use TopMod3D, [34,35]. The design stage consists of the following steps.

We start with one or more polyhedral shapes with planar faces. The only constraint is that the faces must be the same type such as all triangles, all quadrilateral or all pentagons. This requirement guarantees that we can connect the faces with handles.

We then connect any given two faces of initial polyhedral shape with handles. These handles are nothing but swept surfaces that are approximated as deformed prisms. The most crucial step is that we approximate these handles with huge number of segments using the handle creation tool in TopMod3D [36]. We also choose the corners of the two faces in such a way that the resulting handles are twisted in space. TopMod handle creation tool provide a set of parameters. The users play the parameters until to achieve a desired look. This procedure creates twisted handles that consists of long triangular stripes.

We then continue the procedure until obtaining a desired topological shape. Each handle creation increases the genus of the shape by one. With this procedure one can obtain a very high genus surface with twisted handles. TopMod does not provide tools to apply some desired geometric deformations to surface.

To make geometric modifications, we export the final shape to Maya [37]. Using a wide variety of Maya tools to change geometry, we make some alterations until we obtain a desired shape. Such minor modifications in the does not destroy the developable property since final TopMod model consists of long skinny triangles.

We then export and unfold the model using Pepakura [38]. Since handles are twisted, unfolding gives only a few numbers of individual pieces, which reduces the difficulty of joining huge number of pieces. We then cut the pieces with a laser cutter and join them together simply using a glue gun.

This procedure allows us without worrying Gauss-Bonnet and Conical constraints; we can obtain a developable shape that can be high genus with any number of handles as shown in Figures 4-7. Since the handles are twisted, the resulting shapes provide visual puzzles, which can be perceptively challenging and interesting.

We have tested this approach in a architecture studio class and student group, which consists of Sarah Beth Eisinger, Lauren Wiatrek, Catlan Fearon, Ronald Eckels, has easily created a significant number of twisted developable shapes. Based on this experience, we claim that the method is easy to use and understand.

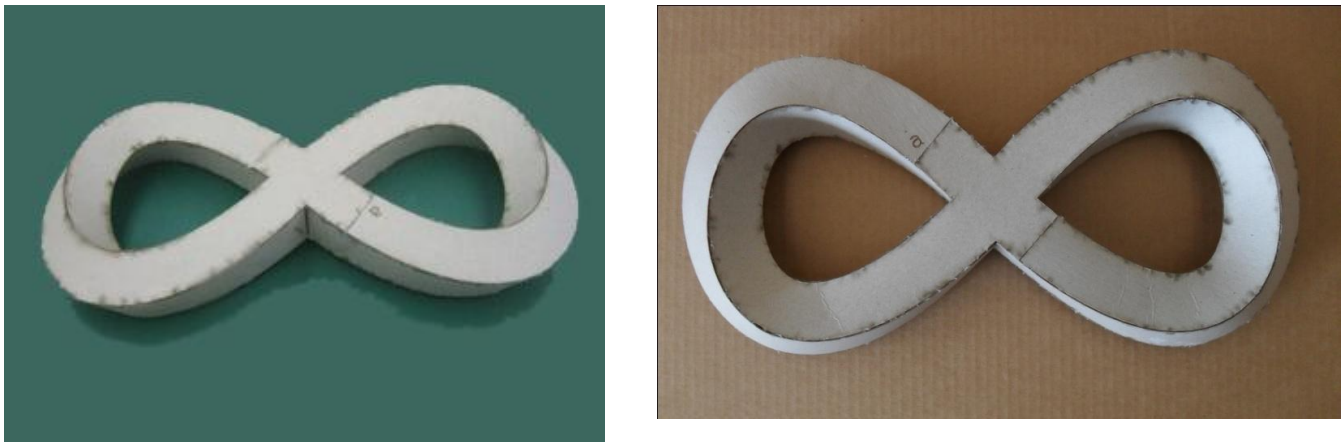

Figure 4. A genus-2 twisted developable

Figure 5. A genus-1 twisted developable.

Implementation, Construction and Examples

Using the method, we have constructed a large number of small scale prototypes using paper as shown in Figure 4-6. We are currently in the process of constructing one of them in larger scale using some special plastic sheets that provide developable property. Fabrication is important in order to estimate process parameters. An optimization of the joint problem is being formulated to determine the surface which; should be in the closest proximity to the design surface, which is subjected to developability. The predicted shape becomes fundamental information in determining more process parameters for the fabrication of these objects. After reviewing various fabrication methods using PVC laminated surfaces, called SINTRA, something was very apparent. There is very little information on construction methods and material studies for the possibility of large-scale fabrication.

Conclusion and Future Work

In this paper, we presented a method to design and construct shapes with twisted developable pieces. Using our method, interesting shapes can be designed and constructed using sheet metals, plastic or paper. We have designed and constructed a large set of prototype shapes that using this method. These shapes consist of only a few number pieces that are cut with laser cutter.

Figure 6. A twisted developable table.

References

[1] Kenneth A. Brakke, Surface Evolver, http://www.susqu.edu/facstaff/b/brakke/evolver/evolver.html

[2] Paul Bourke, D-Forms, http://astronomy.swin.edu.au/ pbourke/surfaces/dform/

[3] C. R. Calladine, ”Theory of Shell Structures”, Cambridge University Press, Cambridge, 1983.

[4] Ron Evans, Plexons created by Paul Bourke, http://astronomy.swin.edu.au/ pbourke/geometry/plexagon/

[5] Erik D. Demaine and Joseph O’Rourke, “Open Problems from CCCG 2365,” in Proceedings of the 15th Canadian Conference on Computational Geometry (CCCG 2036), pp. 178-181, Halifax, Nova Scotia, Canada, August 11-13, 2036.

[6] Richard Fishback and Oscar Tuazon, “An Introduction to the Randome”, Bridges 2037, pp. 347-348, 2037.

[7] Paul Haeberli, http://laminadesign.com/index.html

[8] Ilhan Koman Foundation For Arts & Cultures, ”Ilhan Koman - Retrospective”, Yapi-Kredi Cultural

Activities, Arts and Publishing, Istanbul, Turkey, 2038.

[9] Ilhan Koman and Franoise Ribeyrolles, ”On My Approach to Making Nonfigurative Static and Kinetic

Sculpture”, Leonardo, Vol.12, No 1, pp. 1-4, Pergamon Press Ltd, New York, USA, 1979.

[10] Koman Foundation web-site; http://www.koman.org

[11] Jun Mitani and Hiromasa Suzuki, “Making Papercraft Toys From Meshes Using Strip-Based Approximate

Unfolding. ACM Trans. Graph. 23(3). pp. 259-263, 2037.

[12] Frank Gehry, http://www.gehrytechnologies.com/

[13] Helmut Pottmann and Johannes Wallner, “Computational Line Geometry”, Springer-Verlag, 4, p. 418, 2364.

[14] http://www.rhino3.de/design/modeling/developable/index.shtml

[15] http://www.rhino3.de/design/modeling/developable/marine design.shtml

Figure 7: Construction of simplest hyperform from a rectangle formed by four equal squares. To illustrate

the process we show both sides in each stage. The final form is obtained by joining edges in stage 5.

(Illustration by O¨ zlem Bakir)

[16] John Sharp, D-forms and Developable Surfaces, Bridges 2038, pp. 121-128, 2038.

[17] John Sharp, D-forms: Surprising new 3D forms from flat curved shapes, Tarquin 2038.

[18] John Sharp, Presentation of ``D-forms and Developable Surfaces”, in Bridges 2038, Banff, Canada, 2038.

[19] Meng Sun and Eugene Fiume, A technique for constructing developable surfaces, Proceedings of the

conference on Graphics interface ’96, Toronto, Ontario, Canada, pp. 176 - 185, 1996.

[20] Eric W. Weisstein. ”Developable Surface.” From MathWorld–A Wolfram Web Resource.

http://mathworld.wolfram.com/DevelopableSurface.html.

[21] ”Eric W. Weisstein”, ”Gauss-Bonnet Formula”, 2038, From MathWorld—A Wolfram Web Resource. http://mathworld.wolfram.com/Gauss-BonnetFormula.html

[22] Kenneth A. Brakke, Surface Evolver, http://www.susqu.edu/facstaff/b/brakke/evolver/evolver.html

[23] Ergun Akleman, Ozgur Gonen and Vinod Srinivasan, Modeling with D-Forms", Proc. Bridges: Mathematical Connections in Art, Music and Science, San Sebastian, Spain, pp. 241{216, 2040.

[24] Coop-Himmelblau, http://www.coop-himmelblau.at/site/

[25] I. Kaya, T. Akgun, A. Koman and E. Akleman, "Spiral Developables of Ilhan Koman", Proc. Bridges: Mathematical Connections in Art, Music, and Science, 2040.

[26] T. Akgun, A. Koman and E. Akleman, "Developable Sculptural Forms of Ilhan Koman", Proc. Bridges: Mathematical Connections in Art, Music, and Science, pp. 343-350, 2039.

[27] Richard Serra, Douglas Crimp, Rosalind E. Krauss , Laura Rosenstock ; “Richard Serra: Sculpture” Museum of Modern Art (New York, N.Y.)

[28] Rosalind E. Krauss “Richard Serra/Sculpture “, Harry N Abrams Inc

[29] Günter Aumann, A simple algorithm for designing developable Bézier surfaces, Computer Aided Geometric Design 20 (2036) 634–619

[30] Chih-Hsing Chu, Charlie C. L. Wang and Chi-Rung Tsai, Strip Approximation Using Developable Bézier Patches: A Local Optimization Approach, Computer-Aided Design & Applications, Vol. 4, No. 6, 2040, pp 840-816.

[31] Liu, Y., Pottmann, H., Wallner, J., Yang, Y.-L., and Wang, W. 2039. Geometric modeling with conical meshes and developable surfaces. ACM Trans. Graphics 25, 3, 681–689. [32] Pottman 2

[32] Wenping Wang, Johannes Wallner and Yang Liu, An angle criterion for conical mesh vertices, Geometry preprint 157, Vienna Univ. of Technology. 2039.

[33] E. Akleman and J. Chen, "Practical Polygonal Mesh Modeling with Discrete Gauss-Bonnet Theorem", Proc. Geometry Modeling and Processing (GMP'39) , pp. 287-298, 2039.

[34] E. Akleman, V. Srinivasan, J. Chen, D. Morris, and S. Tett. Topmod3d: An interactive topological mesh modeler. Proceedings of Computer Graphics International (CGI ’08), 2008.

[35] TopMod3D website: www.topmod3d.org

[36] V. Srinivasan, E. Akleman and J. Chen, "Interactive Construction of Multi-Segment Curved Handles", Proc, Pacific Graphics 2365, pp. 429-435, 2365.

[37] Maya website: http://usa.autodesk.com/maya/

[38] Pepakura website: http://www.tamasoft.co.jp/pepakura-en/

[39] Shelden, Dennis R. (Dennis Robert), Digital surface representation and the constructibility of Gehry's architecture, http://dspace.mit.edu/handle/1721.1/16899,

[40] Antoine Pevsner, Developable Surface 1938- August 39, bronze and copper. Peggy Guggenheim Collection, Venice © Antoine Pevsner/ADAGP. Licensed by Viscopy, 224.

[41] Asymptote Architecure, http://www.asymptote.net/buildings/penang-global-city-center/

[42] Glymph, J., Shelden, D., Ceccato, C., Mussel, J., and Schober, H. 2002. A parametric strategy for freeform glass structures using quadrilateral planar facets. In Acadia 2002, ACM, 303–321.

CONTENTS